

Assessment of complex wind turbine wake flow using scanning wind lidar measurements and numerical analysis techniques

Author:

Jonathan N Butler, *PhD Student, CDT Wind Energy Systems*

University of Strathclyde, Scotland

jonathan.n.butler@googlemail.com

October 2014

This work has been funded by the EPSRC, project reference number:

EP/G037728/1

Declaration of Authenticity and Author's Rights

'This thesis is the result of the author's original research. It has been composed by the author and has not been previously submitted for examination which has led to the award of a degree.'

'The copyright of this thesis belongs to the author under the terms of the United Kingdom Copyright Acts as qualified by University of Strathclyde Regulation 3.50. Due acknowledgement must always be made of the use of any material contained in, or derived from, this thesis.'

Signed:

Date:

Acknowledgements

I would like to thank the following people and companies for their support during the course of this project.

All the staff at SgurrEnergy Ltd for their help and encouragement through the closing stages of this work, in particular Ralph Torr, Richard Boddington, Peter Clive and Graham More. Thanks also to Bianca Schulte at AREVA Wind GmbH for her support and assistance, particularly in the closing stages of this project.

All of the staff in the CDT Wind Energy Systems, in particular Drew Smith, David Infield, Bill Leithead and Alasdair MacDonald.

Also to all of the students (ahem cohorts) and Dolphins who I have worked with during this time, it has been an oddball ride, a blast and a real pleasure, it is a sad day to move on.

A big thank you to my friends and family, it may seem like I have been at this for ever, but I could not have done this without you. Thank you.

Finally the biggest thank you goes to Bine without whose tireless devotion and encouragement I would not have got anywhere near finishing this, making this is as much her achievement as it is mine.

Table of Contents

Abstract	7
Nomenclature	9
Chapter 1: Introduction	11
1. Introduction	12
1.1 The wind industry	13
Chapter 2: State of the art technology review	16
Chapter Summary	17
2.1 Background	18
2.2 Remote sensing technology	19
2.2.1 Lidar methodology	21
2.2.2. Off the shelf lidar solutions	32
2.2.3 Lidar recommended practice and standards	41
2.3 Numerical modelling techniques	43
2.3.1 Actuator disk theory	44
2.3.2 Blade Element Momentum Theory	46
2.3.3 Industry modelling packages	47
2.3.4 Turbulence modelling with Reynolds Averaged Navier-Stokes (RANS) equations	56
2.4 Measurement and model comparisons	62
2.4.1 Comparison research	62
2.4.2 Comparison conclusions	71
2.5 State of the art review conclusion	72
Chapter 3: Methodology	74
3.1 Background	75
3.2 Project flow chart	76
Chapter 4: Lidar deployments	78
4.1 Lidar data capture and analysis	79

4.2 Lidar data processing	80
4.3 Onshore lidar deployments	83
4.3.1 Myers Hill/Whitelee wind farm, July 2011	87
4.3.2 Myers Hill/Whitelee wind farm, January 2012	90
4.4 Offshore lidar deployment	96
4.4.1 Alpha Ventus offshore, February 2013 – May 2013	101
 Chapter 5: Numerical Analysis	 109
5.1 Background	110
5.2 Onshore numerical simulations	112
5.2.1 Onshore simulation setup and execution	112
5.2.2 Myers Hill/Whitelee wind farm, July 2011	118
5.2.3 Myers Hill/Whitelee wind farm, January 2012	120
5.3 Offshore numerical simulations	123
5.3.1 Offshore Windmodeller simulations	124
5.3.2 Offshore PARK and Eddy-Viscosity simulations	127
 Chapter 6: Results	 130
6.1 Background	131
6.2 Onshore lidar measurements and comparisons	132
6.2.1 Ten minute averaged, MyersHill/Whitelee wind farm, July 2011	134
6.2.2 Ten minute averaged, Myers Hill/Whitelee wind farm, January 2012	140
6.2.3 Inlet definition and time averaged comparison	145
6.3 Offshore results	150
6.3.1 Lidar measurement wake profile extraction	150
6.3.2 Lidar measured wake centreline profiles	158
6.3.3 Numerical wake centreline comparison results	164
6.3.4 Lidar measured wake width profiles	169
6.3.5 Numerical wake width comparison results	176
 Chapter 7: Results discussion and analysis	 182
7.1 Onshore results discussion and analysis	183
7.1.1 Ten minute averaged, MyersHill/Whitelee wind farm, July 2011	183

7.1.2 Ten minute averaged, Myers Hill/Whitelee wind farm, January 2012	186
7.1.3 Inlet definition and time averaged comparison	189
7.1.4 Measurement uncertainties in onshore comparisons	192
7.2 Offshore results discussion and analysis	195
7.2.1 Wake centreline profile analysis	195
7.2.2 Wake width profile analysis	207
7.2.3 Measurement uncertainties in offshore comparisons	209
Chapter 8: Conclusions and summary	214
8.1 Conclusions	215
8.1 Onshore lidar analysis summary	216
8.2 Offshore analysis conclusions	218
Chapter 9: Future Work	221
References	224
Appendix A: Lidar to mast comparisons	238
Appendix B: Extract from DNV-RP-J101	244
Appendix C: Actuator disk theory methodology	246
Appendix D: Raw lidar data file formats	250
Appendix E: Siemens 2.3 – 93 Power and Thrust Curves	254
Appendix F: AREVA M5000 Power and Thrust Curves	256
Appendix G: Publications and Presentations	258

Abstract

Utilising scanning lidar devices deployed in active wind farms the results presented detail the evolution of the wind speed profile in the wake of wind turbines operating in both the on and offshore environment. The results of each of the deployments are compared against a variety of wake simulation models.

Focussing on the measurement of wake data at hub height, data captured from the nacelle of an offshore wind turbine detailing flow evolution behaviour across a wide range of operational wind speeds and inlet operating conditions is presented.

Binned in 2m/s wind speed bins the measurements clearly show a consistent profile across the captured speed range. This profile encompasses an initial flow deficit from inlet measured on the downstream side of the rotor. For undisturbed inflow this is seen to be around 30%, slightly larger for the disturbed inflow and larger still for waked inflow. Moving downstream the measured flow values indicate a flow evolution to a maximum deficit from inlet at two rotor diameters downstream, the differences between the inflow situations are preserved through to this point. This deficit is at a maximum in the 6-8m/s wind speed bins where the Power Coefficient is at its highest. As the wind speeds increase, and the Power Coefficient decreases, the magnitude of the maximum deficit decreases. Beyond this point the flow recovers towards inlet values. None of the profiles are found to recover fully within thirteen rotor diameters of the rotor plane.

The wake simulation models employed each identify different areas of strength in comparison to the lidar measurements. The Eddy-Viscosity model with a Turbulence Intensity of 6% shows the closest correlation with the results at the maximum deficit through the recovery and into the far wake. It does not attempt to model the flow behaviour in the near wake region.

Nomenclature

$^{\circ}$	Degrees	k	Wake decay constant
ϕ	Elevation angle ($^{\circ}$)	KB	Kilo bytes
θ	Azimuth angle ($^{\circ}$)	kg	kilograms
ρ	Density (kg/m^3)	km	kilometres
$\bar{\rho}$	Mean density (kg/m^3)	kW	Kilo Watt
$\tilde{\rho}$	Variable density (kg/m^3)	K_1	Dimensionless constant, 0.015 (EV)
ρ'	Deviation density (kg/m^3)	l	Length scale of largest eddies
ε	Eddy-Viscosity term	Lidar	Light detection and ranging
μ	Viscosity (kg/sm)	m	metres
η	Length scale of smallest dissipating eddies	m/s	metres per second
δ	Kronecker delta	MB	Mega bytes
$\bar{\tau}_{ij}$	Shear stress tensor	MPE	Maximum Permitted Exposure
A_{∞}	Free-Stream tube area (m^2)	MW	Mega-Watt
A_D	Rotor area (m^2)	p'	Deviation pressure (Pa)
A_W	Wake area (m^2)	\bar{P}	Variable pressure (Pa)
a	Axial induction factor	\bar{P}_i	Mean inlet pressure (Pa)
b	Wake width at x, EV (m)	p_{∞}	Freestream air pressure (Pa)
$^{\circ}\text{C}$	Degrees centigrade	Δp	Change in air pressure (Pa)
C_p	Power Coefficient	$p_{\bar{D}}$	Pressure on downstream side of rotor plane (Pa)
C_T	Thrust Coefficient	$p_{\bar{D}}^{\dagger}$	Pressure on upstream side of rotor plane (Pa)
D	Rotor diameter (m)	PPA	Power Performance Assessment
DC	Direct Current (V)	PPI	Plan Position Indicator scan
D_m	Centreline velocity as % of inlet (%)	r	Radius from centreline (m)
D_{mi}	Initial velocity deficit	RANS	Reynolds Averaged Navier Stokes
D_r	Deficit at radial point r (m)	Re_l	Reynolds Number for largest eddies
DFIG	Double Fed Induction Centre	RG	Range Gate Number
F	Filter function	RGL	Range Gate Length (m)
g	Gravitational acceleration (m/s^2)	RHI	Range Height Indicator scan
GW	Giga-Watt	Sodar	Sound detection and ranging
h	Hub height (m)	SCADA	Supervisory Control and Data Acquisition
I_0	Ambient turbulence (%)	t	Time (s)
I_{Amb}	Ambient turbulence (%)	\bar{T}	Mean temperature ($^{\circ}\text{C}$)
i	Denotes properties in the i direction	\tilde{T}	Variable temperature ($^{\circ}\text{C}$)
j	Denotes properties in the j direction	T'	Deviation temperature ($^{\circ}\text{C}$)
κ	Von Karmen constant	T_0	Temperature at z = 0 ($^{\circ}\text{C}$)
$\bar{\tau}_{ij}$	Shear stress tensor	\tilde{u}_i	Variable initial velocity (m/s)
T.I.	Turbulence Intensity (%)	u_i	Deviation inlet velocity (m/s)

u	Horizontal velocity component (m/s)	$\overline{u_i u_j}$	mean of velocities in i and j direction (m/s)
U_c	Velocity at centreline at location x (m/s)	VAD	Velocity Azimuth Display
U_D	Mean flow speed at rotor (m/s)	V	Voltage
U_i	Inlet wind speed (m/s)	V_{los}	Velocity in the line of sight (m/s)
U_w	Mean wake velocity (m/s)	w	Vertical velocity component (m/s)
U_∞	Free-Stream velocity (m/s)	W_w	Wake width, PARK (m)
\overline{U}_i	Mean inlet velocity (m/s)	x	Distance downstream from rotor plane (m)
U_0	Inlet velocity (m/s)	z_0	Surface roughness (m)

Chapter 1:

Introduction

1. Introduction

On the back of government agreed energy targets [1]0 and incentive schemes, the renewable energy sector has increased in size and capability in recent years. Renewable energy generation sources have begun to capture a larger share of the electricity market both nationally and globally. Led by solar and wind [2] this increase will be bolstered in the coming decades through further deployment of existing technology alongside the development of wave and tidal resources [3].

This expansion is currently incentivised by UK and EU funding programs [4] [5] to promote renewable energy development alongside traditional fossil fuel generation. If the full potential of renewables is to be met further improvements in installation and operational costs, as well as efficiency in design and operation, are vital, in the process allowing a reduction in the comparative cost of green energy [6]. Coupled with improvements in storage and grid management this will allow these energy sources to be incorporated fully into a stable, green and efficient energy supply network [7].

1.1 The wind industry

Wind energy has a vital role to play in assisting the UK in approaching its renewable obligation target of 20% by 2020 [8]. Combined with the Scottish Government's commitment to the equivalent of 100% of Scotland's electricity demand from renewable sources by the same date [9] the expansion of grid connected wind energy will be a major development area in the coming years, both within Scotland and the UK. Such a commitment will require an estimated 11 - 18GW [9] of installed renewable energy capacity, with a significant portion of this commitment being met by onshore and offshore wind turbine developments.

At present fully developed and deployed wind farm technology offers turbines with ratings of up to and above 6MW, utilising rotor diameters of in excess of 100m [10]. To help realise the proposed generation capacities the development of larger turbines, such as the 7MW test turbine installed in Methil, Scotland, [11] will be required. Such devices will allow for higher energy density to be achieved in wind farms while larger generating units combined with advances in manufacturing techniques will allow for reductions in the unit cost of wind energy per mega-watt to be realised [12].

The unique nature of utilising wind turbine power plants for electricity generation requires an understanding of the stochastic and complex flow field in which they operate. A significant factor in these flow fields is the development of the wake behind an operational wind turbine.

Installed as part of a wider wind farm a given turbine will operate for a period of time in the wake of an upstream device. Understanding this wake flow development behind a wind turbine will allow for a greater appreciation of how downstream devices can be affected by the wakes of

those upstream. Such understanding can be facilitated by capturing flow vector measurements along the length of a wind turbine's wake to build up a profile along its' dimensions.

Traditional wind field measurement has involved strategically placed meteorological masts equipped with anemometers and wind vanes that provide wind vector information at their installation location [13]. In recent years a variety of remote sensing devices have been adapted and developed for the wind energy sector that capture wind vector information remote from the device, Chapter 2. Providing measurements across a flow field from a single installation point, wind specific remote sensing techniques allow a more spatially complete picture of the monitored wind flow field to be built up. Measured flow data can be captured relating to wind turbine wakes, forestry edges and airflow over complex terrain, while marinised variants allow for the capture of offshore flow patterns and wake structures [14].

Improvements in the measurement and visualisation of these wake flow effects can aid greater understanding in the wind farm design process. In addition the numerical simulation of these features can provide great assistance in this area. At present a variety of simple and more complex flow models, Chapter 2, have been developed to facilitate the modelling of wind flow through a wind turbine rotor and into the wake. These have been adapted to provide predictions of wind speed and energy for potential wind farms in a number of wind specific simulation packages. While commonly used in industry for potential resource assessment the accuracy of these predictions is often cited as the largest source of uncertainty in the development of a wind project [15].

The availability of wind specific remote sensing devices offers the potential to gather live wake measurements for comparison with these models. In the process reducing the uncertainty involved in the development of large wind farms.

The work undertaken in this project aims to develop methodologies for the use of remote sensing devices in the capture of wake flow information in active on and offshore wind farms. The captured measurements will detail wake development for a variety of inflow conditions and turbine orientations with special resolutions not available from the use of traditional flow measurement methods. These measured data sets will then be compared to a series of numerical wake flow models that are utilised across the wind industry in the analysis of wind farm flow predictions.

The work will allow an understanding of how the modelled wake velocities compare to those measured by the remote sensing devices, while also facilitating a development of best practices when deploying such devices for wake measurement in active wind farms.

Chapter 2:

State of the art technology review

Chapter Summary

The project aim to compare wind turbine wake remote sensing measurements with numerical wake models requires a full understanding of the state of the art technology in both of these focus areas.

The literature review presented in the following chapter details the state of the art in remote sensing and the principals involved in wind flow field measurement and analysis.

In focussing on numerical flow modelling techniques the methodology and characteristics of a variety of flow models developed for the wind industry are also explored.

Finally a literature review of existing academic comparisons between remote sensing measurements and a selection of numerical flow models provides an analysis of work completed in this field of study.

2.1 Background

The wind industry sector is utilising tools and expertise developed for use in a wide variety of different industrial and academic sectors. Aerodynamic tools are used to develop blade technology [16], oil and gas expertise used to develop and deploy offshore structures and networks [17], mathematical modelling techniques are implemented to predict failure rates and electrical grid models [18], and transmission grid expertise is being used to plan and locate connection networks to reduce transmission losses [19]. The focus of the work presented here considers the use of remote sensing technology and computational flow modelling tools in the wind industry that have been developed from other applications [20] [21].

The development of these established technologies into wind specific platforms offers new opportunities to apply their capabilities and ensure a better understanding of the challenging flow regimes in active wind farms. The following review chapter will context the state of the art in wind flow measurement technology and numerical analysis tools for characterising wind turbine performance.

2.2 Remote sensing technology

It is essential for maximising wind turbine performance to understand wind flow characteristics and the complexity of the wind resource. Traditional tools for on-site wind vector analysis are physical and intrusive in nature and require the erection of large meteorological (met) masts equipped with cup anemometers and wind vanes. From these towers, point measurements of wind speed and direction can be recorded at defined heights. Current wind assessment techniques and standards will not consider a site without a year's worth of on-site measured data [22] making them a crucial factor in wind farm developments.

The availability, accuracy and mobility of remote sensing devices is changing the way in which developers and other stakeholders approach site assessment [23]. The ability to create virtual met masts above a device or scan in two dimensions away from it allows for richer more expansive data sets to be gathered. This advance in technology allows a greater level of detail into the behaviour of the wind flow characteristics associated with wind farms and individual turbines.

Allowing measurements to be taken at a range of distances from an installed unit, remote sensing devices offer a distinct advantage over the traditional anemometer and wind vane methods. By utilising sonic and laser technology remote sensing devices allow wind vector properties to be captured at programmable distances from the physical location. The wind industry is embracing this technology in research, performance and characterisation roles [24].

Sound Detection and Ranging (sodar) and Light Detection and Ranging (lidar) devices have previously found uses in various engineering applications. Originally developed by the military and used in target acquisition and tracking [25] both have gone on to be used on separate platforms including NASA’s Mars exploration programs [26]. Their application in the wind sector has been aided by the introduction of affordable, robust and compact laser technology [27] and they are subsequently being used for a variety of different roles in the wind industry. Lidar devices are emerging as the market leader [28] with more versatile and compact products. A variety of companies offer lidar solutions to the wind industry, Halo Photonics’ [29] Galion Lidar [30] (marketed through SgurrEnergy Ltd [31]), QinetiQ’s ZephIR [32] [33] (marketed through Natural Power [34]) and Leosphere’s [35] Windcube [36] have a significant presence in the UK market. Recent developments have led to the availability of smaller more mobile devices, improving the opportunity for potential deployments in proposed or developed wind farm. Table 2.1 gives an overview of the main lidar devices available in the wind industry at present and a summary of their capabilities; the different lidar methodologies utilised are explored in Section 2.1.1., while the devices detailed are explored in more detail in Section 2.1.2.

Product	Manufacturer (Marketer)	Max Range	Methodology			
			Beam Emission	Distance Resolution	D.o.F	Scan Geometries
Galion	Halo (SgurrEnergy Ltd)	Up to 4 km	Pulsed	Time of Flight	2	‘All-Sky Scanning’
ZephIR	QinetiQ (Natural Power)	150m	Continuo- us Wave	Beam Focussing	1	Vertical Only
Windcube	Leosphere (NRG)	200m	Pulsed	Time of Flight	1	Vertical Only

Table 2.1: Commercially available lidar models

2.2.1 Lidar methodology

Each of the lidar technologies presented in Table 2.1 utilise a similar doppler shift technique to obtain the component of the wind vector aligned with the laser orientation (line of sight velocity or V_{los}) at a defined distance from the device. This doppler shift is established through the laser reflecting on microscopic aerosols, or scattering centres, travelling in the wind. The changes in laser wavelength and frequency imposed on the beam correspond to the component of the wind vector aligned with the laser beam and are used to calculate the corresponding line-of-sight component of the local wind vector. The key variables defining a lidar device are the emission method of the measurement beam and the number of degrees of freedom available in controlling the orientation of the beam [27].

Emission method

Wind lidar devices use two types of measurement beam emission principle, continuous wave (ZephIR) or pulsed (Galion and Windcube). The difference between these two technologies is in the way that the distance to the measurement locations is achieved. Continuous wave devices employ a method of beam focussing where the strongest measured reflections are achieved at the focus point of the beam [37]. In contrast pulsed systems use a time-of-flight methodology, determining the distance to the measurement location from the time taken to send the pulse emission and the return of the reflected light [38]. Consequently a number of measurements can be taken simultaneously at different ranges along the laser length.

Laser emission and reception is facilitated from either a bistatic or monostatic source [39], Figure 2.1 shows the basic setup of a bistatic pulsed laser, where the emitted beam is compared to the back scattered properties to establish

the doppler shift properties. The laser emission and backscatter detection optics are separate in a bistatic lidar device; in contrast a monostatic lidar device the emission and detection processes share common optics. The monostatic arrangement is more common. Time of flight calculations are used to find the distance to the scattering centres this is indicated in the system schematic in Figure 2.1.

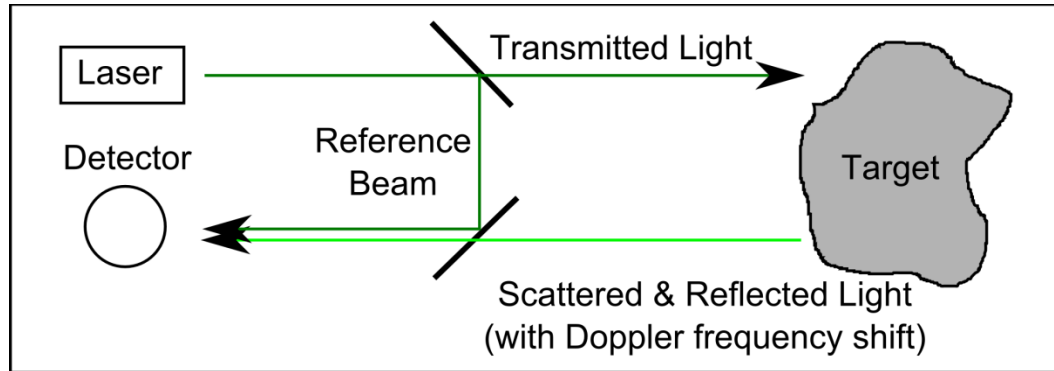


Figure 2.1: Generic bistatic pulsed lidar system [39]

Single degree of freedom lidar devices

Single degree of freedom lidar devices allow the user to vary the azimuth of the measurement beam while the elevation remains constant. To ascertain an absolute wind vector, three or more line of sight velocity (V_{los}) measurements are required to aid in calculating the three unknowns of Equation 2.1.

$$V_{los} = |A \sin(\theta - B) + C| \quad \text{Equation 2.1: [40]}$$

Where:

$$A = u \cos(\phi)$$

$$B = \text{Wind bearing} \pm 180^\circ$$

$$C = w \sin(\phi)$$

ϕ = Beam elevation angle measured from horizontal

θ = Beam azimuth angle measured clockwise from North (0°)

u = horizontal component of measured wind vector

w = vertical component of measured wind vector

The common lidar method of achieving this is by varying the azimuth of the beam in a circular motion keeping the beam elevation from the horizontal plane (ϕ) constant [41], thus defining a conical volume around the zenith above the device [42]. Commonly the elevation angle is held constant at 60° defining a cone with an apex angle of 60° , this method is defined as a Velocity Azimuth Display (VAD) scan.

A single degree of freedom lidar device can be programmed to obtain measurements at a succession of points around a full 360° circle directly above the device, Figure 2.2. From these variations at a constant distance, or height, from the device, a series of line of sight velocity values can be recorded. Under steady state wind flow conditions these values can be plotted against azimuth angle (θ – measured clockwise from North) to follow a sinusoidal pattern, Figure 2.3. This pattern is produced as the laser intercepts the wind flow at different angles and the variations in the line of sight values are plotted. The maximum and minimum measured line of sight values align with the predominant wind direction while the function passes through zero when the azimuth value is perpendicular to the wind direction. Each point in the sinusoid can be fitted against Equation 2.1, derived in [23] [40].

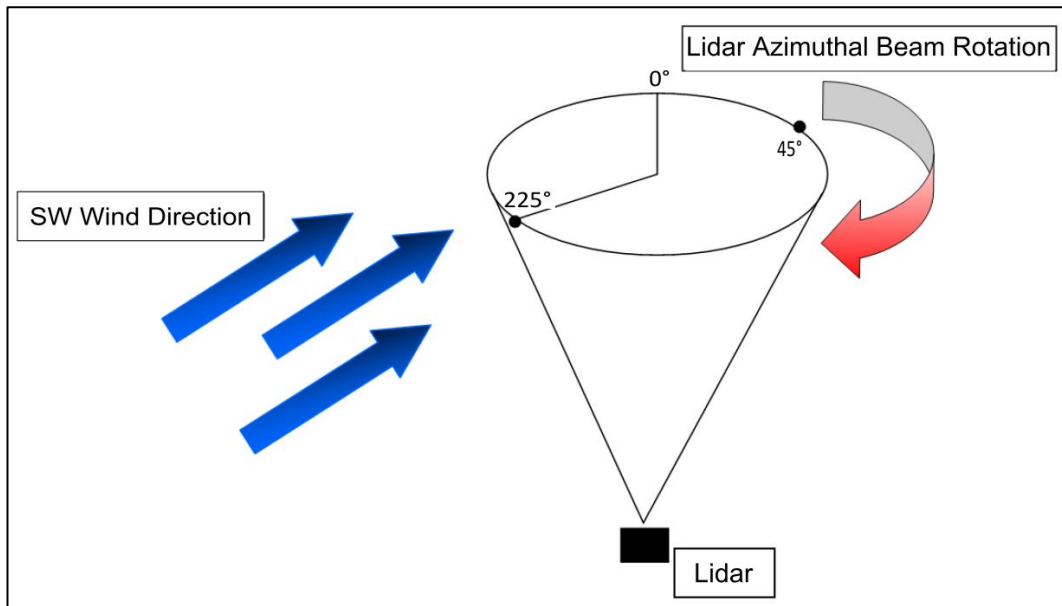


Figure 2.2: VAD formulation diagram

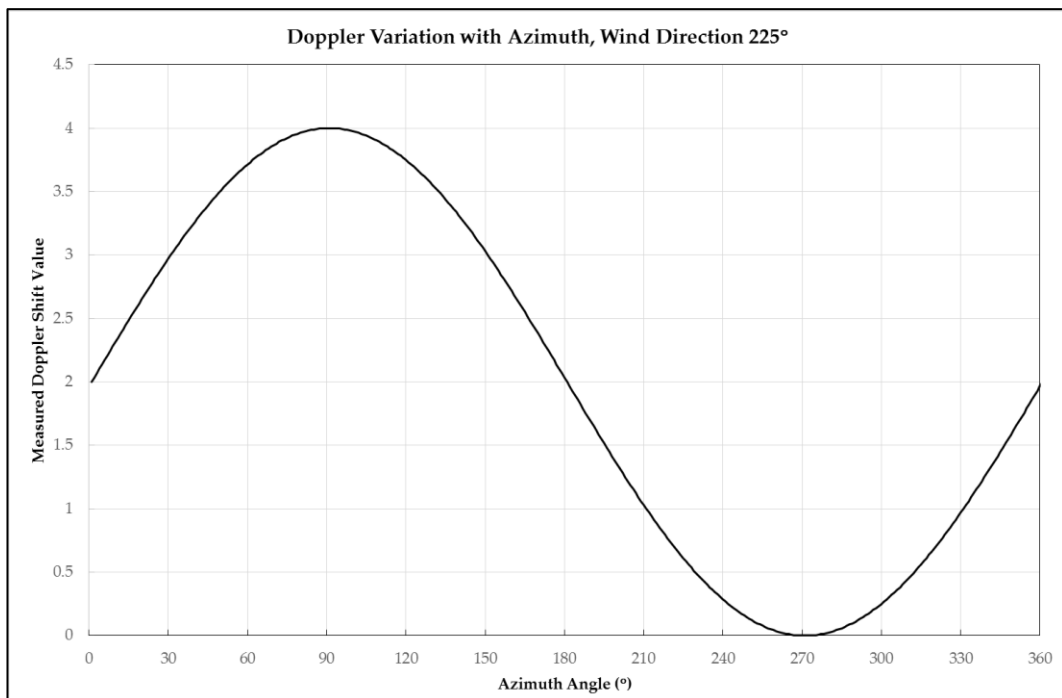


Figure 2.3: VAD scan fitting technique

Given three or more points for V_{los} and their corresponding azimuth value it is possible to determine the three unknown values for horizontal wind speed (u) and vertical wind speed (w) along with the value of the wind bearing, B . This will allow the formulation of a local wind vector at the height the measurements took place.

The definition of this height is reliant on the definition of the distance from the device. Pulsed lidar solutions employ a fixed probe length that is governed by the optics of the device, constraining the measurement location to being multiple of this value. Continuous Wave based devices have greater ability to tailor the measurement height to the user's requirements [37] by allowing a beam focussing methodology to be employed. With this the user specifies the measurement distances required and the lidar focuses on each of these in turn.

Employing a VAD methodology with a pulsed lidar the measurement height above the lidar can be given by:

$$h = (RG \times RGL)\sin(\phi) \quad \text{Equation 2.2}$$

Where:

RG = Range Gate Number

RGL = Range Gate Length

The user specifies the number of probe lengths from the device a measurement is required at, this is known as the Range Gate (RG) number; the distance from the device is then given by this value multiplied by the probe, or Range Gate, length (RGL) [43]. As the Range Gate Length is a constant value controlled by the optics of the device this is the limit for the resolution of lidar data sets captured using a single pulsed device. In most situations the lidar is programmed to probe a maximum number of range gates defined by the user, the required distanced from the device can then be chosen from the results.

This Velocity Azimuth Display method of wind vector formulation is the main measurement technique for single degree of freedom based lidar

devices. In this methodology the lidar device is creating a virtual met mast above the device; it can be employed by all of the referenced lidar devices, Table 2.1. The ZephIR continuous wave device takes a large number of readings around the 360° azimuth in a short scan time, a sinusoid can then be accurately fitted against these measurements. In contrast the pulsed Galion Lidar and Windcube devices rapidly take 3 - 4 readings at a given height and fit the sinusoid to these results. Using the extended range of the lidar devices these virtual masts can attain measurements at heights unattainable by traditional met mast installations.

Although widely used there are a number of weaknesses in the VAD methodology that may limit its effectiveness, particularly in complex terrain and non-uniform flow situations.

The resultant vector is an average over the circular area defined by the measurement points taken; it is therefore not a true point measurement. As the scan is conical, the area of the described circular measurement plane will increase with height. A 60° cone apex angle will result in measurement diameters of 115.5m at 100m and 230.9m at 200m. Thus, the assumption of steady state flow across the measurement plane becomes weaker as height increases. The VAD method has been shown to produce measurement errors in complex terrain in studies where greater values of vertical wind speed may be experienced and turbulent eddies may be prevalent [44]. These difficulties can be resolved as the VAD method shows good correlation with met mast data in simple terrain for the Galion, the ZephIR and the Windcube, these results are covered in Section 2.1.2 below.

Two degree of freedom lidar devices

The ZephIR [33] and the Windcube V2 [36] variant have single degree of freedom scanning capabilities. In both devices this refers to an ability to vary the azimuth of the measurement beam as the elevation stays fixed; this necessitates the use of the VAD scan profiles described in Section 2.1.1.

Systems which have the capability to vary elevation in addition to the azimuth introduce a second degree of freedom in the beam orientation definition. Devices with this functionality include SgurrEnergy Ltd's Galion Lidar [30] and the Windcube 200S [36], these devices are often termed scanning lidars [44]. This configuration coupled with increased measurement range allows for 'all sky scanning' [43] capabilities providing the user with the option to implement any desired arc scan pattern to fulfil their requirements.

Distance resolution is achieved through time of flight measurements. Techniques commonly employed with second generation lidar devices involve holding one beam orientation variable constant while changing the other tracing an arc pattern remote from the device, these techniques echo those used in the aviation industry for radar scanning purposes [45].

Holding the elevation steady and varying the azimuth creates an arc scan across the sky, this methodology can be termed Plan Position Indicator (PPI). In contrast holding the azimuth constant and varying the elevation creates a vertical plane through the studied flow field and is termed and Range Height Indicator (RHI).

Although the PPI method is identical to that of the VAD the elevation value employed is generally applied between 0° and 10° from the horizontal, while the azimuthal range is usually less than the 360° of the VAD method. The

visualised results lead to a plan like image of the flow field measured; Figure 2.4 shows a sample PPI scan. The image shows multiple lidar scans averaged over a period of one hour on the 11th January 2011 between 22:00 and 23:00 as identified in the figure title. The lidar is situated at (0, 0) along the top edge of the scan and is scanning from 90° to 185° relative to North. As the image represents measurements taken from a ground based lidar device the height above the device increases linearly from (0, 0) to the scan edges. This is reflected in the measurements as the measured wind speeds increase towards the bounds of the scan. Several turbines and their associated wakes can be identified in the image.

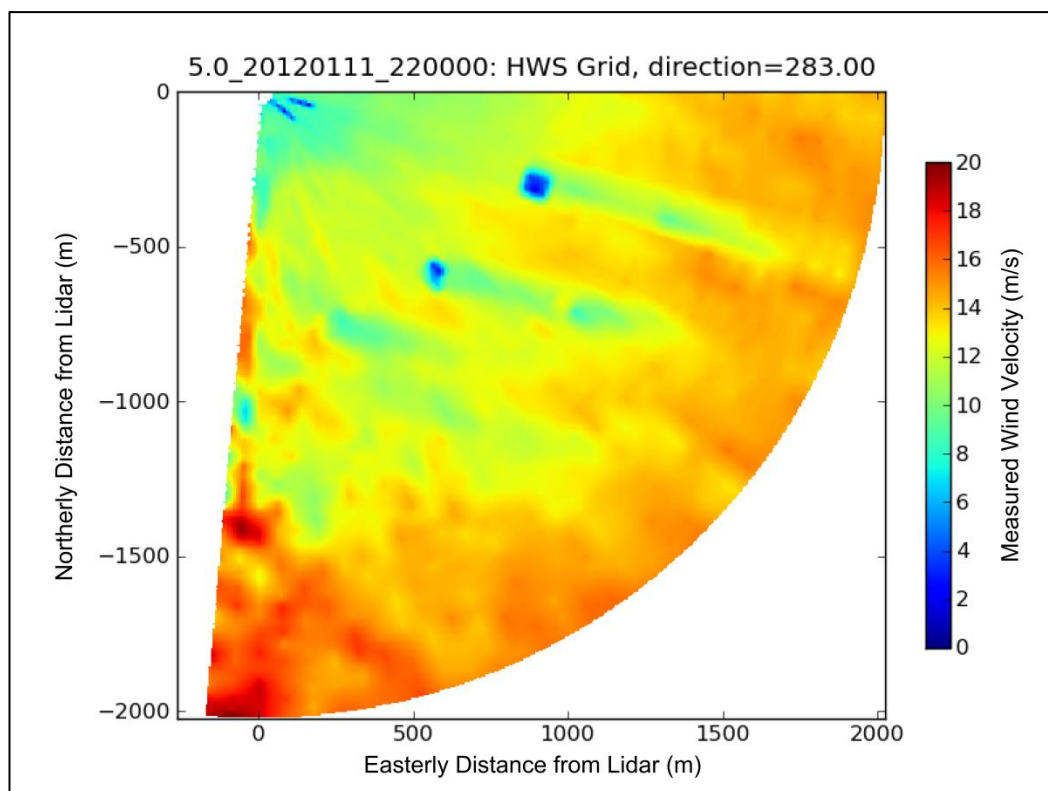


Figure 2.4: PPI Scan, 1 hour averaged

Focussing on the PPI scan methodology it is found that the VAD scan analysis method of fitting a sinusoid to the data sets to ascertain wind direction can be applied to PPI scans given that PPI's are essentially

truncated VAD scans with a lower elevation, usually in a quadrant (i.e. not 360°) of interest.

The RHI method holds the azimuthal value constant and varies the elevation of the beam creating a vertical slice through the flow field. Figure 2.5 presents a sample scan using this technique from a Galion Lidar device, the flow field presented measured wind flow moving right to left towards the device located at (0,0) [43]. The vertical plane scan through the atmospheric boundary layer captures evidence of a low level jet of faster moving air between heights of 80m and 200m. The negative wind speed values indicate flow moving away from the device.

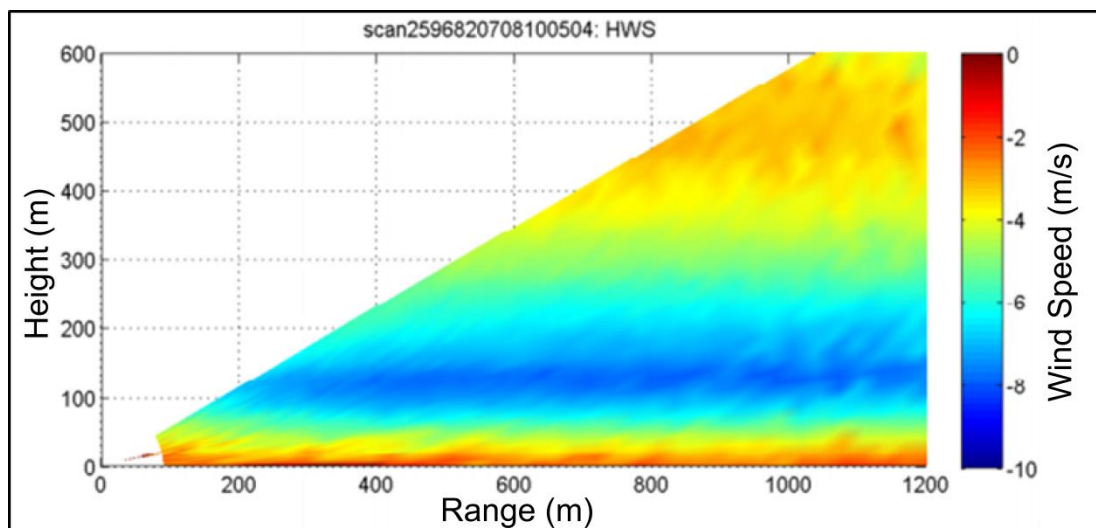


Figure 2.5: Sample RHI scan [43]

Time and space trade-off

Under ideal conditions the air flow into a wind turbine will be turbulence free, horizontal and consistent in direction and speed. The nature of the wind does not allow this to be the case. The wind resource across a given site is shown to evolve consistently; it is influenced not only by physical structures but also by atmospheric conditions such as localised temperature and pressure. These effects can be manifest on a large variety of length scales and

move in a variety of directions regardless of the prevailing wind direction. The resultant flow field is fully three dimensional and highly stochastic in nature. Patterns may emerge at a macro scale but at length scales relevant to wind turbines turbulent eddies and induced structures can dominate the flow. Such behaviour is particularly evident within active wind farms where the rotational and velocity slow down effects created by active wind turbines can extend for tens of rotor diameters downstream from the rotor plane.

In attempting to measure and quantify these structures using scanning lidar technology their varying size, movement and evolution necessitates a trade-off in the resolution of the measured data sets and the time taken to acquire them [46]. Although the time taken to capture the measurements on a single beam orientation is small the time overhead involved in refocusing the devices optics to a new beam orientation is more significant, particularly when high resolution data is required. A 4000m radius scan will take several seconds to gather measurements along the full beam length, repeating this process for a wide scan arc will incur a significant time overhead reducing the time resolution of the measurements.

In the time taken to capture all of the data in the defined arc the flow features measured will have moved on and the resultant data set cannot represent an instantaneous snapshot of the flow field. Reducing the number of measurement points along the beam and beam spacing in the arc scan will increase the speed at which a scan arc can be completed thus increasing the time resolution; this will however reduce the spatial resolution of the attained data set as there are larger spaces between the measurement points. This is the nature of the time and space resolution trade off that exists with the use of scanning type lidar devices for arc scans. The larger the azimuth and distance range of the scans implemented the more these issues will come

into play. Each device has slightly different capabilities that can allow for the optimisation of the scan arc for given situations but this problem cannot be removed completely with the deployment of a single device. To counter these issues a scan setup can use either multiple laser beams or average the data sets across extended time periods.

Averaging the data sets allows data sets to capture permanent flow structures such as turbine wakes or flow circulation areas. This setup assumes steady state flow conditions and cannot capture dynamic turbulent structures or gusts present in the flow. For comparison with steady state numerical models these averaging techniques provide an attractive prospect.

2.2.2. Off the shelf lidar solutions

The three devices considered in Table 2.1 have been deployed successfully in a wide variety of locations and conditions across the globe, Section 2.3. The deployments have been undertaken in a wide variety of complex flow situations where further understanding of flow behaviour is required by clients and researchers. In the following section the characteristics and performance of these three devices are considered for operations in the VAD mode explored above.

The three devices examined are portable and are easily deployed for measurement campaigns after a period of verification and performance testing. When compared to traditional meteorological mast solutions their installation location flexibility and range of measurement heights provide greater possibilities for wind profile measurements and flow analysis.

There are two other wind specific lidar devices becoming available but their development status is unclear, Catch the Wind's Vindicator [47] and LockHead Martin's WindTracer [48].

Halo-Photonics (SgurrEnergy Ltd) Galion Lidar

Developed by Halo-Photonics [29] and SgurrEnergy [31] the Galion [30] is a variant of existing Halo remote sensing technology. At present two Galion Lidar models are available, the Galion G250 and the Galion G4000, with both models offering offshore marinised variants [49]. Table 2. details the technical specifications of the Galion device.

Performance:	Range	250m (Galion G 250) 4,000m (Galion G4000)
	No. of measurement heights	15 + (Galion 250) 130 (Galion 4000)
	Probe length	24m (Galion 250) 30m (Galion 4000)
	Sampling rate	50Hz
	Laser emission	1 x Pulsed Laser Beam
	Scan averaging period	10mins / 1hour
	Speed measurement accuracy	$\pm <0.1\text{m/s}$
	Direction measurement accuracy	$<0.5^\circ$
	Speed range	0m/s – 70m/s
	3D Scanner	Azimuthal scanning
Zenithal scanning		$0^\circ - 180^\circ$
Angular resolution		0.5°
Maximum rotation speed		360° in 20s
Operations:	Temperature range	$-15^\circ\text{C} - +35^\circ\text{C}$
	Power consumption	150 Watts
	Power input, DC	24V DC
	Weight	85kg
Data:	Variables	Horizontal Wind Speed, Direction, Turbulence, Measurement Location, Device Pitch & Roll, Measurement Intensity
	3 second data	3MB/day
	10 minute averaged data	80KB/day
Safety:	Laser classification	Class 1
	Eye safety standard	IEC 60825-1

Table 2.2: Galion technical specifications [49]

Galion performance verification

The Galion has undergone a series of independent testing deployments in order to assess performance against traditional met mast methods. In 2009 at the DTU Risø operated Danish National Test Station for Large Wind Turbines located at Høvsøre, Western Jutland, Denmark [50] the device was tested for four days against Class 1A cup anemometers and wind vanes

mounted on a meteorological mast installed at the site. Each of the mast's anemometers was calibrated to MeasNet Standards [51], at heights of 40m, 60m, 80m, 100m and 116m above ground level. Comprehensive testing was conducted of the Galion's wind vector measurement capabilities against the mast measurements at each height. In addition comparisons of the lidar wind direction measurements were conducted against those of the wind vanes, mounted at 60m and 100m on the mast. The data set was filtered to exclude low wind speeds ($< 4\text{m/s}$), mast and turbine shadow effects (based on direction), excess wind veer (greater than 5° in a 10 minute period) and precipitation during the period of averaging [50]. In the analysis presented ten minute averages and standard deviations were considered for comparison. Figures presented in Appendix A detail the results for standard regression analyses carried out on the test data for the 100m case for horizontal wind speed and wind directions.

Height [m]	Mean Value [m/s]	Standard Deviation [m/s]
40	-0.16	0.31
60	-0.05	0.18
80	-0.07	0.16
100	-0.09	0.17
116	-0.10	0.18

Table 2.3: Mean error value and standard deviation for lidar wind speed measurements at multiple heights [50]

The measured lidar error values, defined as lidar measured horizontal wind speed minus the mast anemometer wind speed measurements [50], are presented in Table 2.3 for each measurement height. The standard deviations of the measurements at each height are also presented.

Analysis of the findings in Table 2.3 show the largest mean error values to be at 40m; this is as a result of the greater scatter seen in the captured data at this height [50]. Beyond the 40m height it can be seen from Table 2.3 that the

mean error value increases with height, while the standard deviation of this error stays reasonably constant. The measurements between 60m and 116m show an acceptable correlation with the cup anemometer measurements with a maximum error value of -0.1m/s and maximum standard deviation value of 0.18m/s at a measurement height of 116m [50].

The lidar measurement performance against the meteorological mast data as captured in this analysis is acceptable but shows slightly increased variations at distance from the device perhaps resulting from the increase of measurement volume [50].

The Galion, and its variants and functionality, have been tested and verified by a number of independent organisations with track records in device certification. The studies verify the device’s wind speed and directional measurement accuracy for a number of challenging environments both on and offshore, details of each of these can be found in Table 2.4. The papers detailed show that the Galion’s capabilities and accuracy levels are acceptable for a wide range of flow conditions.

Organisation	Year	Description	Reference
DTU Risø	2009	Onshore test against heavily instrumented independent met mast at DTU Risø test site, Denmark.	[50]
Deutsche Windguard	2013	Onshore performance verification at the DWG test field in Rysum, Germany.	[52]
DNV KEMA	2013	Reviewed a year’s worth of bank-grade wind data captured by Galion lidar on the ORQA platform, Hong Kong, China.	[53]
Fraunhofer IWES	2013	Verified the accuracy of Galion lidars "remote mast" functionality for providing offshore power curve tests.	[54]

Table 2.2: Galion lidar independent verification tests

QinetiQ (Natural Power) ZephIR

The ZephIR [32] has been developed and manufactured by British company QinetiQ [33], and is now marketed and operated by the renewable energy consultancy Natural Power [34]. It was the first market ready wind specific lidar and achieved a number of firsts for lidar devices in the wind sector [55]. Initially launched in 2003 the ZephIR has been through a number of design iterations, the current primary device available is the ZephIR 300. Other products offered in the ZephIR range include nacelle mounted (ControlZephIR) and offshore (SeaZephIR) variants; these are both based on the same technology found in the ZephIR 300, Table 2.5 details the main ZephIR 300 technical specifications [56] [57].

Performance:	Range	10m – 200m Extended Option - 300m	Range	
	Number of measurement heights	10 user defined		
	Probe length	0.07m @ 10m 7.70m @ 100m		
	Sampling rate	50Hz		
	Laser emission	Continuous (CW)	Wave	
	Scan averaging period	1s upwards		
	Speed measurement accuracy	<0.5%		
	Direction measurement accuracy	<0.5°		
	Speed range	1m/s – 70m/s		
	Operations:	Temperature range	-40°C - +50°C	
		Power consumption	69 Watts	
Power input, DC		12 V		
Weight		55kg		
Data:	Variables	Wind speed, direction, turbulence		
	3 second data	3MB/day		
	10 minute averaged Data	80KB/day		
Safety:	Laser classification	Class 1		
	Eye safety standard	IEC 60825-1		

Table 2.3: ZephIR 300 technical specification [56] [57]

ZephIR performance verification

Each ZephIR 300 lidar is tested and calibrated at the company's test site in Pershore, Worcestershire. The site accommodates a 90m meteorological mast with Vector 100L anemometers [58] calibrated by Risø at heights of 20m, 45m, 70m and 90m. In addition to this met mast each device is bench marked against a reference ZephIR 300 which has been calibrated at the DTU Risø test station in Høvsøre, Denmark. This is the same test station and mast as utilised in the Galion performance verification identified above [50]. ZephIR testing is undertaken to industry approved guidelines and certified for 'finance grade wind resource assessments' if required [57].

Test results for a ZephIR 300 deployed at the Pershore test site are presented in Appendix A. The figures present standard regression analysis applied to the ten minute averaged data comparing mast data to lidar data at heights of 91.5m and 40.5m. The plots compile mast measured horizontal wind speed data against lidar measured horizontal wind speed data. The deployment took place for two weeks in January 2011; low wind speed filters ($< 3\text{m/s}$) were applied to both captured data sets and any erroneous data points visible in the cup anemometer data sets were removed from the comparison [59].

Individual analysis of the errors in the deployments in [59] is not presented, instead the measurement statistics have been averaged over 24 non-concurrent ZephIR 300 deployments. The results presented in Table 2.6 detail the mean slope and standard deviation of the regression analysis aggregated across the 24 deployments, this has been completed for each measurement height.

Height (m)	Gradient		Sensitivity	
	Mean Slope	Standard Deviation	Mean Slope	Standard Deviation
91.5	1.0038	0.0069		
70.5	1.0039	0.0076	1.0350	0.0881
45.5	1.0005	0.0054		
20.5	0.9967	0.0048		

Table 2.6: Regression analysis for data captured by 24 ZephIR 300 devices at Pershore test site [59]

These results indicate that the calibration consistency across the 24 devices lies within 0.5% of the mean value of the regression slope of the analysis for each of the study heights, the standard deviation of this slope is found to be <1% for all heights.

The sensitivity study on the right of Table 2.6 compares the results of the 24 tests to that of a reference ZephIR 300 unit with a sensitivity of unity. The regression analysis results presented shows a 3.5% deviation from the unity gradient of 1.

The results of the Gradient regression analysis show a low level of variation in the mean across the 24 deployments which showcases the consistency in measurement accuracy of the ZephIR device.

Leosphere (NRG) Windcube

Developer Leosphere [35] are an established name in developing laser based atmospheric remote sensing technology. In partnership with NRG, a wind monitoring and analysis specialist, they developed and market the Windcube [36] product line. The main sales model is the Windcube V2, an offshore variant (Windcube V2 Offshore) is also available [60]. Table 2.7 below identifies the key technical specifications of the V2 device.

The V2 device uses a pulsed laser system employing 5 individual laser beams, four point to the cardinal points (N, E, S & W) and the fifth to the zenith (Z). The V2 is claimed to be the only wind specific lidar measuring the absolute values of horizontal and vertical wind speed [60].

Performance:	Range	40m – 200m
	Number of Heights	12 User defined
	Sampling Rate	1Hz
	Laser Emission	5 x Pulsed Laser Beams
	Speed Accuracy	0.1m/s
	Direction Accuracy	2°
	Speed Range	0m/s – 60m/s
Operations:	Temperature Range	-30°C - +45°C
	Power Consumption	45 Watts
	Power Input DC	18V - 32V
	Weight	45kg
Data:	Resolution	1s or 10min
	Variables	Horizontal & Vertical wind speeds Min & Max, direction, Signal to Noise Ratio, Quality Factor, GPS Coordinates
Safety:	Laser Classification	Class 1M IEC
	Eye Safety Standard	IEC 60825-1

Table 2.7: Windcube V2 technical specification [60]

Windcube V2 performance verification

The Windcube V2 model has undergone testing in a variety of flow situations around the world. Renewable energy consultants *res* [61] have carried out a side by side comparison of the Windcube V2 device against a met mast and Triton Sodar device [62], all three devices captured ten minute averaged data sets. The remote sensors are constrained to take measurements at 60m and 80m, the met mast at 62m and 80.2m. Figure A.5 in Appendix A shows a comparison between measured horizontal wind speed for both remote sensing devices and that of the met mast at 80m [61]. The presented

comparison shows that the Windcube performs better in this test than the Triton with less scatter present in the measurement results at both heights

Height (m)	Gradient	Uncertainty	Intercept	Uncertainty	R ²	Valid data
60	1.0100	0.0012	0.0096	0.0081	0.9941	99.52%
80	0.9985	0.0010	-0.0105	0.0071	0.9959	99.92%

Table 2.8: Windcube V2 vs mast data results from Rotsea test [61]

Table 2.8 identifies the key calculations presented in [61] for a standard regression analysis applied to the measured and filtered V2 data set. The correlation gradient at both heights shows a < 1% error to the unity gradient which is within the acceptance test criteria [61].

In addition to the Windcube V2, Leosphere offer a number of further devices with similar technical specifications but with extended range capabilities. A further recent addition to their wind profiler range is the Windcube 200S [63], a scanning lidar device capable of 3D scanning utilising two degree of freedom scanning abilities.

2.2.3 Lidar recommended practice and standards

Lidar devices are not manufactured to set standards governing their construction and measurement methodology; instead the three devices considered in Section 2.1.2 subject each device for a period of testing and calibration before delivery to the customer. The recorded results ensure each device has a traceable history and its' accuracy in a field situation can be guaranteed upon delivery, the figures presented in Appendix A above show standard field test results for each device outlined in Table 2.1.

A multitude of working groups and organisations have looked at developing sets of standards governing the best practice use of remote sensing devices, focussing in particular on the met mast replacement potential of such devices. The Lidar Acceptance Group (LAG) [64], have been looking at developing a set of standards governing the testing and use of remote sensing devices for wind measurements. An outcome of a series of LAG meetings the 2010 Boulder Protocol [65] began the process of formalising the acceptance of remote sensing data. The main topics considered in this brief document identify cases in which remote sensing data is acceptable, methods for verification of the device before deployment, and verification operational constraints for remote sensing use.

In April 2011 Det Norske Veritas (DNV) published a recommended practice document DNV-RP-J101 titled the 'Use of Remote Sensing for Wind Energy Assessments' [66]. The document covers the requirements for a lidar deployment to be considered acceptable for use in Energy Assessments. It states that remote sensing data can be used to quantify the accuracy of extrapolations from tower data, as well as that of the shear coefficients calculate from tower data. Remote sensing data may also be used to capture

hub height wind speed and direction measurements and to quantify wind resource variability across a site [66]. DNV-RP-J101 also describes a number of caveats pointing out relevant features of remote sensing methodologies that must be understood prior to their use; these are described in full in Appendix B.

The text presented in Appendix B and the wider DNV document seeks to establish a set of parameters that define periods in which results captured by a remote sensing device can be used in Energy Assessment procedures and when the data cannot be verified reliably. DNV-RP-J101 [66] also provides guidelines on Site and Operation, Documentation, Instrument Verification, and the Planning and Implementation of Measurements for Energy Assessments. Enacting these principals will allow for the effective use of remote sensing devices in situations where traditional techniques do not provide the flexibility required. This is of particular use where planning permission for met masts is not available, large rotor turbines are being considered, measurements at hub height and across the rotor diameter are required, in addition to locations where the installation of a met mast will be problematic i.e. undeveloped sites and offshore.

Work is underway to develop standards and best practice guidelines governing Power Performance Assessment (PPA) at operational wind farms, in particular IEC 61400-12-1 [67], which covers 'Power performance measurements of electricity producing wind turbines'. If successful this work will allow for the use of remote sensing devices in the power performance assessment of operational wind turbines. Through accurate characterisation of wind turbine inflow and matching this with operational turbine performance data a true picture of how a wind turbine is operating compared to design specifications will be established.

2.3 Numerical modelling techniques

Computer based numerical flow models have been developed and applied to a wide range of engineering problems. Their development for wind turbine simulation applications has allowed them to become a widely used tool in the development of wind farms. Providing solutions to the Navier-Stokes flow equations or incorporating wind turbine wake flow methodologies the aim is to provide models of wind flow through a wind farm and corresponding predictions of potential power and loading characteristics across the site. In the use of Navier-Stokes equations the aim is to produce a complete simulation of flow interactions across a site detailing the flow across each of the mesh [68]. These tools can be used during the planning, deployment and operational stages of wind farm development.

Wind farm flow modelling

With the complexity of the wind turbine flow field there is a need for flow simulation packages tailored specifically to wind simulations with improved accuracy suited to the requirements of the application.

The flow regime experienced across a wind farm site is a complex mix of turbulent flow with a variety of length, mixing and time scales observed. Production of full numerical solutions with mesh sizes capable of modelling all of these scales results is not practical. Laminar solvers have been used across turbulent flow in an attempt to solve this; however solutions from this method do not fully characterise the conditions and hence lack accuracy [69].

In pursuit of workable solutions for wind farm modelling a number of methods have been developed to reduce the complexity of the posed problem. The most common and proven of these are detailed as follows:

2.3.1 Actuator disk theory

Initial one-dimensional models for idealised wind turbine flow were developed by Betz in the 1920s [70] [71] leading to the formulation of the Betz limit of the theoretical maximum power co-efficient possible through a wind turbine rotor. The methodology has since been developed for modern wind turbine flow applications, the basic idea is to impart a pressure drop on the incoming flow at the rotor plane; Figure 2.6 illustrates the major concept and the behaviour of the flow properties under investigation.

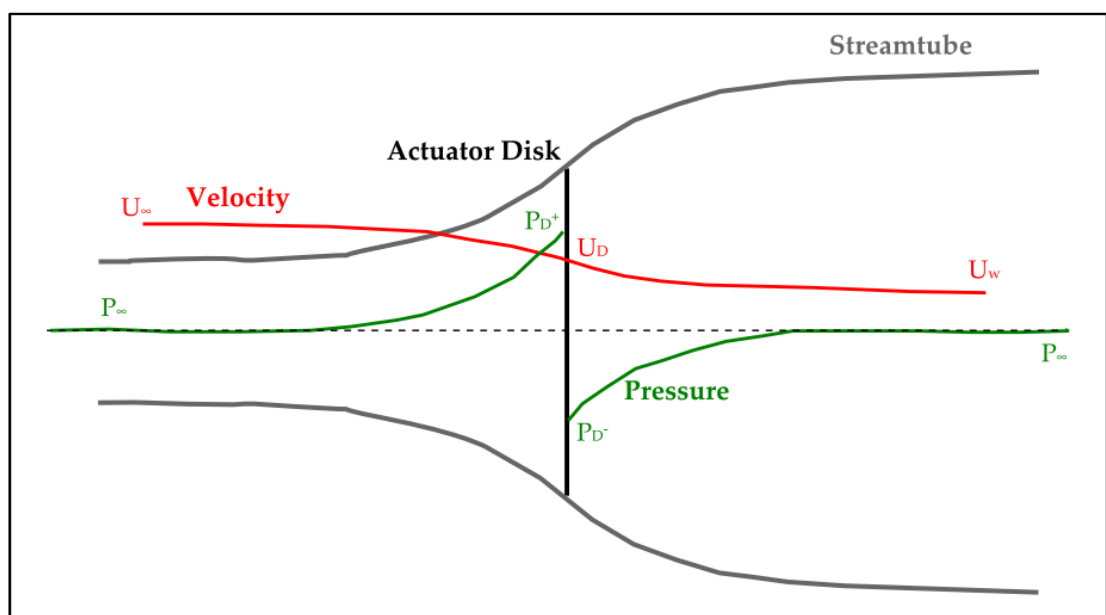


Figure 2.6: Actuator Disk concept [68]

In Figure 2.6 U represents velocity and P pressure, while the subscript ∞ represents freestream conditions, w conditions at the wake and D conditions at the rotor.

The idealised flow assumption incorporates steady-state conditions at the boundaries of the control volume along with uniform thrust across the rotor. Rotational aspects of the flow present in the wake are not modelled. The ambient pressure is assumed to be equal to the local pressure at the inlet and

outlets of the control volume. The methodology employed by Actuator Disk Theory concept is explored in Appendix C.

This theory has proven highly reliable for the modelling of simple flow situations but does not provide the depth of resolution required from numerical solutions, in particular in the evolution flow velocities in the wake and the subsequent recovery towards inlet conditions. In modern CFD programs it is often used to infer the upstream inflow velocities based on boundary conditions input by the user [72].

2.3.2 Blade Element Momentum Theory

In the Betz models described in Section 2.3.1 angular momentum is not taken into account. Blade Element Momentum (BEM) Theory allows for the introduction of the rotational effects of the rotating blades and their impact on downstream flow properties while introducing the conservation of momentum into the system, Figure 2.7 [73].

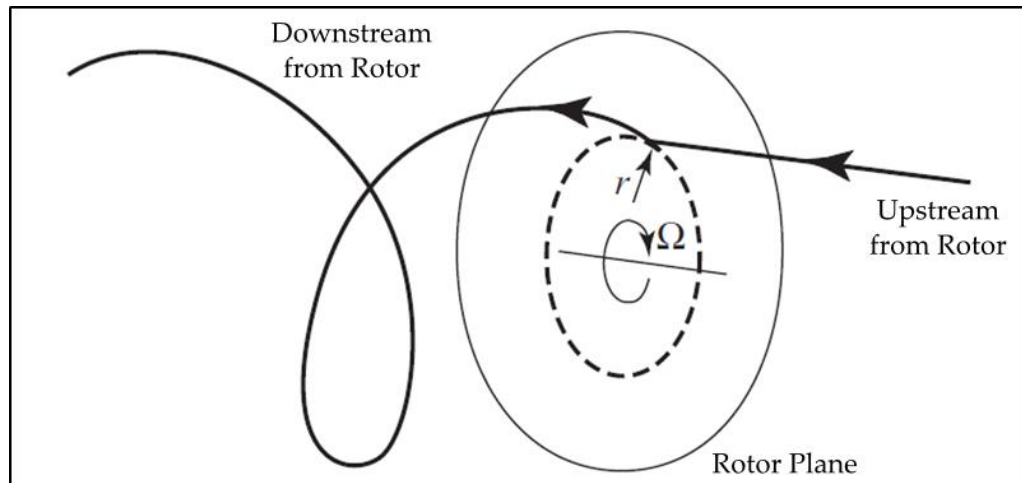


Figure 2.6: The trajectory of an air particle passing through the rotor disk [73]

In Figure 2.7 the flow is moving through the rotor plane from right to left, r represents the radius from the rotor centre and Ω the rotational speed of the blades. Breaking the rotor plane into small discs the BEM model attempts to account for the lift and drag forces of the rotating blades as they pass through the air flow [74]. Additionally employing the Bernoulli [75] equations for the conservation of momentum and treating each annular ring as an isolated system the model allows for the calculation of wake properties developing behind the rotor plane.

The BEM methodology improves upon standard actuator disk theory but it also has a number of drawbacks that limit its accuracy. Expansion in the wake is not taken account of and system losses introduced through turbulent flow interaction and wake losses are not modelled.

2.3.3 Industry modelling packages

In the preliminary design and planning stages for wind farms a number of packages are currently used by industry. Packages such as WindFarm [76], WindPro [77], OpenWind [78] and WAsP [79] are all used by developers to plan and optimise farm layouts based on terrain and local roughness as well as local wind measurements and characteristics. The outputs evaluate wind speed profiles through the analysis domain and the corresponding potential power and loads that can be expected during operation. Incorporating meteorological measurements and predictions for a prospective site they allow developers to assess potential energy yield. These packages make use of a number of accepted flow models, of which PARK and Eddy-Viscosity models are two of the most commonly used.

PARK models

Developed by Jensen [80] and Katic et al [81] in the 1980s this model employs a simple numerical modification to the freestream inlet to account for the initial velocity deficit and subsequent recovery downstream of the rotor. The velocities in the turbine wake are assumed to be uniform across its extents and symmetrical around the wake centre line at any given point downstream of the rotor. Outside the wake bounds the wind speed returns to the freestream value, U_i , as seen in Figure 2.8.

An initial velocity deficit, based on the turbine specific thrust coefficient value (C_T), is applied at the rotor disk. The wake speed value, U_w , then recovers towards freestream related to the distance from the rotor (x) and the wake-decay constant (k), this is demonstrated in Figure 2.8. The horizontal arrows represent the size of the local wind vector.

The wake width expansion predicted by the model is calculated using the same variables and is found to expand linearly with distance from the rotor plane. Equations 2.3 - 2.5 show the formulae for PARK wake speed evolution calculation.

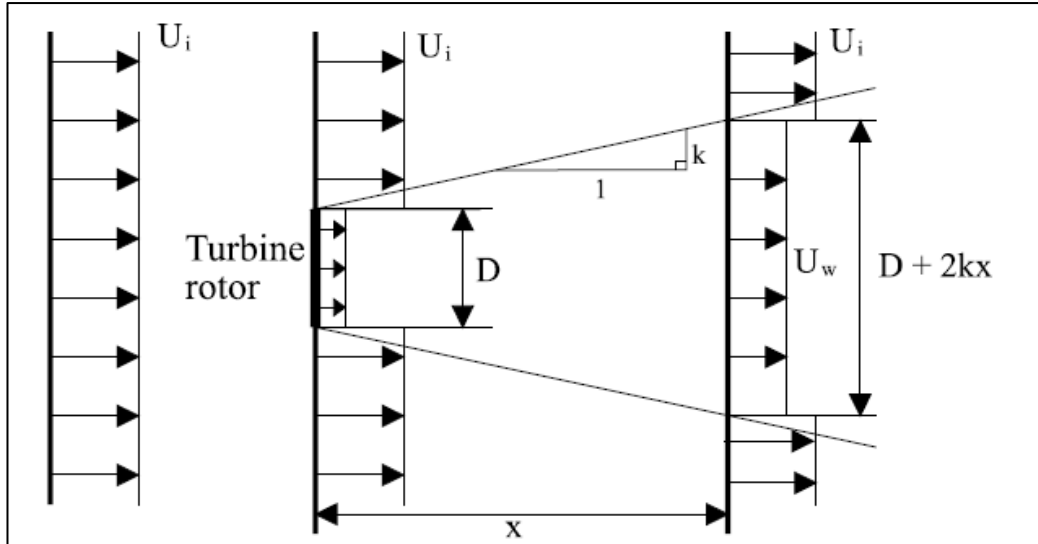


Figure 2.8: PARK Model Wake Velocity Development [82]

Velocity in the wake at a given downstream distance x:

$$U_w = U_i \left[1 - (1 - \sqrt{1 - C_t}) \left(\frac{D}{D + 2kx} \right)^2 \right] \quad \text{Equation 2.2 [82] [83]}$$

Wake width at a given downstream distance x:

$$W_w = D + 2kx \quad \text{Equation 2.3 [82] [83]}$$

Where the wake decay constant, k, is:

$$k = \frac{A}{\ln\left(\frac{h}{z_0}\right)} \quad \text{Equation 2.4 0 0}$$

Where z_0 is the surface roughness, h is the turbine hub height, D is rotor diameter, W_w is Wake Width, U_w is velocity in the wake and U_i is inlet velocity.

The profiles presented in Figure 2.9 detail the changes in the PARK model wake velocity behaviour with changes in local surface roughness. The models consider the wake behaviour of a multi mega-watt wind turbine for a range of surface roughness values. The parameters employed include a constant inlet wind speed of 15m/s, thrust coefficient of 0.74 and variable surface roughness values of between 0.0001 and 0.005 which lead to wake decay constants of 0.0365 to 0.0509. The resultant profile shows an initial velocity deficit at the rotor plane, followed by an arc profile that trends towards full recovery at freestream velocity.

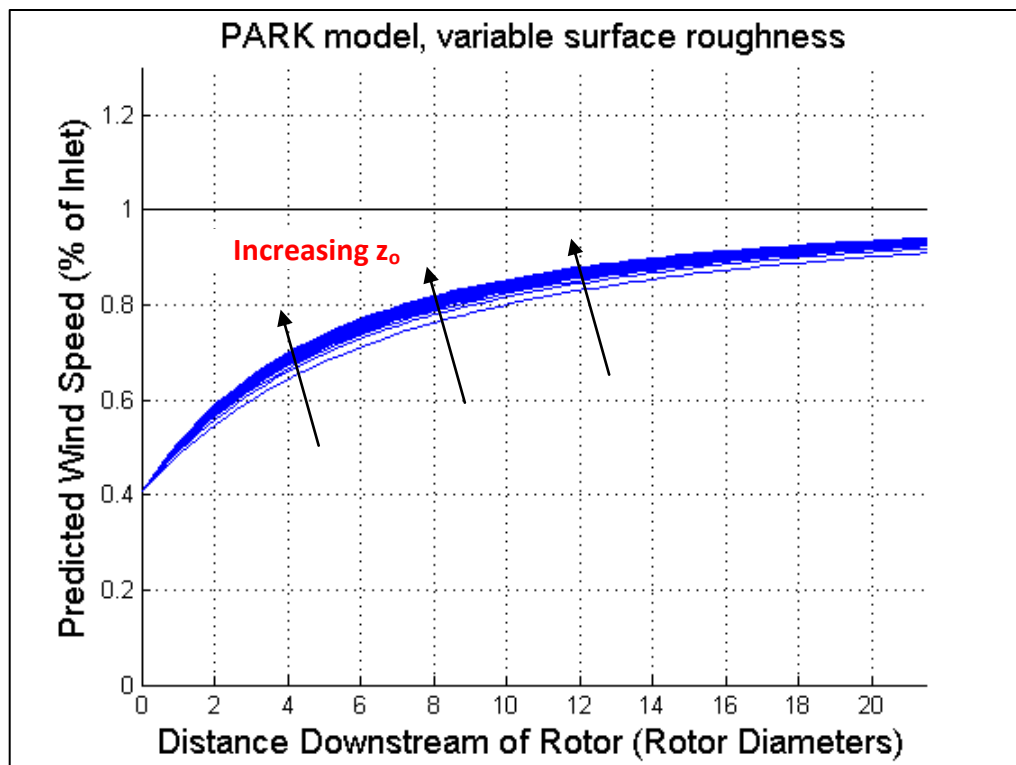


Figure 2.9: PARK predicted variation of wake velocity deficit with distance from rotor plane, z_0 variable (0.0001 – 0.005), wake decay constant, k (0.0365 – 0.0509)

The profiles in Figure 2.9 show that an increasing value of surface roughness (z_0) in the PARK prediction leads to an arc profile with a decreasing radius while having no effect on the initial deficit value at the rotor plane. This change in behaviour indicates that the wind speeds in the wake will recover marginally quicker with increases in local surface roughness levels.

For comparison the profiles presented in Figure 2.10 show the PARK model wake profiles for a range of inlet wind speeds, U_i . The range of U_i incorporated in the analysis is from 5 - 10m/s, at 0.5m/s intervals, and corresponding thrust coefficient range from 0.76 - 0.83.

The results presented show that the inlet wind speed value, and corresponding thrust coefficient, has a direct impact on the deficit from inlet experienced at the model initiation at the rotor plane. Increasing values of inlet wind speed lead to lower initial deficits and the development of flatter wake speed profiles.

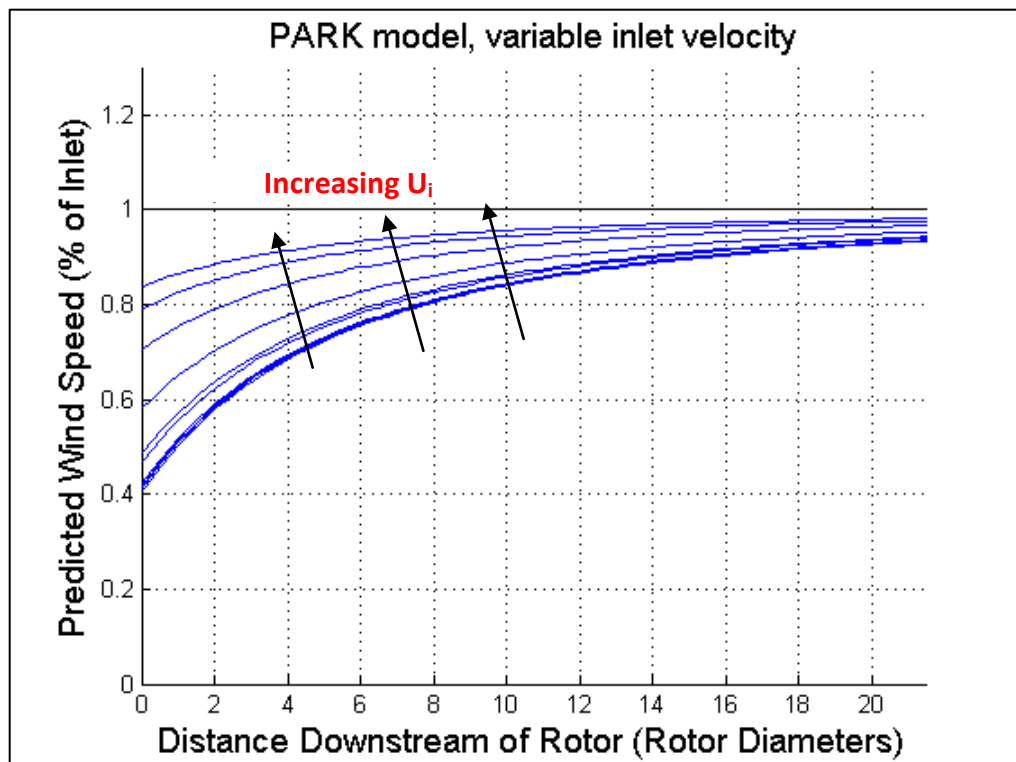


Figure 2.10: PARK predicted variation of wake velocity deficit with distance from rotor plane, U_i variable (5 – 10m/s)

Eddy-Viscosity models

The Ainslie developed Eddy-Viscosity Model [84] offers a CFD approach to solving the Navier-Stokes equations. The formulation sets initial conditions for the wake at two rotor diameters downstream of the rotor plane, Equation 2.6, and the modelling approach predicts wake velocity development downstream. The evolution of flow is given by:

$$U \frac{\delta U}{\delta x} + V \frac{\delta U}{\delta r} = \frac{\varepsilon}{r} \delta \left(r \frac{\delta U}{\delta r} \right) \quad \text{Equation 2.6 [83]}$$

Where U is the velocity in the downstream direction, V is the velocity in the radial direction, x is the downstream distance from the rotor plane, r is the radial distance from the centreline of the wake and ε is the Eddy Viscosity and each downstream (x) location. The system of equations can be solved using a numerical solver such as the Crank-Nicholson Method [63].

The initial wake centre line deficit (at two rotor diameters downstream) is prescribed in Equation 2.7, with the full wake behaviour developing after this point. The width of the wake at any point can be defined as a function of the calculated centre line deficit and the thrust coefficient, Equation 2.8. The initial wake width profile is Gaussian in form with the peak occurring at the wake centreline; the velocity at a given distance, r , from the wake centre line can be calculated from Equation 2.9.

In Equations 2.7 – 2.9; D_{mi} is the initial velocity deficit at two rotor diameters downstream, U_i the velocity in the freestream on the upstream side of the rotor, $U_{c,i}$ the initial velocity at two rotors diameters downstream, C_t the thrust coefficient, I_{AMB} the ambient turbulence the turbine is operating in, b_j the wake width at a given point j downstream from the rotor, $D_{m,j}$ the

velocity deficit on the centreline at the given location j downstream and $D_{r,j}$ the velocity at a radial point r from the centreline.

Initial Velocity Deficit (at two Rotor Diameters):

$$D_{m,i} = 1 - \frac{U_o}{U_{c,i}} = C_t - 0.05 - \left[\frac{(16C_t - 0.5)I_{Amb}}{1000} \right]$$

Equation 2.7 [84]

Wake Width at point j downstream:

$$b_j = \sqrt{\frac{3.56C_t}{8D_{m,j}(1 - 0.5D_{m,j})}}$$

Equation 2.8 [84]

Gaussian Wake Width Profile at point j downstream:

$$D_{r,j} = U_{c,j} \left(1 - D_{m,j} e^{-3.56 \frac{r^2}{b_j^2}} \right)$$

Equation 2.9 [84]

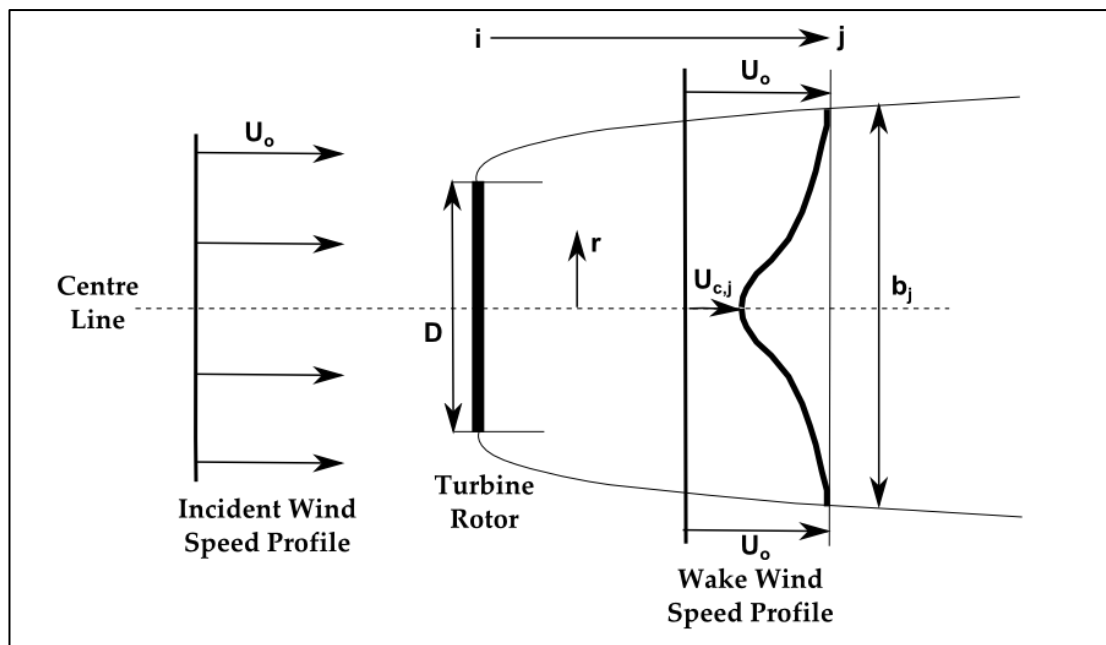


Figure 2.11: Eddy-Viscosity Wake Speed Development [82]

The Ainslie predictions show a Gaussian wake width profile recovering with radial distance from the maximum deficit at the centreline to the freestream velocity at the predicted bounds of the wake, Figure 2.11 details this behaviour. The maximum extent of this deficit is at its peak at the model inception at two rotor diameters downstream, before recovering towards the freestream.

Simplified Eddy-Viscosity Model

While the original Ainslie models are used in the software mentioned above a Renewable Energy Systems [85] developed 'Simple Solution to the Eddy-Viscosity Model' [86] offers highly accurate results when considering wake velocity development behind the same initial conditions described by Ainslie above. Given that for wake profiling the centreline velocity is solved for first, the paper observes that the Ainslie wake model can be re-written as:

$$\frac{dU_{c,j}}{dx} = \frac{16\varepsilon(U_{c,j}^3 - U_{c,j}^2 - U_{c,j} + 1)}{U_{c,j}C_T} \quad \text{Equation 2.6 [86]}$$

Where the variables are defined as below 0:

$$U_{c,j} = U_0(1 - D_{m,j})$$

$$\varepsilon = F(K_1 b(U_0 - U_c) + K_m)$$

In which 0:

$$K_1 = 0.015$$

$$K_m = \kappa^2 \frac{I_{AMB}}{100}$$

$$\text{If } x < 5.5, \quad F = 0.65 + \left(\frac{x - 4.5}{23.32}\right)^{\frac{1}{3}}$$

$$\text{If } x \geq 5.5, \quad F = 1.0$$

κ is the Von Karmen constant, 0.41.

A Runge-Kutta [87] [88] numerical solver can be applied to Equation 2. in order to calculate the evolution of the velocity deficit along the wake length. The Wake Width and Gaussian Width profile can then be described for each point using Equation 2.7 and Equation 2.8 respectively. The behaviour identified in Figure 2.12 shows the velocity recovery as predicted in the Simplified Model for range of turbulence intensity (T.I.) values with inlet velocity kept constant. Increasing values of ambient turbulence intensity are seen to induce greater mixing between freestream and wake flow and cause a faster recovery towards freestream velocity values.

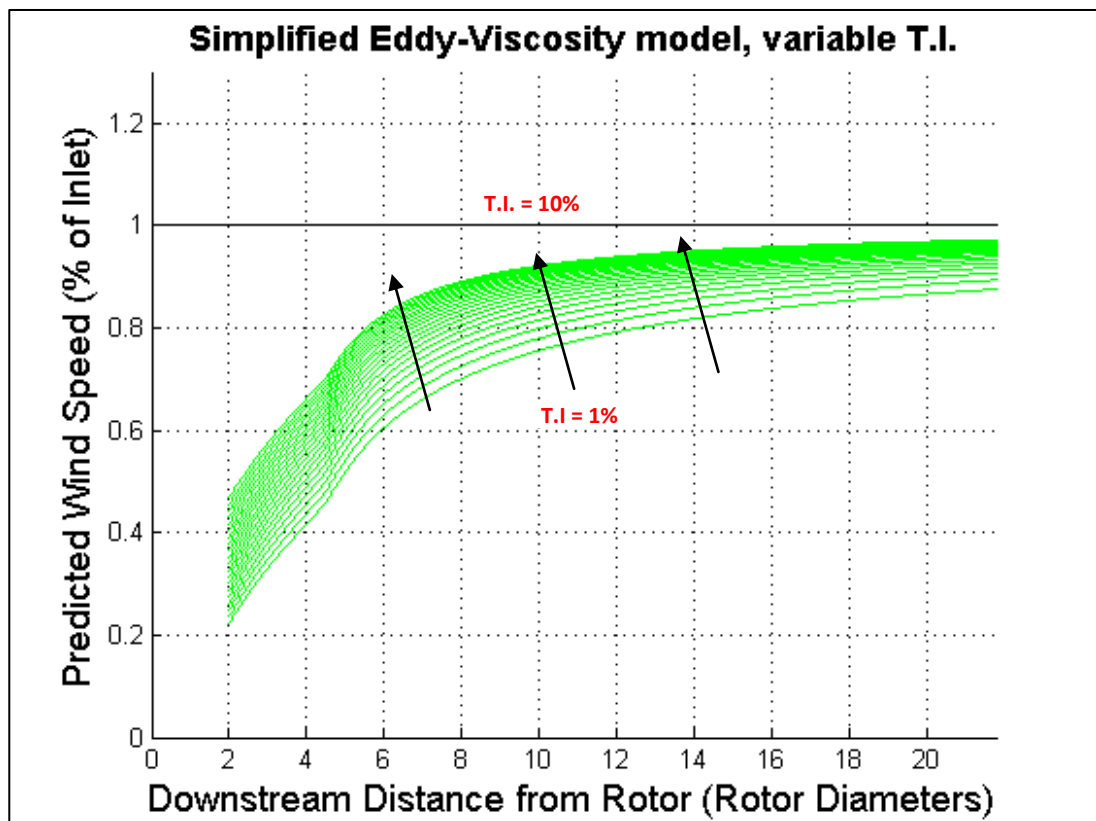


Figure 2.12: Simplified Eddy-Viscosity predicted variation of wake velocity deficit with distance from rotor plane, T.I. variable (1 - 10%)

The behaviour presented in Figure 2.13 presents the velocity profiles predicted by the Simplified Eddy-Viscosity model for variations in inlet wind speed, U_i (5- 15m/s), while the T.I. is held constant. As the inlet wind speed increases up to 10m/s there is little effect on the profile described. Above 10m/s the deficit from inlet values at the boundary of the model is less significant. This behaviour results in shallower initial recovery rates and a flatter profile towards freestream conditions than at lower wind speeds.

In this model the defined inlet wind speed is not directly used in the calculation of the wake profile. Instead the turbine specific thrust curve in combination with the inlet wind speed is used to calculate a thrust coefficient value that is used in the calculations. The inlet velocity term in the equations is kept at unity throughout.

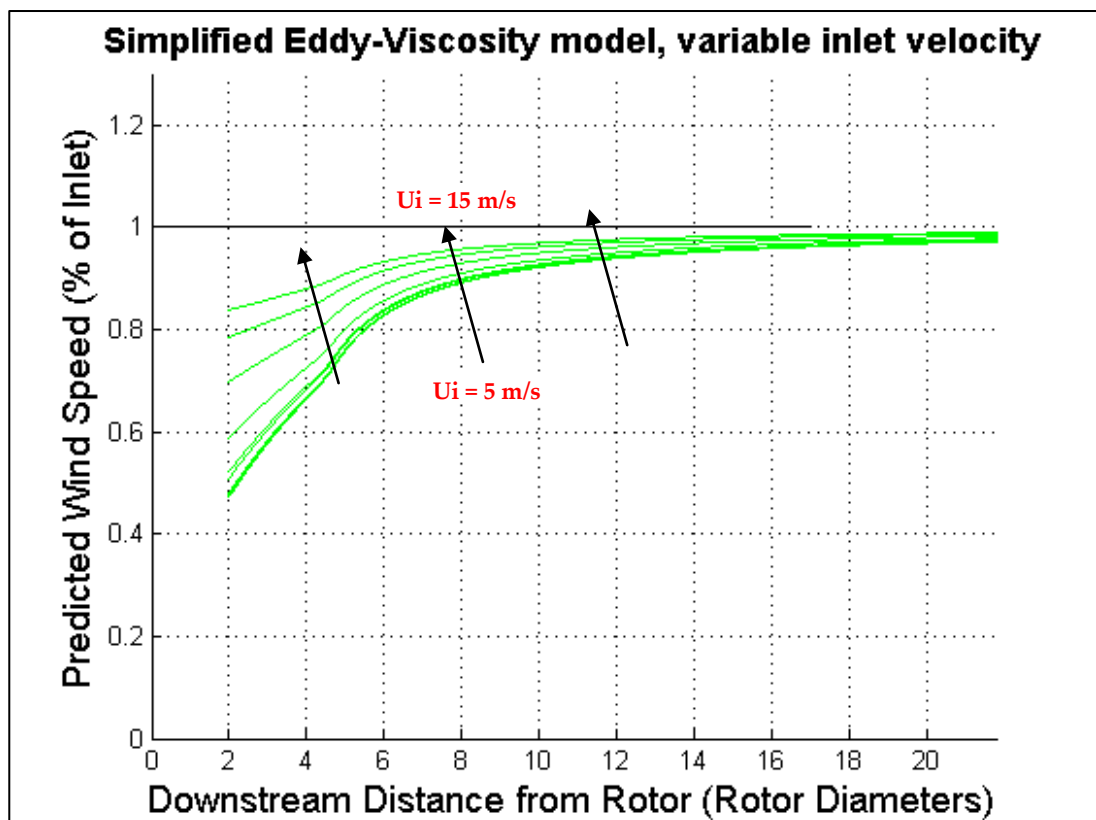


Figure 2.13: Simplified Eddy-Viscosity predicted variation of wake velocity deficit with distance from rotor plane, U_i variable (5 – 15m/s)

2.3.4 Turbulence modelling with Reynolds Averaged Navier-Stokes (RANS) equations

Computational modelling methods first established in fluid flow analysis have been applied to a variety of wind farm specific packages using solutions to the RANS equations, some of the modelling packages available are listed in Table 2.9 [72] [89].

Model	Primary Method	Turbulence Closure Method
Riso (1) (RISOE) [90]	- Actuator disk method interfaced to aero elastic code - Iterative method	
Riso (2) [90]	- Semi-Analytical engineering model	
MIUU, Uppsala University (MIUU) [91]	- Based on Taylor hypothesis using the transport time for the wake development	
GH Windfarmer (GH) [92]	- Axis-symmetric NS solver - initiates at 2D downstream - Gaussian initial profile varies according to C_t and ambient turbulence intensity	- Eddy Viscosity using turbulence in wake
Robert Gordon University (RGU) [93]	- Fully elliptical turbulent 3D solver - Requires upstream boundary layer profiles for velocity and turbulence	- $k-\epsilon$ turbulence closure
University of Oldenberg (UO) [94]	- Ainslie wake model - 2D axis-symmetric solving NS momentum and continuity equations	- Eddy Viscosity
Netherlands Energy Research Foundation [95]	- Near wake model uses standard moment theory, adding empirical conditions later	- $k-\epsilon$ turbulence closure
ANSYS Windmodeller [96]	- Wakes modelled with uniformly loaded actuator disk theory, uses C_t and freestream wind velocity - Upstream flow inferred using actuator disk theory from hub speeds - Rotor disk resolved via mesh adaption during solving	Can be chosen from - $k-\epsilon$ standard model - $k-\epsilon$ RNG - $k-\omega$ SST

Table 2.9: Available CFD packages methods [72], [89]

In order to converge CFD numerical solvers, RANS introduce apparent (or Reynolds) stresses into the Navier Stokes equations. Adding a 'second order tensor of unknowns' [97] RANS equations can be solved using a Boussinesq Hypothesis [98] or Reynolds Stress Models (RSM) [99].

The Boussinesq approach is more widely used in modelling as RSM is more computationally costly as it introduces new transport equations related to the stresses that increase the complexity further [97]. The Boussinesq hypothesis instead is based on the introduction of Eddy Viscosity terms to model the momentum transfer caused by turbulence within the flow field.

Incorporating these decompositions into the Boussinesq approximation for instantaneous flow gives the modified NS equations of motion [100]:

Continuity:

$$\frac{\partial U_i}{\partial x_i} = 0 \quad \text{For Mean Flow}$$

Equation 2.7 [100]

$$\frac{\partial u_i}{\partial x_i} = 0 \quad \text{For Turbulent Fluctuations}$$

Momentum:

$$\frac{DU_i}{Dt} = \frac{1}{\rho_0} \frac{\partial \bar{\tau}_{ij}}{\partial x_j} - g[1 - \alpha(\bar{T} - T_0)]\delta_{i3}$$

Equation 2.8 [100]

Where the stress term is defined as:

$$\bar{\tau}_{ij} = -P\delta_{ij} + \mu \left(\frac{\partial U_i}{\partial x_j} + \frac{\partial U_j}{\partial x_i} \right) - \rho_0 \overline{u_i u_j}$$

Equation 2.9 [100]

In which the $-\rho_0 \overline{u_i u_j}$ term is the Reynold's Stress Tensor acting in mean flow.

Heat:

$$\frac{D\bar{T}}{Dt} = \frac{\partial}{\partial x_j} \left(\kappa \frac{\partial \bar{T}}{\partial x_j} - \overline{u_j T'} \right) \quad \text{Equation 2.11 [100]}$$

Algebraic equations are introduced to model the stresses; this includes modelling unknowns in the flow such as turbulent viscosity, kinetic energy and dissipation. These are included depending on resolution required and the computational resource available. The most common type of algebraic models are the Linear Eddy Viscosity two equation models, these solve to find the turbulent kinetic energy (k) as the first variable. The second variable depends on the model but is commonly described as the variable that defines the length, or time-scale, of the turbulence [97] [100]. Some two equation models are briefly considered in the following section.

RANS additional two-equation models

Two equation models are commonly applied in a range of academic and industrial sectors. The two extra transport equations represent the turbulence more completely and allow historical effects to be taken into account [97].

k- ϵ Standard Model: In this closure model the two equations represent turbulent kinetic energy (k) and the turbulent dissipation (ϵ) of the flow, where ϵ is the turbulent and stochastic variations moving the flow [97]. The model developed provides good accuracy in relatively small pressure gradients, particularly in cases of free shear boundary layer flows and internal flows [97]. A single turbulent length scale is used to determine eddy viscosity and thus turbulent diffusion properties.

k- ϵ RNG Model: The Re-Normalisation Group (RNG) is a modification of the standard k- ϵ model developed by Yakhot et al [101] to account for

smaller scales of motion. In the standard model turbulent properties can only be developed at a single length scale. As turbulence occurs at all scales the RNG model was developed to account for this. The approach results in a modified version of the ε equations. The smaller scales are essentially removed from the calculation while their effects are accounted for and incorporated into the rest of the calculations. The result is sub-grid scale models for large eddy simulations which can be processed more accurately [101] [102].

k- ω SST Model: The standard k- ω model has been shown to produce favourable results in modelling right down to wall conditions in the boundary layer but has difficulties in freestream flow. By combining the k- ω approach with the k- ε methodology for modelling freestream flow, the Shear Stress Transport (SST) model produces good results in modelling adverse pressure gradient and separating flow situations. The SST modelling configuration addresses this and improves overall accuracy when compared to a single approach. There is still a tendency in SST formulation to over predict turbulence levels, however it provides better performance in applications with significant flow separation than the standard k- ε approach produces [97] [103].

The turbulence models considered above have been developed for internal flow simulations i.e. flow inside pipes, channels or housings. While producing good results under these flow conditions the adaptation of these methodologies for the complex flow situations experienced in wind farms is at an early stage [72]. The adaption of these methodologies into wind specific packages must account for a change in scale of all of the flow features modelled. The atmospheric boundary layer, in which wind turbines operate, is assumed to have a similar profile to boundary layers in internal driven

flow with a flow velocity of zero at ground level. However, its behaviour is driven by a series of complex relationships with the surface and its local roughness features, temperature, solar radiation and higher altitude winds. Modelling these local, externally driven and constantly varying features accurately is a unique challenge. Atmospheric stability can also be included in the setup of these models incorporating atmospheric features (i.e. stable and instable boundary layers) to accurately model the flow development in the vertical domain.

Large Eddy Simulation (LES)

LES models focus on the larger flow features and interactions, allowing for improvements in computational time when compared to the Direct Numerical Simulation of the NS equations. The smallest flow scales are removed via low-pass filtering and the larger more important turbulence scales can then be solved separately and explicitly. A variety of sub-grid scale models can be used to account for the removed small eddy effects. Based on Kolmogorov's [104] theory of large eddy flow being predominantly dependent on geometry and containing the majority of flow energy, LES has been used widely across CFD applications but has been hampered by the computational cost required when compared to the RANS two-equation models detailed previously [97] [104].

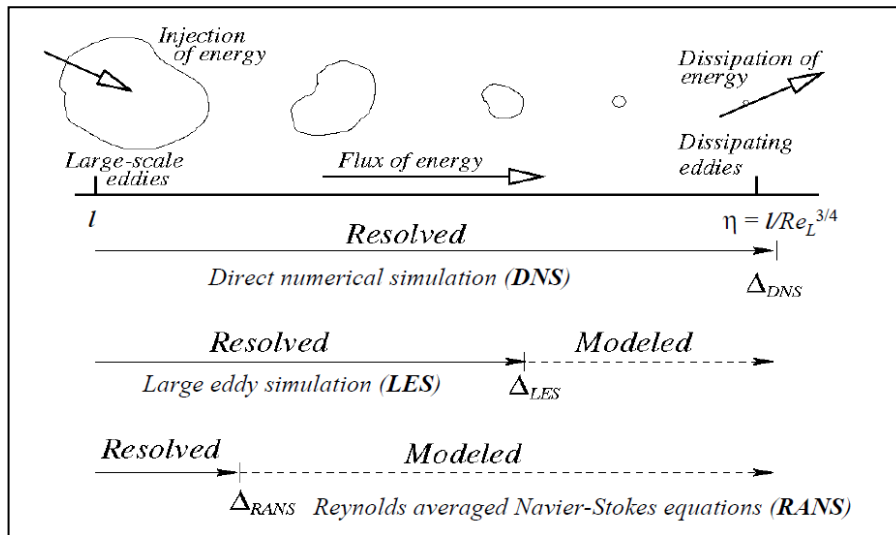


Figure 2.14: Turbulence prediction methods. [104]

The image in Figure 2.14 details a range of turbulence closure methods employed in numerical flow solutions and the length scales associated with these. The range of eddy length scales being solved for is shown moving from larger lengths at the left of the image to smaller at the right. The greater the variety of resolved flow scales the greater the computational cost incurred in running the simulation as each must be solved in turn. As can be seen the Large Eddy Simulation methodology solves for the larger length scales and utilises models to solve for the smaller length scales reducing the computational time needed for solving the Navier Stokes equations [105].

In the Figure 2.14 the eddy flow variables are defined as:

$$l = \text{length scale of largest eddies}$$

$$\eta = \text{length scale of smallest dissipating eddies} = \frac{l}{Re_L^{3/4}}$$

Where Re_L is the Reynolds number of the flow at large eddy scale, η can also be referred to as the Kolmogorov scale [104] [105] [106].

2.4 Measurement and model comparisons

In the following section a series of academic and industrial papers are presented summarising work completed in the comparison of numerical and remote sensing data sets. Detailing a variety of deployment and flow situations these provide context to the state of the art in numerical and experimental analysis applied to wind turbine flow behaviour. An outline of the modelling packages used in the studies can be found in Table 2.9.

2.4.1 Comparison research

Montavon, C., S.-Y. Hui, and e. al., *Offshore Wind Accelerator: Wake Modelling using CFD*, U.C. Trust, Editor. 2009. [72]

This Offshore Wind Accelerator program [107] study utilises commercial ANSYS CFD software applied to operational data from two wind farms, North Hoyle in Wales and Horns Rev in Denmark. North Hoyle is a 30 turbine wind farm in a 6 row and 5 column layout while Horns Rev consists of 80 turbines in an 8 row and 10 column format.

Comparing normalised measured power along each of the wind farm columns the ANSYS CFD normalised power predictions provide a good comparison to the operational data.

The analysis considers the power production behaviour of the wind farms with varying sized directional envelopes of valid data. These are based around a wind direction perpendicular to the columns of each wind farm. The comparisons from the North Hoyle wind farm for two separate valid directional envelope sizes (10° and 30° around 260°) can be seen in Figure 2.15.

For the Horns Rev analysis the valid envelopes are defined as 2° , 10° and 30° around flow originating from a 270° direction, Figure 2.16. In this Figure the Columns have been labelled as Groups. The data used in the Horns Rev analysis has been sourced as part of the UpWind project [108]. For both analyses the $k-\epsilon$ turbulence modelling methodology was applied in this study.

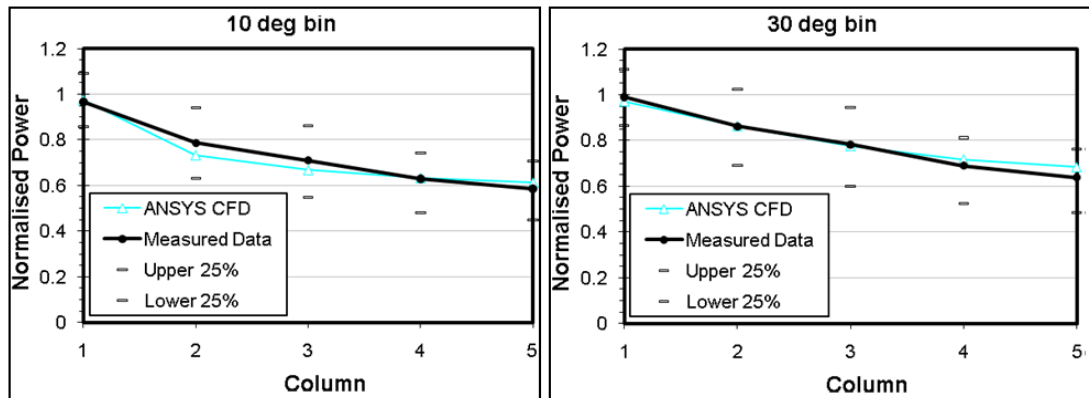


Figure 2.15: Normalised Power comparison (10 Diameter separation), North Hoyle [72]

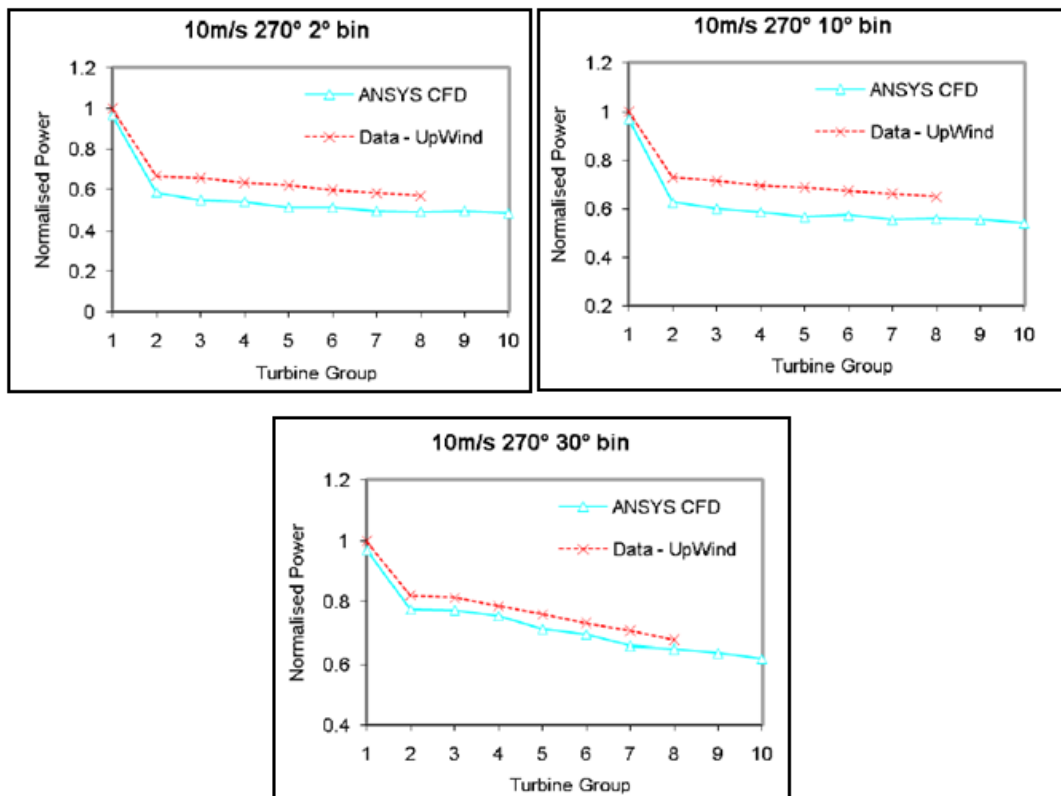


Figure 2.16: Normalised Power comparison (7 Diameter separation), Horns Rev [72]

Comparing the measured data sets with the numerical analysis the results show similar behavioural profiles in both cases. The normalised power is seen to reduce between wind turbine columns. This is to be expected as each column turbines operates in the preceding column's wake and as a result the inflow to each turbine is subject to wake induced vorticity and turbulence, this reduces the energy available at the inlet to the next stage. The numerical results tend to under predict the available power at each row of the comparisons with the exception of columns 4 and 5 in the Horns Rev comparison where there is a small over prediction of normalised power. Comparing the studies this discrepancy is more pronounced in the North Hoyle simulation.

While a number of different local factors can explain this the primary reason is presumed to be the column separation [72]. The seven diameter separation at North Hoyle is modelled more accurately than the ten diameter separation of Horns Rev where beyond the second column a constant power deficit from the measurements is modelled. This deficit would translate into an underestimation of power output from the site.

The turbine models at both sites are identical with the main difference in the simulations being the spacing between the turbines and the incident upstream turbulence intensity employed; 7% at North Hoyle and 6% for Horns Rev. The resulting analysis indicates that the simulation setup incorporating 7% turbulence provides a more accurate prediction of wake development and recovery in the ten diameter spacing wind farm in comparison to the seven diameters situation.

Rados, K., et al., *Comparison of Wake Models with Data for Offshore Windfarms*, *Wind Engineering* 2001. 25 (No. 5): p. 271-280. [89]

Using single wake data from a Danish offshore wind farm, Vindeby, a number of numerical models are presented and considered against wake data from the active turbine. The details of these models can be seen in Table 2.9 and have been developed by a number of different companies and institutions across Europe. The measured data has been captured from two sea met masts that dependant on wind direction are at varying distance downstream of the turbines in the wind farm. The measurements present vertical wind speed profiles at increasing distance downstream of the active turbines. The images in Figure 2.17 show the velocity profile predictions against the mast measurements at a series of distances along the wake. The undisturbed flow velocity variation with height is also plotted; hub height is indicated by the horizontal line.

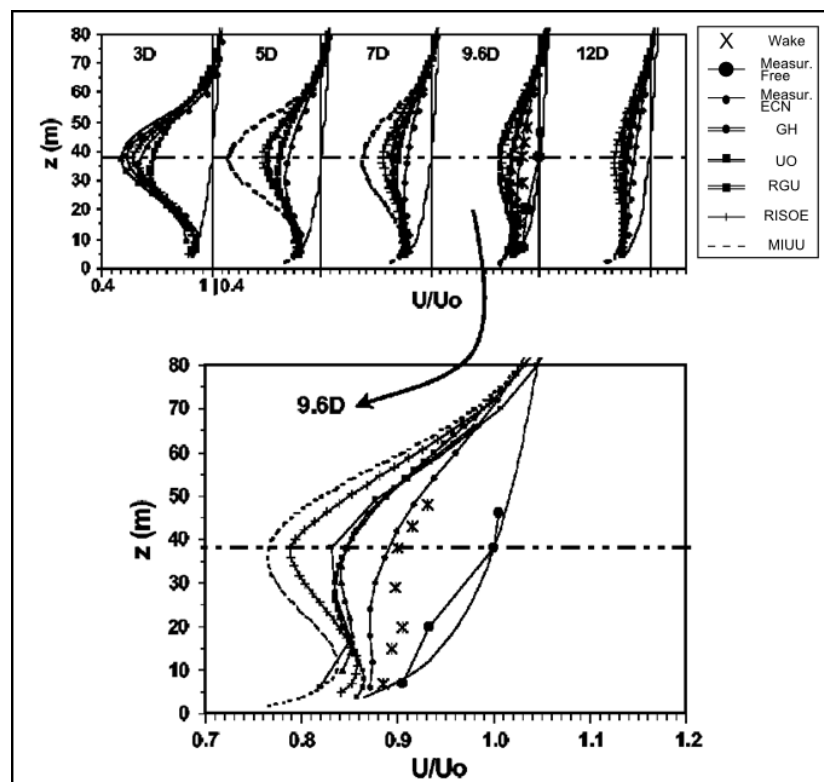


Figure 2.17: Downwind velocity profiles from measurements and CFD [89]

The presented data in the study does not allow clear identification of the individual solver approaches but does allow identification of the overall wake profile. In all simulations the greatest velocity deficit occurs at hub height with different degrees of accuracy attained across the solvers, this level of deficit decreases towards full freestream with distance from hub height, this is known as the 'wake recovery'. As expected the velocity profiles converge towards that of the freestream velocity at increasing distance downstream as seen at the top of Figure 2.17. Each solver models the overall profile well with differences in recovery profile and maximum deficit. Considering the 9.6D wake distance case Figure 2.17 presents a clearer picture of the different solver behaviours. The MIUU [91] solver consistently shows the largest deviation from the measured data with the 3D solver from Robert Gordon University [93] showing a more accurate velocity profile prediction.

I. Dinwoodie, F. Quail, and D.P. Clive, *Comparison of Measured and Modelled Wind Turbine Wakes in Non-Uniform terrain Using lidar and CFD, in DTC Wind Energy Systems, Project One. 2010. [109]*

The work presented models the single wake of an onshore wind turbine at Whitelee Wind Farm, Scotland. Measurements obtained from a ground based arc scan from a Galion Lidar are compared to a numerical analysis of the same turbine and domain using ANSYS Windmodeller. Three separate closure methodologies are considered. Applying actuator disk theory the study considers standard $k-\varepsilon$, $k-\varepsilon$ RNG and the $k-\omega$ SST models as outlined in Section 2.2.4.

The image at the top left of Figure 2.16 shows the captured lidar data with a clearly identifiable wake present at the right hand side of the image. In addition a less distinct area of low wind speeds can be seen at the centre of the image, this corresponds to the wake of another turbine but one in which the angled scan plane dissects the wake at a lower level than is optimum for capturing the wake fully. The hub height simulation planes of the three models can be seen in the rest of the images in Figure 2.18.

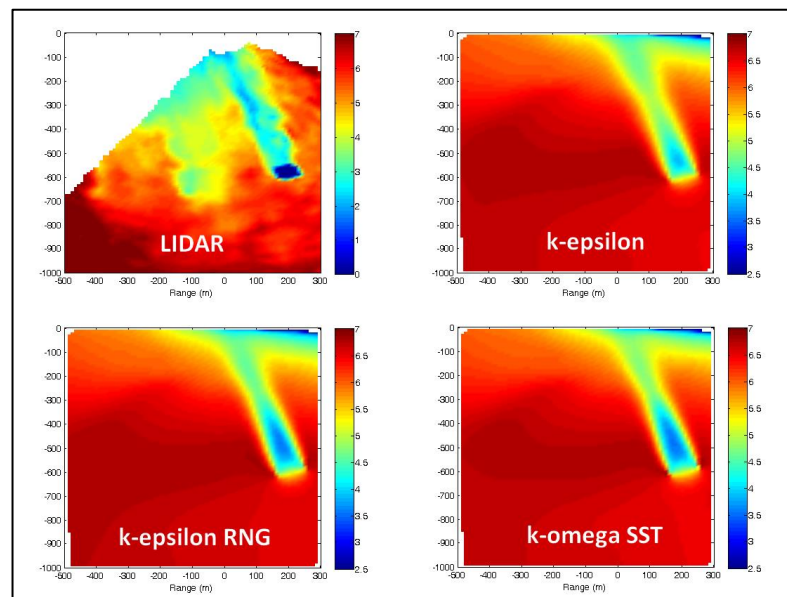


Figure 2.18: Comparison of lidar measurements in an operating wind farm to ANSYS Windmodeller simulations of the same setup [109]

To facilitate a comparison the lidar data has been corrected to hub height by applying a log law for boundary layer evolution [110] to the measurements on the inclined scan plane. The comparison has been completed by extracting data points corresponding to the centreline of the wind turbine wake in the lidar measurements and each of the simulations. The results of a comparison between this corrected lidar data and the three solving methodologies applied details flow evolution both upstream and downstream from the rotor, Figure 2.19.

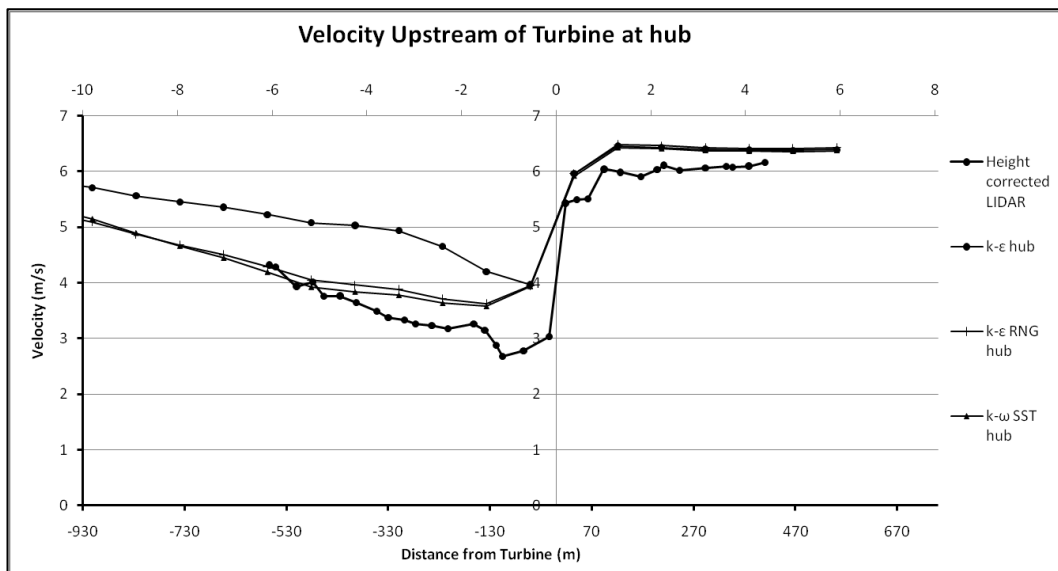


Figure 2.19: Hub height comparison of wind speed velocity [109]

The comparison of the three models to the lidar measured and height corrected profile produces satisfactory results in general behaviour. Each of the data sets can be seen to indicate a steady inlet wind speed profile into the rotor, followed by a drop in speed through the rotor and a subsequent recovery into the wake. The wake deficit imparted through the rotor plane is larger in the corrected measurements when compared to the models, this results in the lidar measurements exhibiting a longer recovery period into the wake. The behaviour of the wake recovery presented in Figure 2.19 shows that the recovery rate is broadly similar between the measured and simulated data, with similar gradients to the presented wake profiles.

The simpler $k-\epsilon$ model presents a far smaller velocity drop through the rotor plane leading to a faster recovery towards freestream when compared to the RNG and SST methods that utilise turbulence models. The recovery rate of all three models is similar.

The lidar data also shows some inconsistencies in measured behaviour profile possibly indicating issues with measurement methodology employed,

in particular the use of a single scan only in the comparison to the steady state profiles simulated in the models.

Creech, D.A.; *Myres Hill Study: A Comparison Between the Heriot-Watt Wind Farm Model and lidar Data*, School of Engineering and Physical Sciences, Heriot-Watt University: Edinburgh; 2009. [111]

A single wake study by Dr Angus Creech at Heriot Watt University compared the Galion Lidar and an in house development of the Fluidity CFD program. Fluidity is an open source multi-phase computational code allowing numerical solutions to the Navier-Stokes equations [112]. The wind turbine considered in the study was a stall regulated 950kW NEG Micon [113] installed at Myers Hill test facility.

The comparison is complicated by a 67° offset in orientation of the wind direction employed in the simulations and that of the measurement campaign leading to uncertainties in the results. This variation results from uncertainties in the location of the lidar and of the flow evolution from the boundary within the measurement domain. Figure 2.20 details a comparison between the wind speeds generated in the wake structure and those measured for increasing distances downstream from the rotor plane. The measurements are seen to end at approximately 145m downstream at which point there is an approximate 1.3m/s deficit to the simulated wake speeds at the same location.

The overall shape of the prediction resembles that produced from the measurement with an initial deficit at the downstream side of the rotor moving to a maximum further downstream. After this both data sets identify

recovery back towards inlet values. The velocity values presented show that the model over predicts the wake deficit at all points downstream.

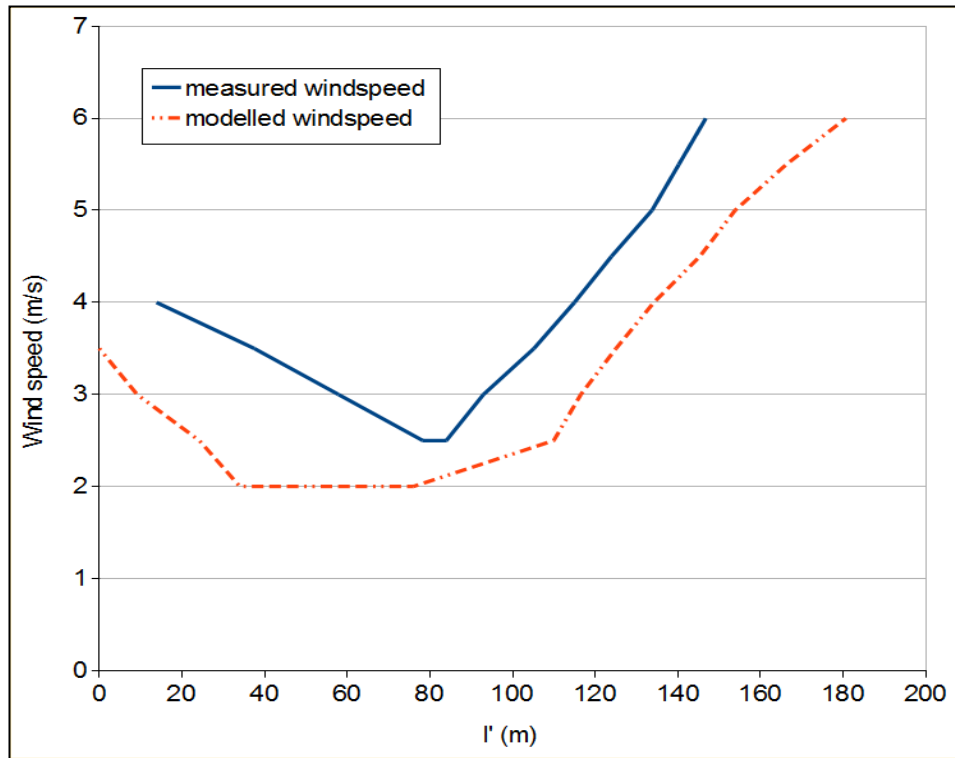


Figure 2.20: Measured vs Modelled wake wind speeds [111]

2.4.2 Comparison conclusions

The works presented in Section 2.3 show comparisons between measured and numerical modelling techniques for a variety of different situations and methodologies. Each comparison details wake profile behaviour in wind turbine wake flow for both measured and simulated situations. The overall profiles of the predicted velocity and power characteristics are shown to reproduce that of the measurements across the different comparative analyses with varying degrees of success. In the modelling of wake flow behaviour the main areas of discrepancy appear in the initial deficit predictions and that of the wake recovery profile. A current challenge is to obtain high resolution measurements of wake flow behaviour to allow accurate corroboration with the numerical models. The point measurements available with met mast data do not provide sufficient detail or flexibility for full wake analysis. In the study presented by I. Dinwoodie ⁰, incorporating measurements from a scanning lidar, the data resolution allowed a more comprehensive comparison with numerical wake development. However, some limitations can be identified in the correction of the lidar measurements to corresponding hub height values using a log law approach. This method of data transformation is not appropriate for complex flow such as experienced in a wind farm. It is also clear from data presented that the initial deficit is an important factor in the wake recovery time rate. None of the modelling approaches considered were found to capture this phenomena.

2.5 State of the art review conclusion

The use of remote sensing devices provides the opportunity to collect detailed data sets without the expense and physical intrusion of met masts. In addition, instead of a single point measurement provided when utilising met masts, devices such as lidar can provide two dimensional measurements of the flow field in the scan envelopes. The study presented by Dinwoodie et al [109] offers the most complete characterisation of wind turbine wake behaviour. In presenting a measured wind speed profile detailing velocities upstream of the rotor, through the rotor plane and the subsequent recovery towards freestream the study demonstrates the potential of a scanning lidar offers to characterise flow structure and evolution through the entire wind turbine stream tube.

Building on this work the deployment of scanning lidar devices within wind turbine arrays for an extended measurement period would allow for the capture of high resolution flow behaviour over a wide range of inflow wind speeds and conditions. Extended deployment and analysis for a variety of installation methodologies will allow the uncertainties and unknowns associated with the deployment of scanning lidars in the complex flow environment experienced in wind farms to be quantified. Resulting in an idea of the best practices involved in utilising this technology.

Focussing on wake research high resolution data sets would allow for the visualisation of wake centreline velocity profiles across the operational envelope of the wind turbine. Of particular interest will be the evolution of this profile under different inflow conditions, such as wind turbine operation in the freestream, under the influence of far upstream turbines or directly under the influence of neighbouring turbines. An understanding of such

flow features will allow wake effects in large turbine arrays to be better understood and incorporated in the design and operation of wind farms.

The comparative studies presented in this chapter clearly show that there is a great deal of uncertainty in the accuracy of flow models available to industry. While this remains the case these uncertainties will continue to limit their use in the development of wind assets. A comparison between high resolution wake data sets and wake flow models, such as explored above, will allow for a unique insight into these flow phenomena as well as providing a greater deal of confidence and understanding in their results.

Chapter 3:

Methodology

3.1 Background

To ensure the success of the project it is vital to develop robust methodologies ensuring the large data sets captured during the lidar deployments are processed consistently to ensure an accurate picture of the measured flow behaviour is presented. In the capture of wake data two different types of lidar deployment installation location have been utilised, ground based and nacelle mounted. As a result two separate data processing methodologies have been developed in order to extract the appropriate wake data from the large data sets captured through these deployments; these are both explored in Chapter 4.

Completing the comparisons with the different models requires the pre simulation setup of each of the different flow models being utilised in the comparisons with measured data. These fall into two categories that require separate methodologies to complete their simulations and extract relevant wake profiles for comparisons. The PARK [80] and Eddy-Viscosity [89] models can be run in tandem with the lidar data processing and profile extraction while the more complex Windmodeller [96] based models require a more involved setup of the simulation domain for each situation, the setup and execution of these models for each deployment are explored in Chapter 5.

The methods outlined in Chapters 4 and 5 identify the broad processes undertaken to extract the relevant lidar data sets and to run the numerical simulations based on the measured inlet values for these such that the full comparisons can be completed. A project flow chart to enable the successful completion of the project has been developed and presented in Figure 3.1 below.

3.2 Project flow chart

Outlined in Figure 3.1 is the envisioned flow chart for the project outlining the structure of the work undertaken over the course of the PhD. The project splits into two main focus areas, lidar data capture and analysis and wake flow modelling, with the two areas being brought together for comparison once complete. These exist side by side with important paths of feedback that inform the numerical models and subsequent lidar deployments ensuring the continued development of the project and consistent improvement in the quality of the data captured and the subsequent comparisons.

Focussing on the methodology outlined the red and blue dashed lines indicate areas of iteration where experiences, procedures and results dictate future projects. Working with SgurrEnergy Ltd [31] in deploying the Galion Lidar [30] devices allows the development of an understanding of the procedures involved and the capabilities of the device in relation to physical placement, scan geometry implementation and data resolution. The knowledge gained allows deployments to be organised more efficiently and effectively for the PhD project. The iterative process allows areas of further research to be identified and explored based on previous work, with the results and experiences allowing qualitative improvements to be made in the deployment and simulation processes.

The dark blue dashed line indicates the cross-over between measurement and simulation work, at this point the selected data sets will be used to inform the computational models and domain, ensuring a valid comparison between measured and simulated data sets.

The outlined methodology is that envisioned for the overall project, as work has continued in these areas the timings, structures and methods have by

necessity become more fluid in concept and execution. Through this it is important that the broad themes remain in place and the iterative nature of the sections outlined remains, ensuring the planned outcomes are achieved and the focus of the project remains true.

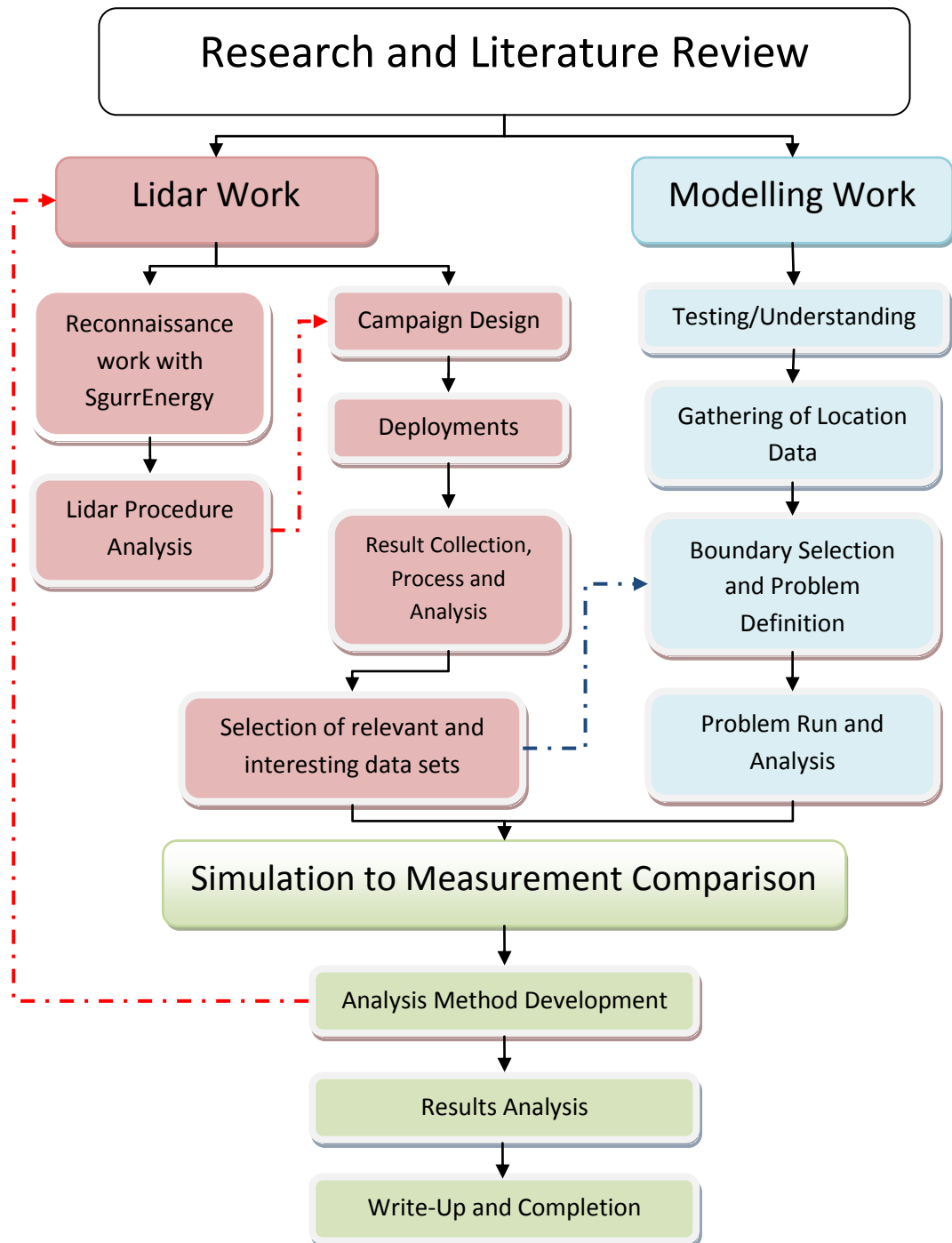


Figure 3.1: PhD methodology flow diagram

Chapter 4:

Lidar deployments

4.1 Lidar data capture and analysis

Capturing wake measurement data sets to support the project required the installation of devices for up to 12 months providing detailed flow measurements over these time periods. The methodologies employed to process the resultant raw lidar data sets are explored in Section 4.2.

Onshore deployments were carried out within the Myers Hill [114] test facility adjacent to the Whitelee wind farm [115] in Scotland. Deploying the device at ground level the lidar was programmed to scan continuously across the wind farm capturing wake behaviour throughout the deployment. The methodologies employed in providing and processing ground based lidar captured data in support of the project are explored in Section 4.3.

The capture of offshore wake data was completed at the Alpha Ventus wind farm [116] in the North Sea utilising two nacelle mounted Galion lidar devices [53]. Deployed for over six months the two lidars operated continuously with the resultant data sets being accessed weekly. The methodologies employed for wake data capture and processing are explored in Section 4.4.

4.2 Lidar data processing

Each scan of the lidar as programmed by the user creates an individual scan file detailing the measurements captured; the structure of these files as produced by the Galion devices utilised in this study are detailed in Appendix D. By employing scanning configurations holding either the azimuth or elevation of the scan constant two dimensional images detailing the measurements across the scan domain can be created.

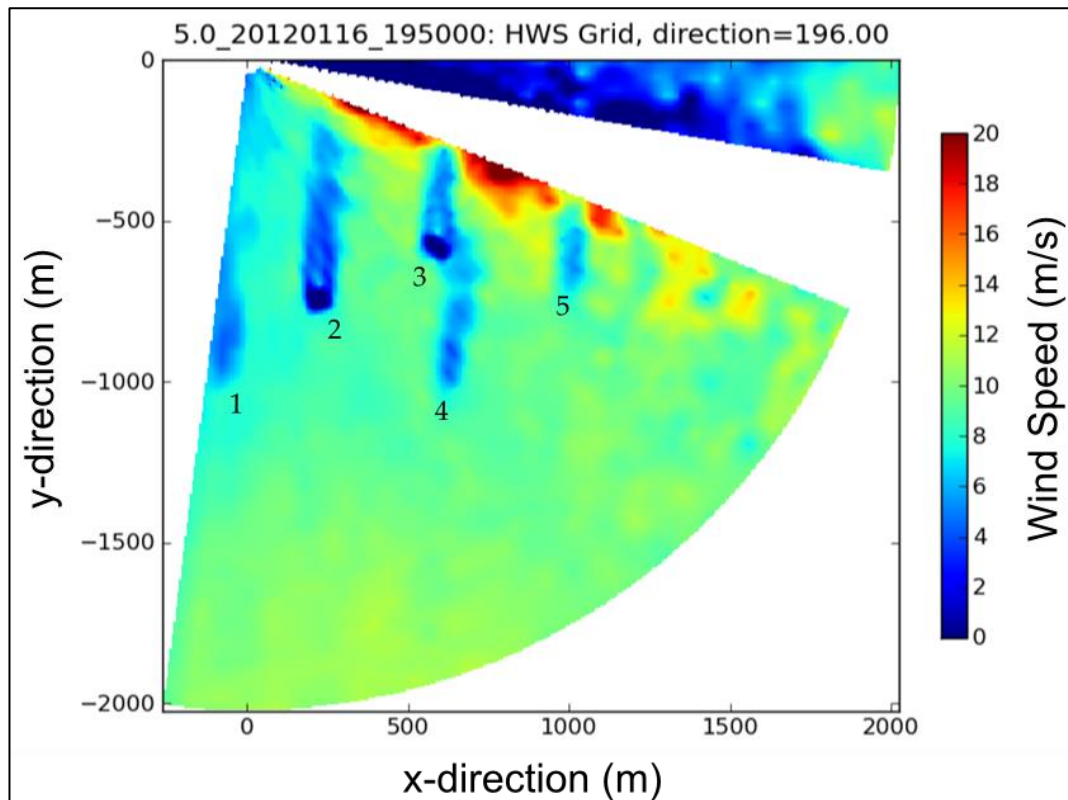


Figure 4.1: Sample ten-minute averaged lidar scan, January 2012 deployment

The image in Figure 4.1 shows a sample ten minute averaged two-dimensional lidar scan from a ground based Galion device lined up with the North. The x and y axis have a unit value in metres (m) and show the distance from the device of the scan points, the device being situated at 0, 0 at the top edge of the image in from the left edge. The colour axis of the image shows measured wind speeds in metres per second (m/s) horizontal to the

ground plane the lidar sits on. Numbered in the image are five wake structures evolving behind the scanned wind turbines. The wind direction measured by the lidar during the scan is displayed in the header as 196° measured from North.

The large blank white slice present across the image represents an area of low intensity in the back scattered component of the results, such that no usable wind speeds could be derived from the measurements in these areas. As is noticeable from the wind direction this pie slice shaped area is centred on a line perpendicular to the measured wind direction when measured from the lidar device. The scanning lidar is measuring the laser aligned line-of-sight component of the ambient wind vector and at this point the component is zero, either side of the line the component is still near enough zero to be indistinguishable. A total of 8° of azimuth are unusable in this image, an inherent problem of using this static configuration for scanning lidar studies. At the lower bounds of the empty data slice a number of regions of high wind speeds are noticeable. These do not correlate with any flow features in the scan envelope and must be treated as anomalies in the measurement translation in this region. As a result the uncertainties of the measurements here must be increased which leads to an increase in the area in which data cannot be used. This again demonstrates the difficulties in using a scanning lidar in this manner.

The processing software allows the user to average the individual scans over a ten minute or over an hourly period if desired. Choosing this option allows the user to visualise permanent flow structures not initially visible in the individual scans due the movement of the airflow between scan beams as the optics manoeuvre.

The project development and comparison with numerical models calls for steady state analysis across a wider flow field, due to this the ten minute averaging function will be the most heavily utilised in comparison with models.

4.3 Onshore lidar deployments

The mobility and flexibility associated with the scanning Galion Lidar device allows for deployments to be carried out in active onshore wind farms. In support of the project two separate deployments at Whitelee wind farm were completed. In both deployments the devices were installed on the ground within the Myers Hill wind turbine test facility adjacent to the wind farm. The deployment location and wind farm layout allowed the device to capture data sets relating to multiple wind turbines.

The image detailed above in Figure 4.1 shows a sample ten-minute averaged PPI arc scan from the ground based lidar devices. The nature of this type of deployment requires that the scan plane have a non-zero elevation resulting in an inclined scan plane capturing data across the boundary layer. When focussing on wakes this inclined scan plane will produce measurements at different heights in the wake.

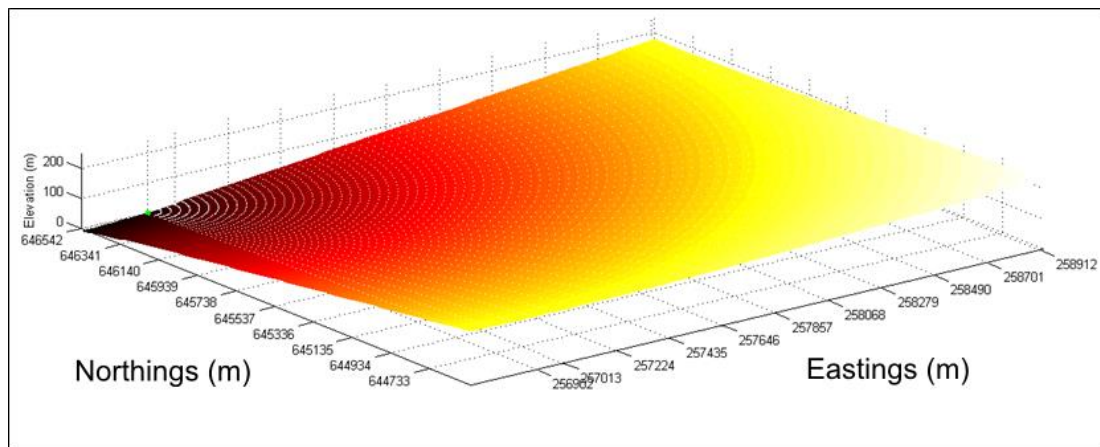


Figure 4.2: Three dimensional lidar scan surface January 2012 deployment

Figure 4.2 shows a sample inclined scan plane in three dimensions with the x and y axis corresponding to the Ordnance Survey [117] map projection locations of the scan range used in this instance. The scan plane identified is that used in the creation of Figure 4.3 below; with the Ordnance Survey

based axis values reflect geographical position of the scan plane. The z-axis identifies the physical height of the measurements above the lidar position. The colour variations applied to the figure allow a more distinct image of the scan plane height increases to be achieved, improving the visual understanding of the scan plane orientation. The white points on the scan plane relate to the individual scan points of the lidar scan arc, as can be seen these get higher and more spread out with distance from the device. The increase in scan height along the length of each beam means that each measurement is higher in the atmospheric boundary layer than the last. In order to fully understand the flow measurements and their development it will be important to gather an understanding of local shear conditions and how the local freestream velocity changes with height.

The point source emission of the measurement beam implies an increasing spread of the scan points with distance from the device. This leads to an increase in the area over which the measurements are combined to calculate local wind vectors as per the lidar methodology explored in Chapter 2. In complex flow this will lead to an increasing uncertainty in the lidar measured wind vectors as distance increases from the device.

The images created from ground based lidar deployments show the formation of wakes behind the devices within range of the device. Dependant on the flow orientation during the time averaged scan these can be seen extending in the corresponding manner behind the device. The stationary nature of this deployment and the passive control of the lidar mean that it is not possible to track the variations in flow orientation at this stage. As a result the extraction of wake behaviour and profiles must be done for each individual image and data set.

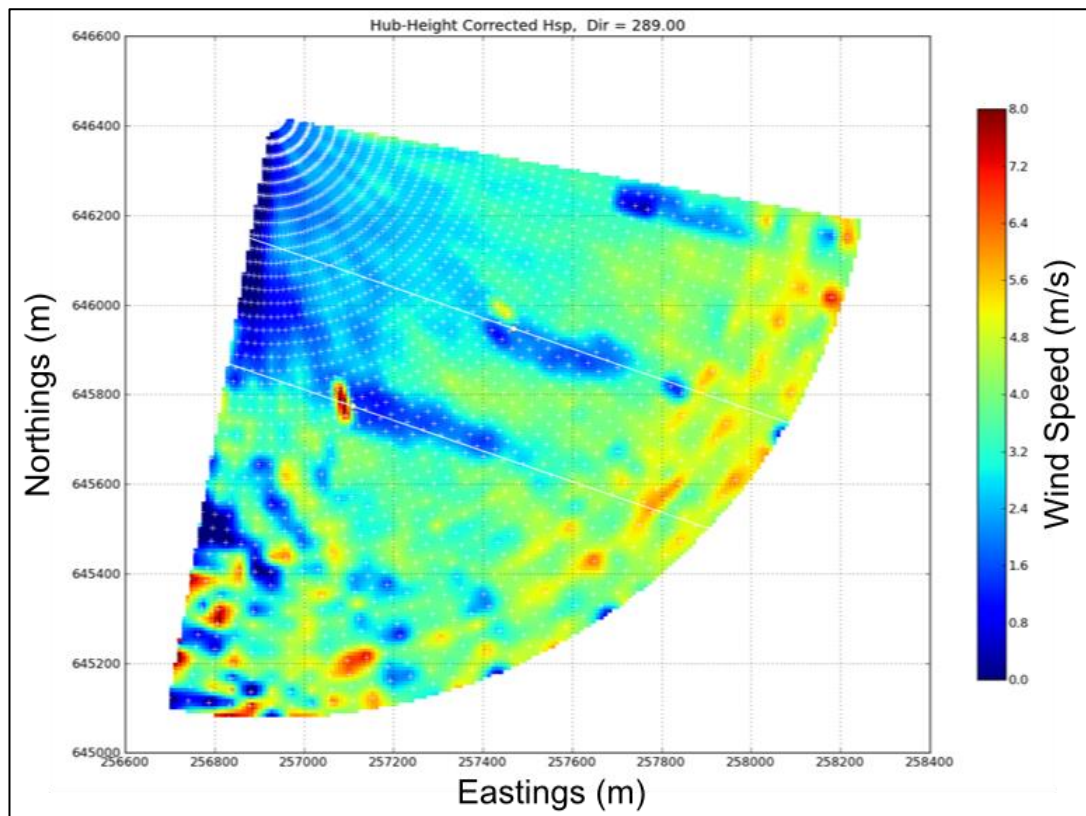


Figure 4.3: Lidar scan points overlaid onto original measured data

From the lidar scan presented in Figure 4.3 the user can extract data corresponding to the theoretical wake and inflow centreline. This is achieved by plotting the individual scan points (white crosses) onto the lidar captured images along with white lines corresponding to the measured wind direction through the rotor location. Selecting points along the line through the rotor the lidar measured centreline inflow and wake profiles can be plotted against distance from the studied turbine's rotor. A small margin of error from the line can be allowed given the inconsistent match up of measurement scan points to the wake's predicted orientation.

The profiles captured from this methodology detail the flow evolution through the rotor plane of the wind turbine into the wake. However the inclination of the scan plane will have a significant effect on the measured results dependant on the relationship between the scan envelope outlined

and the ambient wind direction during the scan being analysed. It is vital that these features are taken into account and understood clearly when performing comparisons and analysis on the data sets captured from these ground based lidar deployments. Sections 4.3.1 and 4.3.2 detail the two separate lidar deployments and the scan methodologies implemented further.

4.3.1 Myers Hill/Whitelee wind farm, July 2011

Deployment Dates:	July 13 th – 18 th 2011
Lidar Location:	N: 256925
(OS Co-ordinates)	E: 646424
	Elevation: 332m
Scan Arc:	100° – 244° Azimuth Range
	2° Beam Intervals
	6° Elevation
Beam Length:	2010m
	67 Range Gates
Individual Beam Time:	0.17 Hz
Total Arc Time:	246s
Number of Points per scan:	4964
Number of Scans:	1953

Table 4.1: Scan geometry for June 2011 Galion deployment at Myers Hill

A single Galion device was deployed at the Myers Hill wind turbine test site over a 5 day period. The campaign was planned to scan wakes in Whitelee wind farm to the South adjacent to the test site. The location of the lidar and the scan arc implemented relative to the turbines of Whitelee are presented in Figure 4.4. The full details of the deployment are indicated in Table 4.1. The initial strategy was to scan from a compass bearing of 100° - 244° with 2° intervals at an elevation of 6° and a range of 2010m. Each beam length consists of measurements at 67 positions (Range Gates) along this length. The lidar device was setup to take 6 seconds to take measurements along a full beam length.

Siemens 2.3 - 93	
Max Power	2,300 kW
Cut-In	3 m/s
Rated	12 m/s
Cut-Out	25 m/s
Hub Height	74 m
Rotor Diameter	120.5 m

Table 4.2: Whitelee wind farm turbine physical characteristics [118]

The defined scan plan surveyed 14 Siemens 2.3MW [118] turbines in the active wind farm, the key physical characteristics of these turbines are identified in Table 4.2. The power and thrust curves for the Siemens turbines are identified in Appendix E. The physical turbine locations are identified with respect to the Ordnance Survey National Grid positioning system [117] in Cartesian coordinates (Northings and Eastings). This measurement strategy would facilitate capture of multiple turbine wakes maximising the potential for usable data sets. In favourable weather conditions it was hoped a detailed data set would be captured that may show turbine wakes and their interactions as well as inflow behaviour in free stream and wake effect turbine operation.

The campaign was initiated in the position shown in Figure 4.4 on 13th July 2011 and left onsite until the 18th July 2011.

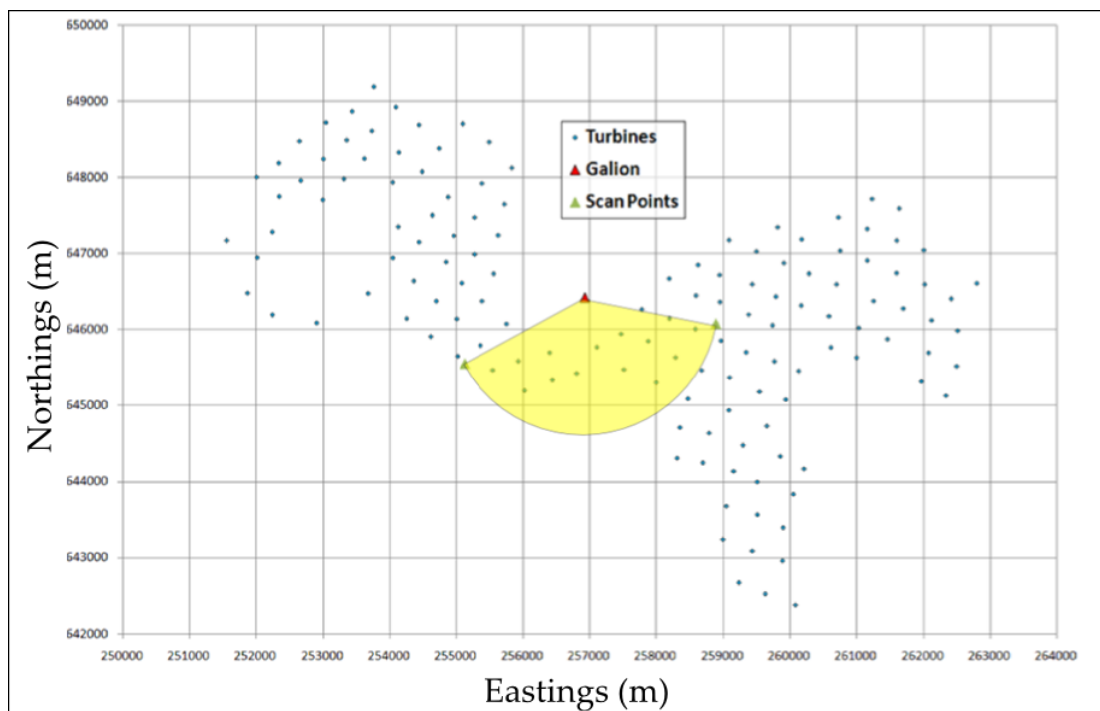


Figure 4.4: Whitelee turbine locations and scan profile

The location at ground level of the lidar device results in the implementation of a scan arc with an elevation of 6° . This elevation was selected to allow the scan plane to intersect the hub height plane as close as possible to the hub location of the nearest turbines. The low elevation also keeps the scan as near to horizontal as is practical from a ground based measurement location. The wind forecast for the duration of the deployment showed an expected directional shift in the wind vector over the 5 days of deployment, the large scan envelope was chosen in order to capture this behaviour. Analysis of the results showed that despite low wind speeds during the deployment a number of usable data sets were captured.

The measurements captured throughout this deployment were averaged over ten minute time periods allowing the visualisation of wake structures in the flow field. The highest quality data sets were then separated and analysed in preparation for further exploration and comparison with numerical models. A single ten minute data set was chosen for further analysis and wake centreline extracted using the methodology outlined above. The numerical simulation setup for the comparison is explored in Chapter 5 and the results explored in Chapter 6.

4.3.2 Myers Hill/Whitelee wind farm, January 2012

Deployment Dates:	January 10 th – 23 rd 2012
Lidar Location:	N: 256860
(OS Co-Ordinates)	E: 646514
	Elevation: 325m
Scan Arc:	90° – 187.5° Azimuth Range
	2.5° Beam Intervals
	5° Elevation
Beam Length:	2010m
	67 Range Gates
Individual Beam Time:	0.33 Hz
Total Arc Time:	151s
Num. of Points Per Scan:	2613
Number of Scans:	6794

Table 4.3: Scan Geometry for January 2012 Galion deployment at Myers Hill

A further deployment at the Myers Hill test site was conducted under identical set up conditions as the previous deployment. The aim of this deployment was to look at the effects of averaging the captured data sets over different time periods along with using different methods to define the simulation inlet conditions. A more focussed scan arc was implemented in order to scan the turbines on Whitelee wind farm. The turbines are the same as identified for the July deployment above in Table 4.2 and Appendix E. The PPI scan arc as described in Table 4.3 featured a narrower azimuthal range of 90° – 187.5° with a lower elevation of 5° and intervals of 2.5°. The increased beam separation interval leads to a lower spatial resolution than the previous deployment with larger distances between the beam lines leading to an increase in the areas measurements are averaged over. As with the previous deployment the range was limited to 2010m with 67 range gates along this length. The device setup was changed to decrease the scan period of each beam to 3 seconds. Coupled with the narrower scan arc and increased beam

separation this allows for a greater time resolution of the captured data sets with the overall time period for each arc scan decreased and more scan arcs captured per time period.

In the employed measurement strategy 11 Siemens 2.3MW [118] turbines were within the bounds of the scan arc with the lower scan elevation facilitating clearer wind turbine and wake structure visibility compared to previous deployments. Depending on operational variables such as visibility, turbine operation and scattering centre concentration some or all of the turbines closer to the lidar should be visible within the results.



Figure 4.5: Panoramic View of Scan Envelope

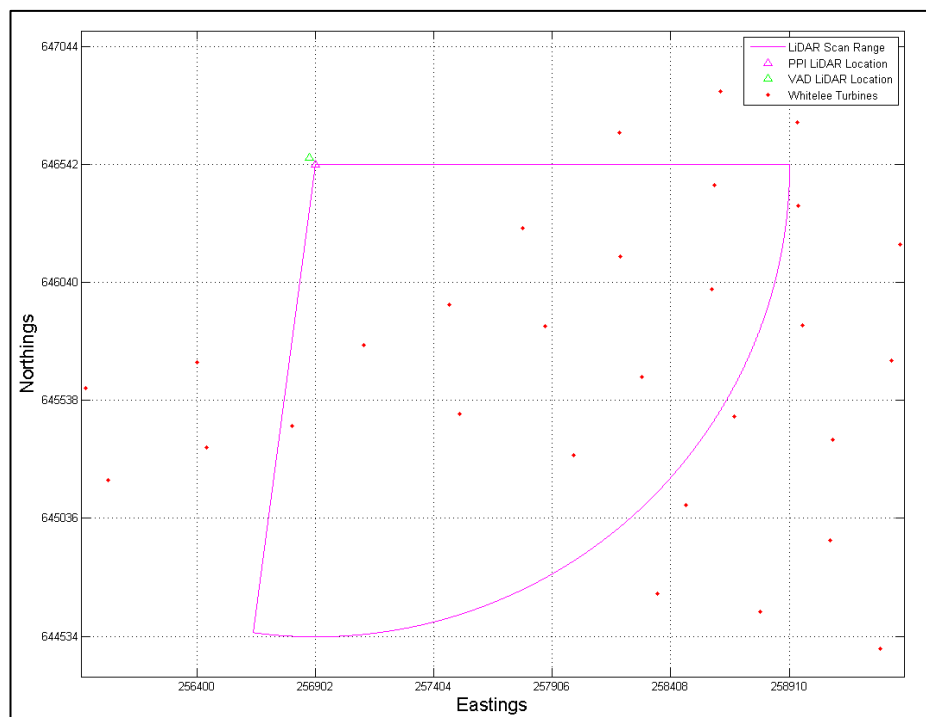


Figure 4.6: lidar scan envelope and Whitelee turbines January 2012 deployment

The scan envelope presented in Figure 4.5 and Figure 4.6 shows the locations of the wind turbines and those expected to be within range of the defined scan envelope. Subject to operational variables such as visibility, turbine operation and scattering centre concentration it was envisioned a significant number of turbines would be visible in the data sets. The lidar scanned continuously throughout the deployment period and the device and data sets were then retrieved for analysis.

Figure 4.7 presents the results of a range of time averaging periods on a sample of the scans from the deployment. Image 1 is an individual scan, Image 2 a ten minute average, Images 3 and 4 are hourly averages.

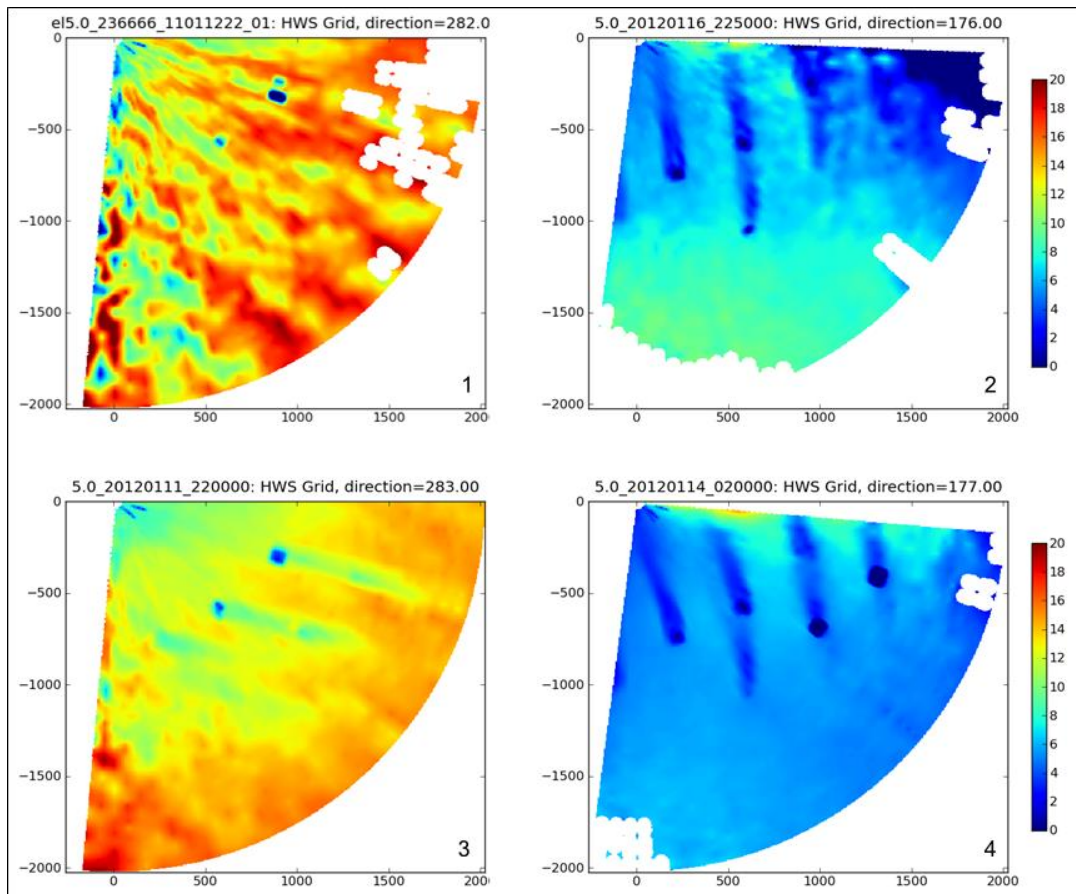


Figure 4.7: Sample processed lidar scan, January 2012 deployment.
1) Single Scan, 2) 10-Minute Averaged, 3) 1- Hour Averaged, 4) 1- Hour Averaged

The measurements presented were captured on different days throughout the deployment period and shows the variation in wind speed and direction experienced. As observed the wakes of the six turbines closest to the device in a South Westerly direction can be seen in images 2, 3 and 4; the ten minute and hour averaged measurements. The averaging period allowing the visualisation of steady state features in the measured flow field. The single scan measurement of images 1 does not show flow structure and wake development and no steady state flow features can be identified. The turbines towards the outer bounds of the scan envelope do not appear in any of the images.

This is a feature of the inclined scan plane enforced by the ground based installation of the lidar. The measurement points increase in height above the device with distance from it and at the further reaches of the beam the measurement height of the scan points has exceeded that of the rotor and its corresponding wake, Figure 4.8. Meaning that no wake induced velocity deficits were recorded in these regions.

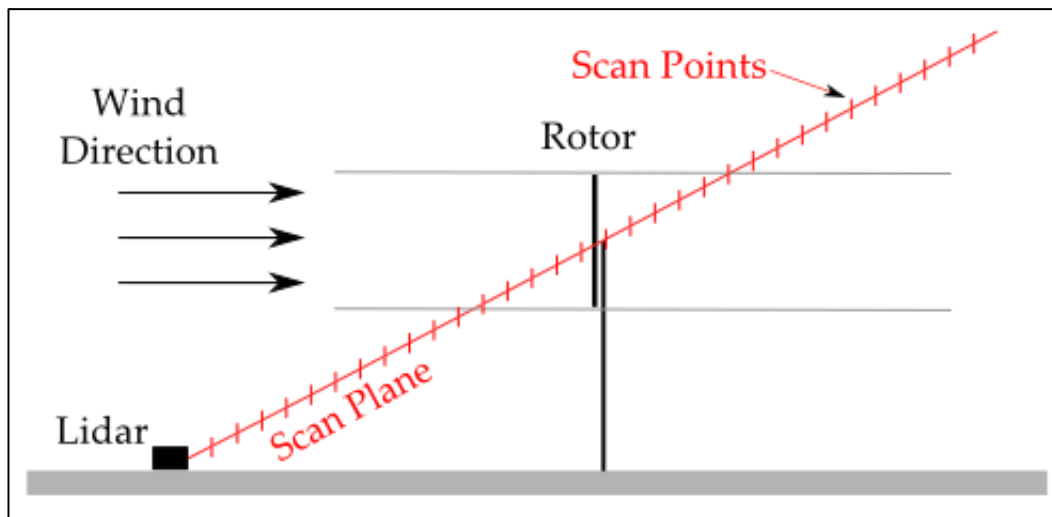


Figure 4.8: Inclined scan plane measurement location height increases

During the deployment a second device was sited at Myers Hill. This device was programmed for Velocity Azimuth Display (VAD) scans throughout the deployment measuring wind vectors at pre-defined heights, essentially acting as a virtual met mast. The location of the VAD device is indicated by the green triangle in Figure 4.6. Measurements were taken at 5m intervals from 40 - 105m directly above the device. The sample rate set on the VAD lidar allowed 19 seconds for the measurements at these heights in the North East, South East, South West and North West directions. Four line-of-sight point measurements were used to create a wind velocity and direction vector at the height of interest, Figure 4.9. These values are assigned to the point at the measurement height, H , directly above the device, accounting for angle of the cone. The data gathered will allow the measurement of the variation of horizontal wind speed with height above the device. Allowing atmospheric and boundary layer conditions to be analysed in parallel to the PPI results. The wind speed measurements will also be used to provide the computational domain inlet conditions where appropriate.

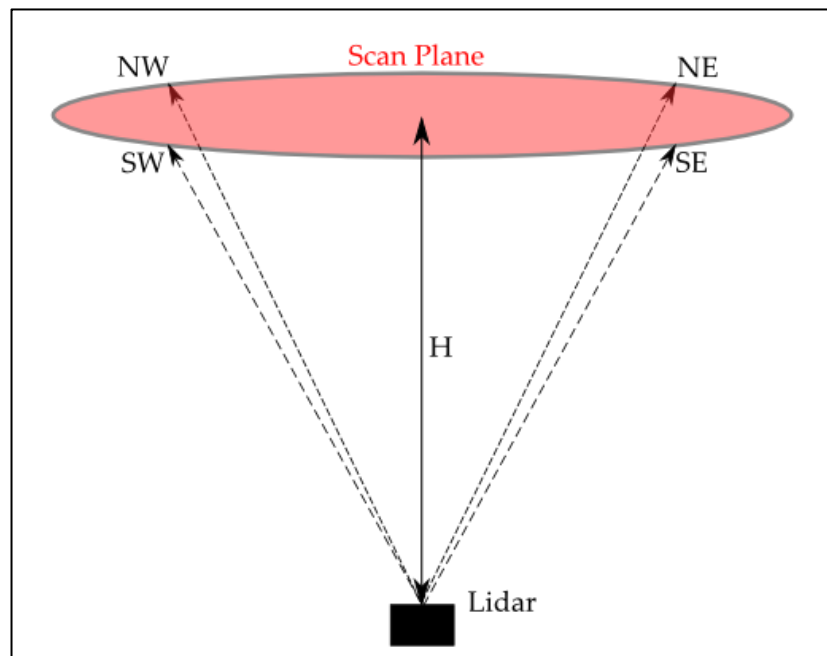


Figure 4.9: VAD scan measurement technique

From the captured scans two separate analysis streams were completed. Analysing both the ten minute and one hour averaged data sets a number of suitable images were selected for comparison with the models. Initially a single ten minute averaged data set detailing uniform inlet wind speed conditions of around 10m/s and resultant distinct wake definitions was chosen for further analysis. In addition the focus of this deployment required selecting a single ten minute lidar data set and a single hour lidar data sets. This allowed comparisons of the two averaging time periods to be made using inlet definitions from both the arc scanning lidar and the virtual met mast lidar. The simulation setups for these are explored in Chapter 5 and the results and comparison in Chapter 6.

4.4 Offshore lidar deployment

The flexibility of the Galion Lidar setup allows for the installation of devices onto the nacelle of active wind turbines. Installation of the device in such a location allows the uncertainties associated with inclined scan planes to be negated. The lidar fixed to the nacelle can also yaw with the turbine ensuring the scan envelopes are constantly optimised for the ambient wind direction. The potential improvement in the results captured from such a deployment is significant. The image in Figure 4.10 shows a sample ten minute averaged data set from a nacelle mounted deployment, clearly seen in the image is the wake of the studied turbine extending down from the top of the image. Also visible are the wakes of adjacent turbines in the wind farm.

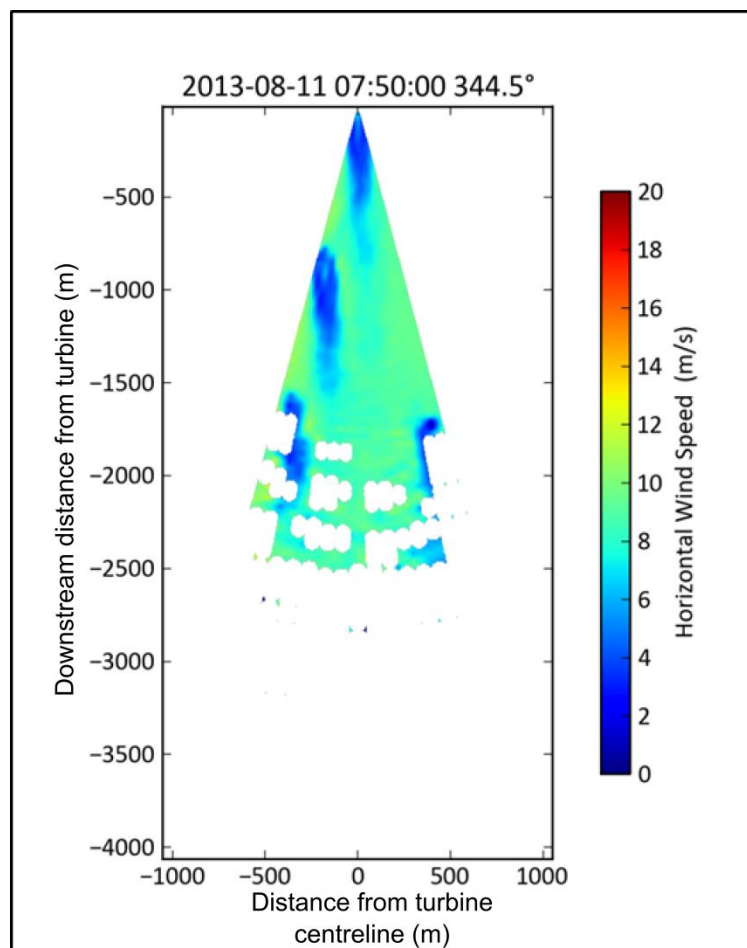


Figure 4.10: Sample rear facing ten minute averaged data set

Aligning a nacelle mounted lidar device with the centreline of the wind turbine allows for scan envelopes to be centred on this axis, with the 0° azimuth pointed upstream and the 180° downstream. In perfect operational conditions a wind turbine wake will be centred on this 180° azimuth of the scans, along the centreline of the turbine [84]. However, due to the variable nature of the wind flow the wake is rarely centred at this point.

The size of multi mega-watt scale operational turbines prohibits their ability to dynamically yaw according to the constantly changing wind direction [73]; as a result the lidar is not aligned exactly towards the wind most of the time. Simply choosing the measurements attributed to the 180° azimuth value will not necessarily capture the wake's centreline, the azimuth corresponding to the wake's centre must be found from the averaged flow field. Employing a selection algorithm to find the minimum Doppler values at each measurement distance from the device it is possible to find an average of this. Extracting the data corresponding to this average azimuth from the measured data then allows the centreline wake profile to be separated for analysis. The wake centreline data can then be plotted to show the evolution of the wake velocity downstream from the turbine rotor.

The advantage of this elevated and yawing installation location means that a series of scripts can be developed to process the data set and extract the wake centreline data from each ten minute data set and thus allow the entire set of weekly downloaded data to be processed in one go. In addition the timestamps for each averaged data set can be used to align with the corresponding information from upstream scanning lidar devices, turbine Supervisory Control and Data Acquisition (SCADA) data and nearby met mast data.

All of this information can be used to filter, sort and characterise each data set such that it can be attributed to individual flow characteristics as required such that they can be analysed and trends found for these. The methodology developed to allow the consistent extraction of the wake centreline profile from a nacelle mounted lidar is outlined below:

1. Average all data sets over ten minute time period

- Remove poor quality data sets such as:
 - In complete data sets:
 - where a high percentage of the required data has not been recorded due to low intensity measurement of the back scattered lidar beam
 - Evidence of yawing during averaging period:
 - where multiple wakes can be seen originating from behind the turbine rotor
 - evidence of multiple hard target returns from a single downstream turbine
 - Evidence of beam blockage by hard targets:
 - where data is missing behind a solid structure as the beam has been blocked and cannot register values beyond this point
 - Low wind speeds:
 - where the turbine is not operational and no wakes are generated to measure

2. Isolate each ten minute averaged and filtered data set in turn

3. Find wake centreline of studied turbine in individual scan as it extends behind the device
 - For each measurement distance (range gate) downstream from the lidar find the lowest measured doppler value and the azimuth value attributed to it
 - Continue this for the first 30 range gates (900m) to ensure only data relating to the studied turbine is used and adjacent wakes are not accounted for
 - Take an average of the 30 azimuth values attributed to the minimum doppler values at each range gate
 - Round this average to the nearest beam azimuth value in the defined scan arc
 - Extract all the data from the averaged data set along this averaged azimuth value
 - This data is attributed to the wake centreline for the ten minute period under study

4. Combine extracted centreline data with corresponding time stamped data from other relevant data sets.
 - Wind speed measurements taken at 2.5 rotor diameters upstream of rotor from the second hub height lidar unit
 - Wind speed and direction data from nearby FINO 1 met mast

5. Filter combined data sets according to desired attributes
 - Inlet wind speeds filtered into 2m/s wind speed bins between 4m/s and 20m/s
 - The ambient wind direction measured from FINO 1 is used to establish the inflow conditions to the turbine
 - Undisturbed inflow with no turbines upstream
 - Disturbed inflow where the inflow has come through the wind farm but not from an adjacent turbine
 - Waked inflow where the turbine is operating directly in the wake of an adjacent turbine

This process can be repeated for each of the averaged data sets gathered from the deployment. By filtering the resultant data into defining bins they can be grouped together such that repetitive behaviour and common characteristics in each bin can be captured. The primary method of individual scan filtering is through the use of inlet wind speed measurements. Grouping the data sets into 2m/s wind speed bins across the operational range of the studied wind turbine allows the effects of the varying conditions to be quantified and analysed. The further filtering done according to flow direction allows the isolation of periods where the turbine is operating in the freestream, under directly waked situations or from flow passing through the wider wind farm. As a result the behaviour of the wake for these conditions and differing wind speeds to be analysed together.

4.4.1 Alpha Ventus offshore, February 2013 – May 2013

Three Galion Lidar G4000 Offshore devices were deployed in an offshore measurement campaign in the North Sea as part of the Efficient Offshore Wind Program (EOWP) [119]. All three devices were deployed in the Alpha Ventus [116] wind farm on turbine AV7, a fully instrumented AREVA M5000-116 [120]. Deploying one device on the turbine transition piece and the other two on top of the turbine's nacelle a unique measurement campaign was implemented in partnership with SgurrEnergy Ltd and AREVA Wind GmbH [121].

The three Galion's operated continuously gathering data sets in a variety of scan regimes for a full year. Communication to the devices was enabled through the turbine's communication systems and could be accessed at any time. This direct access allowed the scan envelopes to be restructured throughout the deployment according to data capture needs.

The lidar deployment was complimented by SCADA data from the subject turbine made available by AREVA. As well as full met mast measurements from FINO 1 [122], a nearby offshore research installation providing wind data as well as atmospheric, temperature and sea state data. These measurements are available free of charge from the Research at Alpha Ventus [123] group who maintain the facility.

There are eleven further turbines within the offshore wind farm; these can be seen in the resultant measurements at different times dependent upon wind direction. As the prevalent wind direction varies the wakes developing behind these devices are seen to interact with the turbines downstream. The six Southern turbines are the same model as the subject turbine while the six Northern turbines are Senvion 5M turbines [124].

Lidar installation

Of the three Galion devices available two were installed on the wind turbine nacelle and one on the turbine transition piece in order to characterise flow conditions fully [125]. As indicated in Figure 4.11 and Figure 4.12 the two Galion Lidar devices fixed to the nacelle, referred to as Lidar 23 and Lidar 24 henceforth, were positioned to provide downstream and upstream measurements respectively, staying fixed to the nacelle as it yaws. Lidar 25 was positioned on the transition piece of the turbine to fully capture inflow and power performance assessments. Installed below the nacelle this device scans with varying elevation in order to capture inflow in front of the turbine rotor. Figure 4.13 identifies the location of the turbine AV7 within the wind farm and the horizontal distances between turbines. The information presented in Table 4.4 identifies the basic characteristics of the AREVA and REPower turbines installed in the Alpha Ventus wind farm.

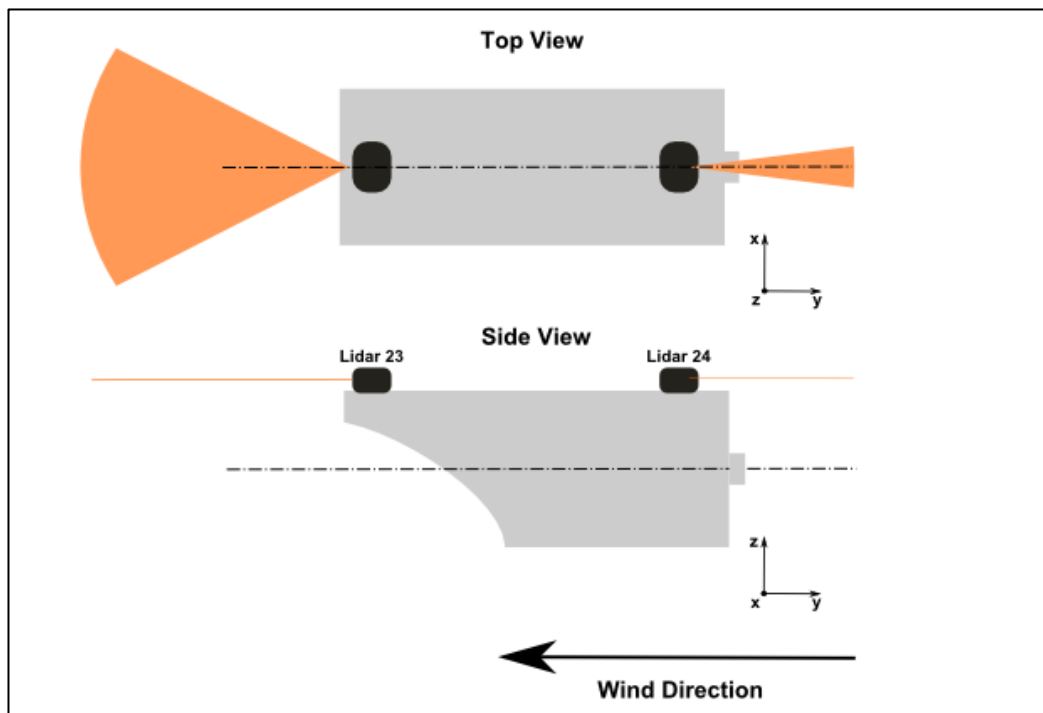


Figure 4.11: Diagram of AV7 nacelle roof lidar installation



Figure 4.12: Image of AV7 nacelle roof lidar installation, Lidar 23 foreground, Lidar 24 background

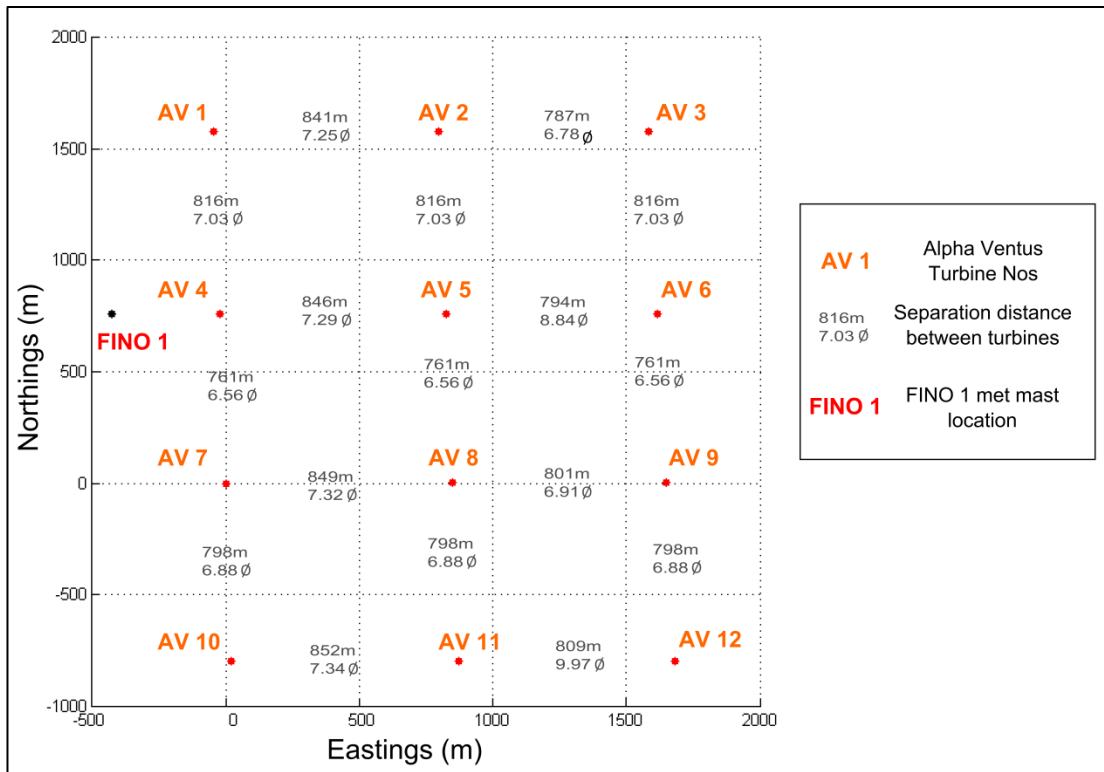


Figure 4.13: Alpha Ventus wind farm map, subject turbine AV7 at (0, 0)

	Turbines AV 1 – 6 REPower 5M	Turbines AV 7 - 12 AREVA M5000
Max Power	5,075 kW	5,000 kW
Cut-In	3.5 m/s	4 m/s
Rated	14 m/s	12.5 m/s
Cut-Out	30 m/s	25 m/s
Topography	Pitch Regulated i = 97 Gearbox Ratio 6-Pole DFIG	Pitch Regulated 1:10 Gearbox Ratio Synchronous PM
Hub Height	92 m	90 m
Rotor Diameter	126 m	116 m

Table 4.4: Alpha Ventus Turbine Properties [120] [124]

Scan envelopes

The deployments yielded a continuous data set during the active operation of the wind turbine. Continuous monitoring of the results and weather forecast facilitated the individual lidar measurement variables to be adjusted to capture high resolution data sets detailing wind turbine wake behaviour for a variety of inflow conditions.

The installation and setup of the three lidar devices offered the opportunity to monitor remote real time measurements. This enabled the scan geometry to be tailored throughout the deployment ensuring the data sets gathered provide insight into projects aims. For wake study the fore (Lidar 24) and aft (Lidar 23) nacelle mounted lidars were programmed to point upstream and downstream respectively. Lidar 24 performed a wide arc scan capturing data pertaining to the flow field in front of the rotor. Lidar 23 initially performed an arc scan to capture wake behaviour down the centreline and in the horizontal plane and was then re-programmed to capture aspects of the wake flow in the vertical centreline plane.

Anchored to the nacelle roof and centred on the wind turbine centreline Lidars 23 and 24 allow the implemented scan envelopes to track with the

turbine ensuring the centre of the arc scans are aligned to the turbine centreline. In addition the installation setup facilitates horizontal arc scans with a scan elevation of zero, thus removing the complications and unknowns of ground based lidar scans producing inclined scan planes that dissect the wake at an angle. Table 4.5 presents the scan configurations used from Lidar 23 to capture wake features in the horizontal plane.

Dates	Envelope	Spacing	Arc Scan Period (s)	Usable Ten Minute Averages
19 th February – 7 th March	120° – 240° - 120°	1°	678	258
6 th August – 18 th August	165° – 195°	2°	68	1205

Table 4.5: Utilised horizontal scan configurations, Lidar 23

The third lidar deployed, Lidar 25, on the transition piece was primarily used for comparisons with the FINO 1 met mast and Power Performance Assessments of the turbine. As this work is focussed on the wake structure created behind the wind turbine the work presented from Lidar 25 is out of the bounds of the work presented here.

Inflow characteristic filtering

The captured data sets encompass a wide range of inlet wind speeds and conditions. The full data sets are averaged over ten-minute periods and filtered according to a variety of criteria. Initially the data sets are filtered to remove:

- Low ambient wind speeds
 - < 4m/s
- Low quality results due to low levels of scattering centres in the ambient wind flow. This results in the intensity of the back scattered results being below the acceptable threshold

- Turbine yaw during the ten minute averaging period resulting in turbine echoes in the results
- Hard target returns from adjacent turbines

The remaining data sets have then been paired with the ten minute averaged time correspondent wind speed measurements at 2.5 rotor diameters upstream from the scanning Lidar 24. This allows an inlet wind speed in front of the rotor plane to be defined. In addition wind direction information from the nearby FINO 1 met mast allows the orientation of the turbine to be estimated.

Each ten minute data set is then sorted and binned according to inlet wind speed, in 2m/s bins from 4m/s to 22m/s, and by inflow condition. The orientation value of the turbine allows the scan to be separated by incident inflow condition. These are Undisturbed where there are no turbines upstream of the device, Disturbed where flow into the turbine rotor passes through the wider wind farm and Waked where flow into the turbine is directly influenced by upstream turbines. The definitions of the range of orientations corresponding to each inflow condition were set during consultation with the project partners [31] [121] and are detailed in Table 4.6. As can be seen the Waked flow directions correspond to a subset of those attributed to the Disturbed inflow directions. Waked inflow conditions are not considered as part of the Disturbed inflow analysis.

The envelopes as defined in relation to the wind farm are presented in Figure 4.14. The information presented in Table 4.7 details the breakdown of the filtered centreline results in each bin with the width breakdown in Table 7.8.

Inflow Condition	Azimuth Range
Undisturbed	200° – 270°
Disturbed	5° – 175°
Waked	85° - 95°

Table 4.6: Inflow condition azimuth definition

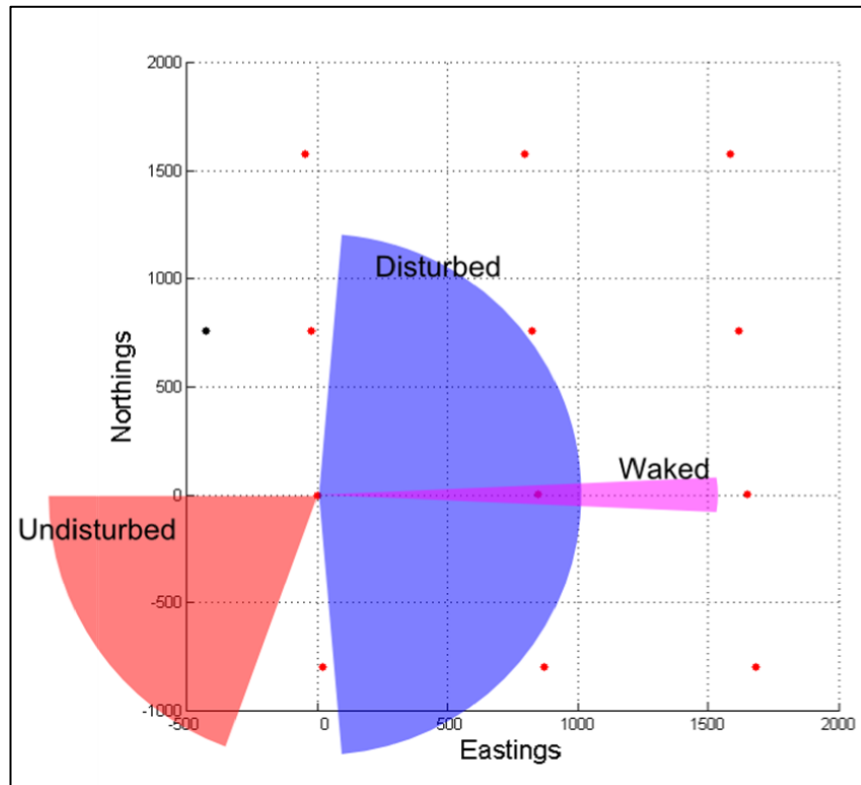


Figure 4.14: Inflow envelope definitions in relation to studied wind farm

Wind Speed Bin (m/s)	Undisturbed Inflow	Disturbed Inflow	Waked Inflow
4 – 6	64	21	0
6 – 8	57	93	7
8 – 10	57	149	26
10 – 12	133	192	44
12 – 14	43	151	39
14 – 16	3	80	30
16 – 18	0	22	7
18 – 20	0	14	2
20 – 22	0	3	0

Table 4.7: Breakdown of ten-minute averaged data sets into each bin

Wind Speed Bin (m/s)	Undisturbed Inflow	Disturbed Inflow	Waked Inflow
4 – 6	-	1	-
6 – 8	-	9	-
8 – 10	-	20	-
10 – 12	-	19	-
12 – 14	-	10	-
14 – 16	-	20	-
16 – 18	-	17	-
18 – 20	-	14	-
20 – 22	-	3	-

Table 4.8: Breakdown of width data sets into each bin

The comprehensive data sets facilitate the analysis of wake flow development to be assessed along two axes:

- Wake centreline profiles along the wake length at hub height
- Wake width profiles at selected distances from the device tracking development of wake velocities out from the centreline at hub height

The methodologies employed in initiating numerical simulations for comparison with the resultant data sets are explored in Chapter 5.

Chapter 5:

Numerical analysis

5.1 Background

The lidar deployments outlined in Chapter 4 provide unique data sets from a variety of installation locations at both onshore and offshore wind farms. The resultant measured data sets allow comparisons with a variety of wind industry flow models to be made.

Onshore the ground based location and inclined scan plane facilitate comparisons with three dimensional solvers modelling the entire wind farm domain. For comparison with the measurements gathered at the Whitelee wind farm the ANSYS Windmodeller platform has been employed. Within this package a number of different turbulence closure models have been considered.

Offshore the nacelle based installation and horizontal scan plane allow comparisons to be completed with the industry standard PARK and Eddy-Viscosity models in addition to the ANSYS Windmodeller [96] platform utilised previously.

The three numerical solvers included in this study require the development of distinct methodologies in order to achieve high quality comparisons with the lidar data sets captured.

The ANSYS Windmodeller flow solver allows for wind flow evolution models to be solved in three dimensions through a simulated wind farm, with wake data being extracted from specified points within this domain. The simulation of the domain and the extraction of wake data for comparison can be split into two separate processes.

- Simulation setup and execution
- Results visualisation and data extraction

For the onshore lidar deployments at Whitelee wind farm the ANSYS Windmodeller simulation setup methodology remains broadly similar with the wind turbine locations, local terrain roughness and elevation information remaining constant. The inlet conditions for each analysis are then specified individually. In contrast the extraction of results methodology is dependent on the nature of the deployment undertaken and the pattern of the measurements to be extracted.

For the PARK [80] and Eddy-Viscosity [84] models the simulation setup is based upon the development of codes to model the flow evolution in the wake as predicted by the models. Measured values of inlet wind speed are used alongside turbine specific power and thrust curves to complete the simulation.

The different methodologies employed for extracting wake simulation data from the onshore and offshore cases are explored in the following chapter.

5.2 Onshore numerical simulations

The inclined scan plane and subsequent three dimensional nature of the onshore measurement campaign data sets provide an ideal platform to utilise the ANSYS Windmodeller wind farm flow simulation package for comparison with wake measurements. Incorporating terrain and roughness features a three dimensional simulation domain can be created encompassing the bounds of the lidar scan plane. The Windmodeller setup also allows the use of variables unique to the studied turbine to be incorporated, improving the accuracy of the simulation.

The turbines at the focus of both studies are Siemens 2.3MW [118] devices, the simulations were setup utilising the turbine specific power and thrust curves. In each case the numbers of turbines encompassed within the scan envelope implemented have been reproduced in the simulation domain. The terrain maps for the wind farm under study also need to be employed and the exact geographical location of the turbines in this identified.

5.2.1 Onshore simulation setup and execution

For the onshore deployment simulations the setup of ANSYS Windmodeller simulation packages is completed through the package's graphical user interface (GUI). This allows the user to define the boundary conditions and domain setup of the proposed simulation. As both onshore deployments took place from similar locations scanning over Whitelee wind farm similar methodologies were used in establishing the simulations. The key input decisions to be made at the setup stage for the onshore simulations are detailed below.

- Domain dimensions

Taking into account inlet locations and required focus area ensuring the bounds of the lidar scan are covered. For each simulation these have been tailored individually to reflect the focus of the study. The specific domain dimension details are presented in Tables at the head of each setup section for each simulation.

- Terrain features

The contours for the terrain within Whitelee onshore wind farm have been applied. The terrain maps of Whitelee wind farm [115] were sourced from the Ordnance Survey Panorama [117] product and incorporate 10m height contours.

- Roughness characteristics

A surface roughness map for Whitelee wind farm has been created using WAsP Map Editor, the resultant .map file is compatible with Windmodeller and can be used for each of the onshore simulations. The values for each surface roughness type found in the wind farm were defined according to the values set out in the WAsP wind farm simulation manual [126]. Values for the separate roughness types are defined as follows:

- Forestry – 0.3, Farmland – 0.08, Grassland – 0.03, Buildings – 0.7, Inland Water – 0.001

- Mesh structure and resolution

ANSYS Windmodeller allows the mesh to be tailored to domain geometry and wind turbine locations. To improve the quality of the simulations higher resolution mesh in the key areas, such as around the

each of the turbine rotors, of the simulation can be implemented to improve simulation results

- In discussions with ANSYS Windmodeller development experts a refinement value of 12-15k nodes per turbine is recommended [127] in order to provide the necessary detail around the turbines to capture the flow evolution through the rotor plane.
- A background mesh with resolution of 40% of the wind turbine diameter is recommended to capture the flow in the rest of the domain
- Turbine locations and characteristics

The locations of each Whitelee turbine within the lidar scan domain are input into the domain setup in terms of x , y and z values. In addition individual turbine hub height and rotor diameter along with turbine specific thrust curves and power curves have been defined.

- Inlet conditions

The inlet for each flow situation being analysed can be defined in terms of its wind speed at the defined height and the direction to be analysed. The ANSYS Windmodeller methodology separates the outer surface of the defined domain into 24 regions, 12 are defined as inlet and 12 outlet. The velocity conditions are defined in the inlet as Dirichlet and the outlet are entrainment with constant pressure [128]. The definition of the 12 inlet and 12 outlet sectors is automated for each simulation based on the defined wind direction. The inlet velocity is applied at the height defined in the simulation setup.

Stability and temperature gradient options are also available that allow the boundary layer characteristics to be defined if enough information is available. For the

- Turbulence closure models to be utilised

The ANSYS Windmodeller software allows the user to define the turbulence closure method employed in each simulation. The user can choose between:

- $k-\omega$, $k-\varepsilon$ RNG, $k-\varepsilon$ STD, $k-\varepsilon$ Modified or Shear Stress Transport (SST)

Running the simulations with the desired criteria produces results files detailing the calculated flow properties across the three dimensional domain implemented based on the inlet definitions supplied. Multiple simulations can be run consecutively with the computational time for each simulation in a 5000m x 1000m domain with twelve turbines being in the region of 2-3 hours region.

Results visualisation and data extraction

Utilising the CFD Post facility the simulation domain and predicted flow evolution through it can be visualised in three dimensions. The required calculated flow properties can then be extracted for each individual simulation. This is completed by loading the .res file into the CFD Post GUI for each simulation the user can create flow evolution visualisations in two dimensional planes across the domain.

In visualising the results it is helpful to represent the simulated flow field at turbine hub height above the ground detailing flow evolution up to the rotor plane and into the wake. Figure 5.1 below details a sample hub height wind speed contour plot for an onshore flow simulation. The simulation was

defined with a 4m/s inlet wind speed and visualised at a hub height of 74m. Two wakes are clearly seen extending behind the turbines in the simulation, the height contours of the local terrain are also presented with interval heights of 10m. The three dimensional simulation and visualisation domain allows the user to repeat this process for any user defined plane and visualise the corresponding predicted flow values across it.

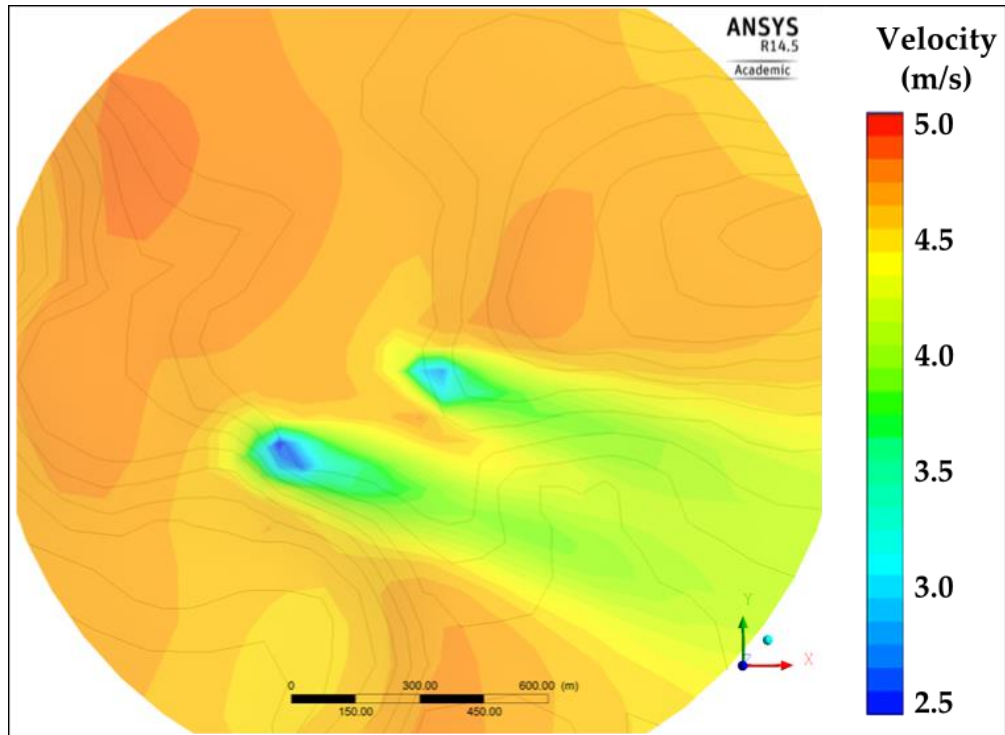


Figure 5.1: Hub height (74m) horizontal wind speed contour plot for onshore simulation, 4m/s inlet wind speed at 74m above ground level

In order to complete the comparison with lidar measurements the simulated data must be extracted from within the computational domain from data points corresponding to the exact same geographical position as that of the measurement points on the lidar scan plane.

In order to complete this process these measurement points must be reproduced in the simulation domain. Each measurement point can be defined as a function of the lidar location, the scan envelope implemented and its distance from the device. To allow a robust comparison between the

measured and simulated data the scan point position in relation to the device must be translated into the corresponding position within the measurement domain. The flow vectors at each measurement point can then be extracted for comparison with the measured data.

For ground based lidar deployments, the inclined scan plane implemented will mean that the measurements points extracted from the scan plane will be at varying heights across the wake profile dependant on the flow orientation being studied, this is covered in Figure 4.8. The changing elevation of the measurements will have a significant effect on the measured results and the subsequent comparison that will increase uncertainty in the conclusions drawn.

This visualisation and data extraction process must be completed for each of the individual flow situations being analysed as well as for each turbulence model used. The detailed simulation setups associated with both onshore lidar deployments at Whitelee wind farm are explored below.

5.2.2 Myers Hill/Whitelee wind farm, July 2011

As was detailed in Chapter 4 a single scan from the July 2011 deployment was chosen for comparison with the Windmodeller numerical models. The domain setup employed for this scan is outlined below in Table 5.1. Based on measurements extracted from the lidar scan the inlet wind speed was set at 4m/s with a wind direction of 289°. This value was extracted from the ten minute average measurements at approximately 2.5 rotor diameters upstream of the rotor. The variables defining the simulation domain are identified in Table 5.1. The simulation assumes a neutral boundary layer.

Geometry Centre (OS Grid reference based)	257469, 645947
Mesh Height	500m
Mesh Radius	1000m
Centre Block Radius Fraction	0.33
Horizontal Resolution	50
Inner Expansion Factor	1.1
Mesh Structure Option	Peripheral Extension
Outer Block Radius Fraction	1.5
Outer Expansion Factor	1.1
Mesh Expansion Factor	1.15
Vertical Resolution	1.15

Table 5.1: Simulation domain setup parameters

An individual simulation was run for each of the turbulence models incorporated within the Windmodeller package, Figure 5.2 shows a hub height (74m) horizontal velocity contour plot extracted from the $k-\omega$ simulation. The characteristics of the Siemens 2.3 turbines modelled are detailed in Table 4.2 and Appendix E. The black lines represent the height contours of the wind farm terrain at 10m intervals; the wakes developed by the two turbines can clearly be seen extending behind the turbines. This simulation method was repeated for each of the turbulence models. A line

corresponding to the wind direction was plotted through each turbine at hub height above ground level in the simulation domain. Data from along these lines can be exported and plotted in the same manner as the lidar data. The comparison results are explored in Chapter 6.

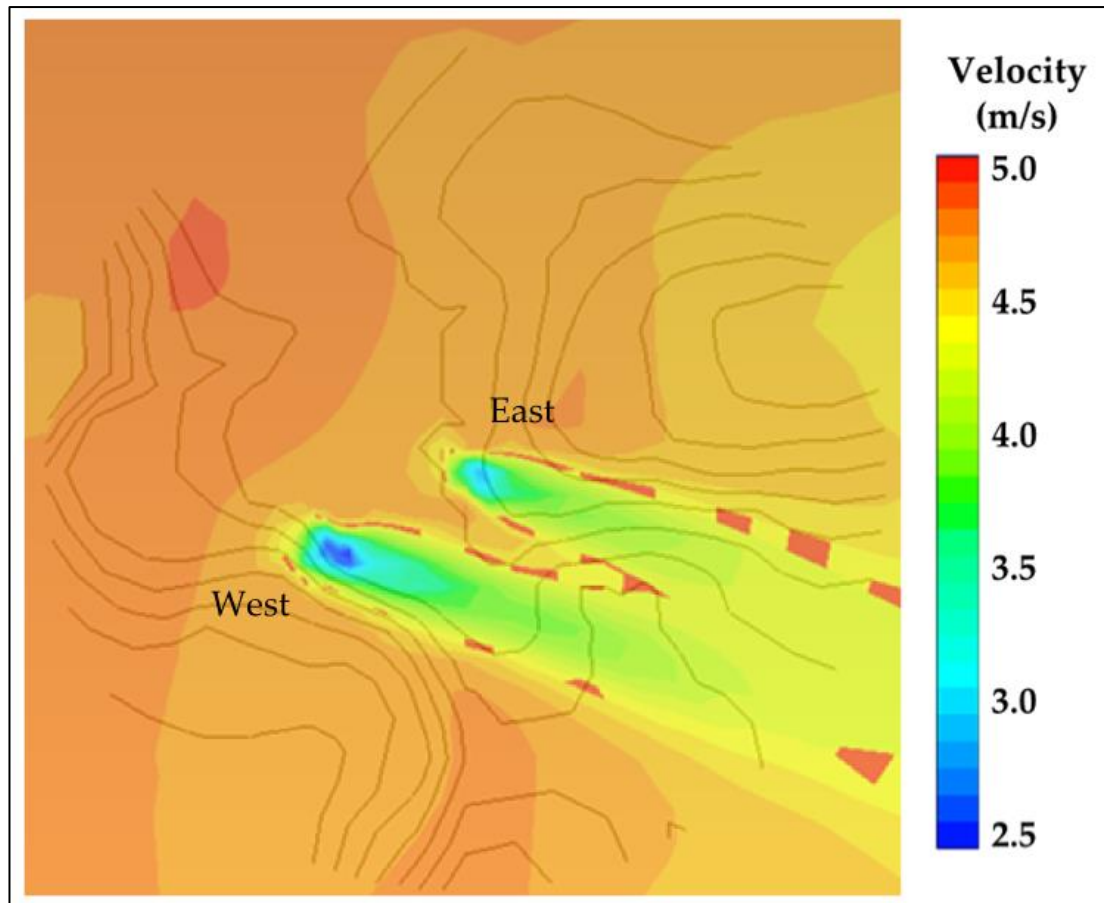


Figure 5.2: Hub height (74m) horizontal velocity plot for Eastern turbine, 4m/s inlet at 74m, Wind Direction 289°, $C_p = 0.47$

5.2.3 Myers Hill/Whitelee wind farm, January 2012

As detailed in Chapter 4 the analyses completed from this January 2012 deployment incorporated two separate focus areas. The first aims to use the same strategy as the previous July 2011 deployment utilising a single ten minute scan to analyse wake centreline flow measurement in this period. The second analysis involves utilising both ten minute and hourly averaged lidar data sets for comparison along with two different methodologies for defining the simulation wind speed and direction inlet conditions. The methodology for initiating the simulation and extracting the results for both the lidar scans and the simulations is the same as that employed in the previous study. While the turbines simulated in the both analysis are the same as in the July deployment, the characteristics for these are identified in Table 4.2 and Appendix E.

As both analyses originate from the same data set the domain setup utilised for both is identical. The variables defining the structure of this domain are identified in Table 5.2.

Geometry Centre (OS Based)	257490, 645713
Mesh Height	500m
Mesh Radius	1000m
Centre Block Radius Fraction	1
Horizontal Resolution	50
Inner Expansion Factor	1.1
Mesh Structure Option	Peripheral Extension
Outer Block Radius Fraction	1.5
Outer Expansion Factor	1.1
Mesh Expansion Factor	1.15
Vertical Resolution	1.15

Table 5.2: Simulation domain setup parameters, ten minute averaged analysis

For the single ten-minute averaged scan the inlet conditions were defined as 10.9m/s from a direction of 178° at a height of 166m above ground level. The wind speed value was extracted from the arc scan lidar measurements upstream of the device and the direction value taken from the calculations of the scan processing program.

For the second analysis in the January deployment multiple simulations were completed in order to compare the different inlet definition and averaging periods. For each simulation the inlet wind speeds and wind directions employed are identified in Table 5.3. The heights of the inlets in Table 5.3 relate to the physical location above ground level of the measurements in each case. The inlet wind speed is defined at these heights in each simulation. All simulations assume a neutral boundary layer.

	Wind Speed (m/s)	Direction (°)	Height A.G.L. (m)
Ten Minute Average			
ARC Scan Input	13.1	278	64
Virtual Met Mast Input	18.5	278	105
One Hour Averaged			
ARC Scan Input	15.8	283	60
Virtual Met Mast Input	18	283	105

Table 5.3: Inlet definitions for Windmodeller simulations, 10min and 1hr comparisons

Using these inlet definition methods in the present deployment means that both the arc and VAD inlet cases require that the turbines and wakes are in the lower left portion of the CFD domain and in close proximity to the edge of the domain. This requires the specification of the mesh parameters to ensure that the domain setup allows for sufficient detail in the areas of interest, Table 5.3.

To ensure the high resolution mesh detail extends to the mesh extremities where the turbines are sited the Centre Block Radius Fraction was set to 1.

This means that the area of high resolution mesh structure extends across the whole domain to its' bounds. This will increase computational time as the number of calculations increases with the number of mesh elements and a finer mesh increase this value. This is an acceptable trade off to ensure the quality of the simulation at the bounds of the domain being analysed.

Running the Windmodeller simulation for the four turbulence models the simulated wind speed measurements for the plotted lidar points locations can be extracted for comparison.

5.3 Offshore numerical simulations

The nacelle mounted location of the lidars utilised in offshore data capture opens up the possibility of employing a variety of models in the numerical analysis. As with the onshore deployments the ANSYS Windmodeller package has been employed. In addition the PARK and Eddy-Viscosity models have also been incorporated into the comparison.

The industry standard PARK and Eddy-Viscosity models have been setup to allow them to be run for each individual ten minute averaged data set captured by the lidar. The inputs are defined by the inlet measurements associated with each scan and the turbine specific thrust and power curves. The complex Windmodeller flow models require a more involved setup and computational overhead such that they are only run for a single simulation at a time. Only the SST model has been included in the analysis of offshore wake behaviour. The methodologies utilised for each of the models employed in the offshore numerical analysis are explored below.

5.3.1 Offshore Windmodeller simulations

The same methodology utilised for setting up the onshore simulation domain in Windmodeller is used for the offshore case. For the offshore simulations however there is no need to incorporate terrain elements and a single surface roughness value can be used instead of a roughness map. For offshore flow simulations a surface roughness value, or z_0 , of 0.0002 is employed. This value is commonly used and accepted by industry to simulate open water [129]. Figure 5.2 below presents a hub height velocity contour plot for an offshore wind farm created in the CFD Post facility. As can be seen the wakes are more clearly defined in comparison to the onshore simulation case. This is as a result of the lower levels of surface roughness and a homogenous ground level producing a consistent and stable boundary layer across the wind farm. This results in less mixing and movement of the air mass surrounding the wakes allowing them to be more defined from the surrounding flow.

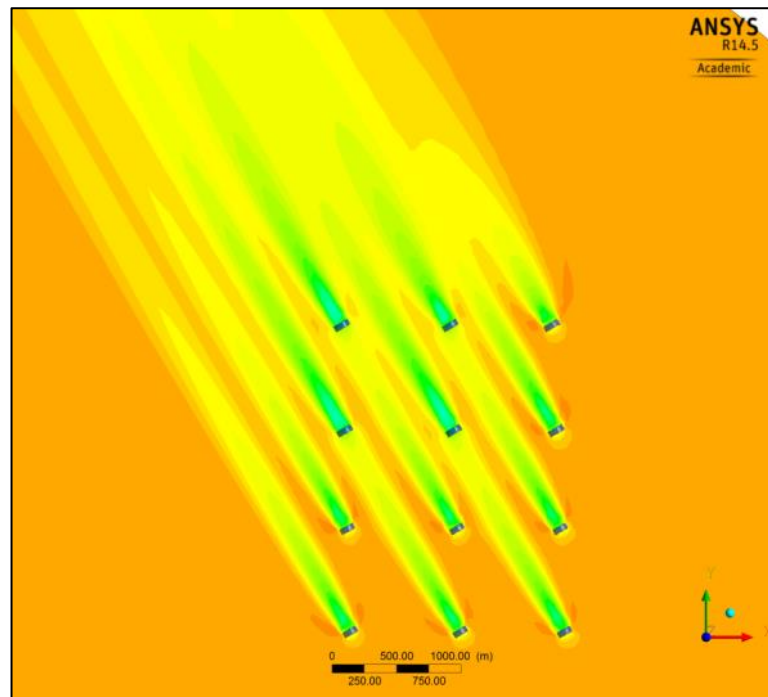


Figure 5.2: Hub height horizontal velocity contour plot for an offshore wind farm

In tailoring the offshore Windmodeller simulations for comparison with the PARK and Eddy-Viscosity models the setup implemented only modelled a single turbine. In Figure 5.2 the wakes of the modelled turbines can be seen interacting with each other downstream while both the PARK and Eddy-Viscosity models employed simulate wake flow behaviour for a single turbine operating in the freestream unaffected by surrounding turbines. To ensure a fair comparison the Windmodeller SST model was run similar conditions with no adjacent turbines modelled. The characteristics of the AREVA M5000 turbines under study are defined in Table 4.4 and Appendix F.

For data extraction in relation to the hub height lidar deployment the wake velocity data can be extracted in the same process as for the onshore case with the individual scan points plotted through the centre of the wake. In this instance there are no issues with the inclined scan plane and the scan points plotted in the domain are all located at the same height. In addition to plotting the individual scan points the user can extract data along a line corresponding to the centre wake of the simulated turbine. This allows for more data points to be extracted and for an improvement in the resolution of the simulated centreline profile.

The simulations employed in the offshore analysis called for comparisons with lidar data averaged across 2m/s wind speed bins. In order to complete a valid comparison with these averaged profiles the numerical models will be run using the average of the inlet conditions measured in each wind speed bin. These measured inlets for each simulation in the Centreline and Width profile analyses are defined in Table 5.4. As only one turbine is modelled in the Windmodeller domain and the terrain is constant across the whole domain the wind direction is will not affect the wake simulations. For this

simulation it was set at 180°. The inlet height is defined at hub height for the AREVA 5M turbine under study, 90m.

Wind Speed Bin (m/s)	Centreline Profile Average Inlet (m/s)	Width Profile Average Inlet (m/s)
4 - 6	-	4.5
6 - 8	7.1	7.1
8 - 10	8.9	8.8
10 - 12	11.1	10.7
12 - 14	13	13.3
14 - 16	15	15.2
16 - 18	-	16.8
18 - 20	-	19
20 - 22	-	20.3

Table 5.4: Inlet wind speed definitions for numerical simulations

For the SST simulation setup the domain was defined as in Table 5.5.

Geometry Centre (OS Based)	0, 0
Mesh Height	1000m
Mesh Radius	5000m
Centre Block Radius Fraction	0.33
Horizontal Resolution	46.4
Inner Expansion Factor	1.1
Mesh Structure Option	None
Outer Block Radius Fraction	1.5
Outer Expansion Factor	1.1
Mesh Expansion Factor	1.15
Vertical Resolution	1.15

Table 5.5: Windmodeller domain setup for offshore numerical simulation

5.3.2 Offshore PARK and Eddy-Viscosity simulations

Utilised in industry standard wind farm simulation packages the Eddy-Viscosity and PARK flow models are commonly used by engineers and developers during the planning and development of new wind farms. Utilised in these packages their methodologies provide wind flow predictions through simulated wind farms and inform the power potential calculations based on these. The equations and methodology behind both models are outlined in Chapter 2. The models use these processes to create a prediction of the wake velocity evolution downstream of the wind turbine rotor. The models also provide a method for calculating wake width and the velocity evolution within this at any given point downstream.

In order to allow the wake models to be incorporated into the comparisons presented a series of scripts to recreate each of the models in turn have been developed in Matlab [130]. The scripts are built to calculate the wake profile development downstream according to the methods and formulae outlined in Chapter 2 for both wake flow models. Separate scripts have been developed to calculate wake centreline and wake width behaviour. These allow the models to be initialised and run based on inputs defined by the user. Both models require a user defined inlet velocity which is used to define the thrust coefficient from the turbine specific thrust. The turbine being studied is the AREVA M5000 [120]. In addition to these values the PARK model requires a user defined Surface Roughness level, while the Eddy-Viscosity model requires a Turbulence Intensity definition. For offshore wind farm analysis a surface roughness of 0.0002 is accepted, leading to a wake decay constant of 0.038 [131]. While a Turbulence Intensity of 6% is common for offshore flow simulations [132]. These values for z_0 and T.I. have been agreed with the project partners [31] [132].

Side by side comparisons of the two models predictions for wake centreline velocity and wake width evolution can be seen in Figure 5.3 and Figure 5.4 respectively. The setup of the numerical simulation for these models allows these wake profiles to be created for each ten minute averaged data set.

These models are simple in nature and do not provide a full calculation of wake evolution in the three dimensional domain. As a result they are not suitable for comparison with data gathered from the inclined scan planes implemented by ground based lidar devices. The results of these simulations provide ideal comparisons with the data captured from nacelle mounted lidar deployments where there are less uncertainties involved with the hub height measurements and comparisons with steady state model predictions.

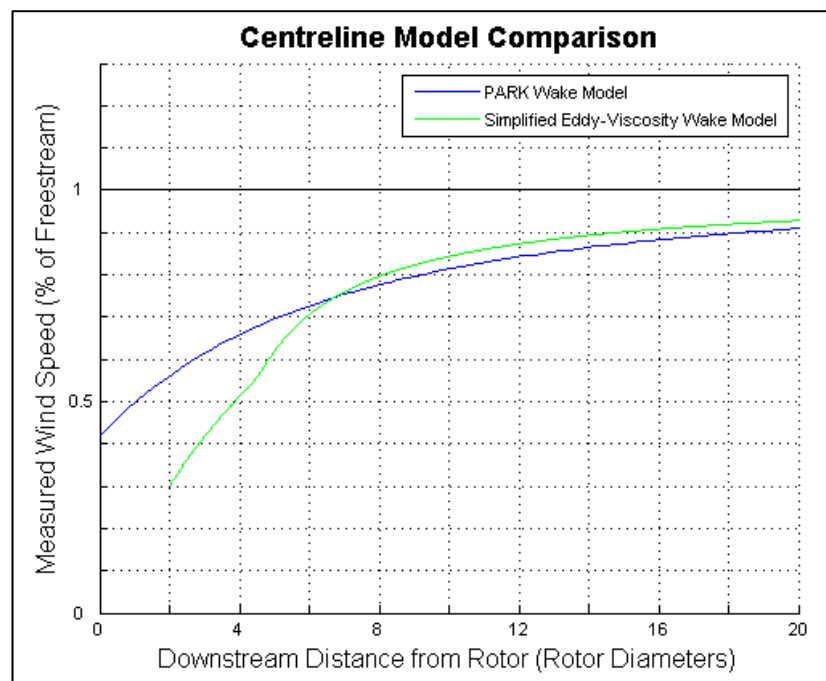


Figure 5.3: Centreline comparison of PARK and Eddy-Viscosity models, Inlet Wind Speed = 10m/s, Turbulence Intensity = 6%, Surface Roughness = 0.0002, Wake Decay Constant = 0.03841

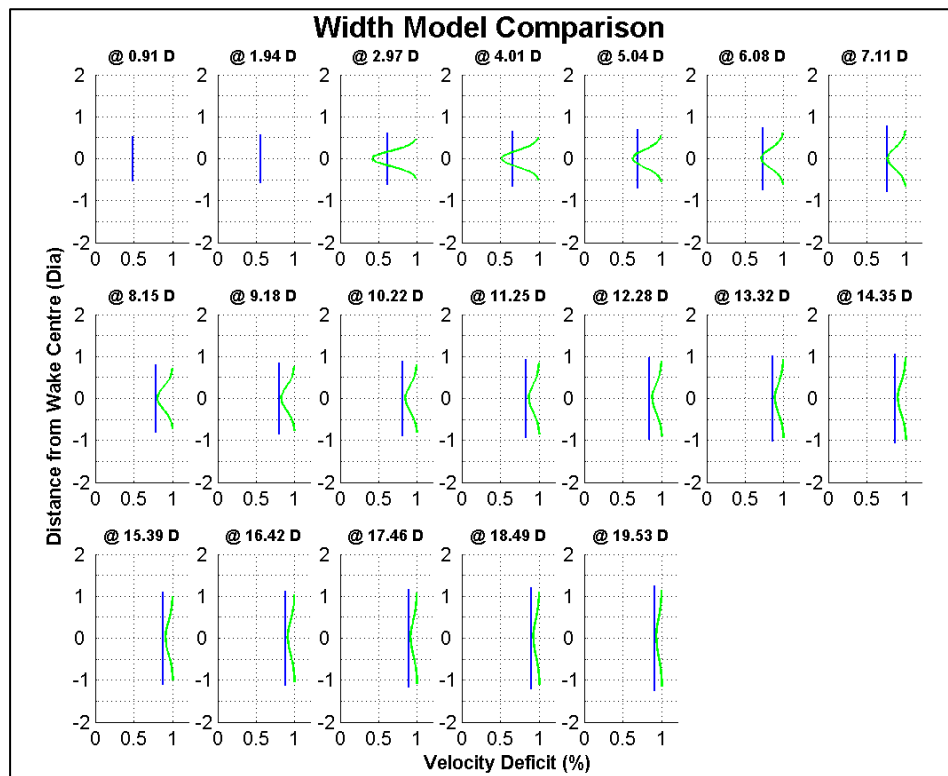


Figure 5.4: Width wake comparison of PARK and Eddy-Viscosity models, Inlet Wind Speed = 10m/s, Turbulence Intensity = 6%, Surface Roughness = 0.0002, Wake Decay Constant = 0.03841

The Eddy-Viscosity model does not appear in the wake width below two rotor diameters downstream predictions in Figure 5.4. It does not attempt to model the near wake velocity and as a result values for the wake width predictions can only be found beyond this point.

As in the Windmodeller simulations identified in Section 5.3.1 the model was run for each wind speed bin using the inlet wind speeds defined in Table 5.5. There is no need to define wind directions or inlet heights for these models.

Chapter 6:

Results

6.1 Background

The deployments outlined in Chapter 4 each yielded a large number of data sets for further analysis and comparison with the numerical wake models. From the onshore deployments a number of single time period averaged scans were chosen and analysed. While for the offshore deployment the lidar installation utilised facilitated a more in depth and complete analysis across the operational range of the turbine. The following chapter presents the lidar data sets chosen from each deployment alongside the corresponding wake analysis and simulation results completed.

Primary wake characterisation in this project deals with analysis along the length (x -direction) of the active wind turbine wake; how far the wake extends behind the rotor plane and the velocity profile along that length. The ultimate length of the wake is known to vary dependant on a number of key factors such as inlet wind speed, surface roughness and local turbulence levels. Direct comparison of measured velocities along the centreline and the simulation velocities at the same locations will provide insight into key characteristics and an understanding of wake development for given flow conditions.

Secondary wake characterisation deals with the wake velocity development perpendicular to the wake centreline. This deals with the characterisation of the flow velocities in the horizontal axis. Lidar measurements to capture detail in this axis will provide understanding of the velocity evolution at given lengths downstream, from the maximum deficit at the turbine centreline back towards the freestream velocities at the wake boundaries. These measurements will allow a picture of the variation in the ultimate wake width with distance and wind speed to be captured and the velocity

profile out to this point. Modelling approaches generally assume that the wake is symmetrical around the centre line in all directions. This is unlikely to hold true as flow boundary layer properties and local surface roughness will affect the velocity evolution in the vertical plane. In the horizontal plane there is likely to be a more symmetrical behaviour around the centreline however the effect of the wake rotation is unknown.

CFD Simulation Limitations

The comparisons with numerical models completed for the two deployment types make use of the four models incorporated in the ANSYS Windmodeller software along with the PARK and Eddy-Viscosity models. All three methodologies have been used for the offshore comparisons while only the ANSYS Windmodeller simulations have been used for onshore cases.

In completing the comparisons with the three dimensional models in ANSYS Windmodeller each simulation was setup up to reflect the conditions encountered. The unique setup parameters used for each simulation are detailed in the associated Tables in Chapter 5. For each case the inlet parameters have been chosen to recreate the conditions incident upon the studied turbine. In addition the mesh resolution and associated expansion factors in the domain have been tailored to provide maximum resolution at the focus areas of each simulation. Every effort has been made to ensure that the available data has been used to provide the highest quality comparisons possible with the measured data sets. However, it must be noted that there are short comings in the setups and comparisons that limit the quality of the simulations and their suitability for analysis with the measured wake data. These issues are outlined below:

- No mesh sensitivity studies were completed on any of the analyses to assess the quality of the simulations and tailor the defined domain to each flow situation.
- The inlet locations defined in the domain do not always reflect the location of the measured data used to define them, this increases the uncertainties associated with their definition. For the offshore simulations these uncertainties are smaller given there are no terrain or variable roughness effects in the domain.
- The data utilised has not captured boundary layer conditions associated with the measured flow field and these have not been included in the setup.
- No data has been captured to allow the characterisation of atmospheric stability during the period of measurements, neutral conditions have been assumed.

As a result of the above issues the ANSYS Windmodeller simulations, while providing a good comparison with the measured wake profiles and other numerical models, cannot be treated as providing anything more than indicative simulations of the model behaviour. There are clearly a number of features that will affect the wake flow evolution that have not been represented in the domain setup and inlet conditions definition in a cases.

6.2 Onshore lidar measurements and comparisons

Three separate onshore analysis streams have been completed based on the ground based lidar deployments to Myers Hill/Whitelee [114] [115] in July 2011 and January 2012. The lidar data sets chosen and the resultant wake profiles and comparisons are presented below. The results are discussed in Chapter 7.

6.2.1 Ten minute averaged, MyersHill/Whitelee wind farm, July 2011

The single scan and data set chosen from the July 2011 lidar deployment for further analysis is presented in Figure 6.1 below. Evident in the images is the clear development of wakes behind two turbines in the right side of the scan; these turbines are identified as East and West. The prevailing wind direction at this time was found to be a West to East orientated 289° with an average freestream wind speed of approximately 4m/s.

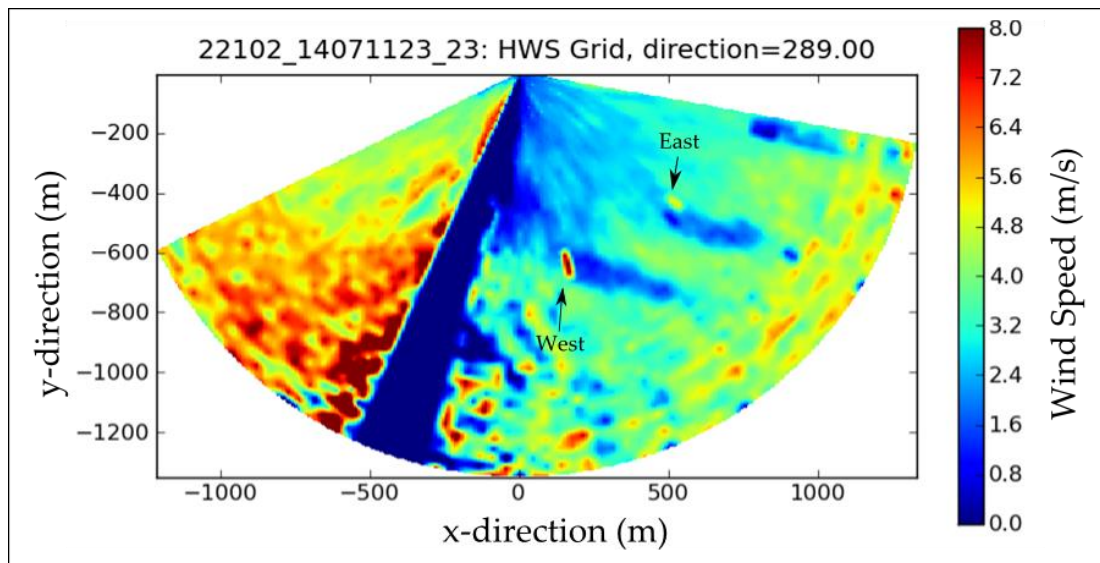


Figure 6.1: Ten minute averaged scan, MyersHill/Whitelee wind farm, July 2011
x-axis (m), y-axis (m), z-axis (m/s)

The large blue 'no data' slice of the arc scan relates to the attempted measurement of flow orientated perpendicular to the measurement beam. At this angle the velocity component of the wind vector aligned with the

measurement beam, V_{los} , is zero and no flow vector can be calculated using Equation 2.1. This results in the area of zero value measurements in this region. This is an inherent difficulty in using a scanning lidar to measure across a flow field from a static ground based location. The methodology outlined in Section 2.2 for lidar velocity measurement and formulation covers this effect more fully. To the left hand side of this blue slice the measured flow field shows far less structure and higher wind speeds than the rest of the image. It is unclear what this represents and there are no known obstacles in the area that could have biased the results. It likely indicates wind speed formulation errors resulting from utilising data in the 'no data' slice. This shows the limitations of the measurement methodology employed and the uncertainties associated with it in particular the use of scans with a section of measurements taken perpendicular to the ambient wind direction.

For the extraction of wake centreline profiles the methodology employed for each turbine is outlined in Section 4.3. The results detail the velocity profile corresponding to the turbine centrelines for the East and West turbines. These velocity evolution profiles plotted against wind turbine diameters up and downstream from the rotor are presented in Figure 6.2. Each measurement point chosen is within a 10m distance of the projected wake centre line. Wind flow in Figure 6.2 is left to right; negative values indicate locations upstream of the turbine rotor. The freestream is approximately 4m/s.

As explored in Chapter 4 the inclined lidar scan plane means that the measurement points obtained increase in height with distance from the device. With the wind flow orientation of the scan under analysis this means that the measurement heights in the wind turbine stream tube get higher in

the flow direction through the rotor, thus measurement points to the left of Figure 6.2 are lower than those to the right, this demonstrated for the lidar centreline measurement points in Figure 6.3.

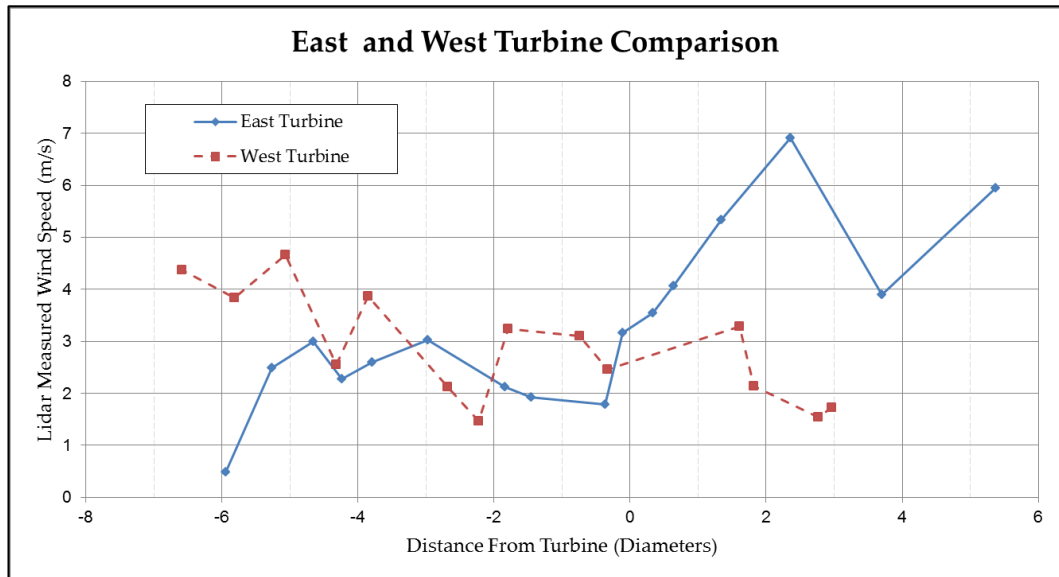


Figure 6.2: Two turbine lidar wake measurement comparison, Ten minute averaged, MyersHill/Whitelee wind farm, July 2011

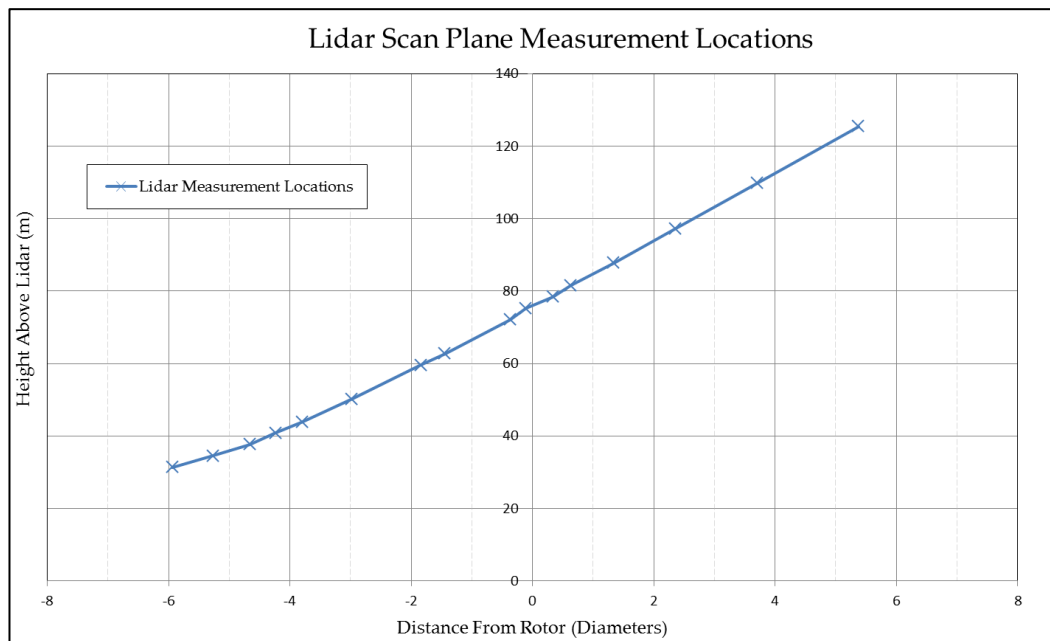


Figure 6.3: Lidar scan plane measurement locations, East Turbine

Focussing on the results for the East turbine a numerical Windmodeller [96] analysis was setup for the four available turbulence models for the flow conditions measured. The inlet value was set at a wind speed of 4m/s and a wind direction of 289°. The wake centreline profiles extracted from the numerical results can be seen in Figure 6.4. These values were all extracted from a plane corresponding to hub height in the simulation domain.

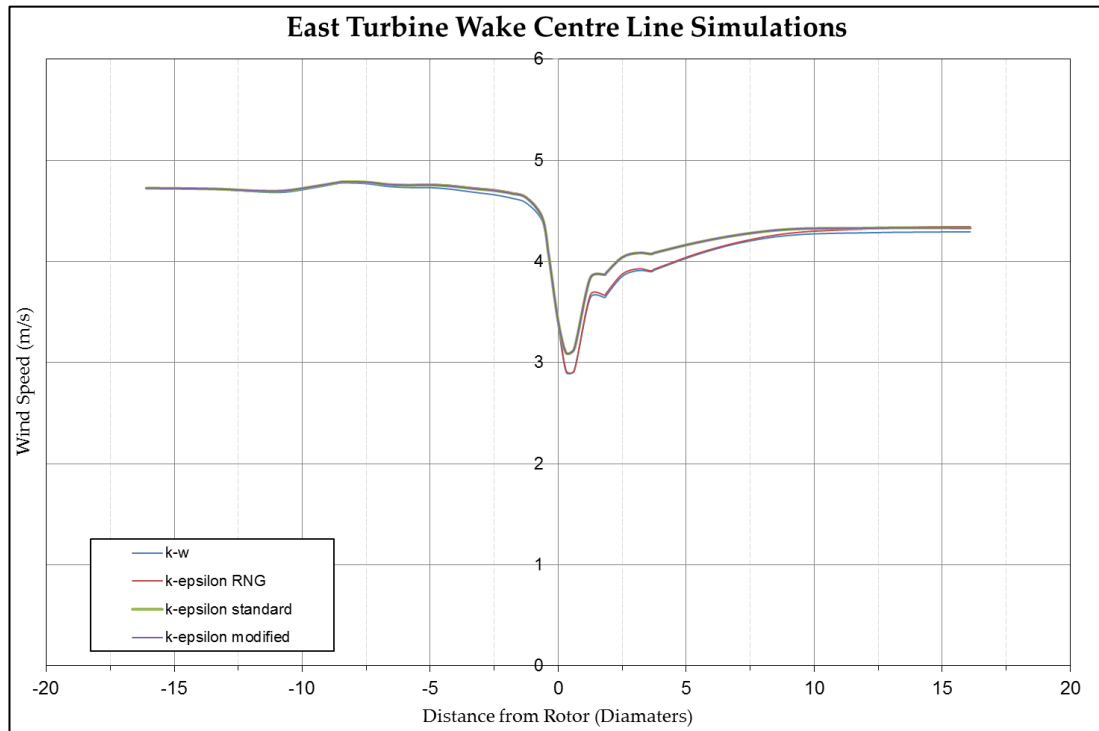


Figure 6.4: East turbine Windmodeller turbulence model comparisons, hub height

The Windmodeller simulation results presented in Figure 6.4 predict a clear hub height velocity profile that is broadly similar for all four turbulence models. The inlet wind speeds remain constant through to the inlet to the rotor stream tube. From this point the flow is seen to slow dramatically through the rotor plane leading to a maximum deficit value downstream of the rotor, this is followed by a gradual recovery towards the free stream velocity.

A direct comparison between wake data extracted from the lidar measurements and that extracted at representative hub height from the simulations would be of little benefit as the varying discrepancies in height between the measured and simulated points will result in significant errors. These will result as the flow within a wind farm will be affected not only by boundary layer interaction but also by areas of flow recirculation, wake effects and turbine induced flow structures that cannot be predicted and are difficult to model.

For comparison the lidar measured velocity values plotted against the corresponding numerical analysis at the same points in the model are shown in Figure 6.5. The numerical results show a smooth profile in line with actuator disk model predictions, predicting a gradual slowing of flow velocity upstream of the rotor followed by a larger drop through the rotor and a subsequent recovery towards freestream beyond the rotor. The measured results show a significantly less stable profile that does not agree with the models. Upstream of the rotor lower wind speeds are measured while the wind speeds are found to increase through the rotor plane and downstream of the rotor.

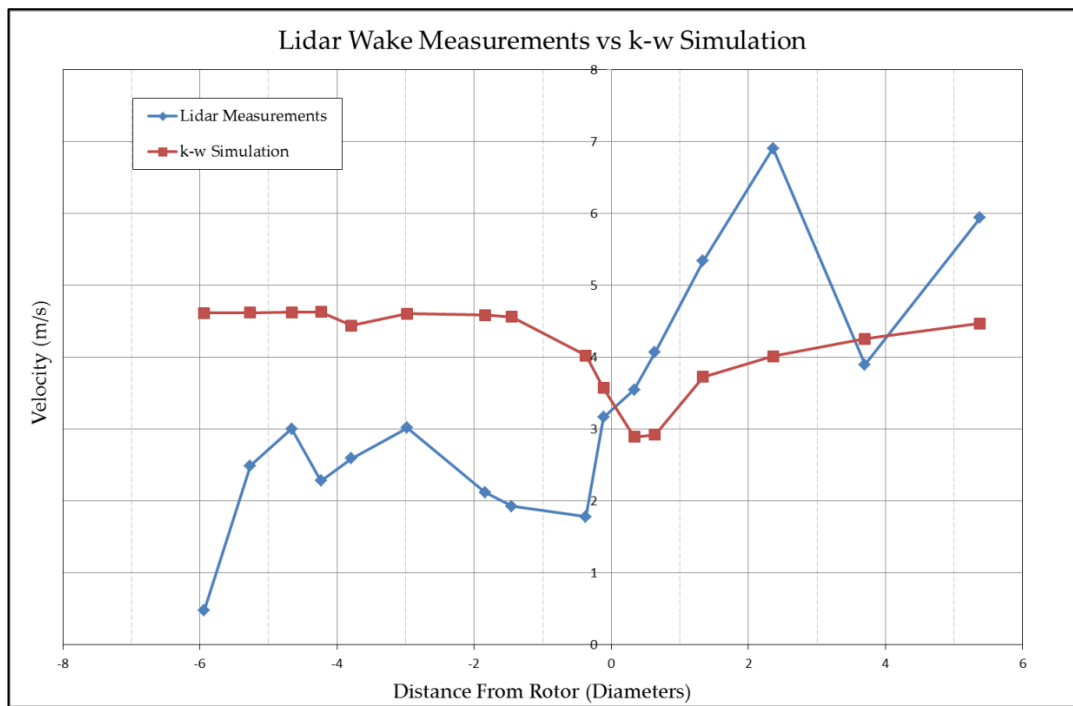


Figure 6.5: Lidar vs Windmodeller k- ω model, 14th July 2011, 23.55.12

6.2.2 Ten minute averaged, Myers Hill/Whitelee wind farm, January 2012

The first analysis undertaken from the January 2012 lidar deployment incorporated the analysis of a single ten minute averaged scan. The wind direction during this time was measured as 178° with a freestream velocity of close to 10m/s. The ten-minute averaged scan chosen for further analysis is shown in Figure 6.6. In this image six wind turbine wakes can be clearly identified moving towards the top edge of the scan envelope behind the turbines present. In addition some less well defined features are present. Upstream of the 6th wake some indistinct flow features can be also be identified, these are likely to relate to upstream turbines in the wider wind farm that are not present in the scan envelope. Also visible at the top right outer edge of the scan envelope a large area of near zero wind speeds can be identified. It is not clear what this relates to and as the measurement heights at the extremities of the scan are higher than the turbine wakes it is likely to be a feature in the flow field above the turbines and not of the wind farm.

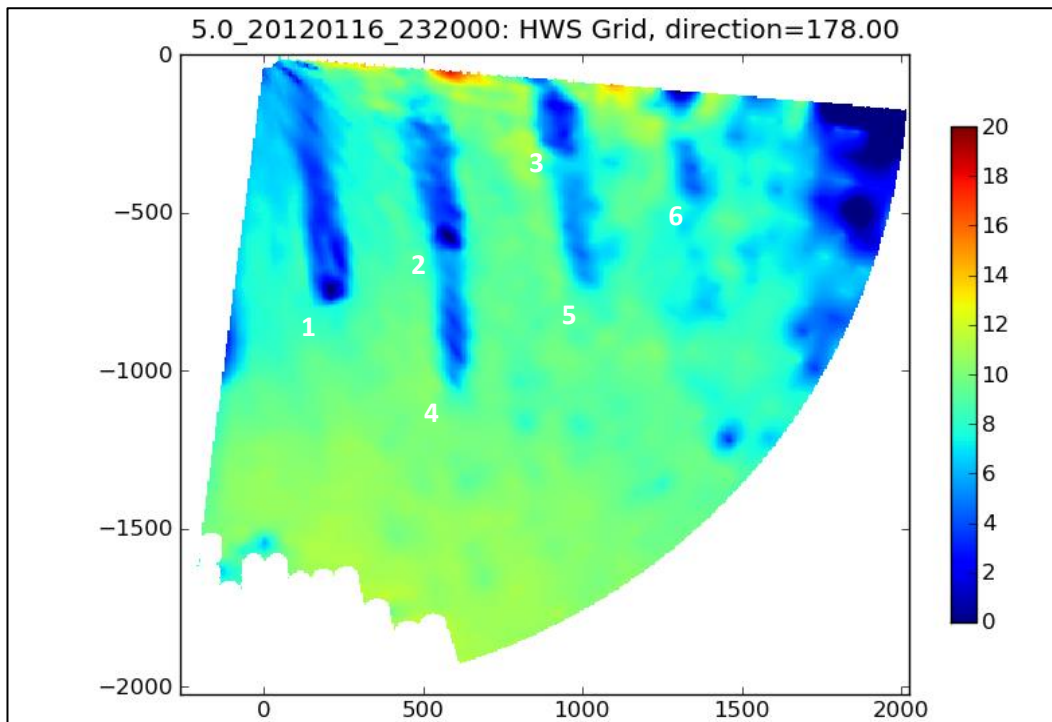


Figure 6.6: PPI arc scan from lidar deployment, 16th January 2012, 2320-2330

In order to compare wake centreline velocity evolution with the corresponding numerical predictions the same approaches for extracting wake centreline data from a ground based lidar deployment detailed in Chapter 4 can be employed. These have been completed for each of the six turbine wakes identified.

Analysing the freestream operating Turbine 1, the lidar measurement height profile in Figure 6.7 indicates that the scan plane passes very close to the hub of this device making it ideal for use in comparisons. The turbine rotor diameter of 90m dictates that upstream of the turbine the scan points fall within the hub diameter while downstream all but the final two scan points remote from the turbine are outside. These downstream points are still likely to fall within the wake given the expansion predicted. The wind flow in Figure 6.7 is from left to right; negative x-axis values indicate upstream positions.

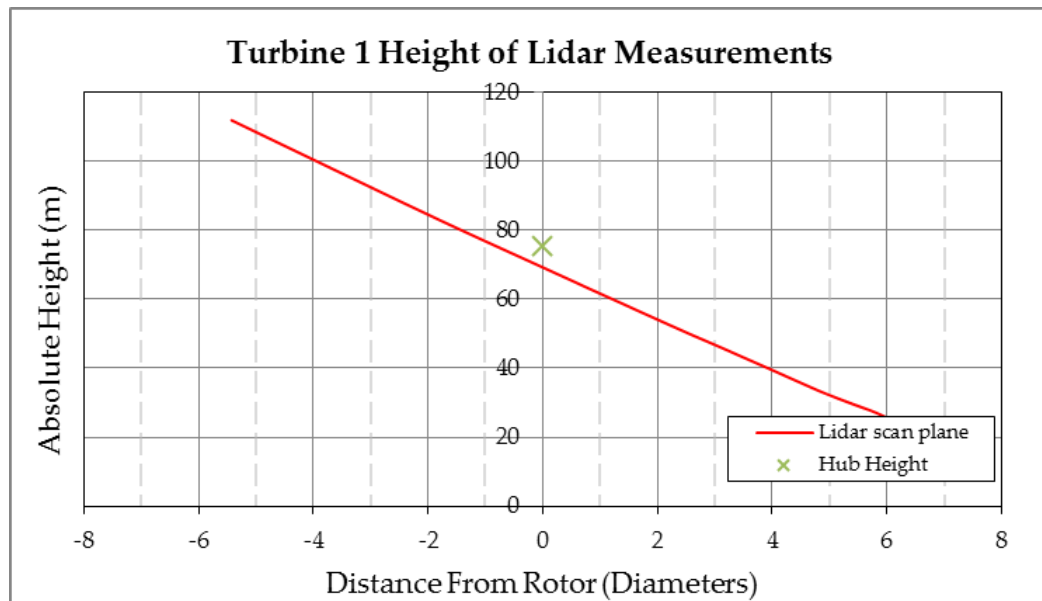


Figure 6.7: Lidar measurement plane, Turbine 1, January 2012

Using lidar measurements on the line indicated in Figure 6.7 the numerical model considers the wake flow evolution of Turbine 1. The plot of the data extracted to create the measured wake centreline velocity profile can be seen in Figure 6.9 (black line).

The methodology and domain parameters outlined in Chapter 5 allow a simulation of the measurement domain to be completed. The values input at the setup of the Windmodeller simulation are a direction of 178° with an inlet velocity of 10.9m/s . The simulation was run with the six turbines identified in the lidar measurements and for each turbulence model available in the Windmodeller package, the $k-\omega$, $k-\varepsilon$ RNG, $k-\varepsilon$ STD and $k-\varepsilon$ Modified models.

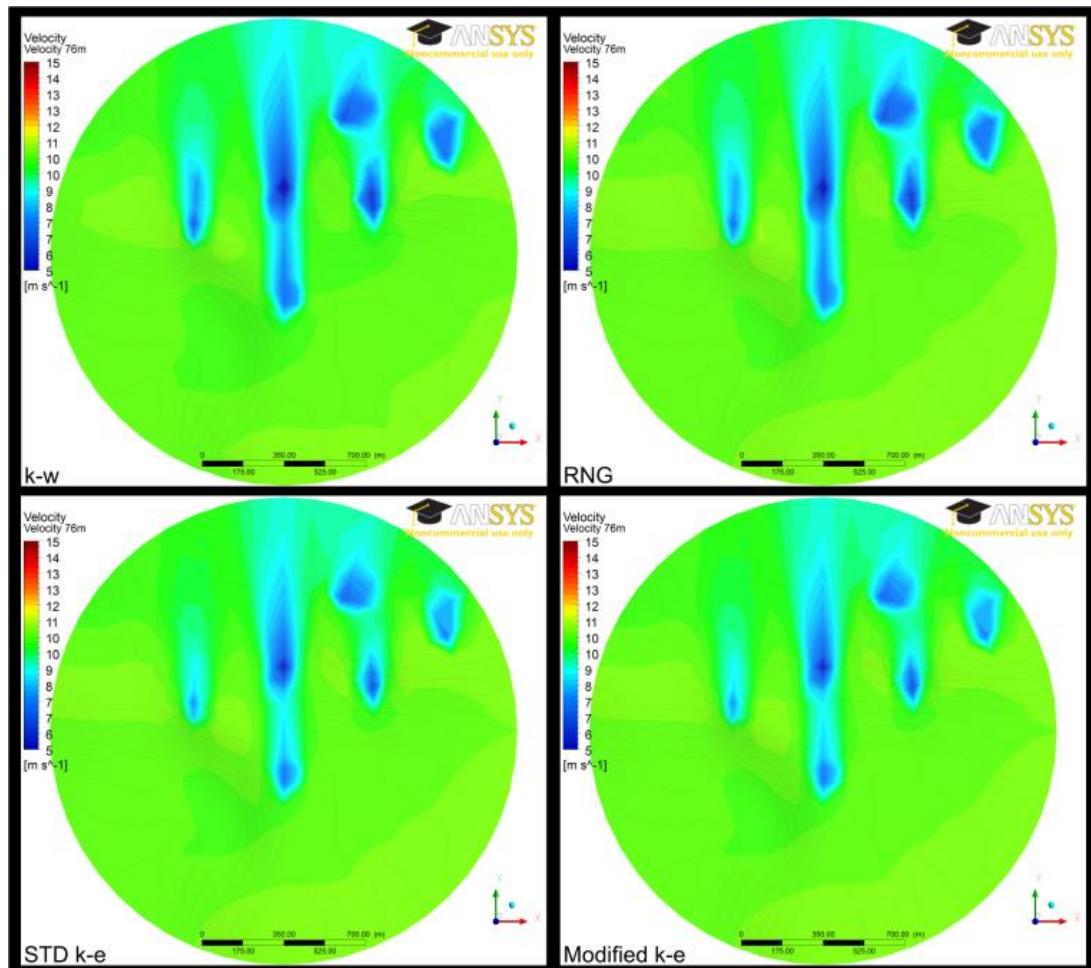


Figure 6.8: Windmodeller Turbulence model comparison, Wind Direction 178°

The four images in Figure 6.8 present the Windmodeller simulation visualisations for the four turbulence models. The velocity profiles are plotted on a horizontal plane at hub height above ground level in the domain; this corresponds to as to hub height for the Whitelee turbines. As in the lidar data the six modelled turbine wakes can be seen extending towards the top of the domain, the same turbine numbering system as in the lidar scan can be used to identify the turbines. Focusing on the presented wake structures it is clear that the turbine wakes that extend to the domain edges show unexpected behaviour and are truncated by the flow interactions at the domain edges. As a result these turbines and associated wakes are not appropriate for use in comparison with the lidar models

Extracting wake centreline data for the Turbine 1 lidar measurement points in the simulation domain a comparison with the lidar measurements can be presented, Figure 6.9. The flow direction in the figure is from left to right with the turbine situated at zero on the x-axis.

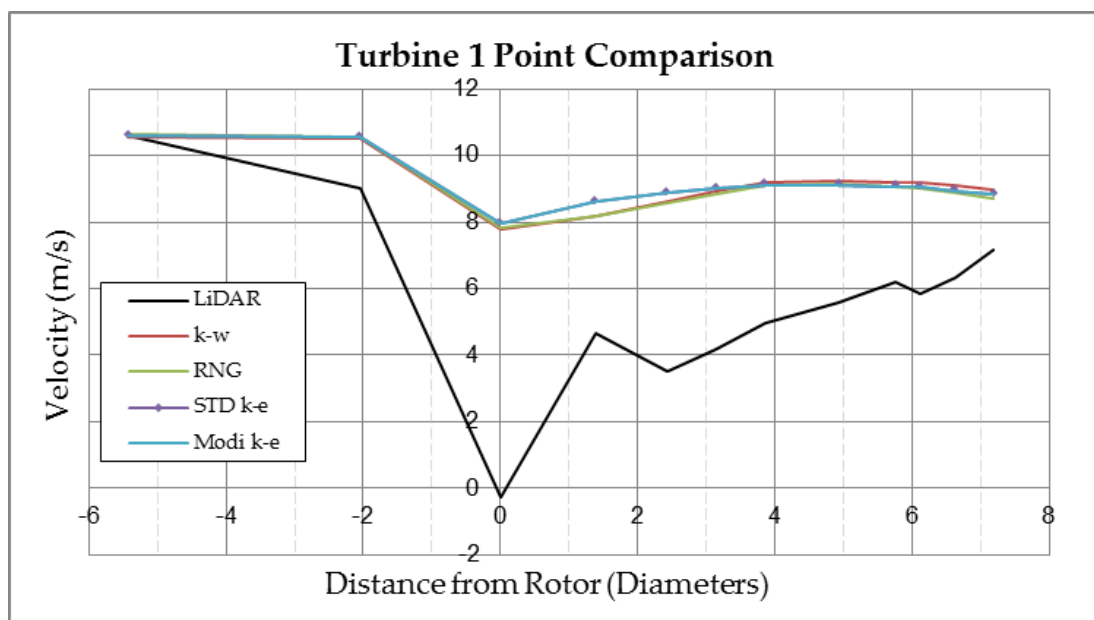


Figure 6.9: Turbine 1 centreline horizontal velocity comparison

The lidar measurements presented in Figure 6.9 show the measured velocity evolution through the rotor plane. Upstream of the rotor a gradual slow down towards the rotor plane is followed by a large drop through the rotor to a negative value which is followed by a subsequent recovery towards freestream. The steep drop through the rotor plane is far larger than is expected and indeed the negative value indicates a flow reversal at the rotor plane. This feature does not agree with any theory of flow evolution and is likely to be a feature resulting from the measurement location. As the scan plane at the rotor plane passes close to the hub it can be surmised that this measurement has been affected by the structure of the turbine itself and is not a true flow measurement.

The four numerical flow profiles presented show broadly similar behaviour to each, indicating a velocity profile in keeping with expected theory with a velocity drop through the rotor plane followed by a subsequent recovery towards freestream. The $k-\omega$ and RNG models show a slightly larger predicted velocity drop across the rotor. There is then a resulting increased recovery time than the two $k-\varepsilon$ based models, which appear to have strong correlation throughout. Beyond four diameters downstream of the rotor disc the wake behaviour of the four models is almost identical. However, towards the end of this recovery it is seen that the simulated velocities begin to fall again as the measured recovery stalls. This feature is brought about as the lidar scan points used to extract the data from the measurement domain are steadily decreasing in height with length along the wake, Figure 6.7.

6.2.3 Inlet definition and time averaged comparison

Utilising data sets captured from the same lidar deployment as the work undertaken in Section 6.2.2 comparisons for a different flow orientation at Whitelee wind farm are presented. The data sets chosen encompass different time averaging periods, ten minutes and one hour. In addition the deployment described in Section 4.3.2 utilises a second Galion lidar deployed onsite during the deployment, Figure 4.6. This device is constrained to measure vertically creating a virtual met mast at its location.

Visual analysis of the resultant images allowed a single data set relating to each averaged time period to be selected for further analysis, Figure 6.10 and Figure 6.11. The six turbines focussed upon are visible to the south east of the device in the ten minute and one hour averaged images.

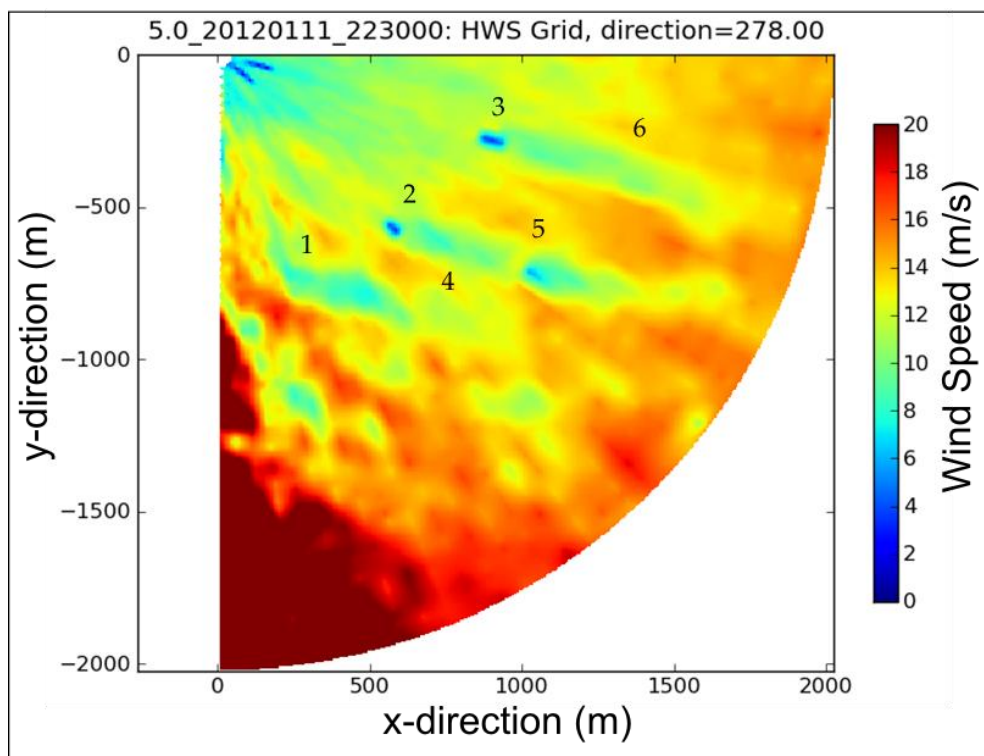


Figure 6.10: Ten Minute averaged lidar scan

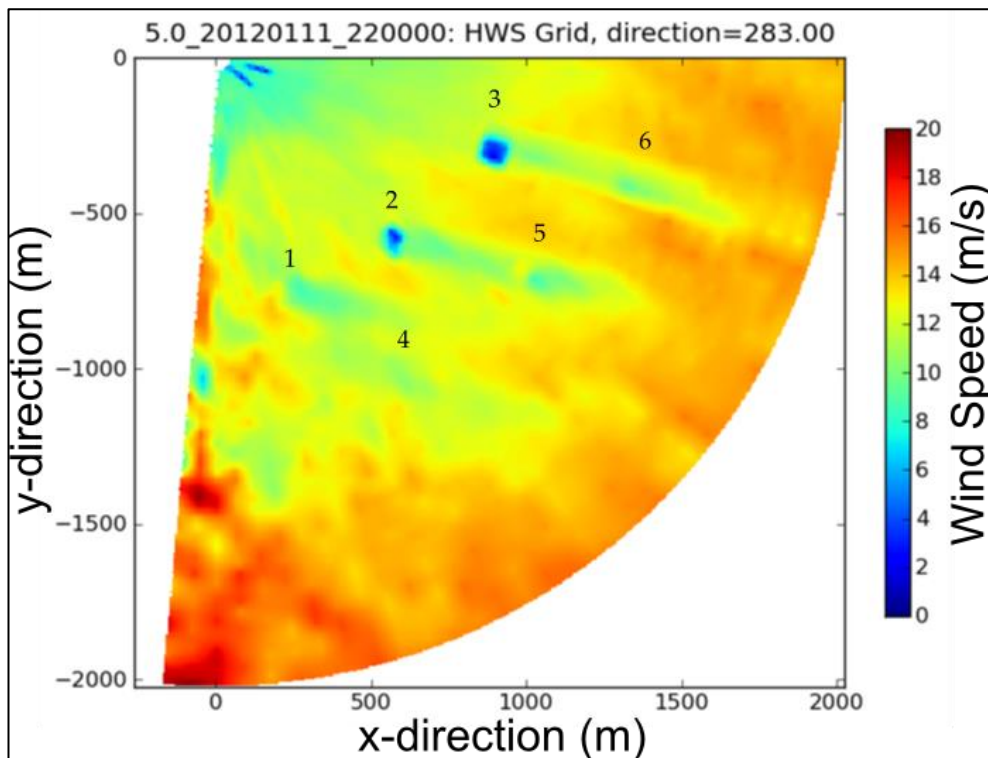


Figure 6.11: One hour averaged lidar scan

For both time periods the prevailing wind direction was approximately West to East with the breakdown of the wind speed and direction values extracted from each scan presented in Table 5.3. These values have been utilised in defining the inlets of the four numerical simulations. The inlet locations of the domain were chosen to allow the measured definition of the inlet values from either the time averaged arc scans or through the virtual met mast scanning second lidar device.

Where the methodology used requires that the inlet is located within the arc scan the inlet variables must accurately relate to the measurements at the scan point chosen as the inlet location. The domain inlet location is therefore identical to that of the scan point that the inlet wind speed is extracted from. The wind direction will come from the average direction measured by the lidar in the scan period. For the virtual met mast inputs the numerical domain inlet location is defined as the same x and y location as that used for

the arc scan inlets but at the same height as that at which the wind speed value is extracted from. The corresponding velocity and directions used must relate to the values measured during same period of time as the arc scan being considered. The domain definition for these simulations is presented in Table 5.2 with the inlet conditions for each one outlined in Table 5.3. All simulations assume a neutral boundary layer.

The flow orientations selected allow Turbine 1 to operate in a clear inflow and turbine free wake thus making it an ideal candidate for further analysis as there are no external factors affecting it. Utilising the same methodology for extracting wake centreline measurements from the averaged scans as used in the previous section the lidar measured data corresponding to the wake centreline for Turbine 1 can be extracted for each time period.

The lidar measured wake centreline measurements are presented in Figure 6.12, with the charts labelled to reflect the averaging periods and inlet definition method they relate to. Wind direction is from left to right with the turbine situated at zero on the x-axis. The charts show velocity on the y-axis against the absolute distance from the turbine rotor of the measurement point in diameters (90m) on the x-axis.

The numerical models in each image have been run based on the inlet conditions defined in Table 5.3. Each of these values have been measured during the same time period under study and are extracted from either the ARC scan data upstream of the device or the second virtual met mast scanning lidar. The heights defined for the inlet location are taken from the measurement height above the ground level.

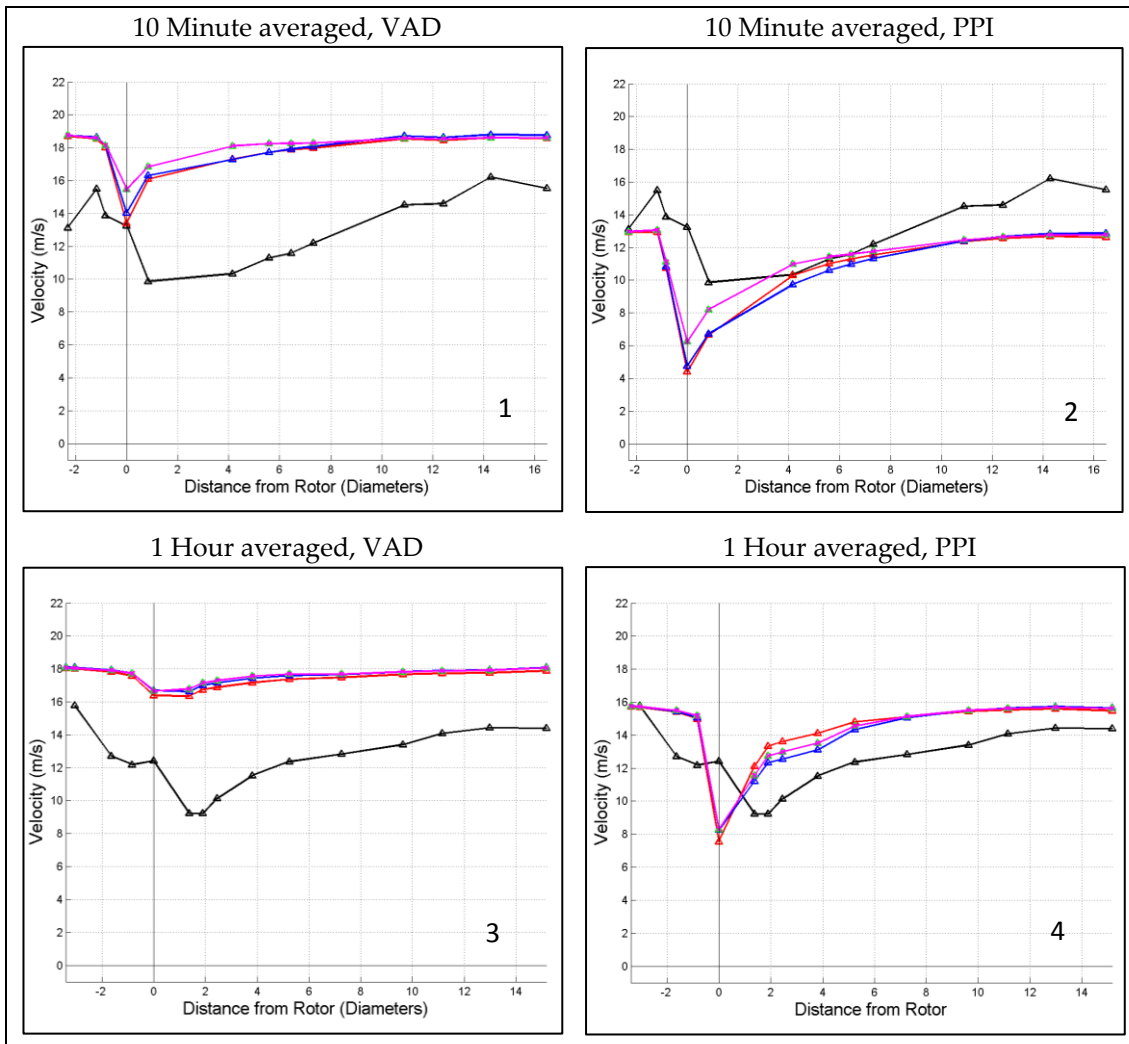
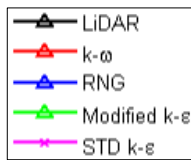


Figure 6.12: Turbine 1 wake centreline comparisons, multiple inlet definitions

The ten minute wake centreline profile presented in Image 1 and Image 2 in Figure 6.12 shows an immediate rise in wind speed from the inlet followed by a slowing down through the rotor plane to a minimum on the downstream side of the rotor. As the flow moves downstream it is seen to recover towards freestream with an initial shallow gradient increasing after 4 rotor diameters. The one hour averaged wake centreline profile in Image 3 and Image 4 in Figure 6.12 shows a decrease in wind speeds from the inlet

and through the rotor plane to minimum on the downstream site of the rotor. The downstream recovery towards freestream identifies a sharper initial gradient to the recovery that decreases with distance downstream. At the rotor plane there is a slight increase in measured velocity from that measured immediately upstream of it.

Using the exact locations of the scan points extracted for the lidar profiles the numerical simulation data can be extracted for comparison. The resultant numerical model profiles for each case are presented alongside the lidar data in Figure 6.12. The models again predict behaviour in keeping with that described in theory and presented in previous numerical analysis in Section 6.2.1 and Section 6.2.2. It is observed that the four turbulence models show similar behaviour patterns along the length of the wake with small variations in magnitude found in the recovery towards freestream. These are most prominent in the region up to eight rotor diameters downstream of the rotor.

6.3 Offshore results

6.3.1 Lidar measurement wake profile extraction

Wake centreline profile extraction

The procedures outlined in Chapter 4 allow for the extraction of wake centreline velocity profiles for each ten-minute data set captured from the Alpha Ventus [116] offshore wind farm. Custom Matlab [130] scripts developed for this project facilitate the production of the visualisation of this centreline velocity profile. An example of a measured wake centreline velocity evolution profile for a single averaged scan is presented in Figure 6.13.

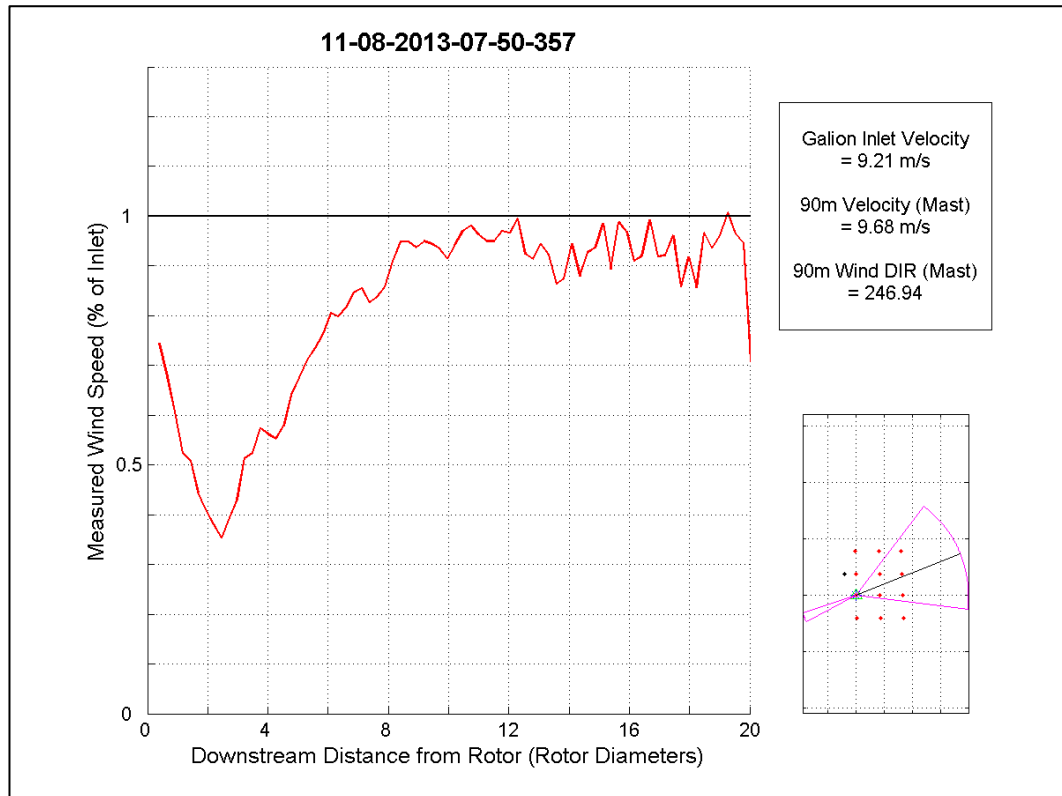


Figure 6.13: Single ten-minute average measured wake centreline velocity evolution

The red line in Figure 6.13 represents the measured data. The orientation of the turbine during the ten minute time period in comparison to the wide wind farm is presented in the image at the bottom right of Figure 6.13. At the

top right of Figure 6.13 the time correspondent lidar measured inlet velocity and mast measured velocity and direction are also identified.

The wake centreline data is plotted to show the magnitude of the velocity downstream from the rotor plane. The measured velocity data is presented as a percentage of the upstream lidar measured inlet velocity and the distance downstream of the rotor disk as a function of rotor diameter. The diameter of the studied turbine is 116m [120] in this case.

The overall trend described in Figure 6.13 and throughout the experiments follows a distinct pattern. An initial velocity drop from the inlet is evident at the rotor plane, evolving to a maximum deficit a number of diameters downstream in the near wake. Recovery towards inlet conditions is experienced; however this occurs well into the far wake behind the turbine. The results presented in Figure 6.13 however are not seen to prescribe a smooth and predictable trend but a more fluctuating profile around a predicted mean value.

Each ten minute averaged data set is binned according to the inlet wind speed and the inflow conditions. Plotting all of the data sets for a single 8-10m/s undisturbed inflow wind speed bin as detailed in Figure 6.14 highlights the extent of this fluctuation within each bin to be visualised. This level of fluctuation is evident in all of the wind speed bins analysed for each inflow condition. These bins are identified in Table 4.6.

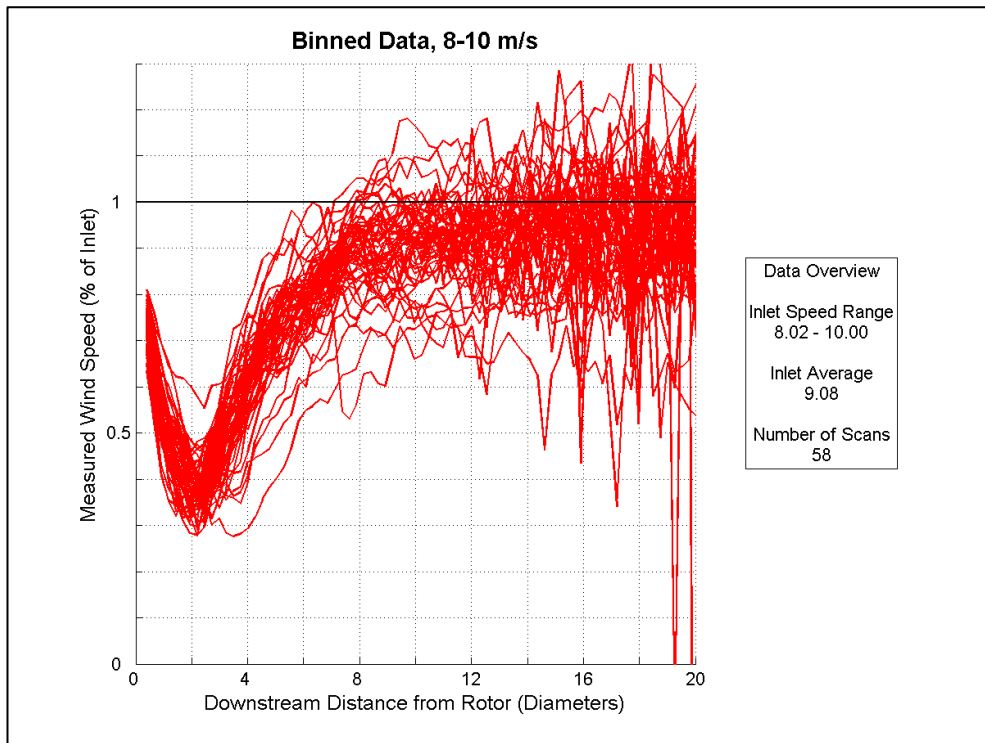


Figure 6.14: All centreline velocity profiles, 8-10m/s bin undisturbed inflow

In order to consider a more representative analysis of the wake centre line data each wind speed bin data set can be averaged for each distance downstream. The results as detailed in Figure 6.15 for the 8 - 10m/s bin show a more stable characteristic profile of wake flow behaviour for each of the bins and the three inflow characteristics. For each measurement position downstream the standard errors of the measurements around the mean can also be plotted using Equation 6.1, Figure 6.16.

$$\text{Standard Error of the Mean} = \frac{\sigma}{\sqrt{n}} \quad \text{Equation 6.1 [113]}$$

Where σ is the standard deviation of the measurements around the mean at the location downstream and n is the number of measurements at the same location.

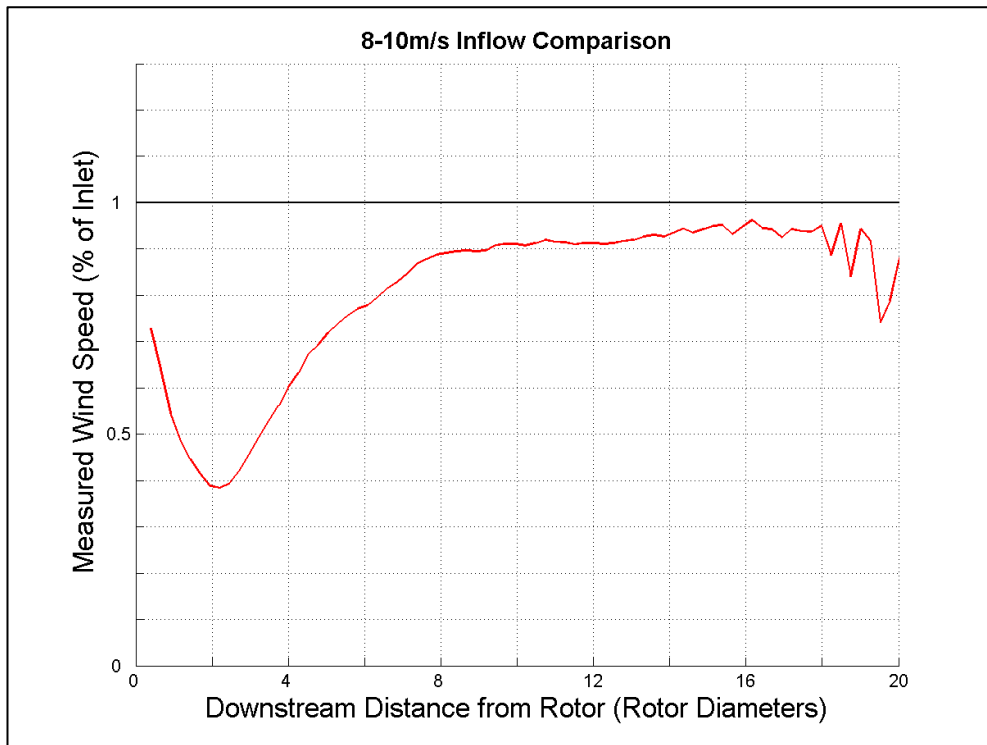


Figure 6.15: Averaged centreline measurements, 8-10m/s undisturbed inflow

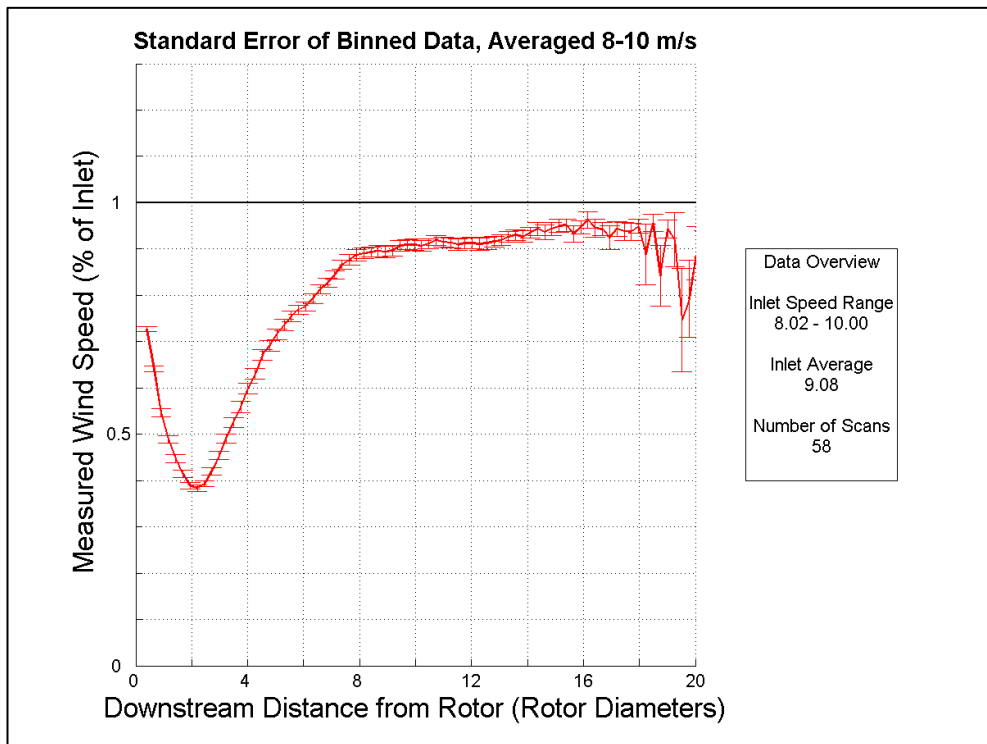


Figure 6.16: Standard error at each measurement point along wake centreline, 8-10m/s bin

The above process can be repeated for the three inflow conditions in a given wind speed bin to allow a direct comparison of the measured flow behaviours for each bin. The inflow condition comparative results for the 8-10m/s wind speed bin are presented in Figure 6.17; the thrust coefficient (C_t) in this speed range is between 0.827 and 0.831. The numbers of ten minute averaged data sets used in defining each binned wake profile are presented in the captions below each of the figures.

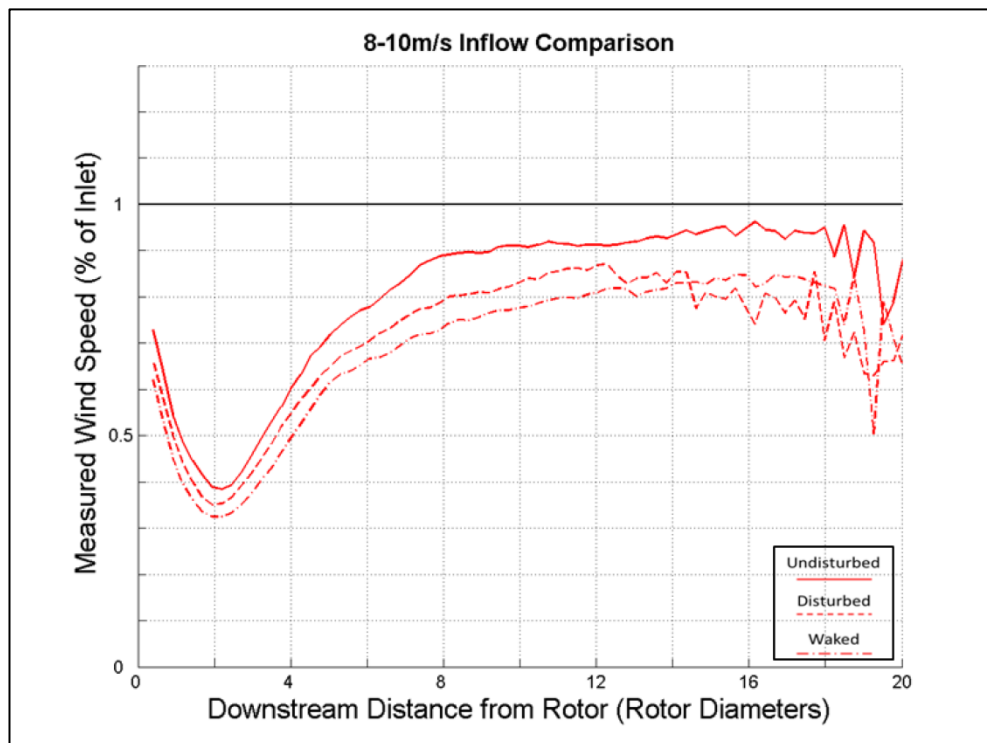


Figure 6.17: 8-10m/s wind speed bin inflow comparison, $C_t = 0.827 - 0.831$
 Undisturbed (Ave=8.9m/s, 149 profiles), Disturbed (Ave=9.1m/s, 57 profiles),
 Waked (Ave=8.9m/s, 26 profiles)

Wake width profile extraction

In contrast to the centreline analysis, where data is extracted from one azimuth only, wake width analysis can be considered by looking at data corresponding to multiple azimuths in an arc across the measured flow at discrete distances along the length of the wake. The resultant measurements can be plotted to show the velocity evolution out from the wake centreline in the horizontal plane. Selecting points equidistant along the wake centreline the evolution of the wake width with distance from the rotor plane can be plotted; Figure 6.18 details the measurements for a single scan.

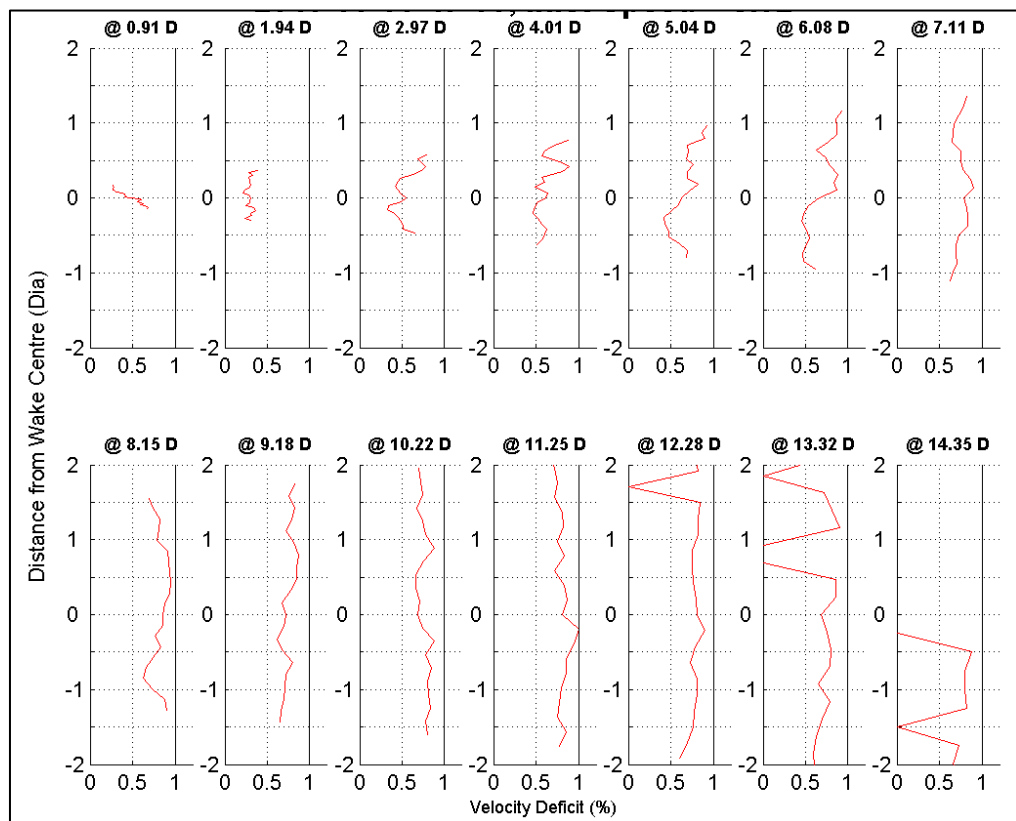


Figure 6.18: Lidar measured single scan wake width profiles, disturbed inflow

Data sets for width analysis require high resolution measurements across the wake. From the scan envelopes identified in Table 4.4 only the data set utilising a 1° beam separation provides sufficient resolution to complete this analysis. The envelope identified incorporates a 60° scan back and forth

across the wake centred on the turbine centreline. As the period of this scan exceeds ten minutes averaging the data over ten minutes, as in the centreline analysis data, does not produce a true average as in some cases only one data value at each location is available. As a result the width data sets are not averaged over ten minutes before they are binned; the single scans on their own therefore show a larger variation in measured behaviour with a less defined profile, Figure 6.18. At farther distances from the device the intensity quality of the data points begins to drop causing incomplete wake width profiles. Repeating the same averaging process across the points and bins as completed in the centreline analysis a more complete profile across the results appears. The wake width profile plot for the 8 – 10m/s wind speed bin under disturbed inflow conditions is presented in Figure 6.19 with the number of individual samples used to create the average profile identified in Table 4.7. The full analysis across the speed range captured is presented in Section 6.3.4.

Due to the scan configurations utilised, and the ambient wind conditions when the width profile measurements were captured, only data sets corresponding to width evolution during disturbed inflow conditions have been captured.

For the measurement locations closer to the device data is not available across the full rotor diameter and the width profiles cannot be completed, this is as a consequence of the scan envelopes implemented. The width plot at distances greater than 2.97 rotor diameters show measurements across the full rotor diameter and beyond.

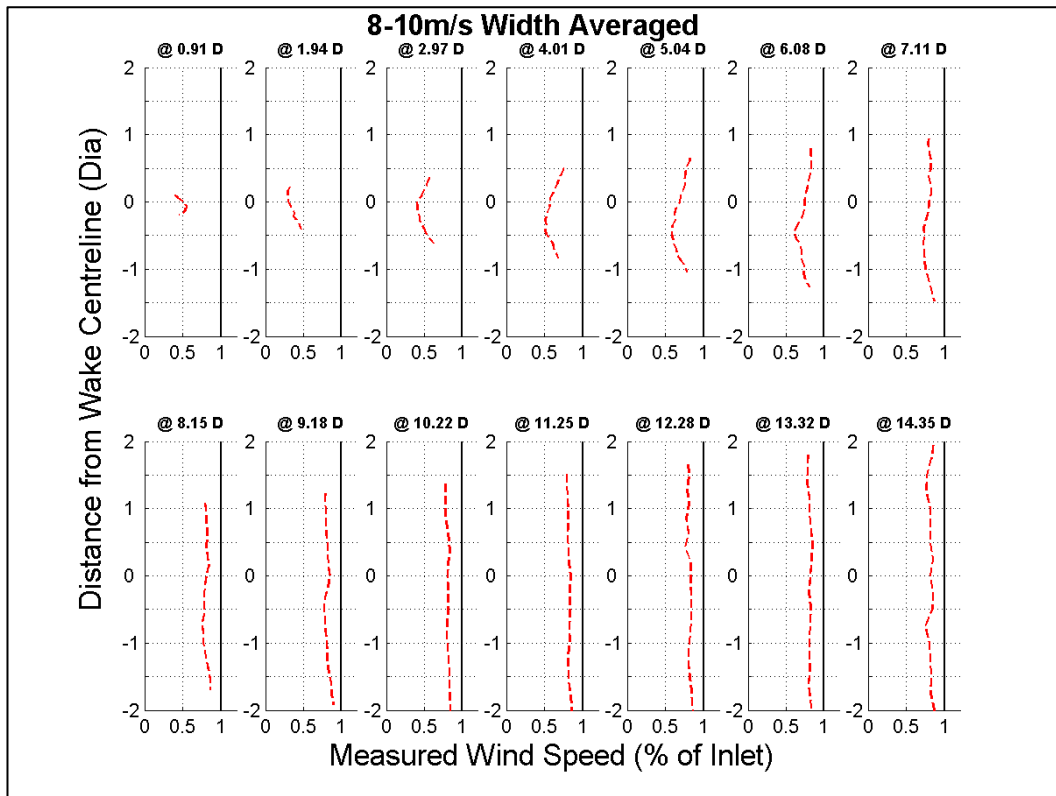


Figure 6.19: Lidar measured wake width averages, 8 – 10m/s wind speed bin, disturbed inflow, $C_t = 0.827 - 0.831$, Ave = 8.8m/s, 20 profiles

6.3.2 Lidar measured wake centreline profiles

The Alpha Ventus deployment has allowed the capture of unique data sets presenting wake flow behaviour from an active offshore wind farm. The captured profiles show wind speed measurements along the wake centreline up to 20 rotor diameters downstream at 30m intervals. The deployment duration has also allowed for wake profile capture across the wide range of wind vector operational conditions experienced by the turbine as well as the opportunity to capture some key wake phenomenon. Analysis of the centreline measurements for the three inflow conditions reveals a number of interesting and challenging observations.

Following the process outlined in Section 6.3.1 the evolution of the centreline velocity profiles for each of the wind speed bins (subject to the availability of data for all three inflow conditions) between 6m/s and 14m/s can be presented. The average inlet speed and the number of scans under each condition are detailed in the Figure captions.

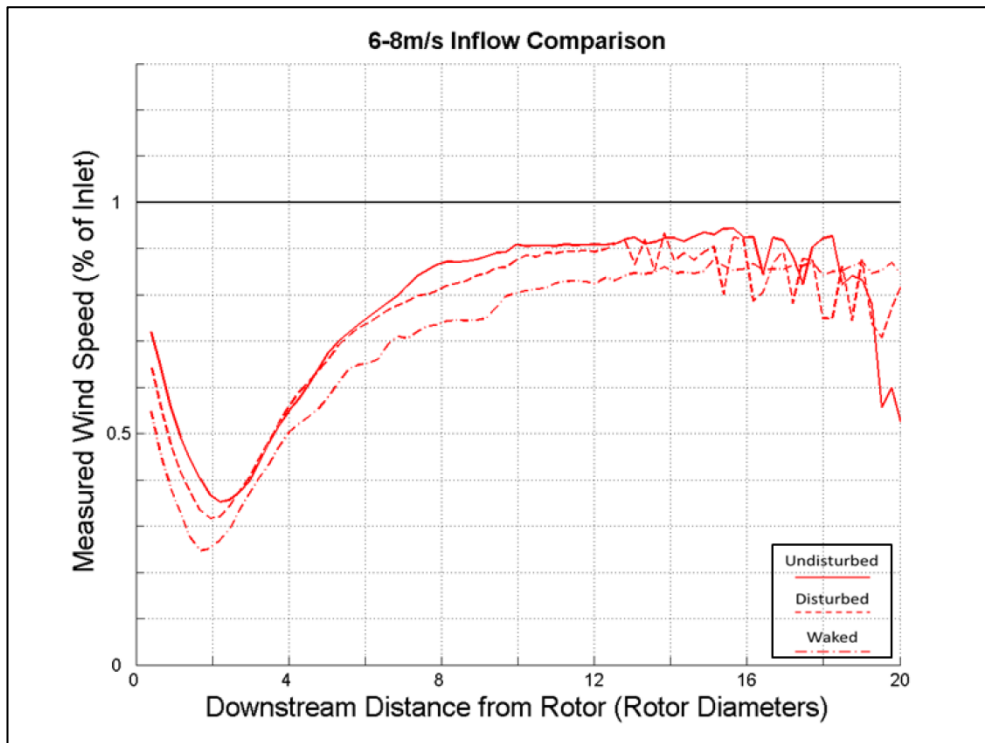


Figure 6.20: 6-8m/s wind speed bin inflow condition comparison, $C_p = 0.326-0.447$
 Undisturbed (Ave=7.1m/s, 93 profiles), Disturbed (Ave=7m/s, 57 profiles),
 Waked (Ave=7.1m/s, 7 profiles)

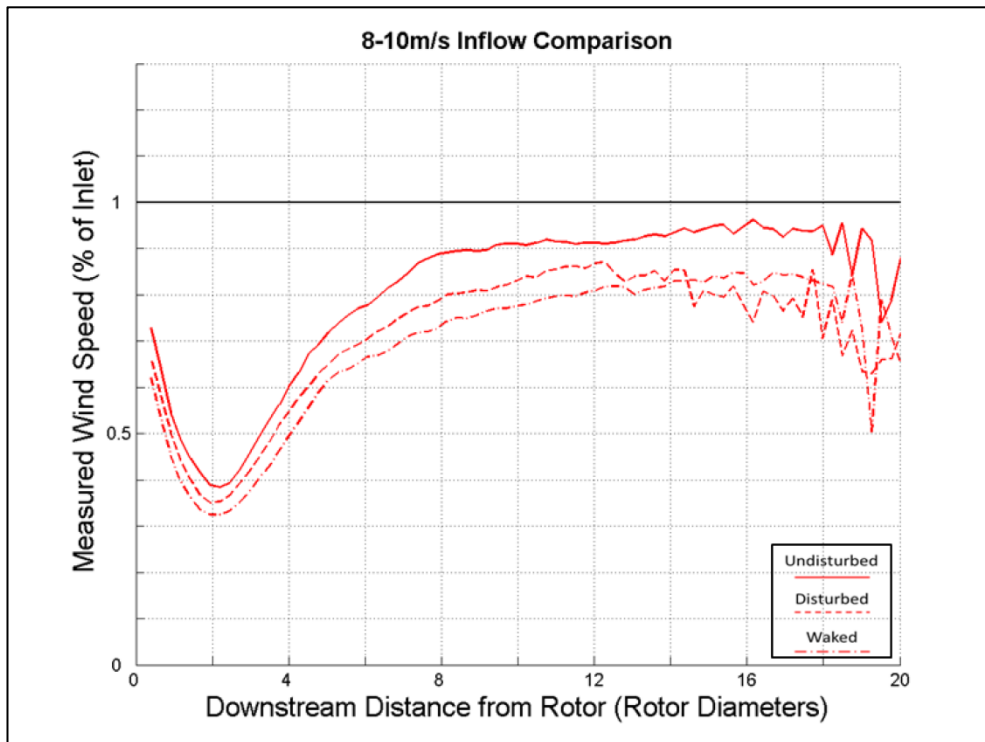


Figure 6.21: 8-10m/s wind speed bin inflow comparison, $C_p = 0.447-0.472$
 Undisturbed (Ave=8.9m/s, 149 profiles), Disturbed (Ave=9.1m/s, 57 profiles),
 Waked (Ave=8.9m/s, 26 profiles)

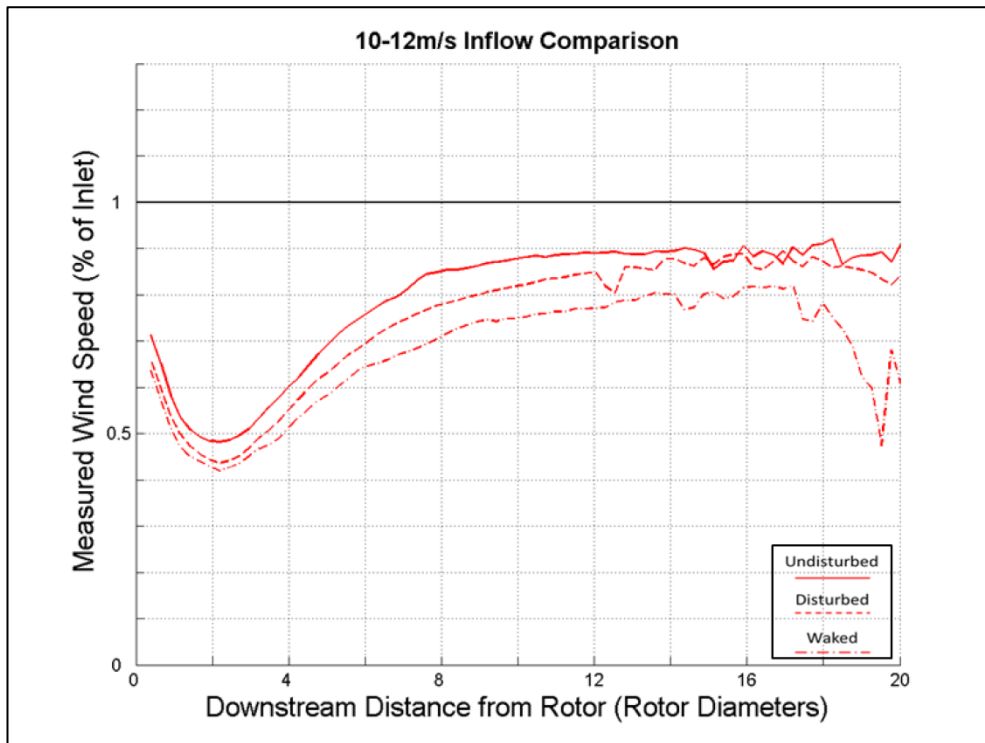


Figure 6.22: 10-12m/s wind speed bin inflow condition comparison, $C_P = 0.472-0.423$
 Undisturbed (Ave=11.1m/s, 192 profiles), Disturbed (Ave=11.1m/s, 133 profiles),
 Waked (Ave=11.1m/s, 44 profiles)

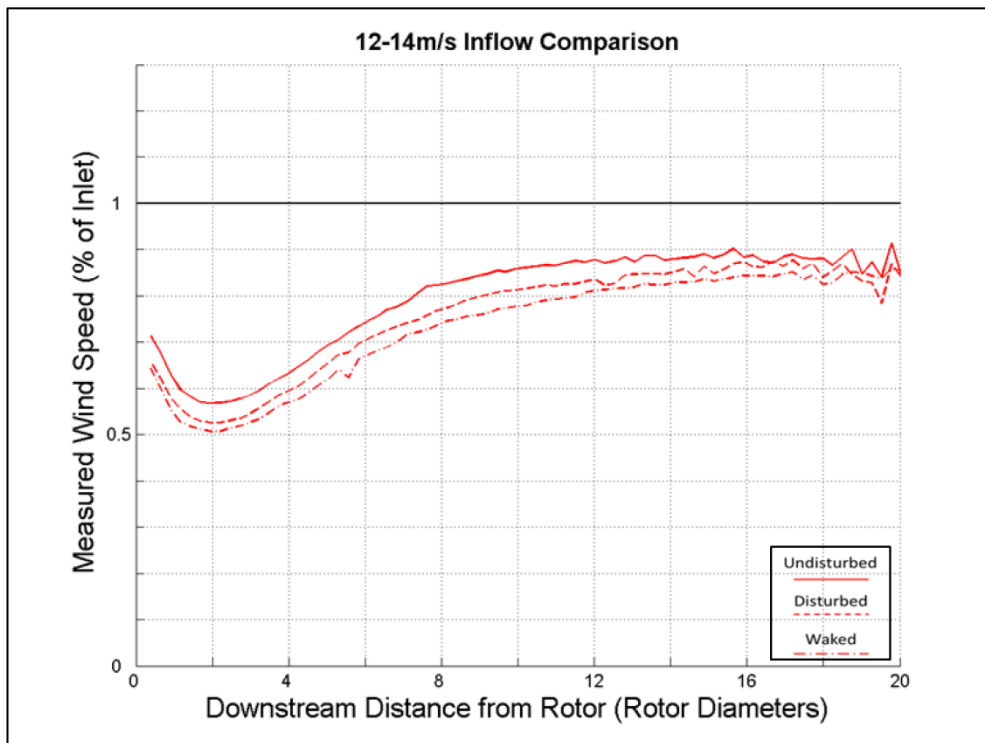


Figure 6.23: 12-14m/s wind speed bin inflow condition comparison, $C_P = 0.423-0.281$
 Undisturbed (Ave=13m/s, 151 profiles), Disturbed (Ave=12.6m/s, 43 profiles),
 Waked (Ave=12.9m/s, 39 profiles)



Figure 6.24: 14-16m/s wind speed bin inflow condition comparison, $C_p = 0.281-0.189$
 Undisturbed (Ave=15m/s, 80 profiles), Disturbed (Ave=14.5.6m/s, 2 profiles),
 Waked (Ave=15.1m/s, 30 profiles)

Considering the wake centre line velocity deficit and downstream evolution, presented in Figure 6.20 - Figure 6.24 a clear pattern of behaviour is evident. As the air flow approaches and passes through the rotor plane a significant velocity deficit is experienced in the downstream flow observed as a velocity drop from inlet windspeed after the turbine rotor. The value of this velocity deficit is of the order of magnitude of approximately 30% deficit from the inlet value for most of the speed ranges studied, 35% for the disturbed inflow and close to 38% for the fully waked inflow.

For lower inlet wind speeds there is a further velocity reduction behind the rotor. The position of this maximum deficit occurs at around two rotor diameters downstream for the 6-8m/s wind speed bin, Figure 6.20. This distance is consistent across each of the wind speed bins up to 12m/s. At wind speeds above this value the wake profile in the initial three rotor

diameters downstream is essentially flat at the same initial deficit value as measured at the downstream side of the rotor plane. The average wind speed for the site falls into the 8-10m/s wind speed bin [116] Figure 6.21, where the maximum velocity deficit is found to be around 40% of the inlet values at a distance of two rotor diameters downstream.

The recovery from the maximum deficit value in the lower wind speed bins exhibits a steeper high gradient recovery in the initial stages before levelling out to a more gradual low gradient trend towards inlet values, Figure 6.20 – Figure 6.24. This trend continues until the 14–16m/s wind speed bin, Figure 6.24, where the recovery is more consistent along the length of the wake measured. The overall behaviours described are consistent between the undisturbed, disturbed and waked inlet conditions across the wind speed bins up to thirteen rotor diameters.

While the overall profile is similar for the undisturbed inlet measurements in each wind speed bin compared to the other inflow situations there are subtle differences between the profiles. In the wake measurements presented in Figure 6.20 – Figure 6.24 it appears that the initial and maximum deficit values are very closely matched for all of the flow situations, with the initial and maximum deficit values increasing from the undisturbed to disturbed inflow by approximately 5% and again to the waked inflow by approximately 3%. Beyond the maximum deficit point however the gradient of the initial recovery phase shows minor yet consistent differences between the inflow situations. For the disturbed inflow the gradient of this initial recovery is less than the undisturbed inflow situation leading to lower experienced wind speeds in the recovery stage, this in turn leads to a larger radius to the recovery curve as the gradient decreases towards a more flat profile into the far wake. This behaviour deficit is repeated in the disturbed

to waked inflow situations. For the four wind speed bins between 6m/s and 14m/s, Figure 6.20 – Figure 6.24, this behaviour is consistent for the three inflow situations, except in the 6–8m/s bin, Figure 6.20, where the disturbed recovery gradient is initially identical to that of the undisturbed situation before tailing off later in the recovery. In the 14-16m/s wind speed bin, Figure 6.24, the waked and disturbed inflow situations present near identical behaviour along the wake centreline. The undisturbed inflow case in this bin presents a lower initial deficit that is preserved until around five rotor diameters when the three profiles gradually begin to converge, eventually doing so around twelve rotor diameters downstream.

Beyond fourteen rotor diameters the averaged velocity profiles for all three inflow conditions in Figure 6.20 – Figure 6.24 begin to exhibit a higher degree of variance and mean error. This is particularly evident in the 14-16m/s wind speed bin presented in Figure 6.24 with large variations evident between the three inlet conditions. This behaviour is as a result of a reduction in the quality and consistency of the back scattered results captured by the lidar in each scan. This can be interpreted as an increase in the uncertainties associated with the measurements beyond this point, the greater variability in results increasing the associated uncertainty at each point. As a result it is not possible to draw conclusions about the wake behaviour from the lidar measurements beyond fourteen rotor diameters.

6.3.3 Numerical wake centreline comparison results

The analysis with the three numerical models is completed by repeating the processes outlined in Chapter 5 for nacelle mounted model comparison. The comparisons presented below in Figure 6.25 - Figure 6.29 present the numerical predictions for the PARK [80] and Eddy-Viscosity [84] models along with the SST closure model. In each wind speed bin the models are setup using the averaged inlet wind speed of the measurements in the bin for the undisturbed flow situation. As covered in Section 5.3 the Eddy-Viscosity and PARK models used create wake flow predictions for a single turbine operating in undisturbed flow, the SST model has been simulated under the same principles in order to allow a consistent comparison between the models. In addition no effort has been made to tailor the models to the three separate inlet conditions by varying the turbulence or surface roughness values associated with each model. These values stay constant with a Turbulence Intensity (T.I.) 6%, a surface roughness (z_0) of 0.0002 and a wake decay constant of 0.038. The inlet wind speeds for each of the simulations have been defined as the average of the Undisturbed wind speeds presented in the captions of each Figure below.

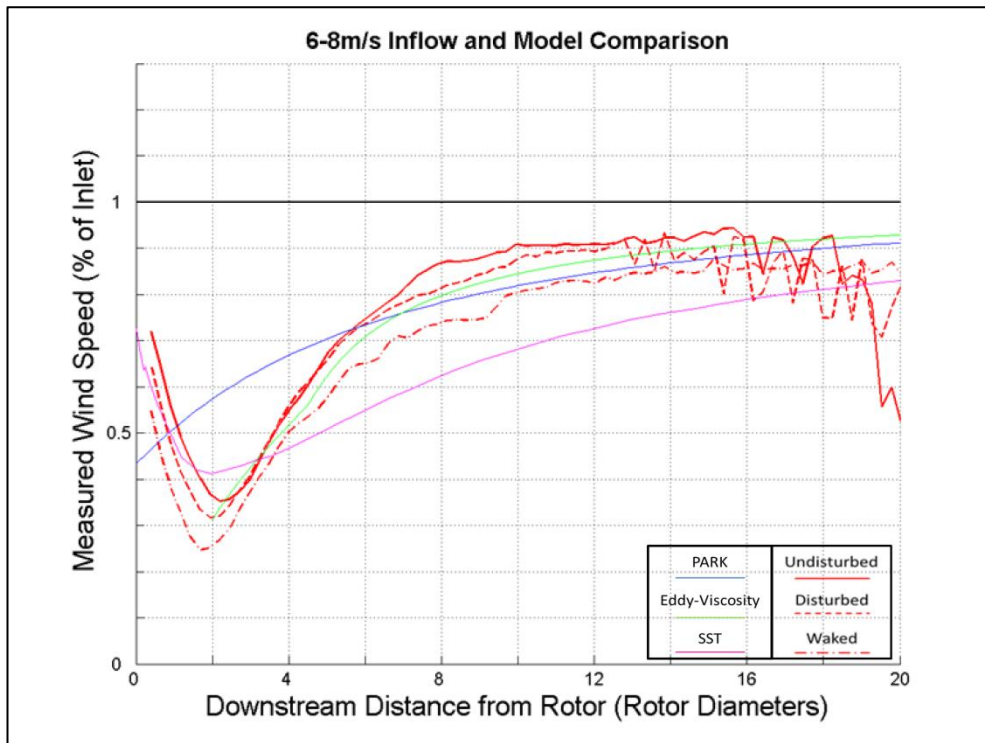


Figure 6.25: 6-8m/s wind speed bin inflow and model comparison, $C_P = 0.326-0.447$
 Undisturbed (Ave=7.1m/s, 93 profiles), Disturbed (Ave=7m/s, 57 profiles),
 Waked (Ave=7.1m/s, 7 profiles)

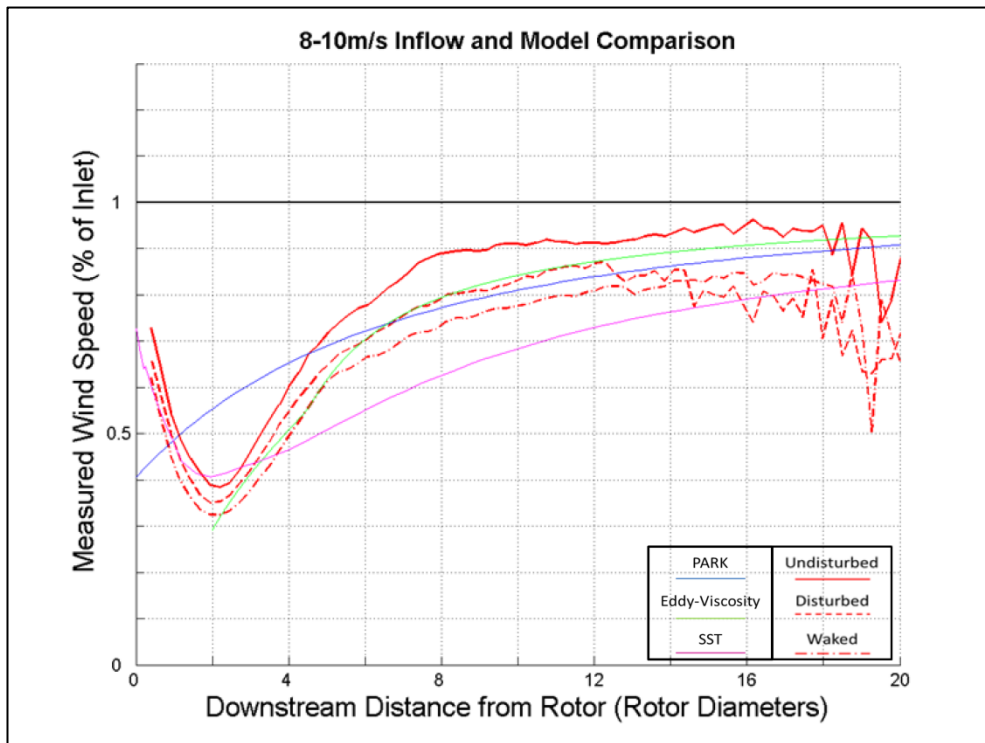


Figure 6.26: 8-10m/s wind speed bin inflow and model comparison, $C_P = 0.447-0.472$
 Undisturbed (Ave=8.9m/s, 149 profiles), Disturbed (Ave=9.1m/s, 57 profiles),
 Waked (Ave=8.9m/s, 26 profiles)

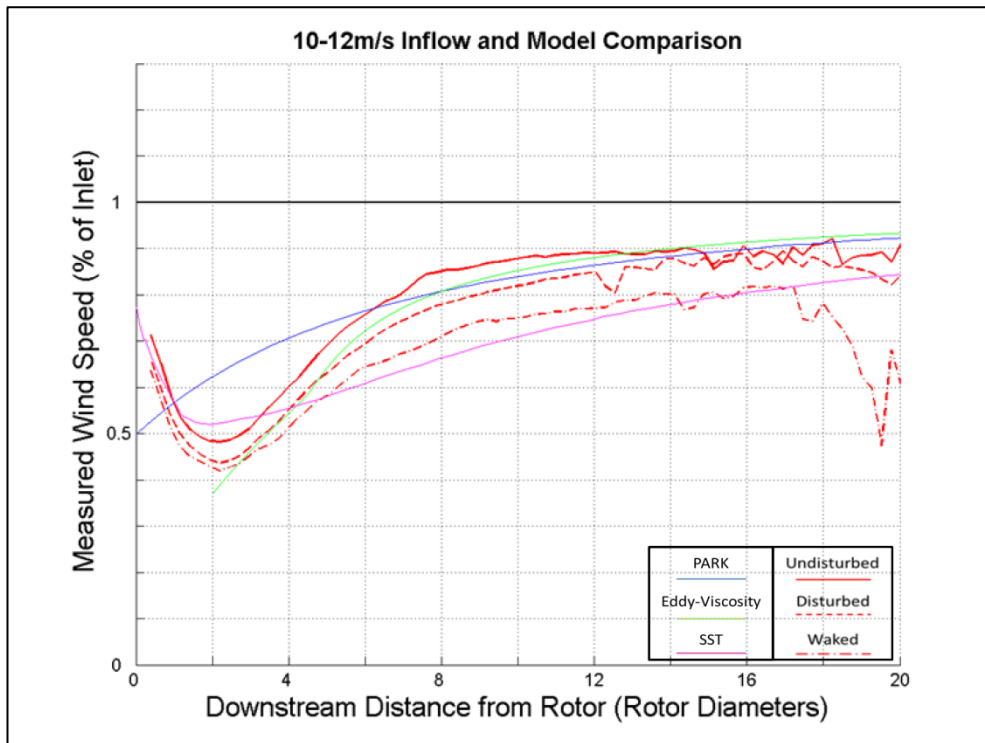


Figure 6.27: 10-12m/s wind speed bin inflow and model comparison, $C_p = 0.472-0.423$
 Undisturbed (Ave=11.1m/s, 192 profiles), Disturbed (Ave=11.1m/s, 133 profiles),
 Waked (Ave=11.1m/s, 44 profiles)

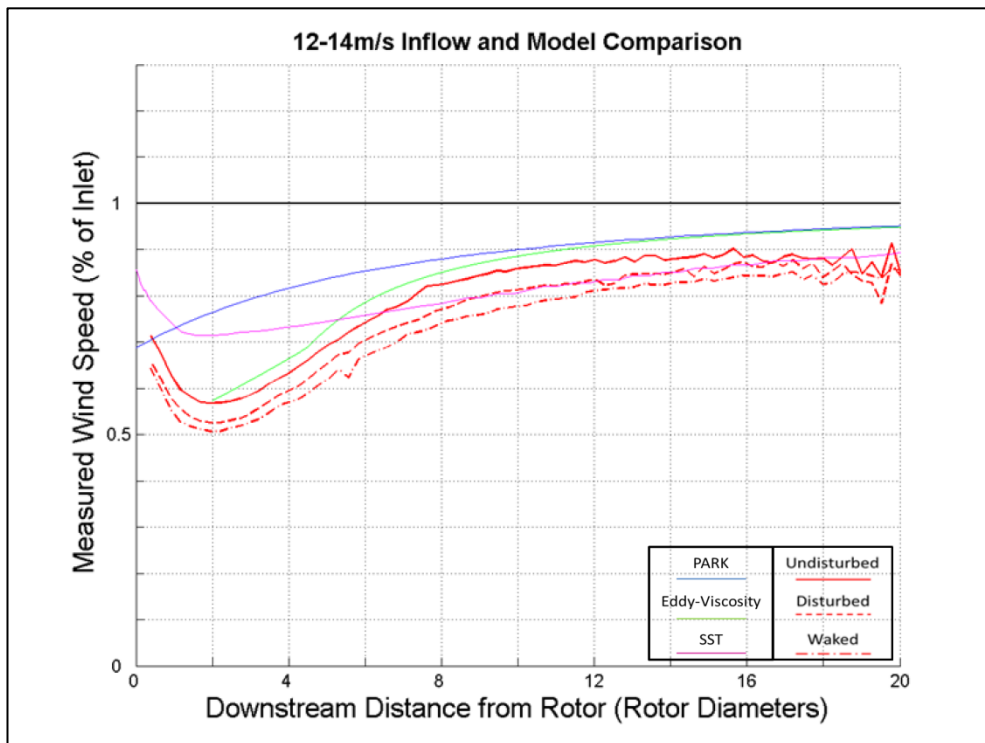


Figure 6.28: 12-14m/s wind speed bin inflow and model comparison, $C_p = 0.423-0.281$
 Undisturbed (Ave=13m/s, 151 profiles), Disturbed (Ave=12.6m/s, 43 profiles),
 Waked (Ave=12.9m/s, 39 profiles)

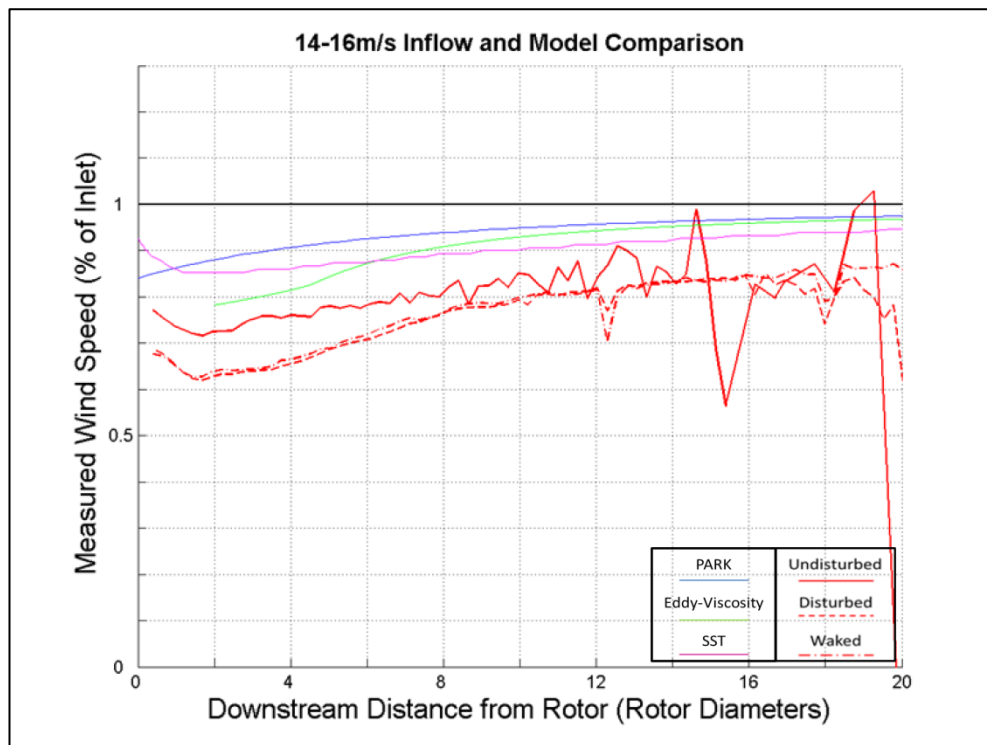


Figure 6.29: 14-16m/s wind speed bin inflow and model comparison, $C_p = 0.281-0.189$
 Undisturbed (Ave=15m/s, 80 profiles), Disturbed (Ave=14.56m/s, 2 profiles),
 Waked (Ave=15.1m/s, 30 profiles)

The numerical model velocity profiles can also be analysed by initial flow phase and wake recovery phases as in those identified in the lidar measurements in Section 6.3.2.

The behaviour of the initial flow phase in the models present in Figure 6.25 – Figure 6.29 can be described in two ways depending on the models. The PARK and Eddy-Viscosity models both initiate with an initial velocity deficit value driven primarily by the inlet wind speed or the corresponding thrust coefficient respectively. Both simulations predict the largest deficit at the model initiation before a recovery towards inlet velocity. The location of initiation in the PARK model is at the rotor plane, while the Eddy-Viscosity setup initialises the model at a distance of two rotor diameters downstream. In both models the maximum deficit from inlet values decreases in magnitude as wind speed increases. The SST model behaviour has been

extracted from the three dimensional simulation domain identified in Section 5.3.1. The extracted wake centreline profile therefore details flow moving from the rotor plane and is seen to closely track the captured lidar profile behaviour with an initial deficit moving towards a maximum deficit. The initial deficit value of close to 30% for lower wind speeds evolves to a maximum deficit at approximately 1.5 rotor diameters downstream. As in the measurements the initial 30% deficit starts to reduce as wind speed increases above 12m/s.

In each of the models presented in Figures 6.25 – 6.29 the wake recovery phase has a high gradient profile that gradually decreases with distance from the maximum deficit location. The PARK model recovery begins immediately at the rotor plane exhibiting an initial high gradient recovery that continually reduces into the far wake. The Eddy-Viscosity approach has a higher still initial recovery gradient at its initiation at two rotor diameters downstream, this initial gradient profile remains mainly constant, with a slight kink, through the initial stages of the model before tailing off into a lower recovery gradient in the far wake. The slight kink in the recovery profile of the Eddy-Viscosity model results from a change in the definition of the Filter Function at 5.5 rotor diameters; this is outlined in Equation 2.6. By contrast the SST model has a shallower initial recovery gradient than the other models or experiments leading to a significant under prediction of velocities in the wake recovery phase. For wind speeds up to 12m/s the SST predicted recovery reaches the values measured by the lidar beyond sixteen rotor diameters. At lower wind speeds the recovery gradients decrease further into the wake while for higher wind speeds the recovery gradient remains constant in the plotted results.

6.3.4 Lidar measured wake width profiles

Following the processes outlined in Section 6.3.1 wake width profiles can be plotted. The analysis has been completed for each of the wind speed bins in which data was available. In order to provide a high quality measurement of the width profile it is necessary to use data sets with 1° separation between the azimuths of the scan arc implemented. As a result only data from the second scan arc identified in Table 4.4 can be used. Due to the wind directions experienced during the implementation of this scan arc only data relating to the Disturbed inflow condition was captured. These profiles are considered at fourteen distances downstream of the rotor plane in Figure 6.30 – Figure 6.38. The average inlet wind speed and the number of scans captured in each bin are presented in each of the figure captions.

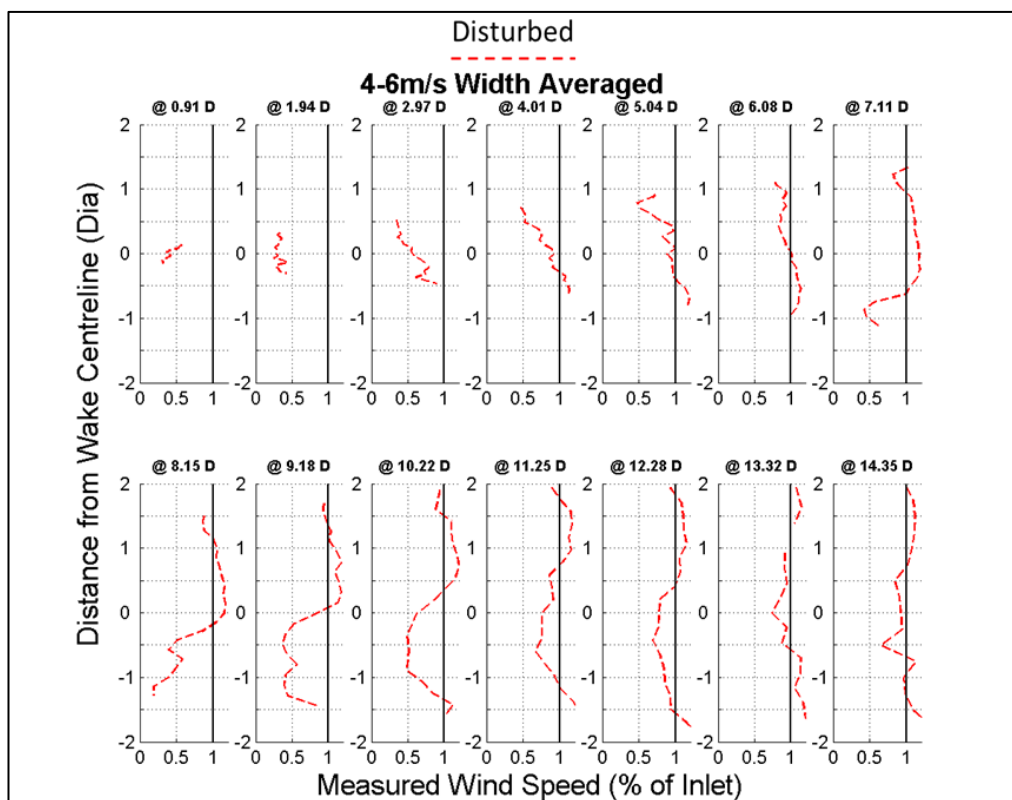


Figure 6.30: 4-6m/s wake width profiles, disturbed inflow, $C_p = 0.200 - 0.326$
(Ave=4.5m/s, 1 profile)

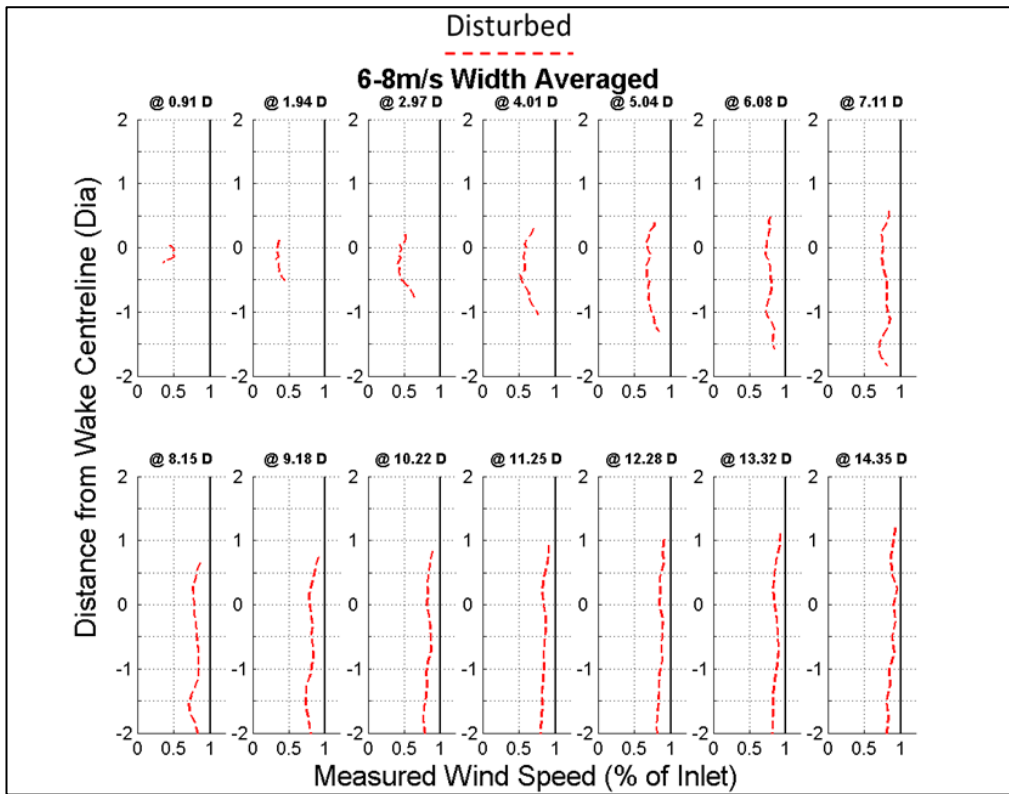


Figure 6.31: 6-8m/s wake width profiles, disturbed inflow, $C_p = 0.326 - 0.447$
(Ave=7.1m/s, 9 profiles)

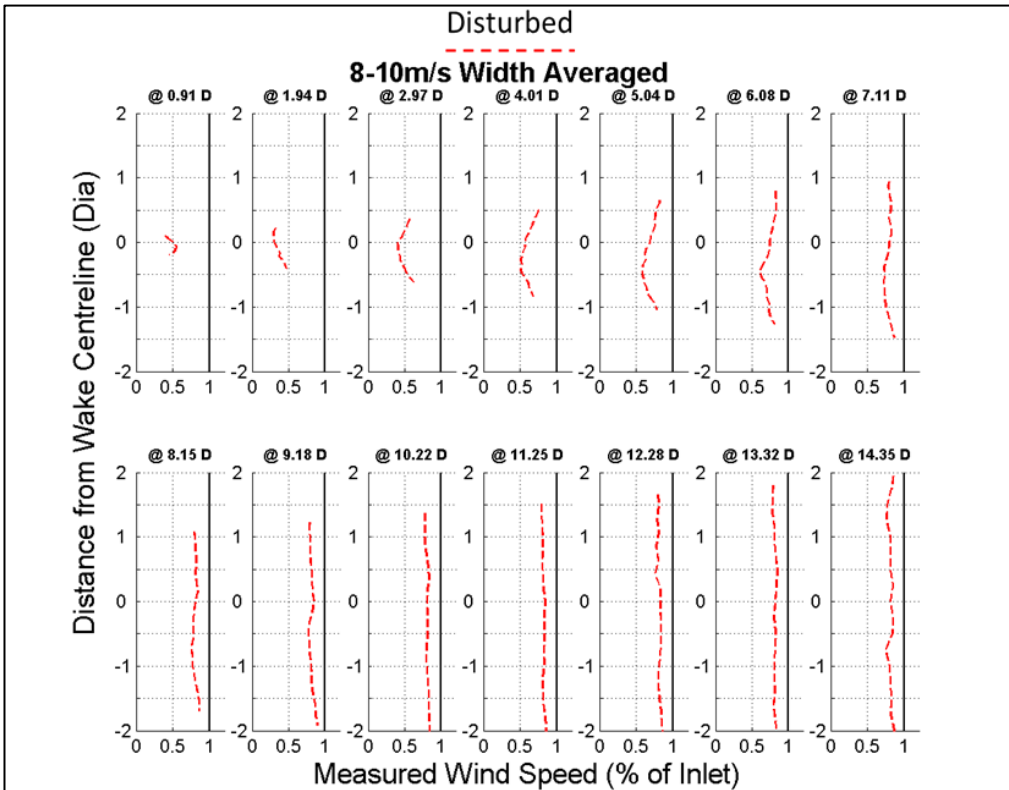


Figure 6.32: 8-10m/s wake width profiles, disturbed inflow, $C_p = 0.447 - 0.472$
(Ave=8.8m/s, 20 profiles)

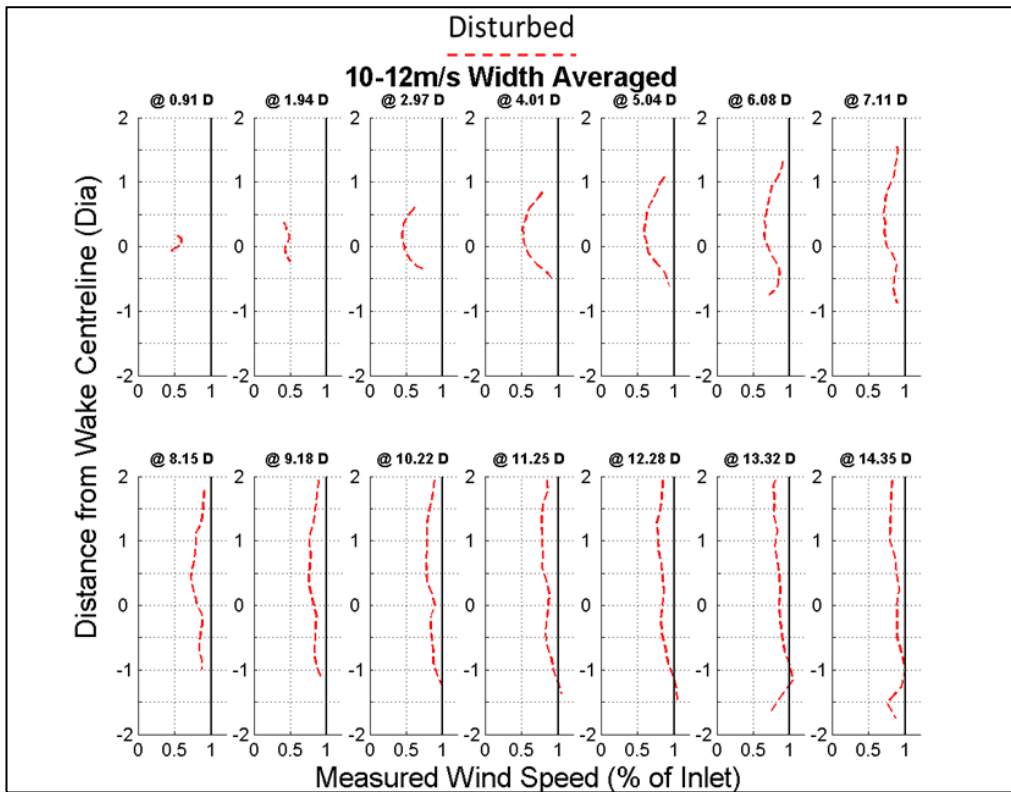


Figure 6.33: 10-12m/s wake width profiles, disturbed inflow, $C_p = 0.472 - 0.423$
(Ave=10.7m/s, 19 profiles)

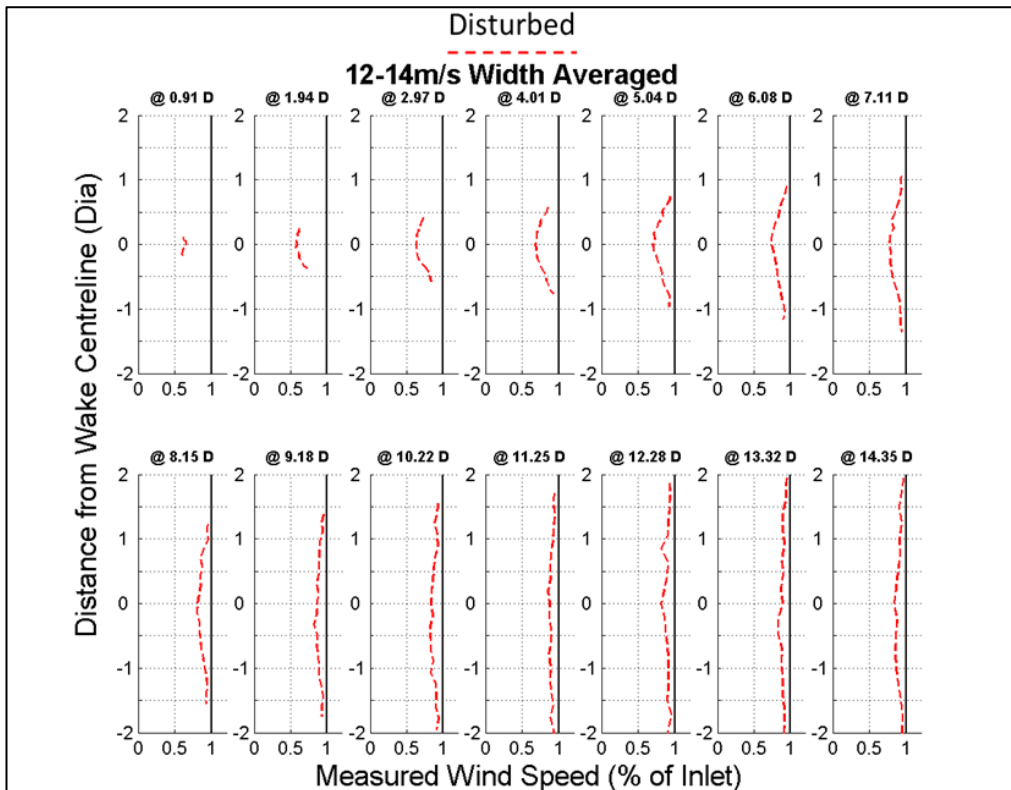


Figure 6.34: 12-14m/s wake width profiles, disturbed inflow, $C_p = 0.423 - 0.281$
(Ave=13.3m/s, 10 profiles)

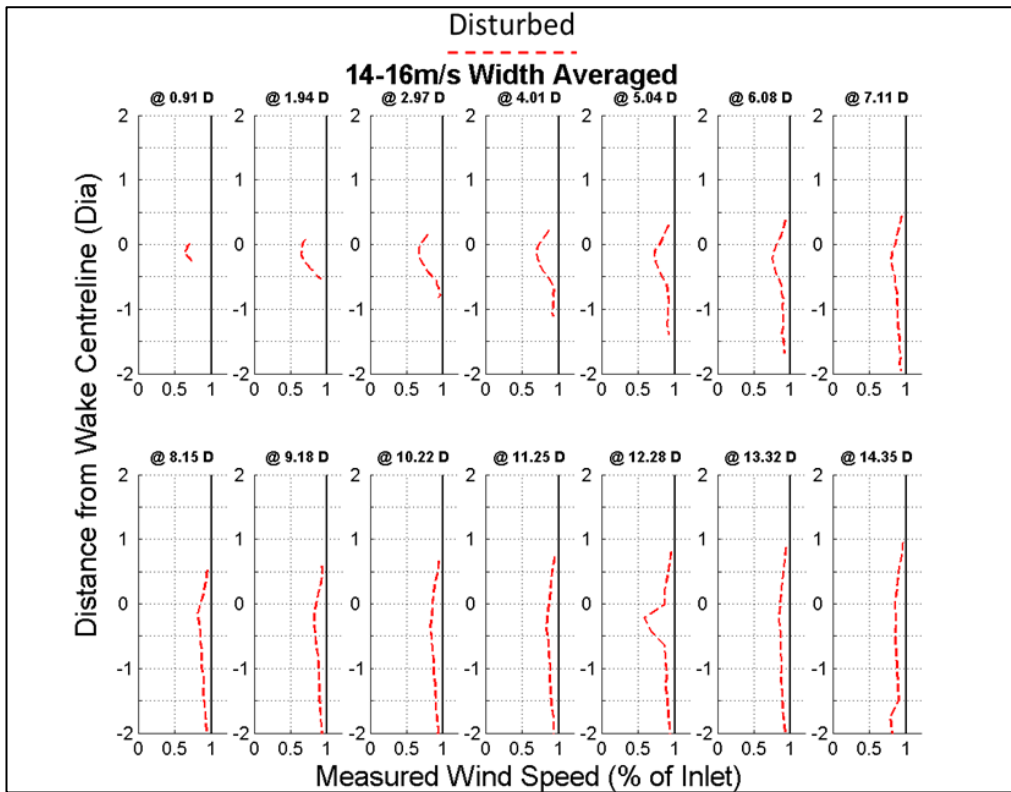


Figure 6.35: 14-16m/s wake width profiles, disturbed inflow, $C_p = 0.281 - 0.189$
(Ave=15.2m/s, 20 profiles)

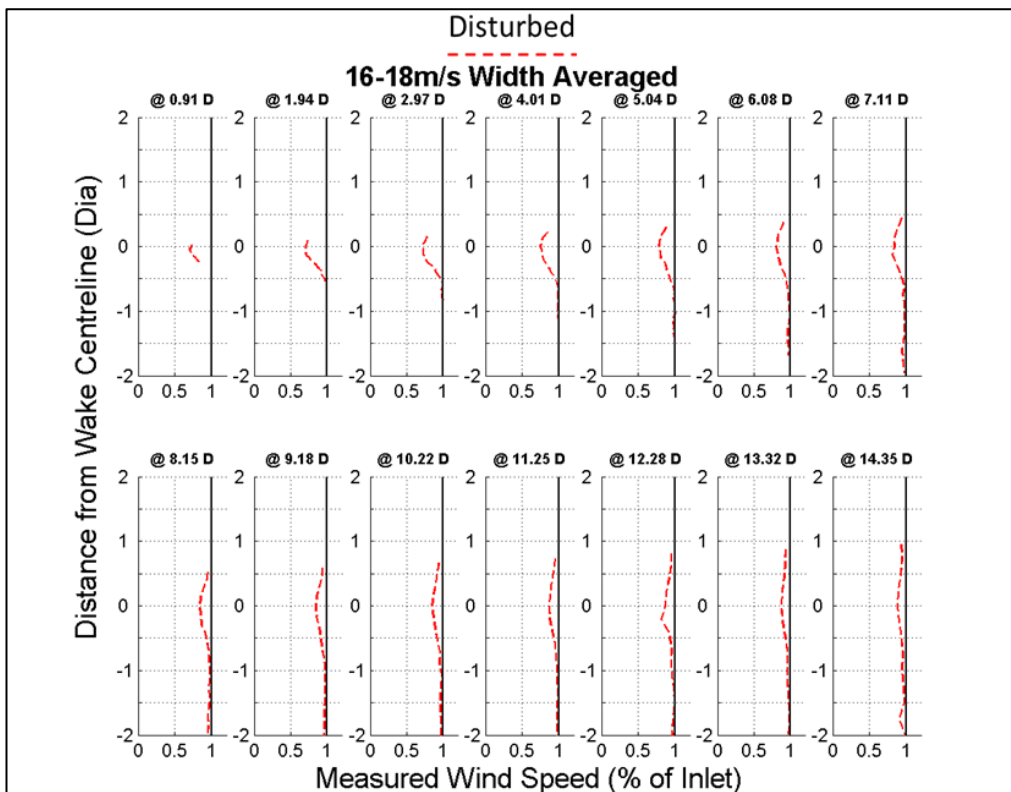


Figure 6.36: 16-18m/s wake width profiles, disturbed inflow, $C_p = 0.189 - 0.132$
(Ave=16.8m/s, 17 profiles)

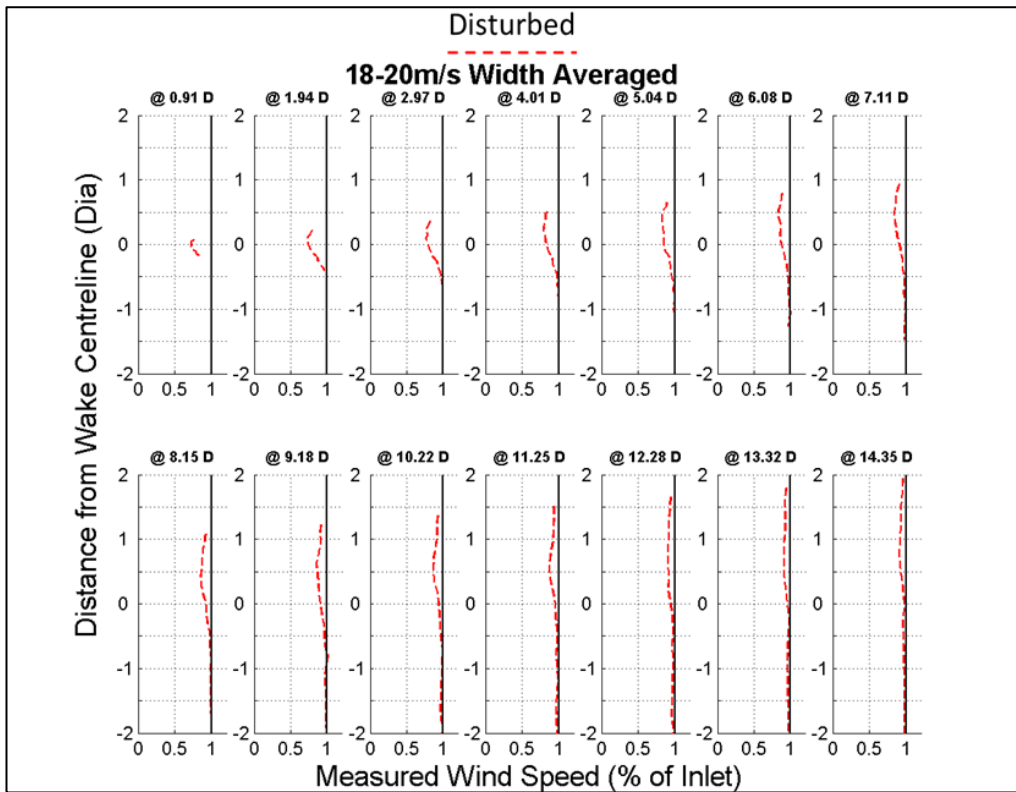


Figure 6.37: 18-20m/s wake width profiles, disturbed inflow, $C_P = 0.132 - 0.097$
(Ave=19m/s, 14 profiles)

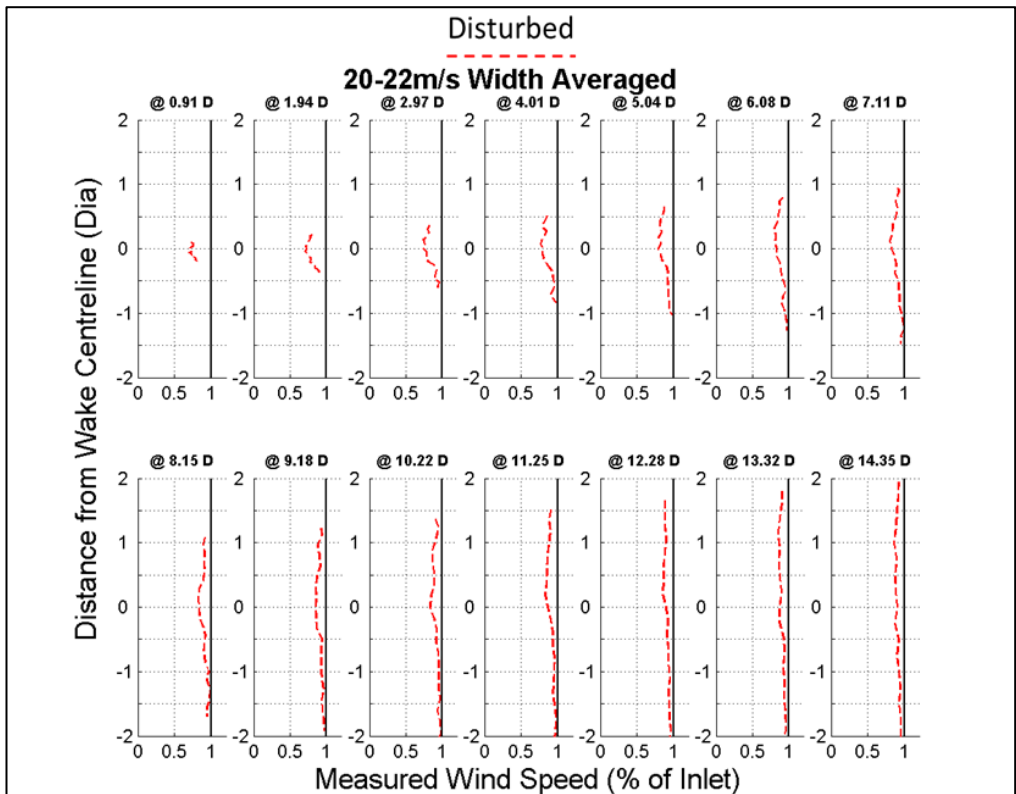


Figure 6.38: 20-22m/s wake width profiles, disturbed inflow, $C_P = 0.097 - 0.073$
(Ave=20.3m/s, 3 profiles)

The presentation of wake width analysis in Figure 6.30 – Figure 6.38 facilitates greater understanding of the dimensions of the wake structure, in particular how much the velocity deficit spreads into the surrounding flow. The width profiles presented in Section 6.7.1 detail the evolution of the width measurements across the wind speed bins, for a separation between cross wake profiles of 1.04 rotor diameters. This distance is fixed by the device optics and the measurement methodology employed, Table 2.2.

In each of the data sets presented in Figure 6.30 – Figure 6.38 it is clear that measurements closer to the lidar, below 2.97 diameters downstream, do not exceed the dimensions of the rotor. As a result it is difficult to derive much meaning from these as they do not represent data captured across the full width of the wake. Above 2.97 rotor diameters however a more pronounced profile is evident in each image. Between the 2.97 and 7.11 rotor diameter ranges a pronounced arc to the measurements can be seen close to the wake centre line at 0 on the y-axis. The peak of this curve signifies a maximum wind speed deficit at each distance on, or close to the centreline. This deficit recovers towards the inlet velocity close to the bounds of the wake and with distance from the rotor. As would be expected from the results obtained in the centreline results in Section 6.3.2 the magnitude of the maximum deficit of the curve gets smaller as inlet wind speed increases. In tandem with this feature the radius of the wake arc increases. Above 7.11 diameters in each wind speed bin the arched wake profile has a far shallower appearance and is almost linear.

For wind speeds below 10m/s, Figure 6.30 – Figure 6.32, the measured wind speeds do not show a return to an inlet value of 1 on the x-axis at any distance downstream. This indicates that the measurements captured do not allow the visualisation of the bounds of the wake profile for these wind

speeds and that the wake profile for these wind speeds is much wider than predicted. At wind speeds above 10m/s, Figure 6.33 – Figure 6.38, the wake bounds are more focussed and are visible within the captured measurements, with more defined arc profiles to the measurements on or near the wake centreline. The measured wakes show that at farther distances the wake width is around two rotor diameters; beyond this the flow has recovered to inlet values.

The measurements captured show the evolution of the wake profile with distance along the centreline a wide range of inlet wind speeds. Across the measurements a clear evolution of the profiles with few departures from the evolving profiles is presented. However in Figure 6.35 at 12.28 diameters downstream a clear peak in measured deficit that does not fit with the measurements around it either at that distance or either side of it is presented. This indicates a local disruption in the flow measurements at this distance, twenty scans have been used in the formulation of this image so it is not an instantaneous anomaly. As the wind direction during these scans results in there being no other turbines in the wake of the studied AV7 turbine that could affect the flow it is unclear what the anomaly can be attributed to.

6.3.5 Numerical wake width comparison results

Completing the comparison for wake width analysis, the PARK and Eddy-Viscosity models for each wind speed bin considered were run and plotted against the processed data sets, Figure 6.39 – Figure 6.47. The inlet wind speeds used to define the models is taken from the averaged lidar measured inlet wind speeds for each bin. Wake width data for the SST turbulence models were not available.

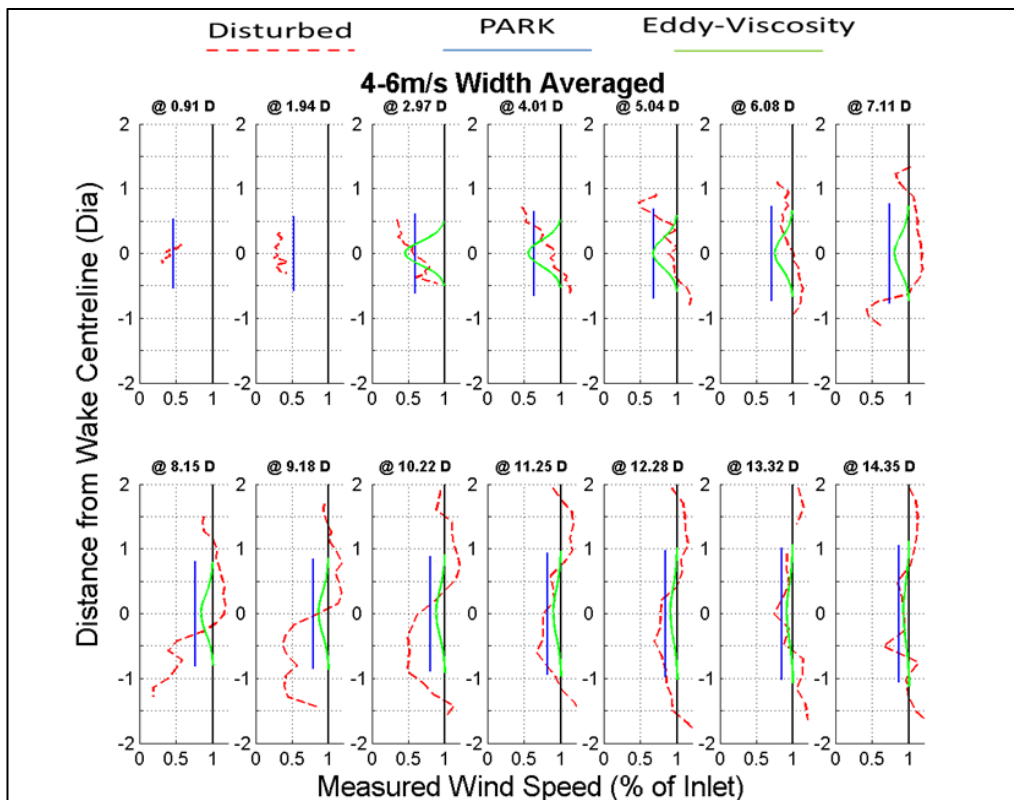


Figure 6.39: 4-6m/s wake width profiles and model comparisons, $C_p = 0.200 - 0.326$ (Ave=4.5m/s, 1 profile)

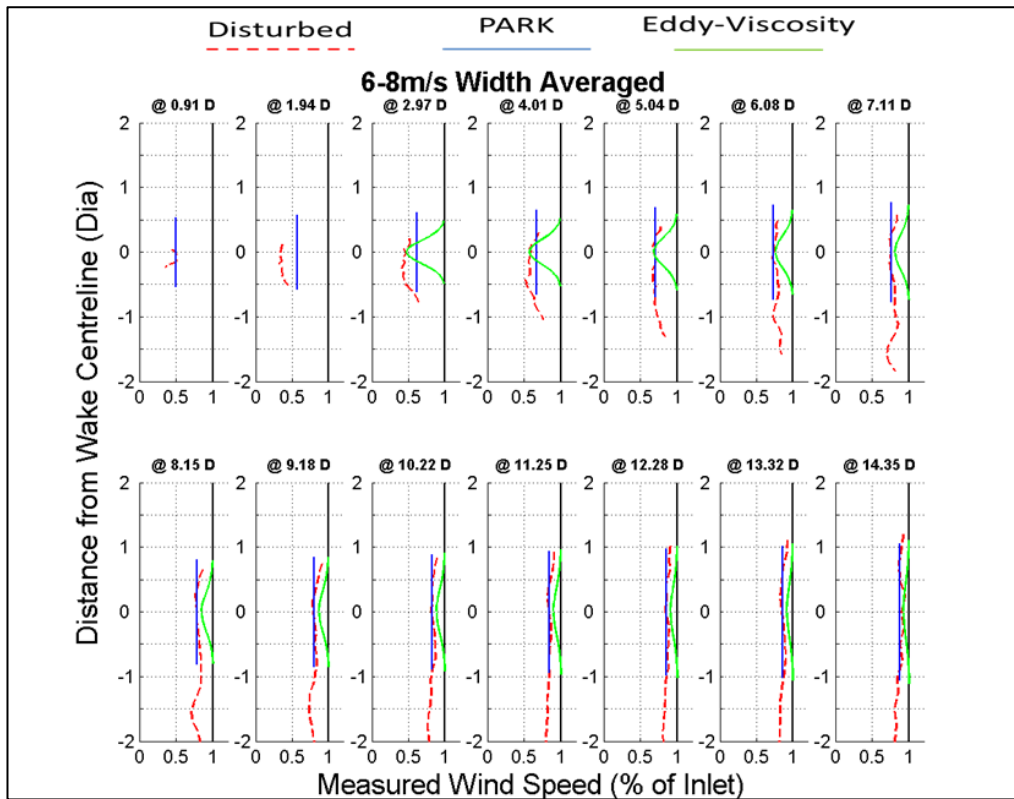


Figure 6.40: 6-8m/s wake width profiles and model comparisons, $C_P = 0.326 - 0.447$ (Ave=7.1m/s, 9 profiles)

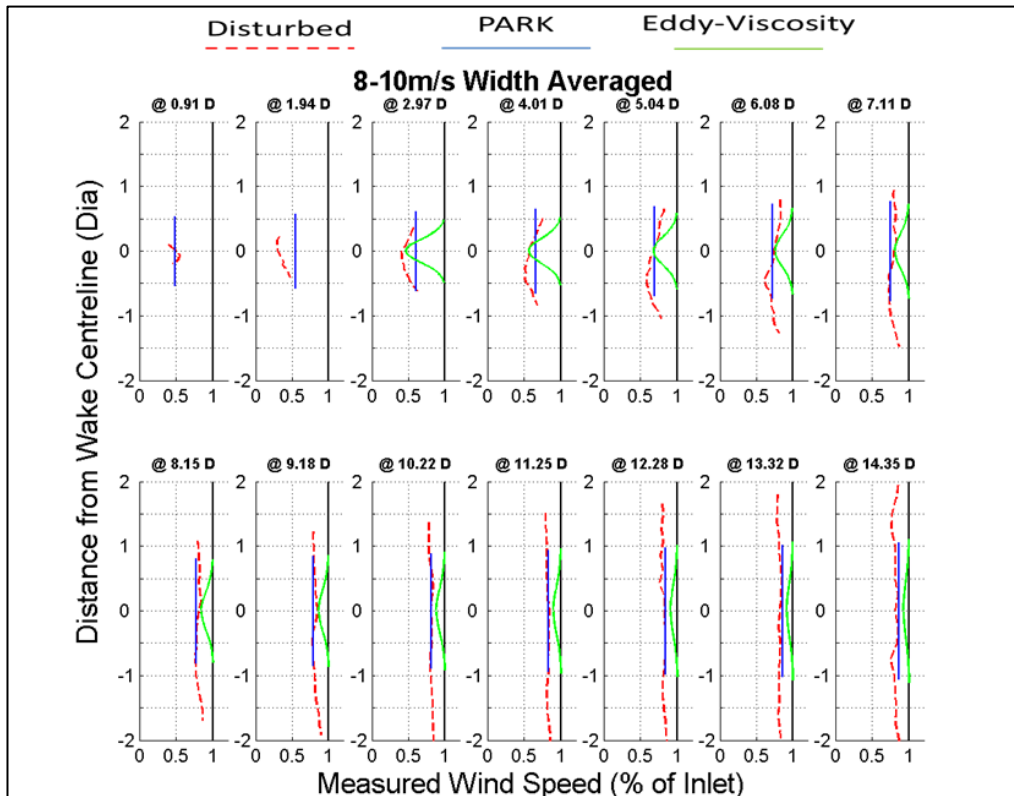


Figure 6.41: 8-10m/s wake width profiles and model comparisons $C_P = 0.447 - 0.472$ (Ave=8.8m/s, 20 profiles)

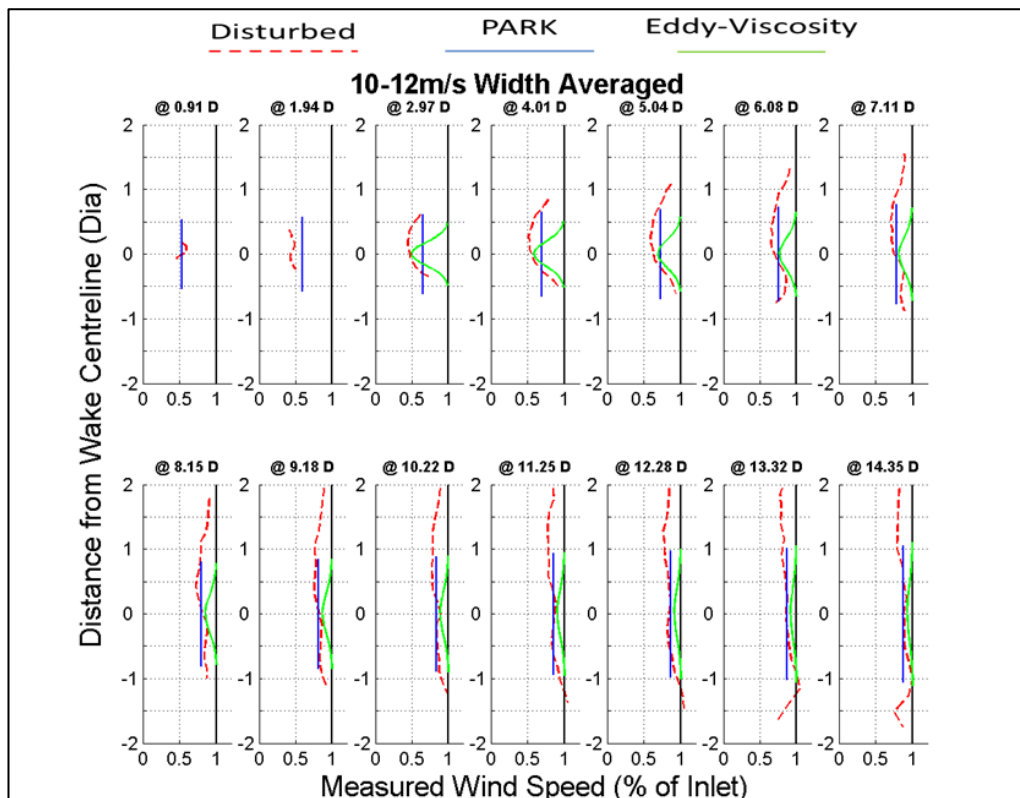


Figure 6.42: 10-12m/s wake width profiles and model comparisons, $C_P = 0.472 - 0.423$ (Ave=10.7m/s, 19 profiles)

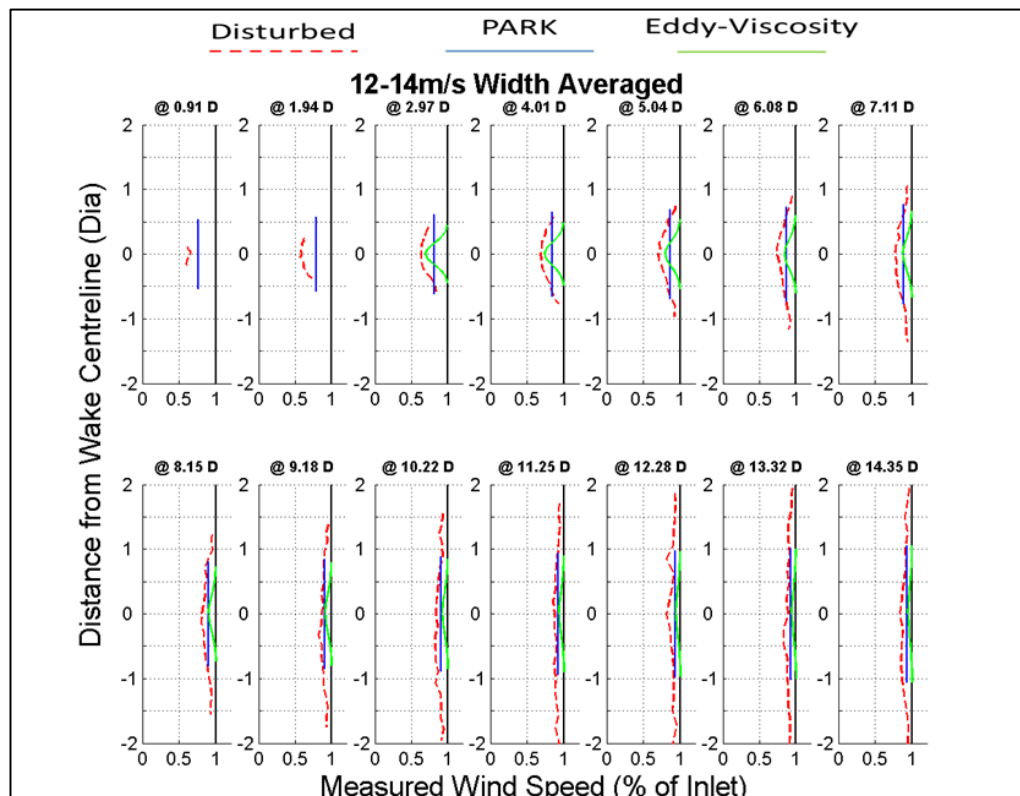


Figure 6.43: 12-14m/s wake width profiles and model comparisons, $C_P = 0.423 - 0.281$ (Ave=13.3m/s, 10 profiles)

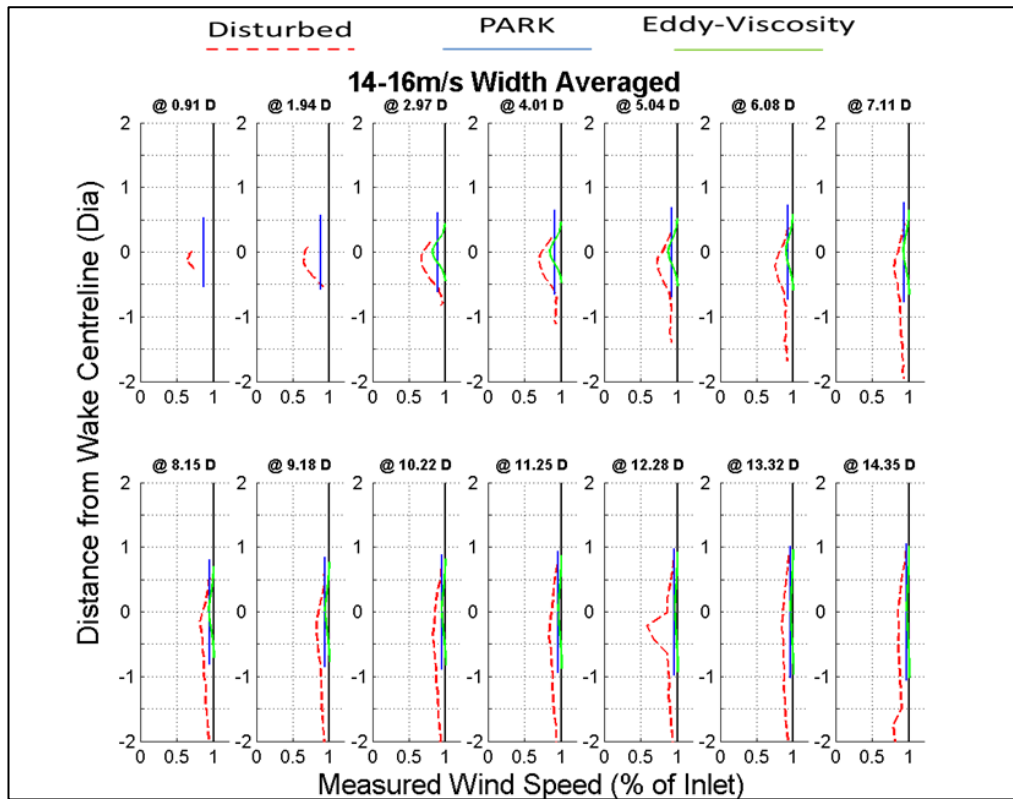


Figure 6.44: 14-16m/s wake width profiles and model comparisons, $C_P = 0.281 - 0.189$ (Ave=15.2m/s, 20 profiles)

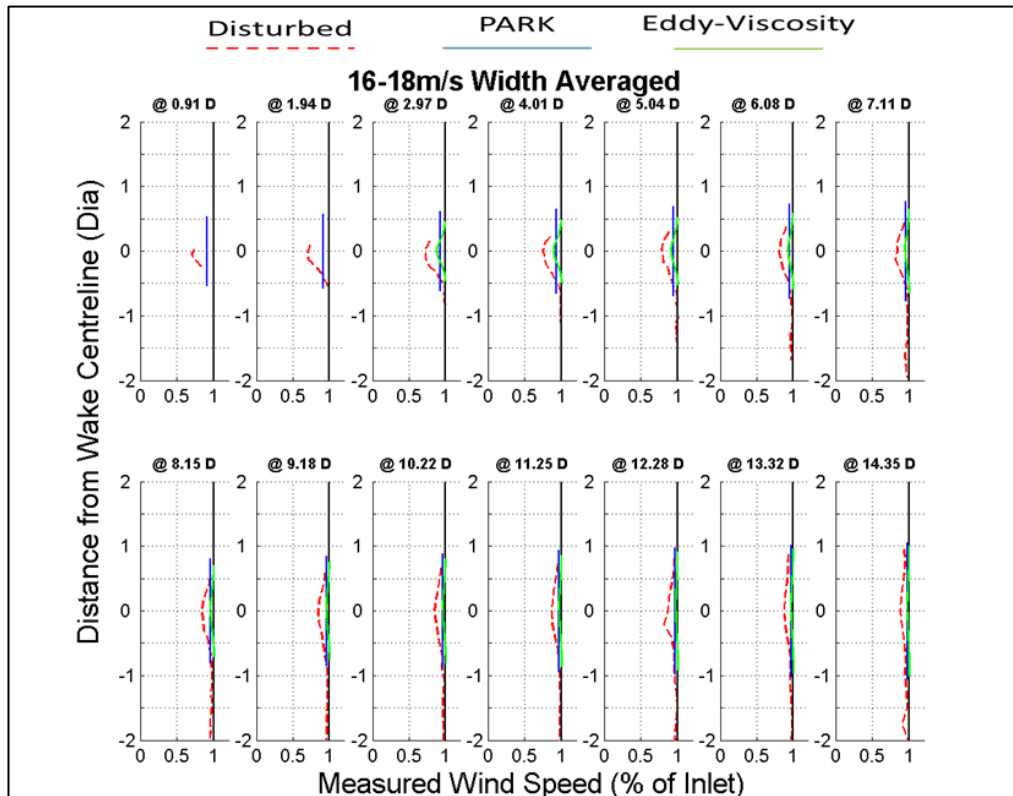


Figure 6.45: 16-18m/s wake width profiles and model comparisons, $C_P = 0.189 - 0.132$ (Ave=16.8m/s, 17 profiles)

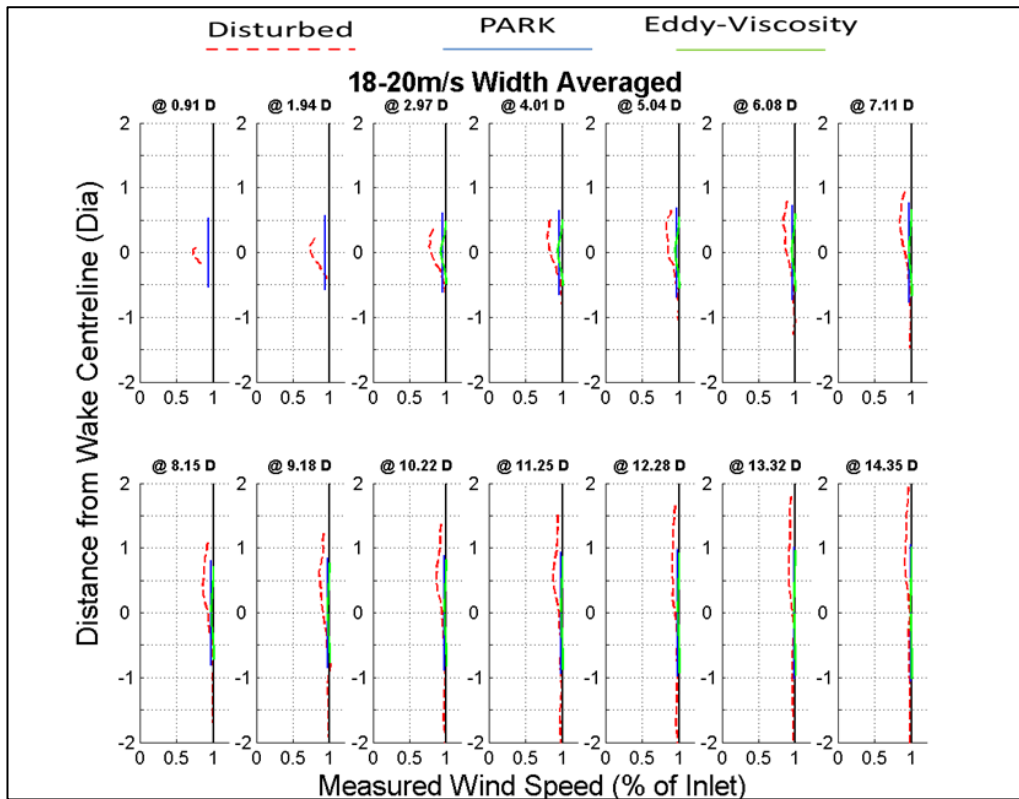


Figure 6.46: 18-20m/s wake width profiles and model comparisons, $C_P = 0.132 - 0.097$ (Ave=19m/s, 14 profiles)

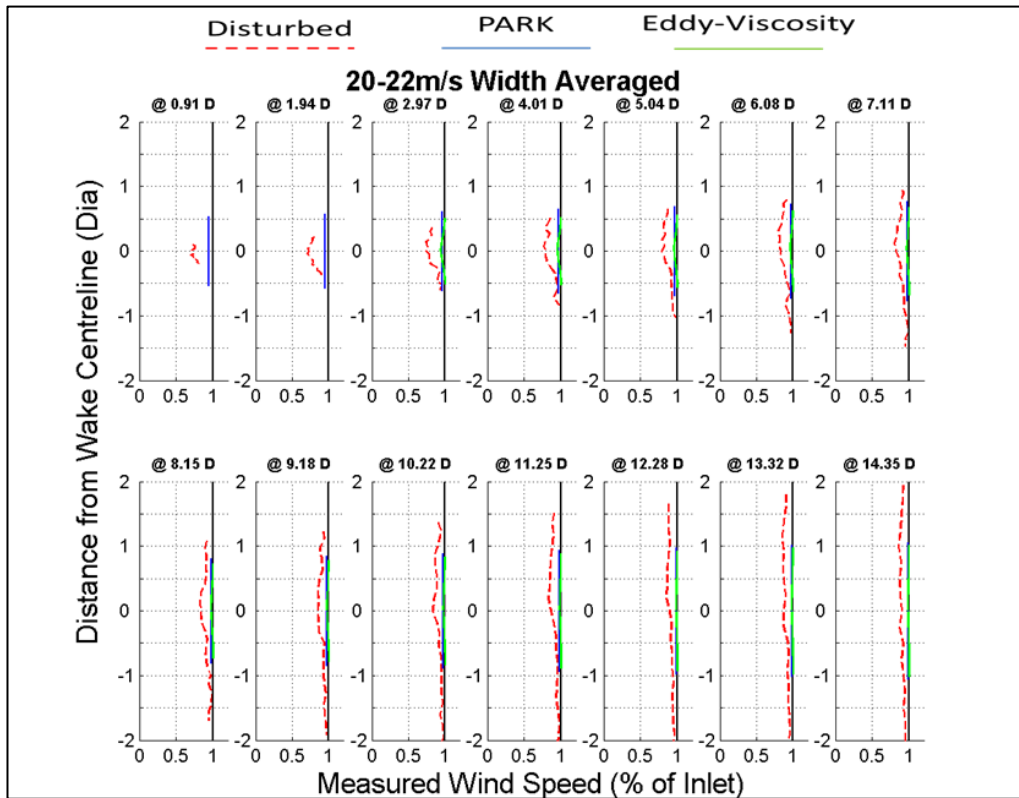


Figure 6.47: 20-22m/s wake width profiles and model comparisons, $C_P = 0.097 - 0.073$ (Ave=20.3m/s, 3 profiles)

The wake width models visualised in Figure 6.39 - Figure 6.47 show that the PARK and Eddy-Viscosity numerical models predict symmetrical profiles around the centreline of the wake and rotor that get wider with distance from the rotor plane.

The PARK model assumes a deficit from the inlet that is uniform at all points across the width of the wake at a given distance, the magnitude of this deficit decreases with distance from the rotor plane. The wake width at a given point is a function of the distance downstream from the rotor, the inlet wind speed (and corresponding thrust coefficient) as well as the wake decay constant, Equation 2.11 and Equation 2.12. At a given distance downstream the magnitude of the deficit from inlet is seen to decrease as wind speed increases.

The Eddy-Viscosity model presents a Gaussian wake profile symmetrical around the wake centreline. The resultant profile across the wake width details a peak deficit at the wake centreline reducing to the inlet velocity at the wake bounds. The magnitude of the peak deficit is seen to decrease with distance from the rotor plane as well as with increasing wind speed for a given distance. The deficit at the centreline is the same for the given point as is defined in the wake centreline analysis and is a function of distance, thrust coefficient, turbulence intensity and inlet wind speed. The wake width is a function of this deficit from inlet and thrust coefficient, Equation 2.7. While the half profile across this width is a function of inlet wind speed, centreline deficit and distance from the centreline, Equation 2.8.

At the bounds of the predicted profiles the PARK and Eddy-Viscosity profiles predict an immediate return to inlet wind speeds; this behaviour is detailed in Figure 2.8 and Figure 2.11 for the two models respectively.

Chapter 7:

**Results discussion
and analysis**

7.1 Onshore results discussion and analysis

7.1.1 Ten minute averaged, MyersHill/Whitelee wind farm, July 2011

The lidar data measurements presented in Section 6.2.1 detail flow measurements averaged over a ten minute time period for two operational wind turbines, Figure 6.1. It can be seen in the figure that the measured wind speed velocities through the wind turbine rotors were close to 4m/s during the ten minute period. Such low wind speeds mean that turbulent eddies and atmospheric instabilities will dominate the flow field as steady state flow cannot establish itself. This is reflected in the lidar wake centreline measurements, Figure 6.2, where the two profiles presented do not show consistent behaviour in comparison to each other.

The simulation results presented in Figure 6.4 shows that the $k-\varepsilon$ Modified and the $k-\varepsilon$ STD produce almost identical results. The $k-\varepsilon$ RNG and $k-\omega$ models show similar behaviour and both predict a larger velocity deficit within the near wake and a corresponding longer recovery time. The $k-\omega$ model shows a longer length and appears to recover to a lower value. Upstream of the turbine all models have almost identical behaviour with the $k-\omega$ model showing a slightly earlier slow down before the turbine rotor than the other models. This study was repeated for the west turbine with similar behavioural patterns visible.

The comparison between the measured and $k-\omega$ simulated results for the East turbine has produced an unsatisfactory correlation between the two data sets, Figure 6.5. The smooth profile presented by the model is in contrast to the variable results captured by the lidar measurements. There are a number of reasons for this:

- The inclined scan plane created by the lidar measurement scan arc, Figure 6.3, measures velocity values at increasing heights through the boundary layer. This results in natural velocity increases as the height above the lidar of each measurement point increases.
- It is clear that the low wind speeds are not optimal for comparing remote sensing and numerical predictions of wind turbine wakes. A wind speed of approximately 4m/s is insufficient to overcome the instabilities within the atmosphere. Thus turbulent eddies and gusts dominate the flow field and a steady state wake structure cannot be formed skewing the comparison.
- The effect of ambient atmospheric stability cannot be included in the analysis as temperature data was not measured at the time of deployment and calculation of its properties cannot be completed.
- The approximation of the reference wind speed used to define the numerical model inlet was taken from an analysis of the wind speeds measured in front of the turbine by the lidar. Therefore the domain inlet location and defined wind speed were unsuitable for informing the simulations accurately as the chosen lidar measurement points were not exactly at the corresponding inlet location.

While not producing a satisfactory comparison the deployment and the experience gained, along with the subsequent analysis has provided a proof of concept for the next stage of this study. Lessons learned from the results allowed for a number of improvements in the subsequent lidar deployments in order to gather higher quality data sets. These are:

- Reduce the width of the measurement arc and thus increase the time resolution of the deployment while focussing the measurements around specific turbines.
- Employ a lower scan elevation value in order to reduce uncertainties arising from measuring at different heights across the wind turbine streamtube.
- Average the captured data over ten minute and hour periods in order to capture steady state flow behaviour.
- Incorporate the capture of accurate ambient condition measurements in order to improve the physics setup and definition of the models. In particular temperature and pressure values.
- Gather data during a wider range of wind speed and direction conditions, in particular data from wind speeds around the average for the site under study.

7.1.2 Ten minute averaged, Myers Hill/Whitelee wind farm, January 2012

The lidar data measurements presented in Section 6.2.2 detail flow measurements at the same wind farm as the previous July deployment. For the January 2012 deployment the lower scan angle implemented and extended range employed allowed six turbines to be encompassed within the scan envelope. The visualised flow field from lidar data averaged over ten minutes is presented in Figure 6.6. Extracting data from the freestream operating Turbine 1 a clear wake profile has been presented in Figure 6.9 for comparison with the numerical models.

It is evident from Figure 6.9 that while the profiles offer similar behaviour patterns there is significant variance in the predicted flow values between the simulations and the measured scanning lidar results for Turbine 1. The numerical and experimental data sets both indicate a gradual reduction from freestream velocity as the flow approaches the rotor disk; this is followed by a larger deficit across the rotor disk. Actuator disk theory [68] suggests that the predicted velocity drop for the measured inlet wind speed of 10.9m/s and corresponding Thrust Coefficient of 0.65 for this turbine should be close to 20% from freestream conditions. This is in close agreement with the current numerical prediction but not the measured lidar data.

The lidar data shows a much larger velocity drop through the rotor plane than the modelled results and appears to suggest a flow reversal with a negative wind speed value measured at the rotor plane. This is clearly an error in the measurement which is likely brought about by the presence of the physical structure of the turbine at the measurement point. This behaviour indicates either the measurement of flow effects relating to the blockage effects of the nacelle and tower, or the physical presence of the

turbine on the measurement beam with the structure creating a false measurement at this location. Analysis of the measurement point location shows that it is at the nacelle location for this turbine and reflection or blocking of the measurement beam would likely cause a bias upon the measured results at this location. As a result the uncertainty of the measured velocity at this point is significant.

Downstream of the rotor plane in Figure 6.9 the predicted recovery towards freestream velocity takes longer in the measured centreline data compared to the numerical models. As a result the recovery is not captured completely in the lidar scan range of seven rotor diameters downstream. Wind turbine theory suggests ambient atmospheric conditions as the primary driver in wake recovery as a greater local Turbulence Intensity (T.I.) allows more mixing and a faster recovery. The atmospheric conditions experienced during the deployment were typical for night time winter conditions with a measured T.I. of 6% over the period of the averaged 10 minute data. This T.I. value was calculated from measurements taken by the co-located virtual met mast scanning lidar during the same deployment period. This low T.I. value would facilitate an increase in the length of the wake recovery period as is captured by the lidar results as there will be less mixing between the freestream and the wake.

In the ten minute averaged comparison presented in Section 6.2.2 the wind direction coupled with the scan envelope implemented leads to lower variation in height between the lidar measurements points and the hub height, Figure 6.7, than in the July deployment, Figure 6.3. As a result the influences of the boundary layer and local roughness properties will have a more consistent influence across all of the measurement points leading to a more useful comparison between the measured and simulated data sets.

Using data from the arc scan to define the inlet wind speed and flow direction provides good results when comparing inlet conditions, however it is unclear the effect that the terrain and surface roughness has on the evolution of the flow from the inlet measurement point to the turbine rotor plane.

The comparison presented with the ten minute averaged data set provides a clear indication of wake speed evolution. While useful as a proof of concept it is clear that a more detailed data set capturing the evolution of the wake over a longer measurement domain is required in order to capture more accurate details of wake development. In addition the comparison of multiple ten minute averaged data sets over a wider range of ambient flow conditions would present a more comprehensive indication of wake generation, propagation and dissipation.

7.1.3 Inlet definition and time averaged comparison

The results presented in Section 6.2.3 focus on the effects of different averaging periods on the lidar measurements from the same January 2011 deployment discussed above in Section 7.1.3. The chosen lidar data sets are averaged over two time periods, ten minutes and one hour, and visualised in Figure 6.10 and Figure 6.11 respectively. A second lidar has been used to provide an alternative inlet definition method for the numerical models. Analysing four different combinations of averaging period and inlet definition method Figure 6.12 presents the wake centreline velocity measurements for Turbine 1 against the numerical models. It can be seen that the four comparison cases considered in Figure 6.12 show similar flow features between the profiles of the measured and modelled data sets. Broadly following that expected in wind turbine theory [73] these encompasses a sharp reduction in flow velocity through the rotor plane followed by a longer recovery towards freestream conditions in the wake.

Focussing on the comparisons of the lidar data across the two averaging periods in Figure 6.12 the wake centreline profiles provide a good analysis of the effects of these differing length scales. While the ten-minute and hour data sets exhibit generally similar behaviour the ten minute dataset, Image 1 and 2, suggests more stochastic variations from point to point. In contrast the one hour data, Image 3 and 4, presents a smoother transition between points and across the overall profile. Such effects would be expected as the averaging process reduces the scatter from individual scans using more data points at each location to find the average. For the comparison with steady state numerical modelling this may be considered a desired result. However given the nature of wind flow and turbine operation it is likely the one hour averaging period is losing some key features. As most wind turbines operate

with a ten minute averaging response for their yaw drive actuation it is likely that over a 60 minute period the wind turbine will have moved position and consequently the centreline of the wake will also have moved. The effect of this will not be detailed in the one hour results. It is also clear from both of the lidar measured velocity profiles that the maximum deficit from the freestream is not measured at the rotor plane but at a distance on the downstream side of the rotor. This feature has not been captured in the previous deployments and will be a focus of future work.

The numerical models exhibit behaviour in keeping with that found in previous analyses with a maximum deficit at the rotor plane. While the minimum wind speed measured at the rotor plane is seen to increase as the wind speed increases the difference between this value and the inlet wind speed decreases. The overall magnitude of this deficit through the rotor plane can be said to decrease with inlet wind speed. This modelled feature is not readily evident in the lidar measurements.

Analysis of the numerical results presented in Figure 6.12 show that the use of the virtual met mast definition of inlet wind speed consistently over predicts the wind speeds in comparison to the measurements, Image 1 and 3. At inlet the modelled velocities are approximately 3m/s higher than the experimental results, this deviation is preserved throughout the stream tube along the inlet and into the wake recovery. In the arc scan inlet definition, Image 2 and 4, the inlet numerical and measured velocities are in better agreement, downstream of the rotor the recovery behaviour is similar with velocities closer to those simulated.

The work presented provides a useful comparison of a number of methodologies that can be employed during the analysis of scanning lidar

measured wake data and the comparison to computational simulations. The use of a second lidar onsite to verify results is an attractive concept as it will remove some of the uncertainties associated with the use of lidars in complex flow as explored in Chapter 2. However the distance between the devices along with the complexity of the terrain in this deployment have been shown to introduce too many uncertainties. By comparison the use of data measured in the arc scan directly upstream of the device improves the accuracy of inlet definitions for comparative assessment of the experimental and numerical results. The analysis presented also suggest that ten minute averaged data sets provide steady state analysis for comparison with models while ensuring the effects of turbine yaw and misalignment are accounted for. Furthermore it appears that the models analysed are underestimating the maximum wake speed deficit imparted on the freestream flow by the operational wind turbine. This results in longer recovery period of the wake velocity which will have an effect on the performance of downstream wind turbines. The results presented back up previous work in proving a valid proof of concept for the comparison of experimental and numerical data sets. In addition the comparison of the two time averaging periods and inlet definition methodologies have identified best practices for the measurement and analysis of scanning lidar measured wake data, providing a good test bed and outline for future work.

7.1.4 Measurement uncertainties in onshore comparisons

As has been discussed throughout the work presented a number of uncertainties exist that arise from the use of the Galion lidar measurement technique to capture wind speeds remote from the device. Using the lidar technique described requires the formulation of wind speeds based on 3 or more measurements captured at the same time. The use of a single device, and thus a single emission point, requires that such devices cannot capture such information at the same point. This necessitates the use of the arc scanning technique discussed in Chapter 2. In order to calculate a local flow vector the processing software will use data points either side of a single point as well as the local measurement to calculate the local flow vector at that point. This brings rise to a number of uncertainties in the lidar measurements:

- As a single emission point is capturing flow measurements at multiple points it is impossible for these values to be captured at the exact same time. The measurements are therefore an average in time as well as spatially.
- The calculated values are attributed to a single point but are the result of multiple data points being used to calculate a single value. The measurement can therefore be said to be an average across these points. It follows that the larger the spacing between the measurement points in formulating a point vector the larger the uncertainties associated with those values. The uncertainty is therefore governed by the device characteristics and the scan envelope defined. As the Galion lidar uses a Range Gate value of 30m along each beam between measurements this uncertainty in using this device can only be

controlled by the definition of the azimuth spacing in the arc scan implemented. i.e. the uncertainty associated with spacing can be reduced by employing lower spacing values between the azimuths of each beam in the scan envelope.

Each of the onshore lidar deployments utilised in the works outlined above employ a single arc scanning lidar to capture measurements across the flow field, this device is installed at ground level within the active wind farm. In order to capture wake flow behind the subject wind turbines the arc scan envelope must be constrained to having an elevation of greater than 0° , in the analyses presented 5° and 6° elevations have been used. As a result the measurements along a single azimuth beam increase in height with distance from the device capturing measurements vertically across the atmospheric boundary layer and wind turbine wakes, this feature is demonstrated in Figure 4.8. Again the uncertainties can be controlled by the definition of the scan envelope, a shallower elevation to the arc scan will result in reduced uncertainties as the height difference between measurements is less and the effects of the boundary layer are more consistent across the measurements. However for wake centreline analysis the direction of the flow field being studied can also help to reduce the total changes in height across the measurements. In Section 7.1.2 the analysed flow field is orientated towards the device and as a result the height changes across the utilised measurements are large, Figure 6.7. By comparison the analysis shown in Section 7.1.3 identifies a flow direction that crosses the scan envelope at a distance from the device, this results in less changes in height across the measurements used reducing the uncertainties by comparison.

In order to provide a valid comparison for each of the onshore analyses the varying height lidar measurement points have been reproduced exactly in

the numerical domain. Working in this manner reduces the uncertainty associated with the differing heights, however in the complex flow models of the Windmodeller simulations this moves the uncertainty to the representation of the wakes in the three dimensional domain. A wind turbine wake will contain a rotational component to the wake generated by the rotating blades. While this is modelled in the Windmodeller simulation there is no literature on the accuracy of these simulations and the quantification of this uncertainty.

7.2 Offshore results discussion and analysis

7.2.1 Wake centreline profile analysis

The results presented in Section 6.3 present lidar measurements describing wake flow development across a range of inflow conditions experienced by the studied AV7 turbine operating in the Alpha Ventus wind farm. The results presented in Figure 6.20 – Figure 6.24 outline key flow features and wake velocity development not previously captured in such detail.

Presenting an analysis of cases where the inflow is undisturbed, disturbed or waked (defined in Figure 4.14 and Table 4.5) the results demonstrate that the measured velocity deficit profiles through the rotor plane and into the wake are dependent on a variety of factors and show distinctive behaviour for each condition. As discussed in Section 6.3.2 the deficit from inlet wind speed at the rotor plane appears to be centred close to 30% for all of the inlet wind speed bins in the undisturbed flow condition. While centred around this point it is clear that as the incident turbulence level increases, from the undisturbed to the disturbed to the fully waked situations, the magnitude of this initial deficit increases. This increase is preserved downstream as the flow evolves to a maximum downstream of the rotor in the near wake. It is clear that the maximum deficit is therefore a function of the inlet wind speed and the incident inflow conditions. The measured deficits from inflow for each condition and wind speed bin are presented in Table 7.1. For the majority of conditions the maximum deficit from inlet is found to be in a location ranging between 1.7 and 2.2 rotor diameters downstream from the rotor plane, Table 7.1.

Wind Speed Bin (m/s)	Initial Deficit (%)	Maximum Deficit (%)	Maximum Deficit Location (Ø)	Deficit at 12 Ø (%)
Undisturbed Inflow				
6-8m/s	28.4	64.8	2.2	9.2
8-10m/s	27.2	61.6	2.2	8.7
10-12m/s	28.7	51.8	2.2	10.9
12-14m/s	28.6	43.12	2.2	12.2
14-16m/s	22.9	28.4	1.7	15.8
Disturbed Inflow				
6-8m/s	35.1	68.3	2	10.7
8-10m/s	33.7	65	2	13.1
10-12m/s	33.8	56.4	2.2	15.1
12-14m/s	34.1	47.5	2.2	16.5
14-16m/s	31.3	38	1.7	18.2
Waked Inflow				
6-8m/s	45.1	75.4	1.7	17.6
8-10m/s	38	67.6	2	19.01
10-12m/s	36.3	58.1	2.2	22.9
12-14m/s	35.7	49.3	2.2	18.9
14-16m/s	31.3	37.4	1.4	18.5

Table 7.1: Key measured flow parameters for three inflow conditions, Figure 6.20 – 6.24

It can be seen in Table 7.1 that as inlet wind speed increases the maximum deficit from this value is shown to decrease; at the same time the rotor plane deficit values from this inlet wind speed stay comparatively consistent while increasing slightly as incident turbulence increases. The maximum deficit location does not show any prescribed behaviour.

Focussing on the recovery downstream of the maximum deficit it is shown that at lower inlet wind speeds, Figure 6.20 – Figure 6.22, a sharper initial recovery is observed as turbulent mixing between the wake and surrounding flow field dominates the flow. The gradients of this initial recovery between 2.5 and 4 diameters downstream for each inflow situation are presented in Table 7.2 below.

	Undisturbed	Disturbed	Waked
6-8m/s	0.13	0.14	0.13
8-10m/s	0.13	0.12	0.11
10-12m/s	0.08	0.07	0.05
12-14m/s	0.04	0.05	0.04
14-16m/s	0.02	0.01	0.02

Table 7.2: Initial recovery gradient beyond maximum deficit, Figure 6.20 – 6.24

It is clear in the values presented in Table 7.2 that as the wind speed increases the gradient of the initial recovery decreases. Between the different inflow conditions it is shown that there is little difference between the recovery gradient in each wind speed bin. Beyond this initial recovery the wake speed recovery in the far wake shows a shallower gradient to the recovery in all cases, Figure 6.20 – Figure 6.24. The values presented in Table 7.3 represent the calculated gradient of the curves between 4 and 10 diameters downstream for the rotor plane.

	Undisturbed	Disturbed	Waked
6-8m/s	0.07	0.05	0.05
8-10m/s	0.06	0.05	0.05
10-12m/s	0.05	0.05	0.04
12-14m/s	0.04	0.04	0.04
14-16m/s	0.01	0.03	0.03

Table 7.3: Wake recovery gradient between 4 and 10 diameters downstream, Figure 6.20 –6.24

As can be seen the gradient values calculated in the far wake recovery between 4 and 10 rotor diameters downstream continue to show a decrease with increase in wind speed but are lower than those of the near wake initial recovery. Again the values are similar across the inflow conditions.

Further downstream the wake speed is not found to recover to inlet values within thirteen rotor diameters downstream of the rotor plane for any of the inlet cases. As discussed in Section 6.3.2 beyond thirteen rotor diameters a

greater degree of scatter is seen in the resultant profiles and they cannot be used for further analysis.

As can be seen in the Tables above the observed behaviour is broadly similar for the three inflow cases with the deficits found between the different inflow conditions at the rotor plane being preserved in the measured recovery towards inlet beyond the maximum deficit location. Across each of the measured wind speed bins the measured velocity values are consistently lower for the waked inflow than for those of the disturbed inflow which in turn are lower than those of the undisturbed flow. As the initial recovery gradients stay broadly constant across the three inflow conditions the separation between the inflow profiles in each bin also stays this way. With the exception of the 10-12m/s wind speed bin, Figure 6.22, where the recovery gradient is seen to decrease with the increase in inflow turbulence and the profiles are seen to diverge through the initial stages of the recovery.

The majority of offshore wind farm arrays adopt a wind turbine separation of 7 – 12 rotor diameters [134]. As a result the recovery of the wind speeds in this region is of importance when considering the amount of energy available to downstream operating turbines. Treating the undisturbed flow situation as a base case the percentage difference between this profile and the disturbed and waked profiles a 7.1, 9.9 and 12 rotor diameters downstream are presented in Table 7.4.

Wind Speed Bin (m/s)	Disturbed Difference (%)			Waked Difference (%)		
	7.1 Ø	9.9 Ø	12 Ø	7 Ø	10 Ø	12 Ø
6-8	3.3	3.42	1.6	11.47	10.44	8.45
8-10	8.44	8.04	4.41	13.56	13.49	10.28
10-12	6.37	5.93	4.13	13.52	12.89	11.94
12-14	4.59	4.61	4.26	7.11	8.1	6.71
14-16	-5.62	-1.45	-4.16	-6.79	-1.84	-3.79

Table 7.4: Measured wind speed deficit from the undisturbed profile at selected distances

Analysis of the results in Table 7.4 again suggests a strong correlation between deficits along the wake centreline from the undisturbed profile to that of the disturbed inflow cases and a further deficit to the waked inflow cases. For both the disturbed and waked inflow cases this deficit is largest in the wind farm's dominant wind speed bin of 8-10m/s, Figure 6.20, and at the seven rotor diameter range. The measured deficit values fall slightly with increasing wind speed. In the predominant wind speed bin for the site of 8-10m/s the results show a near 8% deficit at seven and ten rotor diameters, decreasing to 4% at twelve rotor diameters to the disturbed inflow cases. For the fully waked inflow situations these values increase to near 13.5% at seven and ten rotor diameters, falling slightly to 10% at twelve rotor diameters.

As the potential power available to a wind turbine is proportional to the cube of the wind speed [73] this study confirms that there is a reduction in the potential power availability to turbines operating in the wake of an upstream turbine when compared to undisturbed cases. The results also allow an understanding of the evolution of this potential power loss with increases in distance downstream from the rotor plane and increases in inlet turbulence conditions. All of these effects will be compounded in larger wind farm arrays [135] as more turbines increase the levels of turbulence as well as the deficits on the inflow velocities to each turbine.

Analysis of the evolution of the maximum deficit in Table 7.1 and the C_p operating point of the turbine in Appendix F shows that as the operating power coefficient of the turbine decreases with wind speed so too does the maximum deficit from inlet wind speed. The power coefficient is a measure of the percentage of the total energy available to the turbine it takes out of the inlet flow field. The results present a clear correlation between this operational condition of the turbine and the evolution of the deficit from inlet

wind speeds downstream from the rotor. The percentage differences from bin to bin at the maximum deficit position downstream are large with the overall all maximum deficit change from the 6-8m/s bin to the 14-16m/s bin being greater than 30% for all inflow conditions. In the far wake at 12 rotor diameters downstream the same analysis yields a variation of no greater than 8% across the wind speed bins for each inlet condition. It is clear from this that the C_p operating conditions of the turbine have a large effect on the evolution of the flow downstream of the rotor plane. The effect of this are far more apparent in the near wake than in the far wake where only small deviations are measured.

What these results show is that for offshore wind farms with spacing below 6 rotor diameters small variations in this spacing can lead to large variations in the potential power available to a downstream operating turbine. These effects are more marked at lower wind speeds. For larger spacing above 10 – 12 rotor diameters small changes in this spacing will lead to little difference in the available potential power across the wind speed range of the turbine. This emphasizes the importance of maximising spacing between turbines in an operational wind farm.

Analysis of numerical models

It is observed and explored above that the general profiles outlined in the lidar measured wake behaviour in Section 6.3.2 and discussed in 7.2.1 are consistent for each of the three inflow conditions considered. For comparison with these profiles three numerical models have been run and the wake centreline profiles extracted for comparison with the lidar measurements, Figure 6.25 – Figure 6.29. Each of the models utilised have been employed to

model undisturbed inflow wake development for a single turbine only and have not been modified to account for any array interaction or different inflow conditions other than inlet velocity. The initial and maximum deficit characteristics of each model are identified in Table 7.5.

Wind Speed Bin (m/s)	Initial Deficit (%)	Maximum Deficit (%)	Maximum Deficit Location (\emptyset)
PARK Model			
6-8m/s		56.2	0
8-10m/s		59.1	0
10-12m/s		50.4	0
12-14m/s		30.9	0
14-16m/s		18.3	0
Eddy-Viscosity Model			
6-8m/s		68.3	2
8-10m/s		70.6	2
10-12m/s		63.3	2
12-14m/s		47.2	2
14-16m/s		25.3	2
SST Model			
6-8m/s	26.9	58.9	1.97
8-10m/s	26.8	59.3	1.97
10-12m/s	22.3	48.1	1.97
12-14m/s	14.1	28.6	1.97
14-16m/s	7.3	14.7	1.97

Table 7.5: Numerical model deficit key features, PARK, Eddy-Viscosity and SST

It is clear from Table 7.5 that the maximum deficit location remains constant for each model across the different wind speed bins. The PARK and Eddy-Viscosity models have fixed initial deficit locations that are equal to the maximum deficit at 0 and 2 rotor diameters downstream respectively. The SST model has a profile with the same characteristics as the lidar measurements with a maximum deficit downstream of the initial deficit at the rotor plane; it is shown in Table 7.5 that this maximum is located at 1.97 rotor diameters downstream for all of the wind speed bins considered. Focussing on the maximum deficit values presented for all three models there is an initial increase in maximum deficit from inlet value between the 6-

8m/s and the 8-10m/s cases, above these bins the maximum value decreases steadily. The PARK and SST models identify similar values in the maximum deficit for each wind speed bin albeit at different locations. The Eddy-Viscosity model's maximum deficit in each wind speed bin is larger than both of these in all wind speed bins. Focussing on the initial recovery gradients of the three models in Figure 6.26 – Figure 6.29 it is clear that the SST model recovery gradient is less than that of the simpler models. The values of the initial gradient in the two diameters downstream of the maximum deficit for the three models employed are presented in Table 7.6.

	PARK	Eddy-Viscosity	SST
6-8m/s	0.07	0.09	0.002
8-10m/s	0.07	0.1	0.002
10-12m/s	0.06	0.08	0.002
12-14m/s	0.04	0.05	0.001
14-16m/s	0.02	0.02	0.0005

Table 7.6: Initial wake recovery gradient after maximum deficit for three numerical models, Figure 6.25 – 6.29

It is clear from analysis of the simulated initial recovery gradients in Table 7.6 and in Figure 6.25 – Figure 6.29 that the initial rate of recovery of the SST model is far less than that of the PARK and Eddy-Viscosity models which exhibit similar behaviour at this stage. As the recovery of the Eddy-Viscosity and SST model recoveries begin at a similar location this leads to a divergence of the profiles as the SST model recovers slower into the far wake. While the PARK and Eddy-Viscosity models have similar initial gradients their differing initiation points and tailing off of gradient further downstream mean that the models converge downstream. These two models are seen to have profiles very close to each other in the far wake in all of the wind speed bins analysed. The SST model does not recover to the same values as the simpler numerical models in any of the profiles presented in Figure 6.25 – 6.29.

Lidar measurements and numerical model comparison

None of the three models presented as part of the comparisons can be said to closely match the behaviour of the lidar measured profiles along the full length of the wake captured. Each model however has areas of strength and weakness in comparison with these measurements.

It is clear from Figures 6.25 – Figure 6.29 that the PARK [80] methodology fails to capture the blockage and pressure effects of the flow into the turbine's rotor. The more complex SST [101] model more satisfactorily captures this behaviour. As the Simplified Eddy-Viscosity [86] model does not initiate until two rotor diameters it does not attempt to model these effects.

Beyond two rotor diameters it is clear that of the numerical models studied the Simplified Eddy-Viscosity model is the most representative of the lidar measured flow behaviour for the three inflow conditions. Whilst not attempting to model the near wake behaviour the Eddy-Viscosity initiation at two rotor diameters downstream is shown to match closely the maximum velocity deficit locations identified in Table 7.1. At lower wind speeds, Figure 6.25 – Figure 6.27, the value of this maximum deficit is seen to track that of the lidar measurements. Above 12m/s, Figures 6.28 – Figure 6.29, however the maximum deficit value is underestimated in all cases. Through the 6m/s – 12m/s wind speed range, Figure 6.24 – Figure 6.26, the Eddy-Viscosity model can be seen to produce behaviour closest to that of the disturbed inflow condition, while slightly overestimating the velocity deficit of the undisturbed conditions and underestimating that of the waked conditions. Above 12m/s this modelling approach underestimates the velocity deficit from the inlet for all three of the inflow conditions.

The SST model produces an initially accurate profile of the flow evolution towards the maximum deficit from the rotor plane however it underestimates the recovery gradient beyond this. The recovery profile is therefore not in good agreement with the experimental results. The PARK model's initiation at the rotor plane proves a poor comparison to the measured results in the near wake, showing initial overestimation of the experimental results before converging to the measurements around eight to ten rotor diameters. Further downstream both the PARK and SST models follow a similar trend to the lidar measurements but the poor resolution of the lidar results measured beyond thirteen rotor diameters makes it difficult to draw further conclusions on the significance.

Wind turbine separation at the site of interest occurs at close to 7 rotor diameters along the wind farm axis, Figure 4.13, and 9.9 rotor diameters on the diagonals between the rows and columns. The percentage differences between the Eddy-Viscosity model and the different inflow condition wake speed profile measurements for each wind speed bin at these distances downstream from the rotor are detailed in Table 7.7; the variation at 12 rotor diameters is also presented. Negative values indicate situations where the lidar measured deficit from inlet is less than that of the Eddy-Viscosity model, positive values indicate the opposite.

Speed Bin (m/s)	Undisturbed Difference (%)			Disturbed Difference (%)			Waked Difference (%)		
	7.1 Ø	9.9 Ø	12 Ø	7.1 Ø	9.9 Ø	12 Ø	7.1 Ø	9.9 Ø	12 Ø
6-8	-5.5	-6.4	-3.4	-2.2	-2.9	-1.8	6.0	4.1	5.0
8-10	-8.4	-6.9	-4.1	0.0	1.2	0.3	5.1	6.6	6.2
10-12	-3.6	-2.5	-1.0	2.8	3.4	3.1	9.9	10.4	10.0
12-14	3.6	2.8	3.0	8.2	7.4	7.3	10.7	10.9	9.7
14-16	20.8	13.6	12.5	14.0	13.2	12.8	15.2	13.6	12.5

Table 7.7: Percentage difference between the Eddy-Viscosity model deficit and that of the three inflow condition profiles, Figure 6.25 - Figure 6.29

Considering the most frequent wind speed bin for the Alpha Ventus wind farm, the 8-10m/s range, a number of key observations can be made from the values presented in Table 7.7.

For the undisturbed inflow case the Eddy-Viscosity model is shown to overestimate the deficit from inlet conditions at each of the downstream measurement locations detailed, Table 7.7. This overestimation is shown to reduce with distance downstream. This is a clear underestimation of the potential energy in the wind downstream of a turbine operating in undisturbed flow which is of particular significance at the seven rotor diameter location, the spacing at the site under study.

For the disturbed inflow conditions the Eddy-Viscosity model produces a more agreeable comparison between the measured and simulated deficits in the 8-10m/s wind speed bin. The comparison in Table 7.7 shows a 0% difference between the Eddy-Viscosity predictions and the disturbed inflow measurements at 7.1 diameters, a 1.2% underestimation at 9.9 and 0.3% at 12. These differences are small enough to be within the bounds of the standard error deviation at each location, Figure 6.16. Extending the analysis of the disturbed inflow profile the maximum deviation between 6m/s and 12m/s is below $\pm 3.4\%$ from the model to the measurements, again a close correlation.

For the waked inflow situations the comparisons are the inverse of the results for the undisturbed inflow showing an underestimation of the deficit from inlet at each of the downstream locations for each of the wind speed bins considered. At 7 rotor diameters this overestimation is 5.1% increasing to greater than 6% for the ten and twelve diameter locations in the 810m/s wind speed bin, Table 7.7.

Analysis of the results presented above shows that the 6% turbulence intensity value defined at the inception of the Eddy-Viscosity model produces a profile that most closely matches that of the disturbed inflow conditions. Focussing on the predominant wind speed bin of 8-10m/s visual inspection of Figure 6.26 shows that the model and lidar measured profile closely match each other from 3 diameters downstream to 12 diameters where the increasing scatter in the measurements makes further comparison inappropriate. It is clear from the presented results and the simulations of changing turbulence levels in the Eddy-Viscosity model, Figure 2.12, that in order to individually tailor the Eddy-Viscosity model more closely to the undisturbed inflow case the inlet turbulence intensity should be increased. This does not reflect the turbulence conditions of the inlet which will decrease from the disturbed to undisturbed inlet conditions. The opposite behaviour is true for the fully waked inflow where a turbulence intensity decrease allows better correlation between the measured and simulated data sets. Again this feature does not reflect the expected turbulence level changes where they would be expected to increase from the disturbed to waked inflow conditions. The Eddy-Viscosity models suggests that increases in inflow turbulence will lead to faster recoveries towards freestream of each of the models as mixing between the wake and the surrounding air flow is increase. The captured wake measurements do no show this behaviour rather showing the opposite. This is likely brought about by the atmospherically stable offshore flow conditions leading to a more defined wake that does not mix with the surrounding flow fields.

7.2.2 Wake width profile analysis

Analysis of the measured Figure 6.30 – Figure 6.38 wake width profiles suggests behaviour for disturbed inflow that indicates the development of a wake width structure that becomes more defined as inlet wind speed increases. The structure of the measured results at lower wind speeds follows a wider arc that does not reach inlet levels before the bounds of the measurement domain. At higher wind speeds the arc is narrower with a smaller peak with the measured behaviour reaching inlet values before the wake reaches a width of two rotor diameters. These measurements indicate that the wake is consistently wider at lower speeds than at the same distance downstream for higher wind speeds. This therefore increases the likelihood of wake interaction with downstream turbines as the wake spreads out in to the wind farm more. At higher wind speeds this interaction is less likely to occur as the wakes are more defined.

It should be noted that the scan period of 648 seconds of the wake width scans used for the analysis will introduce a larger uncertainty in the measurements. Over such an extended time period the turbulent nature of the winds mean that the features measured will have moved on during the scan and as a result the results are not a true snapshot in time across the wake width. As discussed in Chapter 2 this is an inherent issue with using scanning lidars for such measurements and must be taken into account when analysing the results. Averaging a number of scans in each wind speed bin will allow for a reduction in this error as a more steady state analysis can be completed and features common to each inlet condition extracted.

The comparison with the two numerical models in Figure 6.39 – Figure 6.47 shows that the PARK model methodology does not offer sufficient

functionality to modify the velocity variation radially out from the centreline. The flat wake profile observed does not correspond to the measured behaviour. As presented in the centreline wake deficit analysis of Section 6.3.5 the magnitude of the deficit predicted by the PARK model in this case does not correspond to the measurements and lower inlet wind speeds and distances from the device.

The comparison of the wake width profile predicted by the Simplified Eddy-Viscosity model and the lidar measurements is far more favourable. Both profiles across the wake width exhibit a peak on or near the centreline that reduces in magnitude with distance from the device and as inlet wind speed increase. At lower wind speeds the lidar measured profile is less pronounced and the wake width is observed as significantly wider than that predicted by the numerical analysis. In the higher wind speed bins, where a clearer profile is presented, the rate of recovery towards inlet is less than that predicted. This leads to a shallower recovery in the lidar measured profile that recovers beyond the bounds of the wake predicted by the Eddy-Viscosity model.

The study suggests that at lower wind speeds the width profile is less defined and more prone to mixing with the surrounding flow field. This does not compare well with the established profiles presented by the PARK and Eddy-Viscosity models, particularly in their prediction of an immediate recovery to inlet conditions at the wake bounds. At higher wind speeds, above 10m/s, the measured profile becomes more defined across the width of the wake, with measured speeds returning towards inlet at the measured bounds. This measured wake width at higher wind speeds is wider than either of these models predict.

7.2.3 Measurement uncertainties in offshore comparisons

The deployment of the scanning lidar devices on the nacelle roof of an operational turbine has reduced some of the uncertainties explored in Section 7.1.4 for ground based lidar deployments while introducing new ones.

The nacelle roof location of the lidar allows it to yaw with the turbine ensuring that the measurements are always aligned with the turbine centreline. This installation methodology has allowed for the implementation of horizontal scan planes that capture hub height flow measurements removing the uncertainties associated with the angled scan planes of previous work.

However, no work has been done to correct the lidar scan plane for the dynamic movement of the nacelle. As the wind speed increases so too does the loading on the turbine and blades. This loading produces a bending moment at the tower base which will result in the movement of the nacelle. As the structure is pushed backwards the front of the nacelle will rise and the back will fall. Using a random nacelle tilt of 1° , it can be calculated that this will lead to an increase in the inlet measurement location (2.5 rotor diameters upstream) above hub height of 5m. At measurement locations downstream this change in inclination will result in measurements below the hub plane. At 8 rotor diameters downstream this corresponds to 16m below hub height (or 21m below the inlet measurement height) and at 13 rotor diameters this is 26m (31m below inlet). Figure 7.1 below illustrates this process.

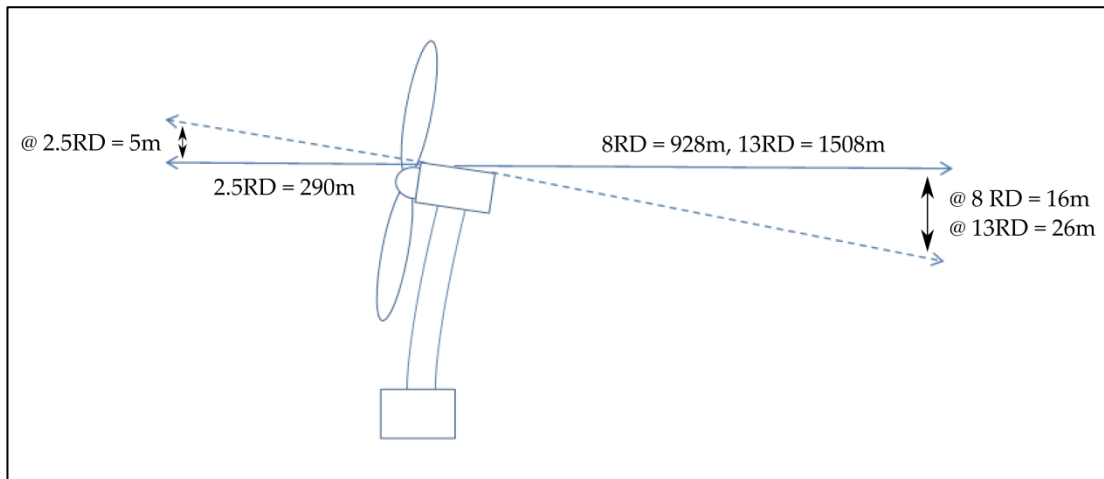


Figure 7.1: Nacelle pitch effects on scan plane

In order to fully quantify the scope of these movements and their subsequent effect on the results further work and analysis is required. The Galion Lidar is equipped with pitch and roll sensors but at this stage it is unclear the operational nature and the calibration of these devices as well as their suitability in measuring the movements of the turbine nacelle in these planes.

What is clear is that any movement in the nacelle in this manner will have an effect on the measurement locations along the scan plane. In discussions with AREVA engineers [132] it was made clear that the magnitude of such movement is not likely to have a simple linear relationship to wind speed and is more likely to have an oscillating profile thus making it very difficult to interpret in the results. This feature will increase the measurement uncertainties in the location of the measurement points used in the analysis.

As described in Section 7.1.4 the uncertainties in using the arc scan methodology increase as the separation between each beam increases. For the wake centreline measurements presented this feature is not present as the raw line-of-sight doppler shift measurements are used to calculate the component of the wake wind speed moving away from the rotor plane. The

surrounding data points have not been used in the formulation of the utilised wind speeds and therefore no formulation uncertainty exists.

The three dimensional wake flows do however contain a strong rotational aspect to it which has not been discussed in the results presented as the use of the lidar measurements in this manner makes no attempt to capture this information. As neither the PARK nor Eddy-Viscosity models attempt to model this behaviour instead simply modelling the wind speed moving away from the rotor plane the comparison of line-of-sight based lidar measurements against these models is valid as like for like. The three dimensional SST model on the other hand does attempt to model this behaviour, a valid comparison with the lidar data is facilitated by only extracting the components of the flow vectors moving perpendicular to the rotor plane as in the lidar data extraction. While the rotational aspect of the flow does exist the measured and numerical data utilised in the presented comparisons only seeks to represent the component of the wind speed moving away from the rotor plane. As the comparison methodology is seeking to compare only the measured and simulated wind vector components moving downstream the uncertainties associated with this methodology are less than those for the ground based measurements. From theory [136] it is likely that the rotational aspect of the wind speed at the wake centreline is at a minimum and thus the uncertainties here are also small.

By contrast the uncertainties arising from the wake width measurements are similar to the onshore deployments. In order to capture the width profile across the wake the arc scan wind speed formulation method employed in the onshore deployments has been employed. While the comparative uncertainty in employing this method is reduced by capturing measurements

in a horizontal plane the uncertainty of calculating wind vectors using three different data points is preserved. A 1° beam separation has been used to reduce this uncertainty and increase the spatial resolution of the width plots. This method has increased the time overhead required to complete the scan arc which increases uncertainties in the time resolution of the measurements, the flow field captured at the minimum azimuth boundary of the arc scan will not be the same as that measured by the time the lidar scan has reached the maximum azimuth boundary.

Discussed above the wake centreline measurements have not tried to account for the wake rotation as at the centreline this expected to be at a minimum. However the wake width profiles capture information from the centreline out to the wake bounds, it can be surmised [136] that the measurements captured will feature increasing levels of rotational flow with distance from the centreline. As the same methodology for simulating and extracting the wake centreline flow speeds has been used for the width profiles this effect has not been accounted for in the comparisons completed. The uncertainties associated with each measurement can therefore be said to increase with distance from the wake centreline.

Each of the numerical models employed requires an inlet definition to initiate the calculations of flow speeds. In the PARK and Eddy-Viscosity model this is simply defined as the inlet wind speed corresponding to the freestream the turbine is operating in. In the work presented the value measured at 2.5 rotor diameters upstream of the rotor plane is used for both of these models. This distance is commonly accepted as it is deemed far enough in front of the rotor to be beyond the wind speed slow down into the rotor predicted by actuator disk theory [73]. In the SST model employed in Windmodeller the inlet is defined by the same wind speed conditions as the

other models but its location is at hub height at the edge of the domain defined in the model. For the simulations completed this is at a distance of 5000m from the rotor plane. This large distance increases the uncertainty and confidence in the accurate definition of the inlet conditions as it is uncertain how these evolve to the rotor plane. However, as the offshore domain is simple with a simple low uniform roughness and no terrain or obstacles between the inlet and turbine these uncertainties are minimal.

Chapter 8:

**Conclusions and
summary**

8.1 Conclusions

The work presented in this thesis demonstrates a unique comparison of high resolution wind turbine wake measurements against numerical models of the same features. Captured using scanning lidar devices in operational on and offshore wind farms the wake measurements allow the evolution of the wind speeds through the rotor plane and into the far wake to be visualised in detail not available using traditional techniques. Both deployment situations represent unique challenges and opportunities the results of which have been presented in the preceding chapters. The findings and conclusions from this work are summarised below.

8.1 Onshore lidar analysis summary

Deploying the scanning lidar device at ground level in an operational onshore wind farm the captured measurements clearly identify the evolution of wake structures behind the operational turbines for a variety of flow speeds and orientations. Deployed over a number of days the data sets present a number of opportunities to capture wake centreline data for extraction and comparison with three dimensional numerical models in ANSYS Windmodeller. The key findings from the results presented in Section 6.2 are:

- Lidar measured data sets capture flow behaviour through the turbine rotor plane and into the wake for a variety of flow conditions.
- The inclined scan plane used from the ground based lidar introduces significant uncertainties as measurements are captured across the boundary layer in complex terrain.
- Comparison of the lidar data averaging time periods in Section 6.2.3 show that the one hour time period improves the consistency of the measured profiles. However, this time period is inappropriate as it misses key details such as changes in flow orientation and turbine yaw. For future analysis ten minute averaging periods are more appropriate.
- The comparison of different inlet definition methodologies in Section 6.2.3 shows the importance in accurately defining these values for the numerical simulations. These values and attributes must be based on values measured in front of the turbine rotor rather than the flow field surrounding it.

The work completed based on the ground based lidar deployments has provided a rich data set for comparison with numerical models and a valid proof of concept for the project. However the methodology employed in capturing wake measurements involves significant uncertainties focussed around the inclined scan plane and use of arc scans over a wide range. The findings outlined above have been used to inform the design and focus of the offshore nacelle mounted lidar deployment.

8.2 Offshore analysis conclusions

Building on the findings from the onshore analysis the offshore lidar deployment captured a unique and comprehensive data set detailing wake flow behaviour for a wide range of inflow wind speeds. Averaged over 2m/s wind speed bins the results allowed for the visualisation of wake centreline profiles for undisturbed, disturbed and fully waked inflow conditions. Wake width profile data was also captured in the same wind speed bins for the disturbed inflow conditions only. Comparisons were completed with the numerical PARK and Eddy-Viscosity wake models as well as the complex SST model in ANSYS Windmodeller. The key findings from the offshore wake analysis study are explored below:

The captured lidar measurements clearly demonstrate the evolution of wake centreline flow behaviour with increasing wind speeds.

- While the deficit from inlet conditions is consistent for all wind speeds at close to 30% the maximum deficit from inlet is shown to be highest at lower wind speeds and clearly shown to decrease as wind speed increases. The maximum deficit value can be shown to decrease as the operational C_p in each wind speed bin decrease.
- The maximum deficit location is consistently found at close to two rotor diameters.
- There is a clear and consistent difference in deficit between the profiles of each of the inflow conditions at each measurement point downstream of the rotor. The undisturbed inflow demonstrates the smallest deficit; the disturbed inflow demonstrates a larger deficit and

the waked inflow a larger still deficit. This behaviour is consistent across all wind speed bins and is preserved from the rotor plane to thirteen rotor diameters downstream.

- The results reiterate the importance of spacing in an offshore wind farm and its potential effects on power availability to turbines operating in disturbed or fully waked flow. Larger spacing leads to more certainty and consistency in the potential available power across the wind speed bins. For lower spacing small variations in this spacing and inlet wind speed can lead to large variations in potential power availability.

The width measurements capture clear profiles across the wake width at discreet distances downstream across the wind speed bins, only disturbed inflow behaviour has been captured.

- The maximum deficit echoes that of the centreline profiles in each bin and location downstream.
- At lower wind speeds the deficit from inlet in the wake is found to extend far beyond the bounds of the measurements taken.
- The wake width profile structure becomes more clearly defined as the inlet wind speed increases.
- At higher wind speeds the width of the wake does not continue to increase with distance from the rotor plane rather it is found to stabilise around a width of two rotor diameters.

The comparisons with numerical models provide a good analysis of the strengths and weaknesses of each modelling approach in comparison to the lidar captured data sets.

- The SST model captures the initial deficit behaviour and outlines a profile with similar behaviour to the lidar profiles. However it tends to underestimate the value of the maximum deficit from inlet and the gradient of the recovery beyond this.
- The PARK model does not capture initial wake behaviour well but is closely matched with the measurements further downstream beyond 6 rotor diameters.
- While not modelling the initial deficit and behaviour the Eddy-Viscosity model provides the closest approximation of the maximum deficit and subsequent recovery towards inlet speeds for the lidar measured profiles.
- The Turbulence Intensity definition of 6% in the Eddy-Viscosity model provides the closest match with the disturbed inflow profiles.
- Eddy-Viscosity model theory suggests that an increase in turbulence will decrease the deficit from inlet at a given point downstream. The opposite is found to be the case in the lidar measured profiles as the increases in turbulence from the undisturbed to disturbed to fully waked inflow conditions lead to increasing values of the deficit from inlet at any given point downstream.

Chapter 9:

Future work

9.1 Future Work

The work completed and presented in this thesis demonstrates the potential of utilising scanning lidar devices in capturing wake flow development in on and offshore wind farms. The installation of nacelle mounted lidar devices has provided a broad data set encompassing a wide range of flow conditions experienced by the active turbine. The data sets captured have provided a unique insight into lidar measured wake development under these conditions. Focussing on these captured data sets further analysis should focus on the evolution of wake profiles through different periods of the day, and for different atmospheric conditions.

The extensive data set captured provides ample data to complete the wake width analysis and comparison for all three inflow conditions. In addition the lidar devices were programmed to capture wake height measurements along the wake length that were not included in this study. Analysis of this data will allow visualisation and analysis of the wake structure and intensity variations in the vertical plane for the conditions analysed. Combined with the work presented in this thesis such work would offer an understanding of the propagation and dissipation of the wake in three dimensions and the effects this can have on optimal performance and wind farm layouts.

Further work should also be completed in the analysis of the pitch of the nacelle in higher winds. The results will allow an understanding of the uncertainties involved in this type of lidar deployment and an exploration of the possible mitigation techniques that can be employed to reduce the uncertainties.

The comparison with a variety of numerical models has pointed towards the accuracy of the Eddy-Viscosity model for this method of flow analysis.

Further work will allow further assessment of these observations leading to improvements in the application of the model to provide a more consistent comparison with the varied inflow conditions experienced. Specifically considering the effect of the definition of Turbulence Intensity for each inflow condition and addressing the contradictory numerical prediction and measured results behaviour. From this work should be completed on how it can be used to best replicate the measurements for these conditions and varying wind speeds.

Completing the data collection procedure and allowing the visualisation of the centreline, width and height profiles will allow a fuller understanding of wake flow development in the offshore environment. Such an understanding will potentially allow further analysis in the field of deep array models and the energy loss experienced within large wind farms. Modification of such models based upon these findings could allow improvements in the spacing and performance of such wind farms.

References

- [1] *UK Renewable Energy Roadmap Update 2012*, Department of Energy and Climate Change, Released 27th December 2012. www.decc.gov.uk, accessed 17/08/2014.
- [2] *Renewable Solar & Wind Energy Produced as Much as 60% Of Germany's Electricity October 3rd*, <http://cleantechnica.com> , accessed 15/10/2013.
- [3] *Wave and Tidal Energy in Scotland*, Published by Scottish Development International, 20th October 2012.
- [4] *Renewable Obligation: Guidance for Generators*, Published by Ofgem, Update draft released 20th December 2012.
- [5] *Feed-In Tariff: Annual Report 2010 – 2011*, Published by Ofgem, Released 21st December 2011.
- [6] *UK Renewable Energy Roadmap*, Published by Department for Energy and Climate Change, July 2011.
- [7] *The future role of energy storage in the UK: Main Report*, Published by The Energy Research Partnership, July 2011.
- [8] *The EU's Target for Renewable Energy, 20% by 2020, Volume 1: Report*, Published by the Authority of the House of Lords, HL Paper 175-I, October 2008.
- [9] *2020 Renewable Routemap for Scotland – Update*, Published by The Scottish Government, Released 30th October 2012.
- [10] *Top 10 Biggest Wind Turbines in the World*, Wind Power Monthly, www.windpowermonthly.com/10-biggest-turbines, accessed 17/08/2014.
- [11] *Samsung 7MW Rises in Scotland*, ReCharge News, October 2013, www.rechargenews.com, accessed 17/08/2014.

- [12] M. Caduff et al, *Wind Power Electricity: The Bigger the Turbine, the Greener the Electricity?* Environmental Science and Technology 2012, 46, pp 4725–4733.
- [13] T. Burton et al, *The Wind Energy Handbook*, John Wiley and Sons, ISBN 0-471-48997-2.
- [14] *Windcube V2 Offshore: Vertical Wind Doppler Lidar*, NRG Renewable Systems and Leosphere promotional material, www.leosphere.com, accessed 17/08/2014.
- [15] J. Bleeg, *Windmodelling Advances Offer Big Project Savings*, North American Wind Power, Issue NAW1305, Volume 10, Number 4, May 2013.
- [16] O. Guillermin and S. Ravi Shankar, *Automating Wind Blade Development from Root to Tip*, Wind Systems Magazine, July 2012.
- [17] *A Guide to Offshore Wind and Oil and Gas Capability*, Scottish Enterprise, SE/3432/Sep11, September 2011.
- [18] I. Dinwoodie, D. McMillan, *Analysis of Offshore Operation and Maintenance Using a Novel Time Domain Meteo-Ocean Modelling Approach*, Proceedings of ASME Turbo Expo 2012, GT2012-68985, Copenhagen, Denmark, July 2012.
- [19] *Our Electricity Transmission Network: A Vision for 2020*, Published by Department of Energy and Climate Change, URN:11D/954, February 2012.
- [20] T. Mikkelsen, A. Peña and C. B. Hasager, *Remote sensing for wind energy*, pages 7–20. Risø DTU, 2011.

- [21] G. Biswas, *Historical Developments in Computational Fluid Dynamics*, CFD Development From Aerospace: Course Notes, Indian Institute of Technology Kanpur, Volume 3, No 2, January 2000.
- [22] *Wind Resource Assessment Handbook*, Published by National Renewable Energy Laboratory, AWS Scientific Inc, Albany, NY, USA, April 1997.
- [23] A. Clifton, D. Elliot and M. Courtney, *Recommended practices for remote sensing for wind energy applications: 1. Ground-based vertically profiling remote sensing for wind resource assessment*, 1st Draft Edition 2012, IEA Wind.
- [24] P. Clive, *Remote Sensing Best Practice*, PO.0322, EWEA Offshore 2011, Amsterdam.
- [25] *Lidar 101: An Introduction to lidar Technology, Data and Applications*, National Oceanic and Atmospheric Association (NOAA) Coastal Services Centre, November 2012.
- [26] J. Whiteway, C. Cook, L. Komguem et al, *Phoenix lidar Characterisation*, Fourth Mars Polar Science Conference, 2006.
- [27] P. Clive, *Second Generation Lidar*, Published in Wind Systems Magazine, October 2011
- [28] *Lidar Gains Market Size and Share in North American Imagery and Value-added Services and Markets*, Published by Frost and Sullivan, May 2004.
- [29] Halo Photonics, Unit 2, Bank Farm Offices, Brockamin, Leigh, Worcester, United Kingdom, WR6 5LA, <http://halo-photonics.com>.
- [30] Galion Lidar G4000 Offshore, Developed by Halo-Photonics, Marketed by SgurrEnergy Ltd. www.sgurrenergy.com.

- [31] SgurrEnergy Ltd, 225 Bath Street, Glasgow, G2 4GZ,
www.sgurrenergy.com
- [32] QinetiQ, Cody Technology Park, Old Ively Road, Farnborough, GU14
0LX, www.qinetiq.com
- [33] ZephIR lidar, Developed by QinetiQ, Marketed by Natural Power.
www.zephirlidar.com
- [34] Natural Power Limited, The Green House, Forrest Estate, Dalry, Castle
Douglas, DG7 3XS, Scotland, UK, www.naturalpower.com
- [35] Leosphere, 14-16 Rue Jean Rostand, Parc Club Orsay Universite, 91400
France, www.leosphere.com
- [36] Windcube lidar, Developed by Leosphere, marketed by NRG.
www.lidarwindtechnologies.com
- [37] C. Slinger, M. Harris, *Introduction to Continuous-Wave Doppler lidar*,
Renewable Energy and Sustainable Energy Institute, Colorado, Internal
Paper, 2012
- [38] P. Clive, *Seeing The Light - The Wind Power Applications of lidar*,
SgurrEnergy Ltd, 204 George Street, Glasgow, G2 4GZ.
- [39] I. Antoniou, et al., *Remote Sensing the Wind Using Lidars and Sodars*, Risø
DTU, National Laboratory, Technical University of Denmark, Roskilde,
Denmark.
- [40] *Wind Energy - The Facts*. 1st Edition ed. 2009: European Wind Energy
Association & Earthscan.
- [41] B.F. Webber, *Convective Wind Fields as Investigated With Doppler Lidar*,
Department of Atmospheric Science, Colorado State University,
Atmospheric Science Paper No. 411, June 1987.

- [42] C. Hill, *Remote Sensing (UpWind WP6) QinetiQ Lidar Measurement Report*, Project UpWind: Contract Number 019945 (SES6), Technical Report (Deliverable 6.1.1), September 2010.
- [43] P. Clive, *2nd Generation Lidar Techniques*, European Wind Energy Conference 2010, Poland, April 2010.
- [44] P. Clive, *Seeing The Light - The Wind Power Applications of lidar*, SgurrEnergy Ltd, 204 George Street, Glasgow, G2 4GZ.
- [45] M.I Skolnik, *Radar Handbook*, Chapter 1, Second Edition, McGraw Hill, ISBN 0-07-057913-X, December 1989.
- [46] J. Mann et al, *Remote Sensing for Wind Energy*, DTU Wind Energy-E-Report-0029(EN), Risø DTU, National Laboratory, Technical University of Denmark, June 2013.
- [47] Catch the Wind/Blue Scout – Vindicator, www.bluescout.com
- [48] LockHead Martin – WindTracer, www.lockheedmartin.co.uk , August 2014.
- [49] P. Clive, *Galion – The Definitive Wind lidar*, Produced by SgurrEnergy Ltd, 204 George Street, Glasgow, G2 4GZ, 2012.
- [50] J. Gottschall, P. Lindelöw-Marsden and M. Courtney, *Executive Summary of Key Test Results for SgurrEnergy Galion*, Riso DTU, CVR-nr. DK 30 06 09 46, July 2009.
- [51] Measuring Network of Wind Energy Institutes (MeasNet), *Anemometer Calibration Procedure Version 2*, October 2009.
- [52] K. Franke; Performance Verification of Galion, Serial No.: 36, Project No. VC12478, Deutsche WindGuard, March 2013.

- [53] *Galion Lidar delivers one year of bank-grade data from Asia's first offshore Lidar platform*, DNV KEMA, SgurrEnergy Ltd, May 2013.
- [54] J. Gottschall; *Galion lidar Performance Verification: Technical Report*, Fraunhofer IWS, May 2013.
- [55] *ZephIR Lidar win prestigious Institute of Physics Innovation Award*, Article on PRWEB UK, accessed 8 July 2013, www.prweb.co.uk.
- [56] M. Harris, *Wind Resource Measurement by Laser Anemometry*, Wind Tech International Volume 3, June 2007.
- [57] I. Locker, A. Woodward, *Introducing the New ZephIR 300*, Windtech International November/December 2010, Published 2010
- [58] Vector Instruments 100L Class 1 Cup Anemometers, Windspeed Limited (Vector Instruments), 115 Marsh Road, Rhyl, Denbighshire, LL18 2AB
- [59] T. Rutherford, *Lidar Calibration and Validation Process*, Natural Power, AWEA 2012
- [60] *Windcube V2 lidar Remote Sensor*, Produced by NRG and Leosphere, 2012 lidar Wind Technologies.
- [61] I. Campbell, *A Comparison of Remote Sensing Device Performance at Rotsea*, res Renewable Energy Consultants, February 2008, Document Reference: 01485-000090.
- [62] Triton Sonic Wind Profiler, Second Wind, 15 Riverdale Avenue, Newtown, MA 02458, USA
- [63] *Windcube 100S-200S Scanning Wind Doppler LIDAR Systems*, Produced by NRG and Leosphere, 2012 Lidar Wind Technologies.

- [64] A. Albers, A.W. Janssen, J. Mander, *How to Gain Acceptance for Lidar Measurements*, Deutsche WindGuard Consultants GMBH.
- [65] P. Clive, *Remote Sensing – the Current Status, The Boulder Protocol*, European Wind Energy Conference, April 2010, Warsaw, Poland.
- [66] *Use of Remote Sensing for Wind Energy Assessments*, DNV-RP-J101 Recommended Practice, Det Norske Veritas (DNV), April 2011.
- [67] IEC 61400-12-1, *Power Performance measurements of electricity producing wind turbines*, Edition 1 2005-2012, International Electrotechnical Commission.
- [68] D. Infield, *Wind Turbine Technology 1*, Department of Electronic and Electrical Engineering, University of Strathclyde, Glasgow, January 2009.
- [69] G.C. Larsen, *ABL flow fields and wake affected flow fields in a wind turbine load perspective*, Risø DTU – National Laboratory for Sustainable Energy, Denmark.
- [70] A. Betz, *Introduction to the Theory of Flow Machines*. (D. G. Randall, Trans.) Oxford: Pergamon Press, 1966.
- [71] *Understanding Coefficient of Power (C_p) and Betz Limit*, Kidwind Science Snack: Betz Limit, www.kidwind.org.
- [72] C. Montavon, S.-Y. Hui, et al, *Offshore Wind Accelerator: Wake Modelling using CFD*, EWEA 2011, Brussels, March 2011.
- [73] T. Burton et al, *The Wind Energy Handbook, Chapter 3*, 2nd Edition, Wiley 2011
- [74] G. Ingram, *Wind Turbine Blade Analysis Using the Blade Element Momentum Theory, Version 1.1*, Durham University, October 2008.

- [75] Y.A. Cengel, R.H. Turner, *Bernoulli and Energy Equations, Fundamentals of Thermal-Fluid Sciences, Chapter 12*, McGraw Hill, International Edition, 2005.
- [76] WindFarm from ReSoft, ReSoft Ltd, Coprnwallis, Burycroft Road, Hook Norton, Banbury, OX15 5PR, www.resoft.co.uk.
- [77] WindPro, EMD International A/S, Niels Jernes Vej, 9220 Aalborg, Denmark, www.emd.dk.
- [78] OpenWind, AWS True Power, 426 New Karner Road, Albany, NY 12205, USA, www.awstruepower.com.
- [79] WAsP – Wind Atlas and Application Program, Risø - DTU National Laboratory for Sustainable Energy, Denmark, www.wasp.dk.
- [80] N.O. Jensen; *A Note on Wind Generator Interaction*; RISO M-2411, 1983
- [81] J. Katic, J. Hostrup and N. Jensen; *A Simple Model for Cluster Efficiency*, EWEC 1986.
- [82] DNV GL Garrad Hassan WindFarmer: Theory Manual, Version 4.2; DNV GL Garrad Hassan, January 2011.
- [83] *OpenWind Theoretical Basis and Validation, Version 1.3*; AWS True Power, Albany USA, April 2010.
- [84] J.F. Ainslie; *Calculating the Flow Field in the Wake of Wind Turbines*; Journal of Wind Engineering and Industrial Aerodynamics, 27 (1988), 213 -224.
- [85] Renewable Energy Systems (res) Ltd, Egg Farm Lane, Kings Langley, WD4 8LR, www.res-group.com.

- [86] M. Anderson, P. Stuart; *Simplified Solution to the Eddy-Viscosity Wake Model*; Renewable Energy Systems, Paper Reference: 01327-000202, Issue: 02, July 2009.
- [87] C. Runge; "Ueber die numerische Auflosung von Differentialgleichungen", Math. Ann., **46** pp. 167-178, 1985.
- [88] W. Kutta, "Beitrag zur naehrungsweisen Integration von Differentialgleichungen", Z.Math. und Phys., **46** pp. 435-453, 1901.
- [89] K. Rados, et al., *Comparison of Wake Models with Data for Offshore Windfarms*, Wind Engineering 2001. 25(No. 5): p. 271-280.
- [90] RISO DTU National Laboratory for Sustainable Energy, Frederiksborgvej 399, 4000 Roskilde, Denmark.
- [91] Meteorological Institute of the University of Uppsala (MIUU), Uppsala, Sweden.
- [92] GH Wind Farmer, Garrad Hassan and Partners Ltd, St Vincent's Works, Silverthorne Lane, Bristol, BS2 0QD.
- [93] Robert Gordon University, Garthdee House, Garthdee Road, Aberdeen, AB10 7QB.
- [94] Carl von Ossietzky University of Oldenburg, Ammerländer Heerstraße 114-118, 26129 Oldenburg, Germany.
- [95] Netherlands Energy Research Foundation, Westerduinweg 3, 1755 LE Petten, Netherlands.
- [96] ANSYS Windmodeller, Developed by ANSYS Inc, ANSYS Inc. Version 13. 2010 SAS IP, Inc., 2010.
- [97] *CFD-Online*. Available from: www.cfd-online.com. Accessed 04/09/14.

- [98] J. Boussinesq, *Essai sur la th´eorie des eaux courantes, M´emoires pr´esent´es par divers savants, `a l’Acad´emie des Sciences, XXIII, 1 1-680, 1877.*
- [99] B.E. Launder, G.J. Reece, W. Rodi, *Progress in the Development of a Reynolds-Stress Turbulent Closure, Journal of Fluid Mechanics, Vol. 68(3), pp. 537-566, 1975.*
- [100] P.K. Kundu, and I.M. Cohen, *Fluid Mechanics (4th Edition).* Fourth ed. Academic Press, 2008.
- [101] V. Yakhot, S.A. Orszag, *Development of Turbulence Models for Shear Flows by a Double Expansion Technique, NASA Contractor Report 187611, ICASE Report No. 91-65, July 1991.*
- [102] V. Yakhot, S.A. Orszag; *Renormalization Group Analysis of Turbulence. I. Basic Theory, Journal of Scientific Computing, Vol. 1(No. 1), pp 3 – 51, 1986.*
- [103] F.R. Menter; *Two-Equation Eddy-Viscosity Turbulence Models for Engineering Applications; AIAA Journal, 32(No.8), pp 1598 – 1605, 1994.*
- [104] A.N. Kolmogorov; *The local structure of turbulence in incompressible viscous fluid for very large Reynolds numbers, Proceedings of the USSR Academy of Sciences, 30: 299–303 (1941)*
- [105] S. Pope; *Turbulent Flows, Cambridge University Press. ISBN 978-0-521-59886-6, 2000.*
- [106] A. Bakker, *Applied Computational Fluid Dynamics: Turbulence Models, 2002.*
- [107] The Offshore Wind Accelerator Programme, The UK Carbon Trust, www.carbontrust.com.

- [108] UpWind Project, Work Package Six: Remote Sensing, EU Sixth Framework Programme (FP6), 2006-20011, www.upwind.eu.
- [109] I. Dinwoodie, F. Quail, and P. Clive, *Comparison of Measured and Modelled Wind Turbine Wakes in Non-Uniform terrain Using lidar and CFD, in DTC Wind Energy Systems, Project One*, 2010
- [110] T.Burton et al; *Wind Energy Handbook, Chapter 1*, 2nd Edition, Wiley 2011
- [111] A. Creech; *Myres Hill Study: A Comparison Between the Heriot-Watt Wind Farm Model and lidar Data*, School of Engineering and Physical Sciences, Heriot-Watt University: Edinburgh; 2009.
- [112] Fluidity Open Source CFD Software; Fluidity Project, <http://fluidityproject.github.io>, accessed 4/10/2014.
- [113] *NEG Micon NM54 Main Specification, Technical Report*, NEG Micon, 2004
- [114] Myers Hill Test Site; Operated by TUV SUD NEL Ltd, Scottish Enterprise Technology Park, East Kilbride, GLASGOW G75 0QF; www.tuvnel.com
- [115] Whitelee Windfarm (*Scottish Power Renewables*), Moor Road, Eaglesham, East Renfrewshire, G76 0QQ.
- [116] *FACT-SHEET Alpha Ventus, As of: Dec. 2012*; Deutsche Offshore-Testfeld und Infrastruktur GmbH & Co.KG; DOTI GmbH & Co. KG, Tirpitzstr. 39, 26122 Oldenburg, Germany, www.alpha-ventus.de.
- [117] Ordnance Survey Map and Contour Download, Land-Form PANORAMA-GB, www.ordnancesurvey.co.uk, ©2012.

- [118] *Siemens Wind Turbine SWT-2.3-93 Fact Sheet*; Published by and copyright © 2009: Siemens AG, Energy Sector, Freyeslebenstrasse 1, 91058 Erlangen, Germany; www.siemens.com/wind.
- [119] *Efficient Offshore Wind Programme*, UK Department for Business, Innovation and Skills, www.bis.gov.uk
- [120] *Offshore Windpower M5000: Efficient. Reliable. Powerful*; AREVA Wind GmbH, Am Lunedeich 156, D-27572 Bremerhaven, Germany; www.arevawind.com
- [121] AREVA Wind GmbH, Am Lunedeich 156, D-27572 Bremerhaven, Germany; www.arevawind.com
- [122] FINO 1 Research Platform in the North Sea, www.fino1.de
- [123] Research at Alpha Ventus (RAVE), Fraunhofer IWES, Kassel, Germany; www.rave-offshore.de
- [124] *REPower 5M: The 5-megawatt power plant with 126 metre rotor diameter*; Senvion (formerly REpower Systems SE), Headquarters, Überseering 10, 22297 Hamburg, Germany; www.repower.de
- [125] Alpha Ventus Deployment Locations Documents, SgurrEnergy Ltd, 225 Bath Street, Glasgow, G2 4GZ; www.sgurrenergy.com, © 2013.
- [126] Mortensen, N.G et al, *Getting Started with WAsP 9 - Risø-I-2571(EN)*, Riso National Laboratory, Technical University of Denmark, Roskilde, June 2007.
- [127] C. Montovan, Correspondence with Author, ANSYS Inc., June 2012
- [128] C. Montavon, I. Jones, C. Staples; *Windmodeller Getting Started: Overview*, ANSYS UK, ANSYS Inc., 2010.

- [129] *WAsP User Guide*; Department of Wind Energy, Technical University of Denmark (DTU), Copyright © 1987-2012.
- [130] MATLAB Version 2011b, The Math Works, © 1984-2012.
- [131] *WindFarmer Theory Manual*; Version 4.2.; GL Garrad Hassan; January 2011
- [132] B. Schulte; Communication with AREVA Wind GmbH, Dated 12/09/2013.
- [133] K.A. Stroud; *Engineering Mathematics, 5th Edition*, Palmgrave MacMillan, Published February 2011.
- [134] G. Habenicht; *Offshore Wake Modelling*, Renewable Energy Systems, Renewable UK Offshore Wind, Liverpool, June 2011.
- [135] S.G. Voutsinas, K.G. Rados, A. Zervos; *On the analysis of wake effects in wind parks*; Journal of Wind Eng. Ind., Aerodyn 14, 204-219, 1990.
- [136] F. Massouh, I. Dobrev; *Exploration of the vortex wake behind wind turbine rotor*, The Science of Making Torque from Wind, Journal of Physics: Conference Series 75, 012036, June 2007.

Appendix A

Lidar to mast comparisons

Galion Lidar regression analysis results

The blue points represent ten minute averaged data sets plotting lidar measured data against that from the cup anemometer in Figure. The wind direction comparisons are presented in Figure A.1, the red line identifies a fitted linear model with offset; the green identifies the model without the offset [50].

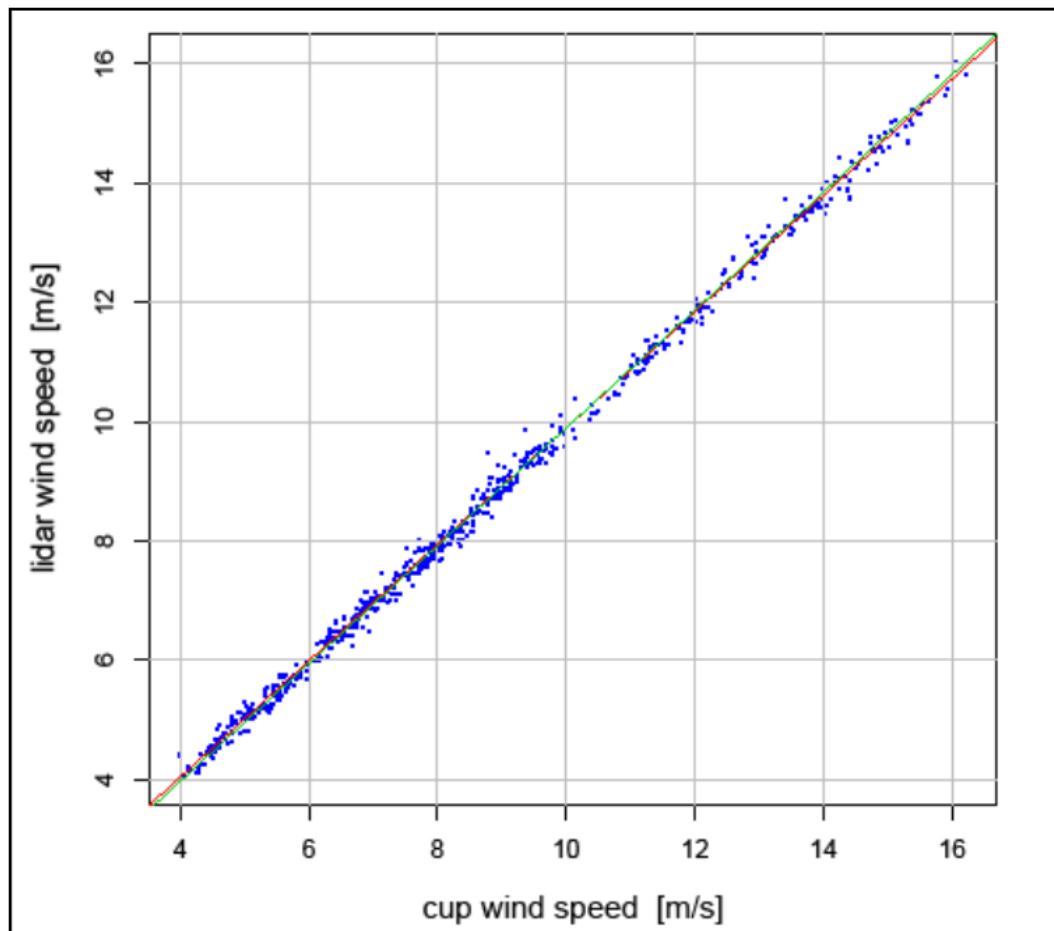


Figure A.1: Standard regression analysis for horizontal wind speed at 100m height [50]

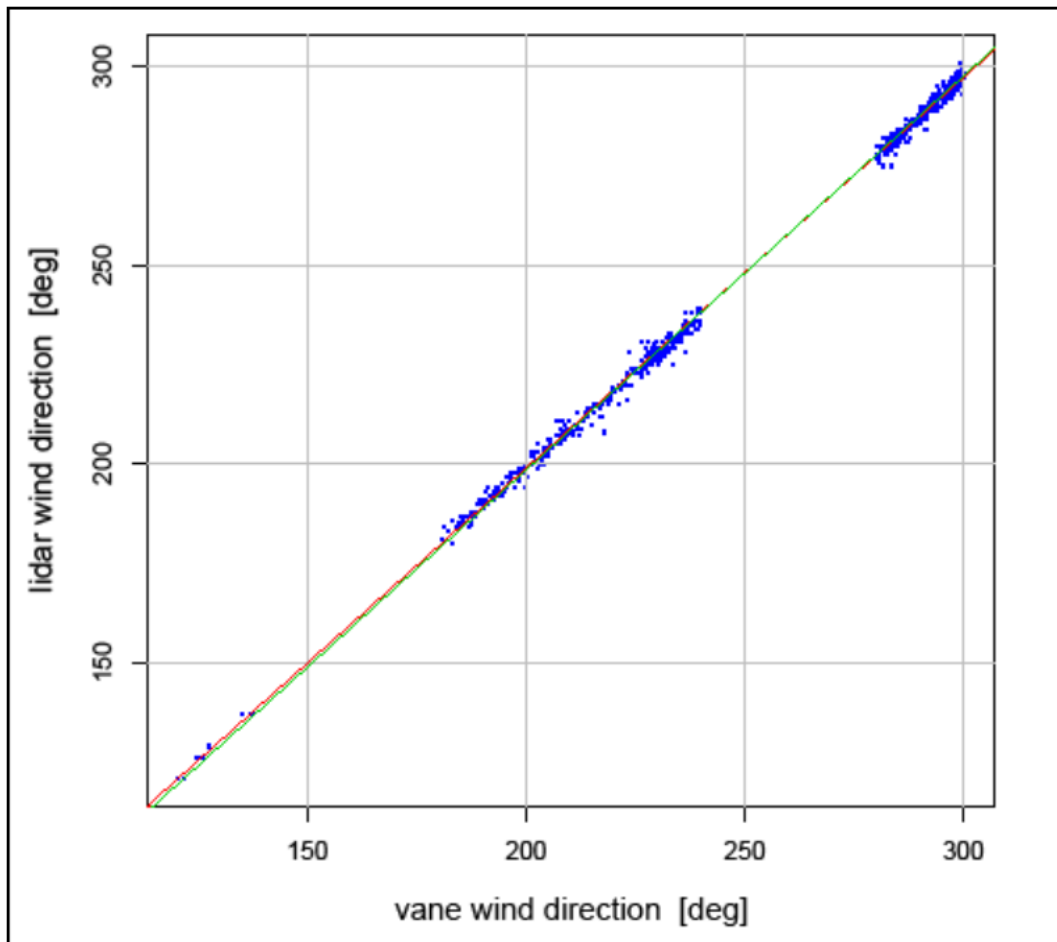


Figure A.2: Standard regression analysis for wind direction at 100m [50]

ZephIR 300 regression analysis results

The blue points represent ten minute averaged data sets plotting lidar measured data against that from the cup anemometer in Figure A.3. The wind direction comparisons are presented in Figure A.4, the red line identifies a fitted linear model with offset; the green identifies the model without the offset [59].

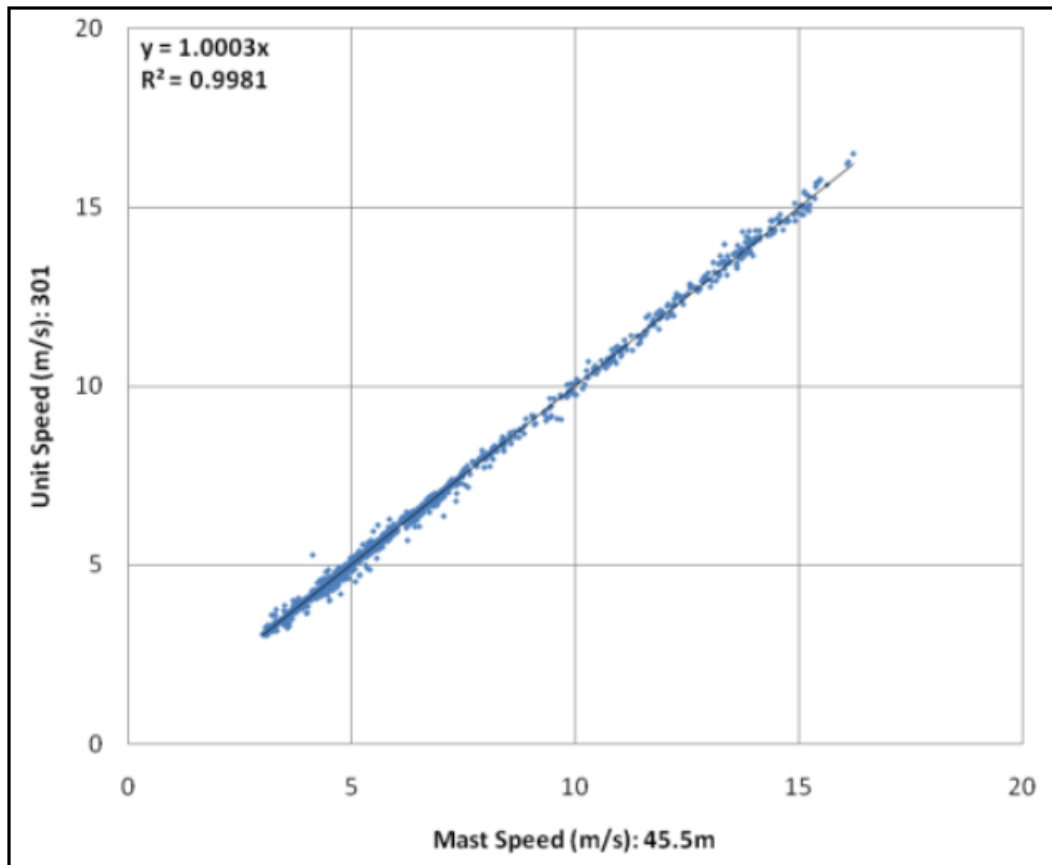


Figure A.3: Standard regression analysis for ZephIR 300 vs mast data at 45.5m [59]

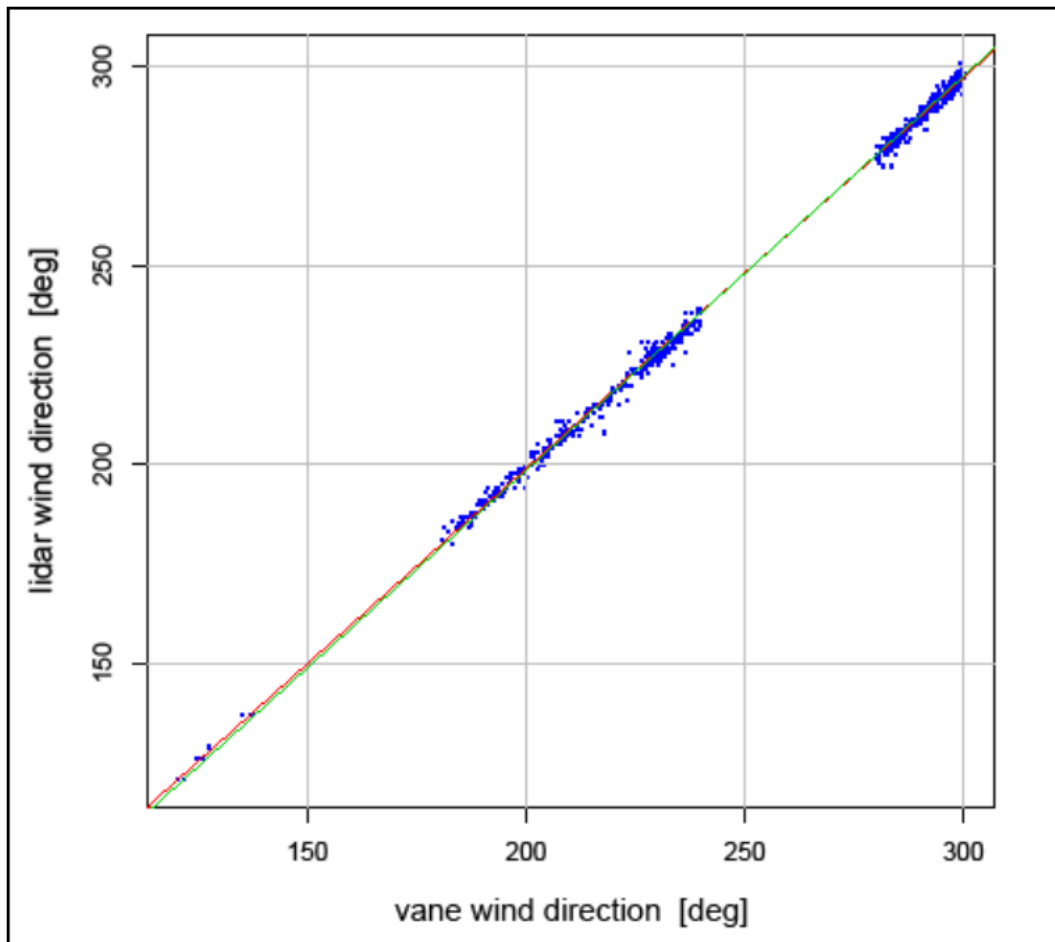


Figure A.4: Standard regression analysis for ZephIR 300 vs Mast data at 91.5m [59]

Windcube V2 regression analysis results

In Figure the red dots refer to data gathered by the Triton SoDAR device and the blue dots to the Windcube V2 data.

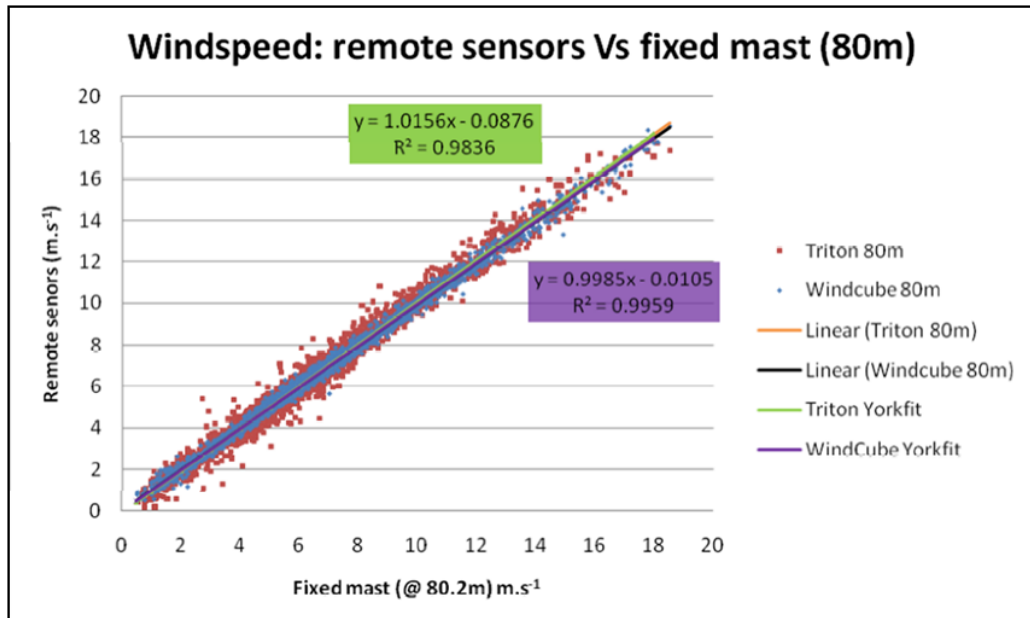


Figure A.5: Comparison of met mast data to Windcube and Triton remote sensing devices at 80m [61]

Appendix B

Extract from DNV-RP-J101, Use of Remote Sensing for
Wind Energy Assessments [66]

The following important aspects of remote sensing technologies must be taken into account to ensure that data are useful for energy assessments:

- Remote sensing technologies are still maturing. Equipment configuration and software changes may affect measurement accuracy, quality, or consistency.*
- Measurement quality may be affected by site positioning. Even perfectly operating Sodars or lidars may provide incorrect measurements in the presence of complex flow (spatially uneven flow) above the instrument. Complex flow may occur in complex terrain or near surface roughness transitions. Additionally, Sodar measurements may be affected by site-specific ambient noises and echoes from nearby objects and surrounding vegetation (“ground clutter”).*
- Remote sensing measurements may be different than those of anemometry. Anemometers provide averages of point measurements of wind speed irrespective of wind direction (“scalar averages”). Sodars and lidars measure average vertical, lateral and horizontal wind speeds. These are usually transformed to provide “vector averages” of wind speed, although some instruments may provide scalar averages. In turbulent conditions, vector averages are lower than scalar averages. These differences mean that remote sensing and anemometry may not provide the same wind speed values although each may be measuring correctly. Each type of measurement system may also provide slightly biased measurements under certain conditions. For example, in conditions with high shear the volume averages of remote sensing instruments are lower than point measurements. In turbulent conditions, anemometer measurements are biased high.*

Appendix C

Actuator Disk Theory Methodology

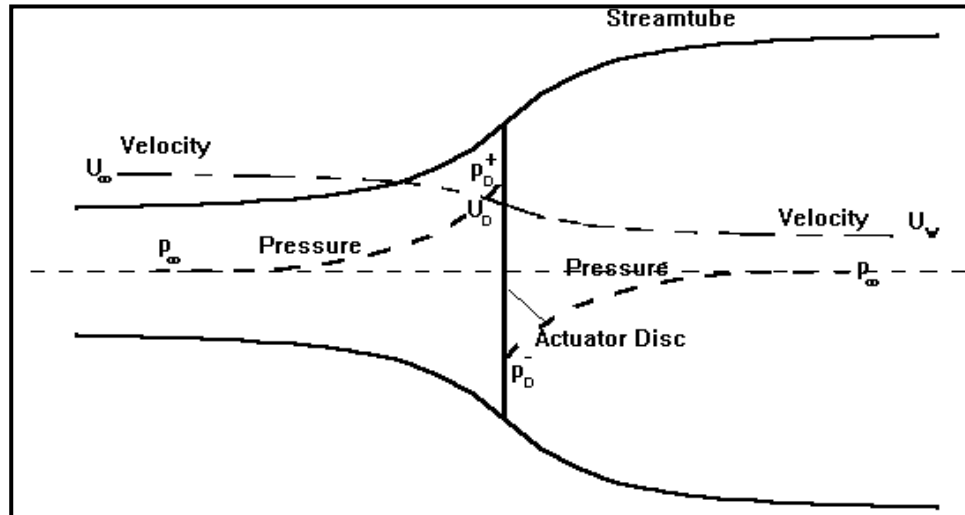


Figure C.1: Actuator Disk concept [68]

In incompressible flow situations the mass flow rate stays constant throughout the domain; Equation C.1 shows the mass flow regime for the wind turbine control volume. For this to hold the fluid properties must evolve in the manner illustrated in Figure C.1. The pressure drop intrinsic to the theory can be seen clearly at the disk plane along with the steady variation in stream tube area and the velocity experienced across this volume.

$$\rho A_\infty U_\infty = \rho A_D U_D = \rho A_W U_W$$

Equation C.1 [68]

$$a = \frac{U_\infty - U_D}{U_\infty}$$

Equation C.2 [68]

The variation between freestream inlet velocity and the axial velocity at the rotor can be accounted for by the introduction of the axial induction factor, **a**

in Equation C.2, this can also be termed the fractional variation between the freestream and rotor plane velocities [73].

Applying the Bernoulli's equations upstream and downstream of the rotor allows the pressure difference variations to be expressed as:

$$\text{Upstream:} \quad p_{\infty} - p_D^+ = \frac{1}{2}\rho(U_D^2 - U_{\infty}^2)$$

$$\text{Downstream:} \quad p_{\infty} - p_D^- = \frac{1}{2}\rho(U_D^2 - U_W^2)$$

Equation C.3 [68]

Subtracting one from the other gives the solution for the pressure difference across the disk in terms of the freestream and wake velocities.

$$p_D^+ - p_D^- = \frac{1}{2}\rho(U_{\infty}^2 - U_W^2)$$

Equation C.4 [68]

Combining Equation C.1 and Equation C.4 with that for the rate of change of momentum caused by the pressure variation:

$$\text{Rate of change of momentum} = \Delta p A_D = (U_{\infty} - U_W)\rho A_D U_D$$

Equation C.5 [68]

Gives:

$$\frac{1}{2}\rho(U_{\infty}^2 - U_W^2)A_D = (U_{\infty} - U_W)\rho A_D U_{\infty}(1 - a)$$

Equation C.6 [68]

Which reduces to:

$$U_W = (1 - 2a)U_{\infty}$$

Equation C.7 [68]

Analysis of Equation C.7 indicates that half of the axial velocity loss takes place upstream of the actuator disc and half after. This is an important concept in actuator disc analysis of wind turbines.

Further analysis allows the thrust and power coefficients to be defined in terms of a .

$$C_T = 4a(1 - a)$$

$$C_P = 4a(1 - a)^2$$

Equation C.5 [68]

It can be noted from the above three equations that a value of a greater than half will produce a negative wake velocity. This can be negated by appropriate modification of the results.

Appendix D

Raw lidar data file formats

The Galion Lidar devices utilised for this project provide output data in a comma separated .scn file format, with a single file produced for each cycle of the scan envelope defined by the user at setup. The following Appendix details the output file format and header explanations from the captured Galion lidar scans.

The top of each scan gives broad details of the scan initiation and individual identifiers in a header before the measurements and location attributes for each individual scan point are detailed line by line. The format presents the measured data for each scan point progressively out from the device ray by ray as identified by the user at scan initiation. Sample scan header and measurement details can be seen in Figure D.1.

1	Filename:	C:\Lidar\Data\2011\201107\20110714\23\22102_14071123_23.scn						
2	Campaign code:	Myres Hill 13 july						
3	Campaign number:	12						
4	Rays in scan:	73						
5	Start time:	23:55:12						
6	Range gate	Doppler	Intensity	Ray time	Az	E1	Pitch	Roll
7	0	-13.670283	1.249598	23:55:12	100.000	6.000	0.213	0.602
8	1	1.333302	1.036100	23:55:12	100.000	6.000	0.213	0.602
9	2	1.523221	1.034960	23:55:12	100.000	6.000	0.213	0.602
10	3	1.903058	1.042783	23:55:12	100.000	6.000	0.213	0.602
11	4	2.358863	1.043288	23:55:12	100.000	6.000	0.213	0.602
12	5	2.415839	1.056589	23:55:12	100.000	6.000	0.213	0.602
13	6	3.023579	1.073210	23:55:12	100.000	6.000	0.213	0.602
14	7	4.277043	1.118480	23:55:12	100.000	6.000	0.213	0.602
15	8	4.409986	1.159011	23:55:12	100.000	6.000	0.213	0.602
16	9	3.859222	1.130912	23:55:12	100.000	6.000	0.213	0.602
17	10	3.669303	1.130756	23:55:12	100.000	6.000	0.213	0.602
18	11	4.049140	1.180655	23:55:12	100.000	6.000	0.213	0.602
19	12	3.859222	1.186098	23:55:12	100.000	6.000	0.213	0.602
20	13	3.194506	1.160021	23:55:12	100.000	6.000	0.213	0.602
21	14	2.757693	1.140188	23:55:12	100.000	6.000	0.213	0.602

Figure D.1: Sample scan header and measurement details

The data in each line details the unique characteristics of each scan point and the measurements taken in 8 columns, the contents of each column is explored below.

Range Gate: Identifies the absolute distance along the beam of the measurement location. The zero range gate is at 45m and each gate after this is at 30m intervals.

Doppler: The measured doppler shift imparted on the measurement beam by the line of sight component of the wind speed velocity at the measurement location.

Intensity: The quality of the back scattered results as measured at the receiving optic of the device. Above and intensity of 1.01 is deemed acceptable.

Ray Time: Gives the hour, minute and second at which each ray begins.

Azimuth: The azimuth value attributed to each ray, constant throughout for Range Height Indicators.

Elevation: The elevation value attributed to each ray, constant throughout for each Plan Position Indicator.

Pitch: The measured pitch of the device at each measurement time.

Roll: The measured roll of the device at each measurement time.

The installed Galion device scans continuously as programmed with each individual scan arc being saved as a new .scn file.

Utilising Galion specific software developed by SgurrEnergy each scan file can be processed to extract the wind speed measurements for the flow field analysed. An example of the process scan file produced from the results can be seen in Figure D.2.

Scan File	Ray Time	Range Gate	Hsp	xCoord	yCoord	wdir	
22102_14071123_23	14/07/2011 23:55:12		1	1.357	29.544	-5.209	289.0
22102_14071123_23	14/07/2011 23:55:15		1	1.851	29.344	-6.237	289.0
22102_14071123_23	14/07/2011 23:55:18		1	3.454	29.109	-7.258	289.0
22102_14071123_23	14/07/2011 23:55:22		1	1.935	28.838	-8.269	289.0
22102_14071123_23	14/07/2011 23:55:25		1	1.245	28.532	-9.271	289.0
22102_14071123_23	14/07/2011 23:55:28		1	1.494	28.191	-10.261	289.0
22102_14071123_23	14/07/2011 23:55:31		1	1.342	27.816	-11.238	289.0
22102_14071123_23	14/07/2011 23:55:35		1	1.307	27.406	-12.202	289.0
22102_14071123_23	14/07/2011 23:55:38		1	1.582	26.964	-13.151	289.0
22102_14071123_23	14/07/2011 23:55:41		1	1.705	26.488	-14.084	289.0
22102_14071123_23	14/07/2011 23:55:44		1	1.482	25.981	-15.0	289.0
22102_14071123_23	14/07/2011 23:55:48		1	1.317	25.441	-15.898	289.0
22102_14071123_23	14/07/2011 23:55:51		1	1.348	24.871	-16.776	289.0
22102_14071123_23	14/07/2011 23:55:54		1	1.542	24.271	-17.634	289.0

Figure D.2: Sample processed out file, July 2011 deployment

The processed out-file contains information for each scan point, detailing more specific values for Range Gate, calculated Horizontal Wind Speed (m/s), x Coordinate (m), y Coordinate (m) and calculated Wind Direction (°). The file name and start time for each ray are also given.

Note: The x Coordinate and y Coordinate locations of each scan point relate to distances in metres from the device location along these axes.

Appendix E

Siemens 2.3 – 93 Power and Thrust Curves [118]

Wind Speed (m/s)	Power (kW)	C_p	C_t
0.25	0.00	0.00	0.35
0.33	0.05	1.47	1.05
0.42	0.09	1.25	1.32
0.50	0.18	1.47	1.23
0.58	0.30	1.53	1.19
0.67	0.46	1.53	1.29
0.75	0.67	1.59	1.29
0.83	0.87	1.50	1.21
0.92	0.96	1.25	1.08
1.00	1.00	1.00	1.00
1.08	1.00	0.78	0.82
1.17	1.00	0.63	0.73
1.25	1.00	0.50	0.65
1.33	1.00	0.41	0.55
1.42	1.00	0.34	0.48
1.50	1.00	0.28	0.42
1.58	1.00	0.25	0.39
1.67	1.00	0.22	0.34

Table E.1: Siemens 2.3-93 Power and Thrust Data

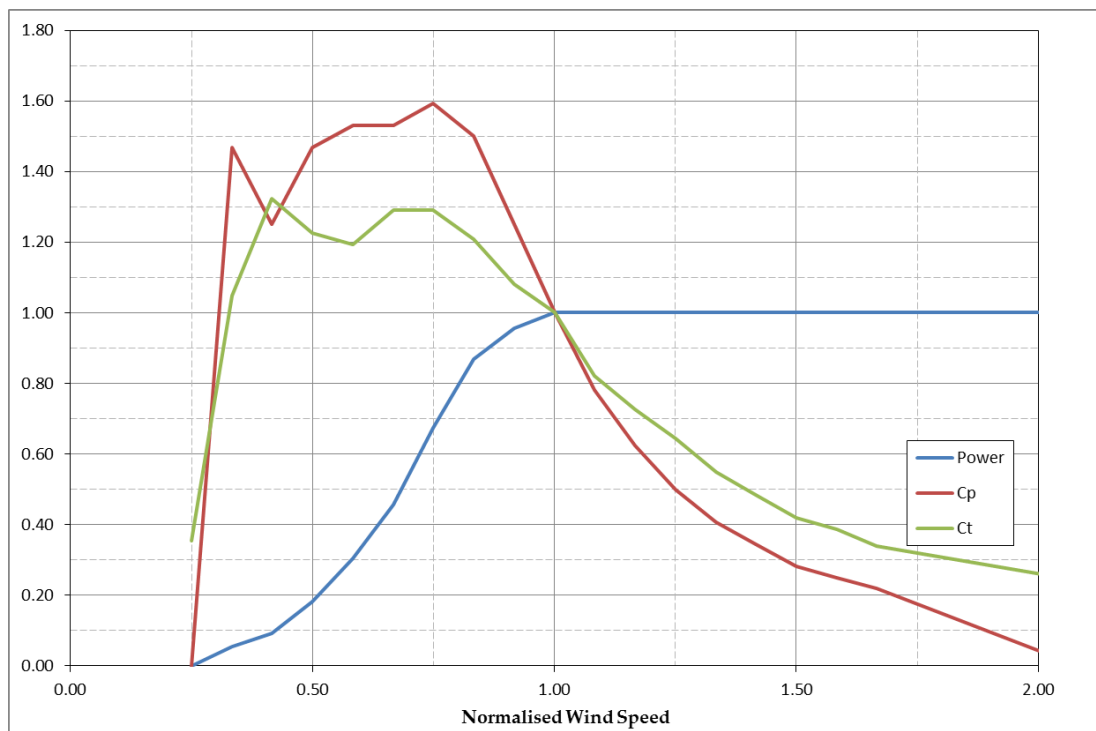


Figure E.1: Siemens 2.3-93 Power and Thrust Curves

Appendix F

AREVA M5000 Power and Thrust Curves [120]

Wind Speed (m/s)	Power (kW)	C_p	C_t
0.23	0.00	0.00	
0.31	0.02	0.60	1.80
0.38	0.05	0.82	1.65
0.46	0.09	0.93	1.55
0.54	0.19	1.22	1.64
0.62	0.30	1.27	1.67
0.69	0.43	1.31	1.65
0.77	0.61	1.34	1.65
0.85	0.76	1.26	1.52
0.92	0.95	1.20	1.32
1.00	1.00	1.00	1.00
1.08	1.00	0.80	0.75
1.15	1.00	0.65	0.59
1.23	1.00	0.54	0.48
1.31	1.00	0.45	0.40
1.38	1.00	0.38	0.33
1.46	1.00	0.32	0.29
1.54	1.00	0.28	0.25
1.62	1.00	0.24	0.22
1.69	1.00	0.21	0.20

Table F.1: AREVA M5000 Power and Thrust Data

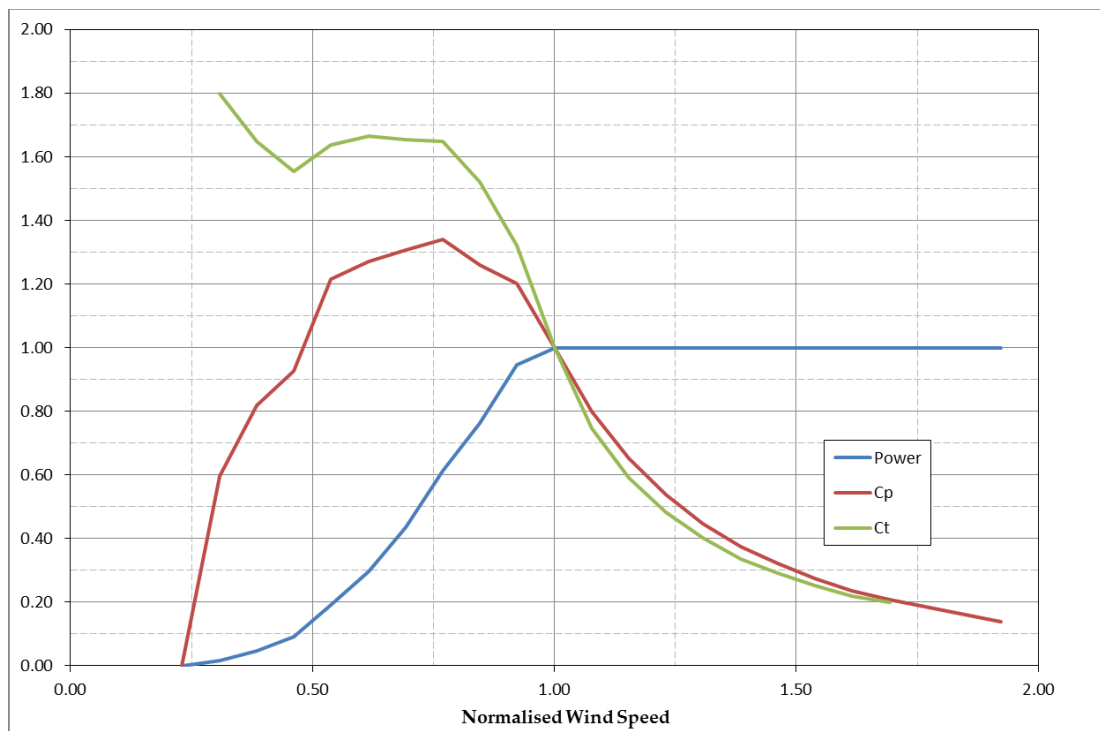


Figure F.1: AREVA M5000 Power and Thrust Curves

Appendix G

Publications and Presentations

Abstracts based on the work completed have been submitted to a number of conferences and journals throughout the course of the student's PhD.

2nd International Conference on SuperGen, Hangzhou, China, September 2012, Presentation and Paper

Title: Comparison of A 2nd Generation Lidar Wind Measurement Technique with CFD Numerical Modelling in Complex Terrain

The abstract submitted was accepted into the Scientific Topic 3: Renewable Power section of the conference. The abstract and paper were based on the initial work done on the Myers Hill/Whitelee January 2012 deployment focussing on data captured from a ten-minute averaged scan. The student attended the conference in Hangzhou in September 2012 to present on the paper and subsequent work. The paper was published in the conference proceedings.

EAWC Making Torque from Wind Conference, Oldenburg, Germany, October 2012, Poster and Paper

Title: Comparison of 2nd Generation LiDAR Wind Measurement Technique with CFD Numerical Modelling

An abstract was submitted and accepted into the 'CFD & Complex Flows' session at the conference. The abstract was accepted with the invitation to present a poster on the work undertaken; an invitation was also given to submit a paper to the conference proceedings. The focus of this work was an analysis of a series of data gathered from the January 2012 Whitelee deployment. This study focussed on comparing the different averaging periods and defined inlet definitions to the CFD simulations.

Vaasa Energy Week 2013, Vaasa, Finland, March 2013, Invited Speaker

Title: Wind Turbine Wake Behaviour, Comparison of 2nd Generation LIDAR Measurements with CFD Simulations

Invited to speak at the Vaasa Energy Week event I presented to Finish industry and academics on the potential for comparison of scanning lidar wake measurements with numerical models.

AWEA Offshore Conference, Providence, Rhode Island, USA, October 2013, Poster and Paper

Title: Analysis of Wake Development and the Effect on Power Output in an Offshore Wind Farm

Based on the work completed on the Alpha Ventus offshore lidar deployment an abstract was submitted to this American Wind Energy Association industry conference. The work presented focusses on measured wind turbine wake development across the operational range of the subject turbine and the associated effect on power availability for downstream wind turbines. This abstract was accepted for poster presentation at the conference.

EWEA Offshore Conference, Frankfurt, Germany, November 2013, Oral Presentation and Paper

Title: Comparison of Offshore Scanning Wind Lidar Wake Measurements with Industry Standard Wake Models

Utilising the extensive offshore measurements from hub height captured during the Alpha Ventus 2013 deployment the abstract submitted was selected for an oral presentation during the Offshore Resource Assessment session at this conference. The paper focus was on the comparison of industry standard and more complex wake models against the captured lidar

measurements. A paper was also submitted in support of the work presented and published in the conference proceedings.